OLFACTORY CONTROL OF *DROSOPHILA* BLOOD-PROGENITOR HOMEOSTASIS AND DEVELOPMENT VIA REDOX REGULATION

A THESIS TO BE SUBMITTED TO

THE UNIVERSITY OF TRANS-DISCIPLINARY HEALTH SCIENCES AND TECHNOLOGY

THE UNIVERSITY OF TRANS-DISCIPLINARY
HEALTH SCIENCES & TECHNOLOGY

FOR THE AWARD OF THE DEGREE
OF DOCTOR OF PHILOSOPHY

BY

MANISHA

UNDER THE GUIDANCE OF

DR. TINA MUKHERJEE

INSTITUTE FOR STEM CELL SCIENCE AND REGENERATIVE MEDICINE, BENGALURU

इन्स्टेम
inStem

MAY 2024

THE UNIVERSITY OF TRANS-DISCIPLINARY HEALTH SCIENCES AND TECHNOLOGY

Private University Established in Karnataka by ACT 35 of 2013

BENGALURU – 560064

DECLARATION BY THE CANDIDATE

I declare that this thesis entitled **"Olfactory control of *Drosophila* blood-progenitor homeostasis and development via redox regulation**" submitted for the award of Doctor of Philosophy to THE UNIVERSITY OF TRANS-DISCIPLINARY HEALTH SCIENCES AND TECHNOLOGY, Bengaluru, is my original work, conducted under the supervision of my guide, **Dr. Tina Mukherjee**. I also wish to inform that no part of the research has been submitted for a degree or examination at any university. References, assistance, and material obtained from other sources have been duly acknowledged.

I hereby confirm the originality of the work and that there is no plagiarism in any part of the dissertation.

Manisha.

Place: **Bengaluru** **Signature of the Candidate**

Date: **7th May 2024**

Name of candidate: **Manisha**

Reg. No.: 20219021222

(November 2020)

THE UNIVERSITY OF TRANS-DISCIPLINARY HEALTH SCIENCES AND TECHNOLOGY

Private University Established in Karnataka by ACT 35 of 2013

BENGALURU – 560064

CERTIFICATE

This is to certify that the work incorporated in this thesis **"Olfactory control of *Drosophila* blood-progenitor homeostasis and development via redox regulation**" submitted by **Manisha** was carried out under my supervision. No part of this thesis has been submitted for a degree or examination at any university. References, assistance, and material obtained from other sources have been duly acknowledged. I hereby confirm the originality of the work and that there is no plagiarism in any part of the dissertation.

Research Supervisor

Dr. Tina Mukherjee
Associate Investigator
Institute for Stem Cell Science and Regenerative Medicine
Bengaluru, 560065
Date: 7th May 2024

ACKNOWLEDGEMENTS

I am deeply indebted to the host of individuals who have made innumerable contributions towards completing my thesis. It is my great pleasure and privilege to express the sense of gratitude and respect to Tina for her meticulous supervision right from the inception to the completion of this work. Her expert guidance helped me to overcome seemingly insurmountable problems. I consider myself fortunate for having had the chance to work under her guidance. I sincerely thank her for always being there for me during the low times. At every step, she has encouraged me to perform better and better. I have learnt a lot from her which has shaped up my scientific thinking.

inStem and BLiSc Campus is undoubtedly one of the best places to pursue research. I thank the present and past Directors, Maneesha, Apurva, Jitu and Shashi for maintaining a conducive and pleasant working environment. I would also like to express my sincere thanks to the faculty members at inStem and NCBS for providing valuable and insightful suggestions. I would also like to thank my thesis committee members Maneesha, Gaiti and Arvind for the critical inputs they offered during the meetings.

The work described in this thesis would not have been possible without the fantastic collaboration with Rams at Purdue University. Scientific discussion and inputs from him have shaped the project and moreover my scientific thinking for which I will always be thankful for. I acknowledge the support of MPF staff, especially Bruce Cooper at Bindley Bioscience Center for giving me the opportunity and provide all the necessary facilities to carry out my research work. They have been instrumental with their timely and genuine advises. Thanks to Vikki Weake and lab members at Purdue University for helping me with the fly work and providing the necessary equipment and space to accomplish my work. I am also thankful to Rams lab members for fruitful scientific discussions in and outside lab.

I am grateful to Utpal Nath and the UTN lab members at MCB, IISc for providing me initial research training and for motivating me to follow my interests.

I'm extremely thankful to the present and past MAD lab members for being so helpful throughout and for all the suggestions regarding the projects. Time spent on campus and especially in the lab would not have been so exciting without all the wonderful people around. It was wonderful experience learning, talking, discussing, arguing and interacting with lively people around and it is not possible to acknowledge everything they have done for me in past 6 years. Next, I thank all the present and the past members of the labs in inStem and NCBS who have shared reagents, graciously allowed me to

use their facilities, when required. My stay at inStem would not have been the same without the various support staff at inStem including Instrumentation, IT, CIFF, fly facility, maas-spec facility, reception, purchase, canteen staff and administration. A special thanks to the staff at the kitchen who made fly media day in-day out. Special thanks too, to Raju, Sunitha, Valsala and Mayur who kept paperwork in order.

My senior and mentor Aitizaz Ahsan deserve special mention in this journey for infusing a sense of learning in me from my masters training onwards and beyond. A special thanks to Zeenat, her words of encouragement gave me a great deal of self-belief and freedom to think independently. I have met several amazing people during various conferences, and I thank Rajesh Gunage for the wonderful discussions about science outside the lab. Every discussion with these people lit a flame of thoughts and kept the passion for doing better in life.

I am thankful to my friends Sonam, Partha, Rohit, Rayees, Shah-e-Jahan, Neha and Naveed. They have always been there to help me in need and support me and made my PhD journey enjoyable.

Thanks to DST-INSPIRE for funding me. I also thank SERB-OVDF for funding my visit and stay at Purdue University. A huge thanks to Ravi Kumar at TDU to help with the PhD registration and further on.

Most importantly, my parents and my siblings- Karan and Taneesha, Kapil and Gaushik deserve the best. Without their love and belief, I may not have embarked on this journey. I will always be grateful to my parents for always encouraging me to pursue my dreams and giving me the freedom to make my choices in life.

(Manisha)

TABLE OF CONTENTS

LIST OF FIGURES

LIST OF TABLES

APPENDIX FIGURES

APPENDIX TABLES

ABBREVIATIONS

AA	Amino acid
ABA	α-Aminobutyric acid
ACN	acetonitrile
Adgf-A	Adenosine deaminase growth factor-A
AGM	Aorta-Gonad-Mesonephros
Antp	Antennapedia
BCA	Bicinchoninic acid
BEH	Ethylene Bridged Hybrid
BrdU	Bromodeoxyuridine
CE	Collision Energy
CHIZ	Combined hematopoietic intermediate zone
Ci	Cubitus interruptus
CMP	Common Myeloid Progenitor
CNS	Central nervous system
Col	Collier
CZ	Cortical zone
DCM	Dichloromethane
EDC	(1-ethyl-3-(3-dimethylaminopropyl) carbodiimide hydrochloride)
EDTA	Ethylenediaminetetraacetic acid
EGFP	Enhanced Green flourescent protein
FOG	Friend of GATA (FOG)
GABA	γ-Aminobutyric Acid
GABBR1	GABA type B receptor subunit 1
Gat	GABA Trasporter
Gcm	Glial cell missing
Gdh	Glutamate dehydrogenase
GFP	Green flourescent protein
GSH	Glutathione (Reduced)
GSSG	Glutathione (Oxidized)
Hh	Hedgehog
HILIC	Hydrophilic interaction liquid chromatography
Hml	Hemolectin
Hph	Hydroxyl prolyl hydroxylase
HPI	Hours post infection
HSC	Hematopoietic stem cells
HSPC	Hematopoietic stem and Progenitor cells
HSS	High Strength Silica
Idh	Isocitrate dehydrogenase
INCA	Isotopomer network compartmental analysis

IP	Intermediate progenitors
ISTD	Internal Standard
IZ	Intermediate Zone
JAK/STAT	Janus kinase/Signal transducer and activator of transcription
JNK	c-Jun N-terminal kinase
LC-MS	Liquid Chromatography Mass Spectrometry
Ldh	Lactate dehydrogenase
LG	Lymph gland
MeOH	Methanol
MPEA	2-Methoxyphenethylamine
Mys	Myospheroid
MZ	Medullary zone
NAC	N-acetylcysteine
NAD/NADH	Nicotinamide adenine dinucleotide
NaHCO3	Sodium bicarbonate
NEM	N-Ethylmaleimide
OBHA	O-Benzylhydroxylamine
OCAID1	Ovarian carcinoma immunoreactive antigen domain-containing 1
OR	Olfactory Receptor
ORN	Olfactory Receptor Neuron
PBS	Phosphate Buffer Saline
PDGF	Platelet-derived growth factor
PN	Projection Neuron
Pnr	Pannier
PNS	Peripheral sensory neurons
PPO	Prophenoloxidase
PSC	Posterior signaling center
Pvf1	PDGF- and VEGF- related factor 1
Pxn	Peroxidasin
QQQ	Triple Quadrupole
RF	Regular food
ROS	Reactive Oxygen Species
RPM	Revolutions per minute
RT	Retention time
SDH	Succinate dehydrogenase
SF	Succinate supplemented Food
Sima	alpha (HIFα) ortholog Similar
Srp	Serpent
Ssadh	Succinate semialdehye dehydrogenase
T3	trifunctionally bonded, low ligand density, C18 bonded phase, with proprietary end capping

TCA	Tricarboxylic acid
TCA	Trichloroacetic acid
TF	Transcription Factor
TGF-β	Transforming growth factor
TIC	Total Ion Chromatogram
TPO	Thrombopoietin
U-13C	Universal-13 Carbon
Ubx	Ultrabithorax
Ush	U-shaped
VEGF	Vascular endothelial growth factor
WOF	Wasp odor food
αKDH	α-ketoglutarate dehydrogenase

SYNOPSIS

Chapter 1: Introduction

Drosophila melanogaster has been used as a developmental model for decades. As our understanding of the complexities of development expands, the significant degree of conservation between *Drosophila* and vertebrate systems has become more apparent (1). During *Drosophila* larval development, lymph gland harbours the blood-progenitor cells akin to the mammalian common-myeloid progenitors (CMP). It disintegrates during the pupal stage and contributes to sessile and circulatory blood cell pool of adult animal. Various signaling molecules and metabolites produced by the local niche (posterior signaling centre, PSC) and differentiating hemocytes, and systemic cues originating from the brain and fat body affect progenitor maintenance (2). Similar to CMPs, the blood-progenitor cells of lymph gland maintain elevated levels of reactive oxygen species (ROS) whose homeostasis is necessary for their development (3–5). While physiological ROS sensitizes progenitor-cells to differentiation cues, its excessive production causes oxidative stress and loss of progenitor homeostasis (3,6). Therefore, the blood-progenitors possess robust mechanisms to maintain their ROS status, but our understanding in this regard remains limited. ROS levels in the hematopoietic stem and progenitor cells are maintained by controlling ROS production and scavenging. A key source of ROS generation in cells is tricarboxylic acid (TCA) cycle and OXPHOS (7–9). The second mode of ROS regulation, ROS scavenging is accomplished by the antioxidant enzymes and compounds like catalase, superoxide dismutase and glutathione etc (10). The goal of this thesis is to characterize the mechanisms and importance of ROS regulation during blood-progenitor development. This work demonstrates the utilization of the sensory cues of olfaction and downstream neuronal release of GABA and its catabolism in controlling blood-progenitor development and lymph gland growth via regulating ROS homeostasis. Olfaction derived GABA catabolism acts as a central regulator of blood-progenitor development during homeostasis (11) and immune-response (11,12) conditions.

The current study titled **‘Olfactory control of blood-progenitor homeostasis and development via ROS regulation’** is divided into seven chapters.

The first chapter highlights and reviews the literature on blood-progenitor development and ROS regulation, as well as discusses open questions. The second chapter describes the objectives of the study highlighting the role of olfaction and downstream systemic GABA catabolism in blood-progenitor development by governing lymph gland ROS homeostasis. Chapter three to five discusses the findings of the thesis. Chapter three of the thesis discussing about the role of olfaction derived GABA catabolism in regulating blood progenitor ROS homeostasis and lymph gland growth is published in journal Development (11). Chapter four highlights the mechanism of glutathione (GSH) biosynthesis by olfaction derived GABA catabolism. Chapter five deals with standardizing and establishing the metabolic flux analysis protocols in *Drosophila* blood-progenitor cells and lymph glands. The sixth chapter deals with material and methods of the thesis, *Drosophila* genetics, immunohistochemistry, confocal imaging and mass-spectrometry (LC/MS) based metabolite analysis has been predominantly utilized to achieve the objectives of the thesis. The work described in this thesis elucidates the role of environment odor sensing and its impact on metabolic pathway regulation and ROS homeostasis during *Drosophila* blood-progenitor development. This work for the first time has utilized the LCMS based flux analysis approach in understanding metabolic status of *Drosophila* lymph gland progenitor cells. The seventh chapter highlights future directions and our contribution to current understanding of similar mechanisms during blood-progenitor development in both invertebrates and vertebrates.

Motivation for this thesis

It is widely known that metabolism is highly dynamic and any small perturbations in the cells lead to metabolic alterations. The hematopoietic niche of the vertebrate system is significantly more complex (13,14) and also relatively inaccessible. Thus, gaining *in vivo* access to metabolic states of blood compartment during its development and understanding the interactions with signaling modules is difficult. While work to address these problems are ongoing, simpler model systems with conserved haematological functions have emerged as significant tools for advancing the idea of metabolism in the control of blood progenitor development. Common myeloid progenitors (CMPs) in mammals maintain increased levels of ROS, which play important role in stem cell state and function (5,15). Interestingly, blood-progenitors in *Drosophila* also maintain elevated levels of ROS, which primes the progenitor towards

differentiation cues. Any reduction in ROS levels during blood-progenitor development leads to loss of progenitor differentiation while, any ectopic production of ROS leads to loss of progenitor homeostasis (3). Any understanding of metabolic or signaling events that enable the sustenance of this fine redox balance and blood-progenitor development remains elusive. The ability to recognize and characterize the roles of the molecular machinery that supports developmental processes is substantially facilitated by the genetic resources available in *Drosophila*. The GAL-4/UAS system is utilized to manage the over-expression or silencing of genes using RNA interference in a spatially and temporally controlled manner. Overall, *Drosophila* lymph gland provides a highly relevant developmental model for investigating the mechanisms that control blood-progenitor maintenance and differentiation. Therefore, mechanisms underlying blood progenitors development coupled to redox homeostasis forms the central focus of current thesis.

Chapter 2: Objectives

This thesis work describes **"the odor mediated control of blood-progenitor development and maintenance via ROS regulation".** *Drosophila* blood-progenitors are an integral component of the hematopoietic organ, lymph gland and various signaling and metabolic cues regulate the development of this compartment. Previous studies have implicated olfaction and its downstream signaling mediated release of neuronally-derived GABA in progenitor maintenance (16) and immune response (12). We have found that olfaction derived GABA release and its catabolism in blood progenitors control lymph gland growth and blood-progenitor differentiation by governing lymph gland ROS homeostasis. Animals that fail to smell also fail to sustain ROS homeostasis, which leads to lymph gland growth retardation.

The specific objectives of this thesis are described below:

1. Investigating the role of olfaction derived GABA catabolism in regulating blood progenitor development and lymph gland growth via controlling ROS homeostasis
2. Exploring and delineating the mechanism of involvement of olfaction derived GABA catabolism in regulation of glutathione (GSH) biosynthesis

3. Standardizing the protocol of metabolic flux analysis in *Drosophila* blood-progenitor cells by utilizing Liquid Chromatography/Mass-Spectrometry (LC/MS) based approach.

Chapter 3-5: Results

3. **Investigating the role of olfaction derived GABA catabolism in regulating blood progenitor development and lymph gland growth via controlling ROS homeostasis**. Previous studies (12,16) have shown the importance of odor-sensing and downstream systemic GABA release in blood-progenitor development in homeostatic and immune-response conditions. We found that odor-sensing is important to maintain blood-progenitor ROS homeostasis. Animals that fail to smell (*Orco-Gal4*, *UAS-Hid*), fail to sustain TCA activity and ROS levels in the blood-progenitor cells, and consequently retarded lymph gland growth. Perturbation of GABA catabolic pathway (*UAS-Gat*^{RNAi} and *UAS-Ssadh*^{RNAi}) in the blood-progenitor cell by utilizing progenitor specific driver (*domeMeso-Gal4;UAS-GFP*) leads to smaller lymph gland size accompanied by an elevation of ROS levels. We investigated the mechanism of ROS generation regulation in the blood-progenitor cells. Since, TCA is a major contribution of ROS generation in a cell, TCA activity was analysed in GABA catabolism perturbed backgrounds. Our data show that loss of GABA catabolic pathway (*domeMeso-Gal4;UAS-GFP, UAS-Gat*^{RNAi} and *UAS-Ssadh*^{RNAi}) in the progenitor cells leads to reduction in active pyruvate dehydrogenase kinase (pPDK) and inactive pyruvate dehydrogenase (pPDH), while the levels of total PDK and total PDH does not show any change. PDH is the rate-limiting enzyme that connects pyruvate to the TCA cycle and to oxidative phosphorylation. Thus, GABA catabolism via PDK activation maintains TCA activity and blood progenitor ROS homeostasis, and supports normal lymph gland growth. Consequently, any perturbations in GABA catabolism lead to heightened TCA activity and impaired ROS homeostasis, which leads to lymph gland growth retardation. Our work shows TCA cycle activity and ROS as one of the prime regulator of lymph gland growth. Further, GABA catabolism mediated restriction on TCA cycle activity is important for progenitor homeostasis and lamellocyte formation upon parasitic wasp-infections (Fig. 1) (11).

4. **Exploring and delineating the mechanism of involvement of olfaction derived GABA catabolism in regulation of glutathione (GSH) biosynthesis.** This part of the

thesis uncovers the function of olfaction derived GABA catabolism in regulating blood-progenitor GSH synthesis by shuttling pyruvate metabolism. We investigated the mechanisms for ROS scavenging regulation by GABA catabolism and discovered that loss of GABA transporter (GAT) and GABA catabolising enzyme $Ssadh^{RNAi}$ resulted in a decrease in GSH levels in lymph glands, an important antioxidant responsible for scavenging reactive oxygen species (ROS). Glutathione is a tripeptide, synthesized from glutamate, cysteine and glycine (17). We found that in the blood-progenitor cells GABA catabolism modulate cysteine levels, which further regulates GSH biosynthesis (Fig. 1). *DomeMeso-GFP>*Gat^{RNAi} and *domeMeso-GFP>*$Ssadh^{RNAi}$ lead to reduction in blood-progenitor cysteine levels, but did not show any change in glutamate and glycine levels, detected by antibodies against glutamate and cysteine. Thus, Cysteine is a key component in GSH production, and its availability is controlled by GABA catabolism. Serine, along with methionine, is known to contribute to cysteine production in cells via the transsulfuration pathway (18). We independently checked the involvement of both serine and methionine in GSH synthesis regulation by GABA catabolism. Our results demonstrated that metabolically, GABA catabolism derived succinate control serine levels in the progenitor cells, which contribute to cysteine and downstream GSH synthesis and thus maintain ROS homeostasis of the blood-progenitor compartment (Fig. 1).

5. **Standardizing the protocol of metabolic flux analysis in *Drosophila* blood-progenitor cells by utilizing Liquid Chromatography/Mass-Spectrometry (LC/MS) approach**. This part of the work deals with utilizing the mass-spectrometry based approach to establish ^{13}C-isotope labelling and metabolic flux analysis in the lymph gland blood-progenitor cells. While recent evidences suggests the distinct metabolic requirements of myeloid cells across systems ranging from mammals to invertebrates, a comprehensive study of this scale has not been attempted (19,20). The current thesis work describes the utilization of LC/MS/MS based methods and ^{13}C-isotope labelling for analysing TCA cycle metabolites, amino acids and GSH:GSSG in lymph gland progenitor cells. Lymph gland are dissected and incubated with 10mM U^{13}C-glucose or 10mM U^{13}C-pyruvate isotopic label in PBS for specific time points and the samples are processed for metabolite extraction. The method of (21,22) are utilized for TCA metabolite analysis.

We show that olfaction derived GABA release and its downstream catabolism in blood-progenitor cells regulate lymph gland growth and blood-progenitor development by regulating ROS homeostasis. A comprehensive study of metabolic pathways and metabolites during blood progenitor development is achieved by utilizing genetics, immunohistochemistry, microscopy (imaging) and mass-spectrometry based approaches. Our findings describe that olfaction-derived GABA catabolism modulates pyruvate metabolism in blood-progenitor cells to maintain ROS homeostasis and blood-progenitor development.

Chapter 6: Materials and Methods

To achieve the above mentioned objectives following materials and methods are utilized, which are briefly outlined here. *Drosophila melanogaster Gal4* and RNA*i* stocks are either procured from BDSC, VDRC or requested from various research laboratories. All fly stocks are reared on corn meal agar food medium with yeast supplementation at 25°C incubator unless specified. The crosses involving RNA*i* lines are maintained at 29ºC to maximize the efficacy of the *Gal4/UAS RNAi* system. *Leptopilina boulardi* (parasitic wasps) are cultured and maintained on w^{1118}. For ROS detection lymph gland were stained with DHE (Sigma, 1:1000 in PBS). For Immunohistochemistry, lymph glands isolated from larvae are stained. Immunostaining on lymph gland is performed majorly with the following primary antibodies: rabbit αpPDHK1(1:200, #11597 SAB), rabbit αpPDH (1:250, abcam #177461), mouse-αPDH (Abcam, ab110334, 1:250), mouse-αPDK (Abcam, ab110025, 1:500), mouse αCysteine (1:20 # sc-69954), Mouse α Myospheroid (1:100 # CF.6G11), rabbit αGABA (1:100, sigma #A2052), rabbit αGlutathione (1:100, abcam #5543), mouse-αGlutamate (1:100, #ab9440). The following secondary antibodies are used at 1:500 dilutions: FITC, Cy3 and Cy5 (Jackson Immuno Research Laboratories and Invitrogen). Samples are mounted with Vectashield (Vector Laboratories). Immuno-stained lymph gland images are acquired using Olympus FV3000 Confocal Microscopy with 40X oil-immersion objective. All images are quantified using ImageJ software. Roughly, middle two confocal Z-stacks are merged and lymph gland area is marked and measured. This is done for respective zones and the area is represented in percent values. Controls are analysed in parallel to the sample conditions every time. For quantifying mean intensities in lymph gland, the relevant stacks of the lymph gland images are selected,

the area to be measured per lobe is defined using the select tool and is then processed for intensity measurements by considering mean intensity values. For all intensity quantifications, the laser setting for each individual experimental set-up is kept constant. For Metabolite supplementation experiments, Succinate (Sodium succinate dibasic hexahydrate, Sigma #SLBM6312V), Serine (0.1%, Sigma), Methionine (0.1%, Sigma), N-Acetylcysteine (0.1%, Sigma) and GABA (3%, Sigma) enriched diets are prepared by supplementing regular fly food with respective amounts by weight/volume measures of succinate to achieve 3% concentrations. Eggs are collected in these supplemented diets and reared until analysis of their respective tissues. For Mass-spectrometry based LCMS analysis, five lymph glands per sample are dissected from the larval stage of interest. Metabolites are isolated from lymph glands using specific methods, and the samples are then subjected to LC/MS analysis. The acquired data is processed further by either MassHunter or MultiQuant software. Statistical analyses are performed using GraphPad Prism software and Microsoft Excel.

Chapter 7: Discussion

It has been well established that ROS as a signaling entity are critical for blood-progenitor development and maintenance (10,23,24). However, mechanisms limiting ROS levels that are critical for its functioning in myeloid progenitor cells remain mostly unclear. We find that blood development in *Drosophila* is strikingly influenced by sensory cues of olfactory in origin. With the current work, we present the developmental role for olfaction in blood progenitor redox balance. Recent research has demonstrated the importance of GABA in myeloid immunity, specifically in metabolic programming of myeloid cells during innate immune training (25–28). These findings point to similarities between the myeloid systems of mammals and *Drosophila*. Our findings in the hematopoietic system of *Drosophila* emphasize many developmental roles of GABA in myeloid development, progenitor homeostasis, and immunity. Upon olfactory stimulation, neuronally derived GABA and its metabolism is linked to limiting pyruvate's entry into the TCA cycle and this restricts TCA derived precocious ROS production (11) and leads to generation of antioxidant, glutathione. Our findings show that myeloid metabolism and ROS balance by controlling both the ROS generation and scavenging axis are sensitive to olfaction-derived GABA. This axis is required for appropriate lymph gland growth and development.

These findings not only reveal novel activities of neurotransmitters like GABA in hematopoiesis, but also expand our understanding of the relationship between animal odor-sensing and systemic modulation of blood progenitor metabolism and redox balance.

Significance and future prospects of the current research

Drosophila and the mammalian hematopoietic system share many conserved characteristics. As a result, the findings in *Drosophila* blood development are intriguing prospects with a lot of potential for translation into the mammalian hematopoietic system as well (19,29). While the *Drosophila* hematopoietic system provides insight into myeloid-like blood progenitor development and immunity, we cannot expect it to entirely mirror the vertebrate immune system. Mammalian hematopoietic niche, bone marrow, is more complex and is controlled by a number of additional modulators. As a result, the metabolic pathways and cross-talks found in this work may have additional layers of complexity during blood-development in higher organisms and the identified mechanism in the fly model must be independently confirmed in vertebrate model systems like mice. Moreover, the complexity of the vertebrate immune system due to presence of lymphoid arm and the existence of additional blood cell types, makes it difficult to delineate mechanisms specific to the myeloid or lymphoid arm. The first step could be to test the existence of these processes or pathways in mammalian systems. Nonetheless, *Drosophila* model provides a multitude of genetic tools for investigating mechanisms underlying development and disease. As we continue to learn more about blood formation and reveal fundamental mechanisms in simpler systems like *Drosophila*, this research can be utilized to develop techniques and approaches for dealing with complex vertebrate systems.

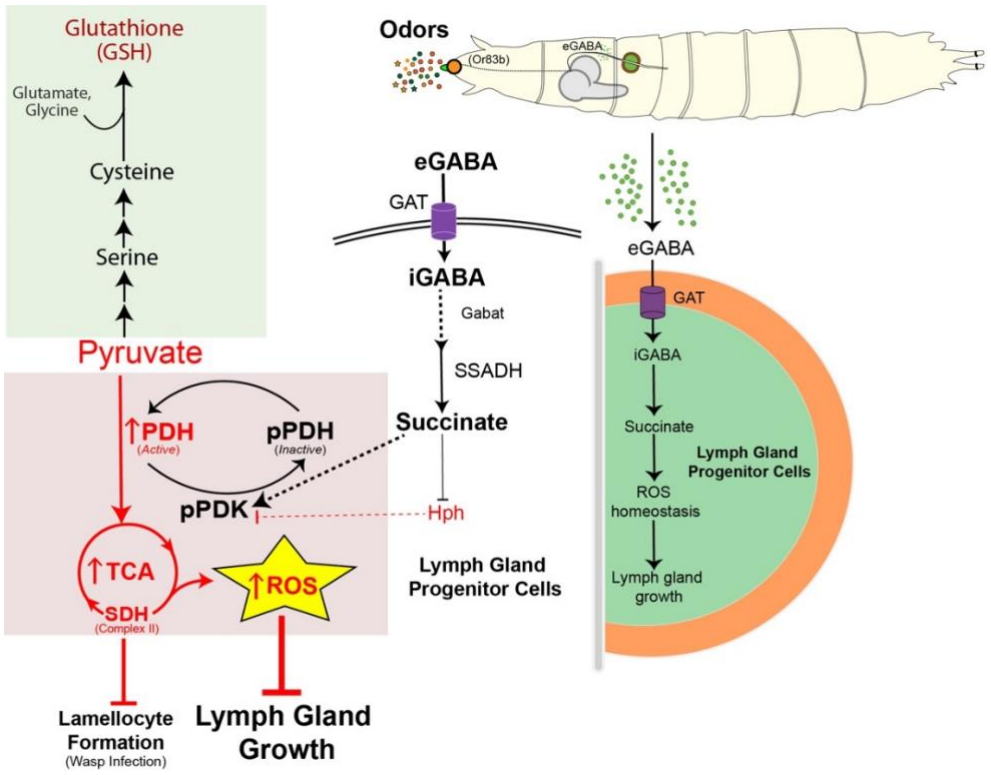

Figure 1. **Olfaction-derived systemic GABA and its catabolism in lymph gland ROS homeostasis and growth control.** The model describes the importance of olfaction-derived GABA metabolism in lymph gland growth control. All elements that repress growth are shown in red, while positive regulators of growth are shown in black. Blood progenitor cells of the *Drosophila* larval lymph gland maintain ROS in them that is derived from the TCA cycle. However, heightened or uncontrolled TCA cycle activity, leading to increased ROS production in progenitor cells, abrogates lymph gland growth and development. GABA catabolism derived TCA regulation is also important for lamellocyte formation during immune response conditions. Secondly, in the blood-progenitor cells, GABA catabolism derived succinate shuttles pyruvate towards gluconeogenic arm and leads to serine and consequently glutathione (GSH) formation.

References of Synopsis:

1. Tolwinski NS. Introduction: Drosophila-A Model System for Developmental Biology. J Dev Biol [Internet]. 2017 Sep 20;5(3). Available from: http://www.ncbi.nlm.nih.gov/pubmed/29615566

2. Banerjee U, Girard JR, Goins LM, Spratford CM. Drosophila as a Genetic Model for Hematopoiesis. Genetics. 2019/02/09 ed. 2019;211(2):367–417.

3. Owusu-Ansah E, Banerjee U. Reactive oxygen species prime Drosophila haematopoietic progenitors for differentiation. Nature. 2009/09/04 ed. 2009;461(7263):537–41.

4. Shinohara A, Imai Y, Nakagawa M, Takahashi T, Ichikawa M, Kurokawa M. Intracellular reactive oxygen species mark and influence the megakaryocyte-erythrocyte progenitor fate of common myeloid progenitors. Stem Cells Dayt Ohio. 2014 Feb;32(2):548–57.

5. Ludin A, Gur-Cohen S, Golan K, Kaufmann KB, Itkin T, Medaglia C, et al. Reactive oxygen species regulate hematopoietic stem cell self-renewal, migration and development, as well as their bone marrow microenvironment. Antioxid Redox Signal. 2014 Oct 10;21(11):1605–19.

6. Dragojlovic-Munther M, Martinez-Agosto JA. Multifaceted roles of PTEN and TSC orchestrate growth and differentiation of Drosophila blood progenitors. Development. 2012/09/07 ed. 2012;139(20):3752–63.

7. Kaplon J, Zheng L, Meissl K, Chaneton B, Selivanov VA, Mackay G, et al. A key role for mitochondrial gatekeeper pyruvate dehydrogenase in oncogene-induced senescence. Nature. 2013;498(7452):109–12.

8. Quinlan CL, Orr AL, Perevoshchikova I V, Treberg JR, Ackrell BA, Brand MD. Mitochondrial complex II can generate reactive oxygen species at high rates in both the forward and reverse reactions. J Biol Chem. 2012/06/13 ed. 2012;287(32):27255–64.

9. Starkov AA. The role of mitochondria in reactive oxygen species metabolism and signaling. Ann N Y Acad Sci. 2008;1147:37–52.

10. Bigarella CL, Liang R, Ghaffari S. Stem cells and the impact of ROS signaling. Development. 2014/11/06 ed. 2014;141(22):4206–18.

11. Goyal M, Tomar A, Madhwal S, Mukherjee T. Blood progenitor redox homeostasis through olfaction-derived systemic GABA in hematopoietic growth control in Drosophila. Dev Camb Engl [Internet]. 2022;149(8). Available from: http://www.ncbi.nlm.nih.gov/pubmed/34850846

12. Madhwal S, Shin M, Kapoor A, Goyal M, Joshi MK, Ur Rehman PM, et al. Metabolic control of cellular immune-competency by odors in Drosophila. Lemaitre B, Akhmanova A, Dolezal T, Kacsoh BZ, editors. eLife. 2020 Dec 29;9:e60376.

13. Morrison SJ, Scadden DT. The bone marrow niche for haematopoietic stem cells. Nature. 2014 Jan 16;505(7483):327–34.

14. Batsivari A, Haltalli MLR, Passaro D, Pospori C, Lo Celso C, Bonnet D. Dynamic responses of the haematopoietic stem cell niche to diverse stresses. Nat Cell Biol. 2020 Jan;22(1):7–17.

15. Suda T, Takubo K, Semenza GL. Metabolic regulation of hematopoietic stem cells in the hypoxic niche. Cell Stem Cell. 2011 Oct 4;9(4):298–310.

16. Shim J, Mukherjee T, Mondal BC, Liu T, Young GC, Wijewarnasuriya DP, et al. Olfactory control of blood progenitor maintenance. Cell. 2013 Nov 21;155(5):1141–53.

17. Lu SC. Glutathione synthesis. Biochim Biophys Acta. 2013 May;1830(5):3143–53.

18. Zhu J, Berisa M, Schwörer S, Qin W, Cross JR, Thompson CB. Transsulfuration Activity Can Support Cell Growth upon Extracellular Cysteine Limitation. Cell Metab. 2019;30(5):865-876.e5.

19. KS G, K B. Drosophila as a model for the two myeloid blood cell systems in vertebrates. Exp Hematol. 2014;42(8):717–27.

20. Zuo H, Wan Y. Metabolic Reprogramming in Mitochondria of Myeloid Cells. Cells. 2019;9(1).

21. Tan B, Lu Z, Dong S, Zhao G, Kuo MS. Derivatization of the tricarboxylic acid intermediates with O-benzylhydroxylamine for liquid chromatography-tandem mass spectrometry detection. Anal Biochem. 2014;465:134–47.

22. Walvekar A, Rashida Z, Maddali H, Laxman S. A versatile LC-MS/MS approach for comprehensive, quantitative analysis of central metabolic pathways. Wellcome Open Res. 2018 Sep;3(3):122.

23. Harris JM, Esain V, Frechette GM, Harris LJ, Cox AG, Cortes M, et al. Glucose metabolism impacts the spatiotemporal onset and magnitude of HSC induction in vivo. Blood. 2013;121(13):2483–93.

24. Vincent A, Crozatier M. Neither too much nor too little: reactive oxygen species levels regulate Drosophila hematopoiesis. J Mol Cell Biol. 2009/12/17 ed. 2010;2(2):74–5.

25. Shao L, Elujoba-Bridenstine A, Zink KE, Sanchez LM, Cox BJ, Pollok KE, et al. The neurotransmitter receptor Gabbr1 regulates proliferation and function of hematopoietic stem and progenitor cells. Blood. 2020/09/04 ed. 2021;137(6):775–87.

26. Steidl U, Bork S, Schaub S, Selbach O, Seres J, Aivado M, et al. Primary human CD34+ hematopoietic stem and progenitor cells express functionally active receptors of neuromediators. Blood. 2004/03/16 ed. 2004;104(1):81–8.

27. Zhu F, Feng M, Sinha R, Murphy MP, Luo F, Kao KS, et al. The GABA receptor GABRR1 is expressed on and functional in hematopoietic stem cells and megakaryocyte progenitors. Proc Natl Acad Sci U A. 2019/08/28 ed. 2019;116(37):18416–22.

28. Fu J, Han Z, Wu Z, Xia Y, Yang G, Yin Y, et al. GABA regulates IL-1β production in macrophages. Cell Rep. 2022 Dec;41(10):111770.

29. CJ E, V H, U B. Thicker than blood: conserved mechanisms in Drosophila and vertebrate hematopoiesis. Dev Cell. 2003 Nov;5(5):673–90.

LIST OF PUBLICATIONS FROM PH.D. STUDIES

1. **Goyal, M.,** Tomar, A., Madhwal, S., & Mukherjee, T. (2022). Blood progenitor redox homeostasis through olfaction-derived systemic GABA in hematopoietic growth control in *Drosophila*. Development (Cambridge, England), 149(8), dev199550. https://doi.org/10.1242/dev.199550
2. Madhwal, S., Shin, M., Kapoor, A., **Goyal, M.,** Joshi, M. K., Ur Rehman, P. M., Gor, K., Shim, J., & Mukherjee, T. (2020). Metabolic control of cellular immune competency by odors in *Drosophila*. eLife, 9, e60376. https://doi.org/10.7554/eLife.60376.

LIST OF PH.D. WORK PRESENTATION IN CONFERENCES

1. **Gordon Research Seminar (GRS), Developmental Biology** meeting from June 24th-25th 2023, held at Mount Holyoke College, MA, USA. (Oral Presentation)

2. **Gordon Research Conference (GRC), Developmental Biology** meeting from June 25th-30th 2023, held at Mount Holyoke College, MA, USA. (Poster Presentation)

3. **Annual *Drosophila* Research Conference 2023**, from March 1st-March 5th, held at Chicago, USA. (Poster Presentation)

4. **International Society for Stem Cell Research (ISSCR) meeting 2022**, from June 14-June 20, held at San Francisco, California, USA. (Poster Presentation)

5. **Asia-Pacific *Drosophila* Research Conference (APDRC5),** held at Pune, INDIA from January 6th-10th 2020**.** (Poster Presentation-Best Poster Award)

1 Introduction

1.1 Hematopoiesis and its developmental phases

Hematopoiesis is a term derived from greek words haima (blood) and poiēsis (to produce). It is the process of blood cells formation and has been studied extensively for over a century using a range of model systems. The various blood cell types that animals have and the processes that produce them have rapidly diversified and become more complex during evolution. Even though some differences do exist, the general hematopoietic mechanisms are conserved across metazoans. Organisms from different phyla such as, *Drosophila*, zebrafish, and mammals (e.g., mouse, human) share many conserved traits that drive blood cell development, despite the temporal and spatial heterogeneity (1,2). The existence of two major developmental phases of hematopoiesis is an important conserved aspect, which establishes the existence of similar types of regulatory mechanisms during blood development.

In both vertebrates and invertebrates, hematopoiesis is a biphasic event and the two phases are spatially and temporally distinct (1–3). In vertebrates, the first wave of hematopoiesis, also known as primitive hematopoiesis, occurs in the blood islands within the yolk sac after the onset of gastrulation during embryonic development and give rise to primitive erythrocytes, megakaryocytes and macrophages (Fig. 1) (3–6). The main function of primitive hematopoiesis is to produce erythrocytes that can facilitate tissue oxygenation and energy during rapid embryonic development. Primitive hematopoiesis is transitory and is replaced by the second wave during later stages of embryonic development (7,8). The second wave of hematopoiesis, termed definitive hematopoiesis, happens in the aorta-gonad-mesonephros (AGM) region and produce hematopoietic stem cells (HSCs, Fig. 1) (9). HSC is at the pinnacle of hematopoiesis and is defined by two fundamental properties: the ability to self-renew, and the ability for multipotent differentiation into mature blood-cell lineages from the later embryonic stages till adulthood (9,10). As the fetal development ends, hematopoietic stem cells migration starts towards the bone marrow, which acts as primary site of postnatal hematopoiesis in adults. HSCs in vertebrates replenishes the pool of blood cells throughout the life span of an organism.

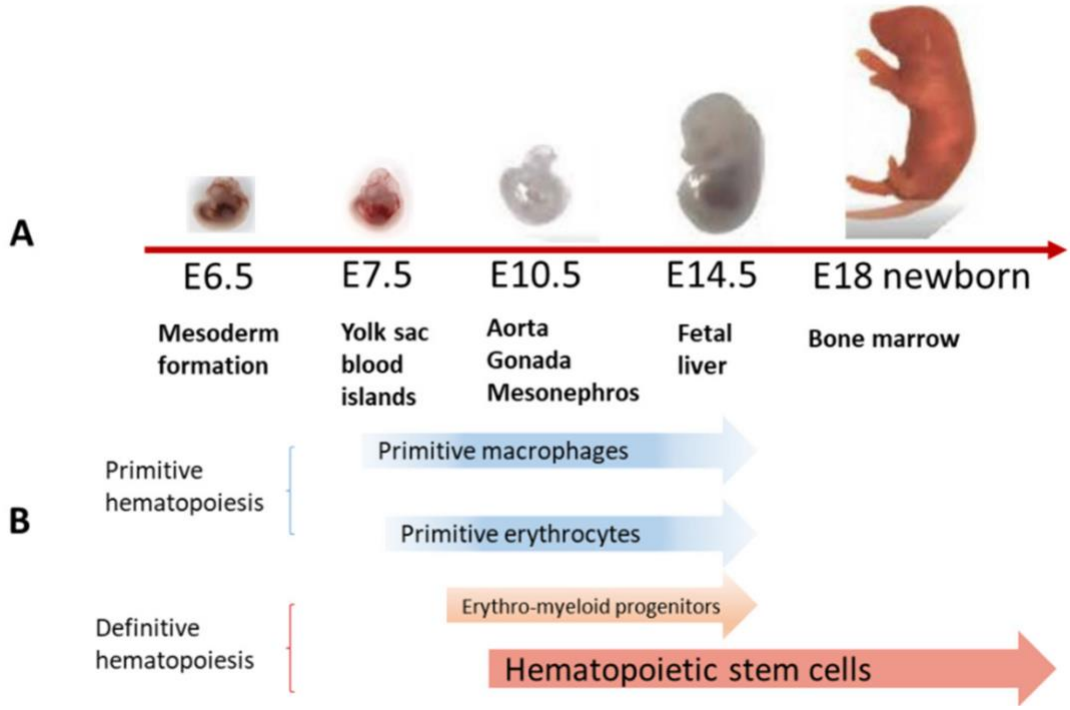

Figure 1. Vertebrate hematopoietic development.
(A) Diverse hematopoiesis sites during mouse development, **(B)** temporal and spatial localization of primitive and definitive hematopoiesis, adapted from (11).

In invertebrates like *Drosophila*, primitive hematopoiesis occurs in the head mesoderm and hemocytes are specified during late stage 10 embryo (Fig. 2) (12). These hemocytes differentiate from a common population of precursor cells called the prohemocytes and at late stage 11embryo around 700 hemocytes are observed and these differentiates into macrophages, known as plasmatocytes (12,13) and platelets like crystal cells (14) whose primary function is wound healing and melanisation during immune response (15,16). During later embryonic stages, the plasmatocytes migrate and populate the entire embryo and these cells circulate throughout the haemolymph in developing larvae (17).

The definitive wave of hematopoiesis originates from the cardiogenic mesoderm during late-embryogenesis and it forms lymph gland, the larval hematopoietic organ (Fig. 2) (18). The lymph gland comprises multipotent prohemocytes that actively proliferate and expands into a multilobed structure spanned across either side of dorsal vessel (19). During larval development, the prohemocytes of lymph gland differentiates into blood cell types with specialized function akin to the vertebrate myeloid lineage, indicating the similarities between vertebrate and invertebrate hematopoietic system (20,21). Specifically, the first wave of hematopoiesis fulfils the energy requirement for rapid

embryo growth, and the successive second wave of hematopoiesis give rise to hematopoietic precursors and contributes to functionally diverse blood cell types during animal development.

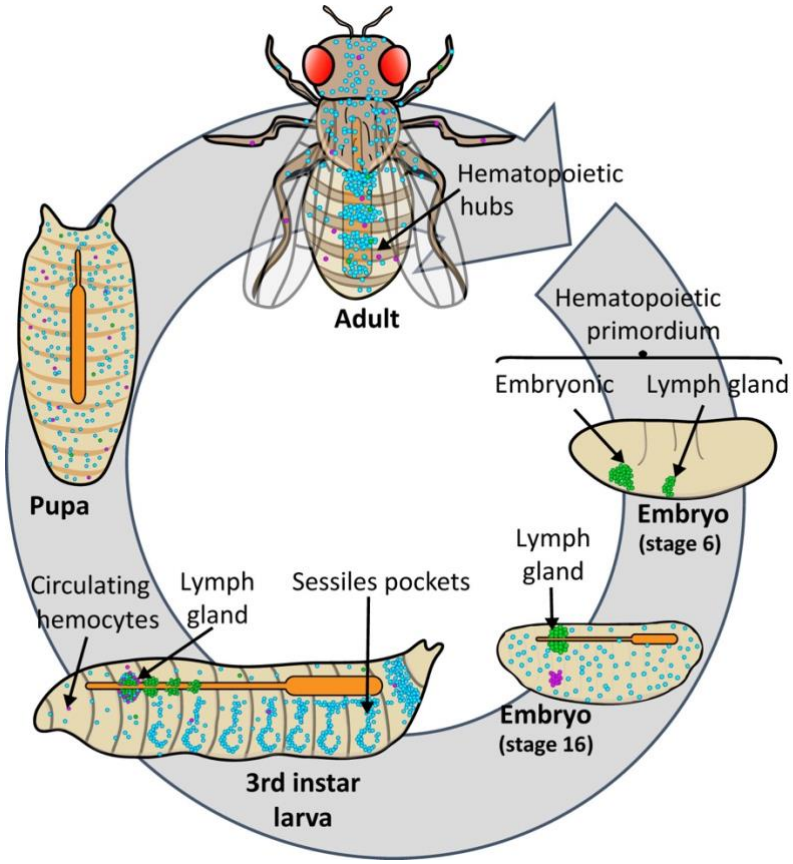

Figure 2. *Drosophila* life cycle and hematopoietic development.
First wave of hematopoiesis occurs at embryonic stage 6 and definitive wave gives rise to lymph gland at embryonic stage 16 (22).

1.2 Molecular mechanisms of hematopoietic development

Molecular circuits that regulate hematopoietic development are highly conserved in animals ranging from invertebrates to mammals. The conservation exists at different levels from existence of similar transcription factors regulating hematopoiesis to presence of conserved signaling pathways to control blood cell development. Although, invertebrates like *Drosophila* lack hematopoietic stem cells (HSCs), the blood cell lineage originate from a common set of hematopoietic precursors. In both invertebrates and vertebrates, GATA family of zinc finger transcription factors are the conserved transcription factors that regulate both primitive and definitive hematopoiesis. GATA, known as Serpent in *Drosophila,* is the early hematopoietic marker which specifies the mesodermal cells towards hematopoietic fate (23,24). GATA-1, GATA-2 and GATA-

3 are fundamental transcription factors (TFs) involved in specification and development of mouse hematopoietic lineage (Fig. 3) (24–28). Other conserved transcription factors include friend of GATA (FOG) and Runx, that have important function in erythropoiesis and definitive hematopoiesis respectively (29,30). U-shaped modulates the function of GATA and is a member of FOG family of zinc finger TFs. U-shaped (Ush) is required for specification of plasmatocytes and it represses the crystal cell fate specification (29). Similarly, FOG-1 zinc finger transcription factors in mouse have been shown to regulate the fate specification of erythrocytes and megakaryocytes in association with GATA-1 transcription factors (31–34) and FOG-2 regulate the fate of heart morphogenesis in conjugation with GATA-4 (35–37). Disruption of Runx family of transcription factors causes loss of definitive hematopoiesis in mice models (38–41) and its *Drosophila* ortholog, *Lozenge* is fundamental for crystal cell fate specification (13,42).

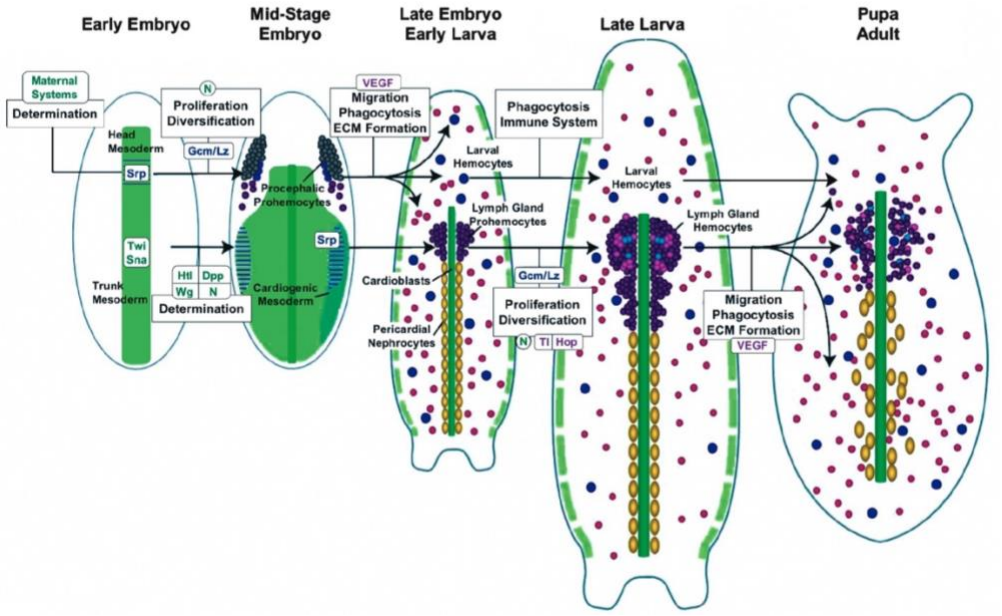

Figure 3. Regulation of *Drosophila* hematopoiesis during the primitive and definitive waves.
Diverse cell fate specification markers involved in *Drosophila* blood development from early embryonic stages till later stages of development (20).

Along with transcription factors, signaling pathways that influence hematopoiesis are conserved across animals. Notch is a major signaling pathway that regulate hematopoiesis in *Drosophila*, mouse and humans alike (43–46). Notch ligand Serrate in *Drosophila* and its homolog jagged-1 in mouse is known to regulate various hematopoietic processes (45,47,48). Moreover, Dpp/BMP and Fibroblast Growth Factor (FGF) signaling pathways regulate definitive hematopoiesis by controlling the

specification of the AGM region from the lateral mesoderm in vertebrates (49,50) and similarly, the Dpp/BMP and FGF pathways control the specification of *Drosophila* cardiogenic mesoderm which form lymph gland and heart during definitive wave (Fig. 3) (51,52). Vascular endothelial growth factor receptor (PDGF/VEGF receptor, Pvr) regulates hemocytes migration in *Drosophila* (53), and angiogenesis and vasculogenesis, during homeostatic development and in pathological conditions in mammals (54). Other important conserved signaling pathways include JAK/STAT and Toll/Cactus pathways that regulate proliferation of hematopoietic precursors and immune function (55–58). Hematopoiesis is a tightly regulated process and perturbation of any of these signaling pathways lead to haematological disorders.

Although, *Drosophila* and higher vertebrates possess differences in their developmental and morphological body plan, the fundamental mechanisms of genetic control are conserved. Existence of similar homeotic gene clusters responsible for anterior-posterior (A/P) axis formation during development is a clear evidence (59). Similarly, *Drosophila* and vertebrates organisms have conserved transcription factors and signaling pathways regulating hematopoietic development. Additionally, presence of fewer blood cell types and relatively simpler blood development systems makes *Drosophila* an excellent model to study the mechanisms controlling blood development (20,21). It offers a great potential in identification of molecular mechanisms and pathways that are relevant to vertebrate blood development.

1.3 Drosophila hematopoietic system

Drosophila proves to be an excellent genetically tractable model system to understand complex mechanisms of development. Presence of various genetic tools, shorter life cycle and cost-effectiveness are additional factors that greatly facilitate the use of *Drosophila* in identification and characterization of complex molecular mechanisms regulating development and disease. Gal4/UAS system (60) allows for spatial and temporal knockdown and overexpression of genes allowing the identification of novel function and regulators in developmental processes. Talking about the hematopoietic system, as discussed previously the existence of conserved mechanisms of development makes it an interesting model to study mechanisms of hematopoietic development.

1.4 Drosophila hematopoietic organ: the lymph gland

The hematopoietic organ of *Drosophila*, lymph gland is present dorsally in the larva and attached to ring gland and dorsal vessel (Fig. 4) (61). Lymph gland is derived from cardiogenic mesoderm and is the hub for hematopoietic precursors and differentiated cells that contributes to the larval and adult hematopoietic pool. Lymph gland development starts in late embryonic stage and continues till wandering third instar larval stage (62) and disintegrates during pupal to adult metamorphosis.

Embryonic lymph gland comprises pool of 20 pre-progenitor cells. During the first-instar larval stage, progenitor cells arise from these pre-progenitors and cluster around the dorsal vessel. This is followed by a series of divisions by the progenitor cells, giving rise to a larger population of progenitor cells (approx. 200 cells) during the second instar larval stage and also the posterior lobes starts appearing at this stage. The proliferation happens maximum at the third instar larval stage (ten-fold increase) and it continues till late third instar larvae (62). During the course of lymph gland development, the progenitor cells starts to differentiate and diversifies into various cell types located spatially within this compartment. The differentiation happens majorly in the primary lobes of lymph gland, while smaller secondary and tertiary lobes show significantly lower hematopoietic activity (1,62).

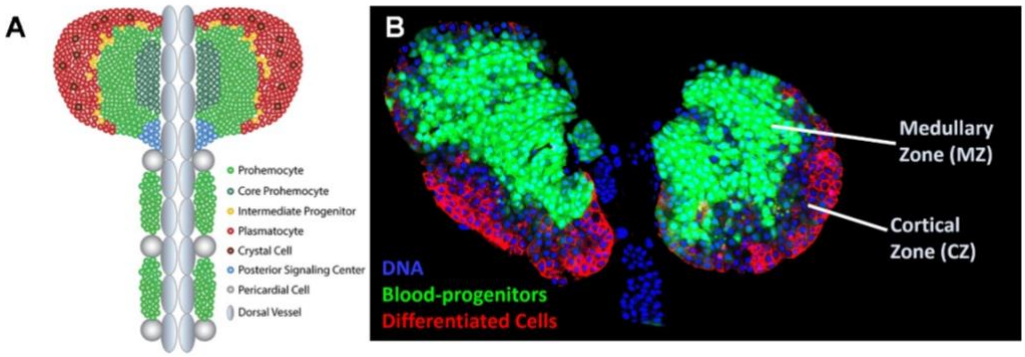

Figure 4. *Drosophila* larval lymph gland.
(A) Schematic representation of the lymph gland showing various zones and cell types (63), **(B)** Confocal Image of lymph gland tissue, blood-progenitor cells are marked green with dome and comprises Medullary Zone (MZ), differentiated cells (Plasmatocytes, red) are marked with P1, component of Cortical Zone (CZ) and DAPI marks DNA.

The primary lymph gland lobes are major hematopoietic compartments and are divided into various subcellular zones, comprising different cell types (Fig. 4).

1.4.1 Zonation of lymph gland primary lobes

1.4.1.1 Posterior Signaling Centre (PSC)

This is the first zone to be characterized as a separate cell population. Posterior signaling centre (PSC), is cluster of 35-40 cells that acts as niche to control progenitor maintenance (Fig. 4A) (45). PSC is localised at posterior end of primary lobe and is separated from the secondary lobe by a single pericardial cell and these cells are characterized by their expression of Hh, Antp and Collier (45,64,65). The PSC niche is a reminiscent of HSCs niche (66,67) equivalent to bone marrow at later stages of mammalian development. The cells of PSC show active proliferation during early stages of development and their number comparatively remains same during later stages of larval development (65). It has been shown that collier and serrate autonomously regulate the homeostatic development of PSC cells in the lymph gland (68) and non-autonomous regulation happens through various independent mechanisms from other lymph gland cell types (69). The PSC cells neither give rise to the progenitor cells nor differentiate, these cell relay signals for progenitor maintenance and differentiation and maintain the homeostasis of progenitor cells either directly or indirectly. Various signaling cues including hedgehog (hh), Antennapedia (Antp) (65), Wingless (Wg) (70,71), Notch and Serrate (68), ROS (72,73), Pvf1/Pvr (74), Collier (col) (75), Dpp (66) , TGF- β and calcium signaling (76) regulate progenitor homeostasis and signals like Toll/nuclear factor κB (NFκB) from the PSC regulate immune response conditions (Fig. 5) (77).

1.4.1.2 Medullary Zone (MZ)

The different zones of primary lobe were first characterised by differential appearance of inner and outer region of lymph glands, the medial region being more compact and smooth, whereas the distal region showed a granular appearance (Fig. 4) (62). The inner zone of cell show progenitor specific markers such as Serpent, Odd, thioester-containing protein 4 (*Tep4*, (78), domeless, ROS (72), Wg, E-cad (62), and very low levels of Collier (68,79–81), and comprises the medullary zone (MZ). During early stages of lymph gland development, a small subset of dome$^-$ cells from medial portion of lymph gland located close to the dorsal vessel, marked as pre-progenitors (62) give rise to dome$^+$ progenitor cells of medullary zone (66,82). Various internal and external signaling pathways regulate the fate of progenitor cells in the medullary zone (Fig. 5). Wingless is expressed in MZ and it regulate the expression of shotgun (DE-cad

homolog) to maintain progenitor population (71,83). JAK/STAT pathway receptor domeless (dome) is used as MZ marker and loss of JAK/STAT signaling leads to progenitor differentiation (62,68). Several other factors that regulate MZ homeostasis include u-shaped, FGF receptor, heartless, ROS, lipids and adenosine or systemically-derived like insulin, amino acids and GABA from neurons (1).

1.4.1.3 Cortical Zone (CZ)

The loosely arranged cells present on the periphery of lymph gland are differentiated cells, marked by collagens (84–86), early differentiation marker Hemolectin, Hml (87,88), Lozenge, Lz (45), Peroxidasin, Pxn (89) and P1 antigen, plasmatocytes marker (84,90). This zone is termed as cortical zone (CZ) and harbours the differentiated hemocyte populations (Fig. 4). The majority of the differentiated cells present in the cortical zone are plasmatocytes (macrophage like) (Fig. 4B), accompanied by a small proportion of crystal cells. Genes governing plasmatocytes fate specification are relatively unknown, it has been shown that STAT92E, Metal-responsive Transcription Factor-1 (Mtf-1), a conserved zinc finger protein is required for maturation of plasmatocytes (91,92). Crystal cell development is widely studied and it is regulated by notch signaling pathway (45). Another differentiated blood cell type, that is not present in the healthy organism, but appears during parasitic wasp-infection is lamellocytes. Lamellocyte induction is majorly regulated by JNK pathway (93), Toll signaling (57) and GABA shunt derived succinate through Sima stabilization (94). In depth characteristics of the differentiated cell types are detailed in the following section.

1.4.1.4 Intermediate Zone

The medullary and cortical zone are separated by a thin layer of transitioning cells, which express the markers for progenitors (dome+) and early differentiation markers such as Pxn and Hml. These cells comprise the intermediate zone (IZ) and are termed as intermediate progenitors (Fig. 4A) (95). These subset of cells lack the expression of terminal differentiation markers of mature cell types such as plasmatocytes (P1) and crystal cells (Lz, PPO). To better characterize the contribution and regulatory mechanisms of intermediate zone, an IZ specific gal4 driver has been constructed, named as CHIZ-gal4 (CHIZ stands for combined hematopoietic intermediate zone). The IZ progenitor cells show a unique cell-cycle profile and are multipotent to differentiate into all the lineages of blood cell types. Utilizing Notch ligand serrate, the IZ cells also direct the fate of neighbouring cells (96).

1.4.1.5 Posterior lobes of lymph gland

The posterior lobes or the secondary and tertiary lobes of the lymph gland are majorly composed of the progenitor cells and these remain less mitotically active during the development throughout (Fig. 4A) (62). These appear during the second instar stage of larvae and mechanisms of their development are relatively less explored. These lobes of lymph gland are derived from a subset of pericardial cells and are bi-potent hematopoietic/nephrocyte progenitors (97). Recent studies have highlighted both developmental and immune function of these progenitor cells (98,99). Posterior lobes of lymph gland have been shown to act as the source for the hubs of progenitor cells during adult hematopoiesis (98). Like the progenitor cells of primary lobes, the posterior lobes progenitor cells undergo differentiation in a JAK/STAT dependent manner and during wasp-infection scenarios activity of JAK/STAT in posterior progenitors goes down directing these cells towards lamellocyte formation and combating infection (99). It has been described that posterior lobes progenitor dynamically express ultrabithorax (Ubx) and collier (col) serving as a niche for the posterior lobe cells to regulate their maintenance and differentiation (100). However, posterior lobes are also shown to have increased differentiation, more numbers of lobes, or increased size under the conditions when primary lobes undergo precocious differentiation and/or lose progenitors (70,72,74,101–103).

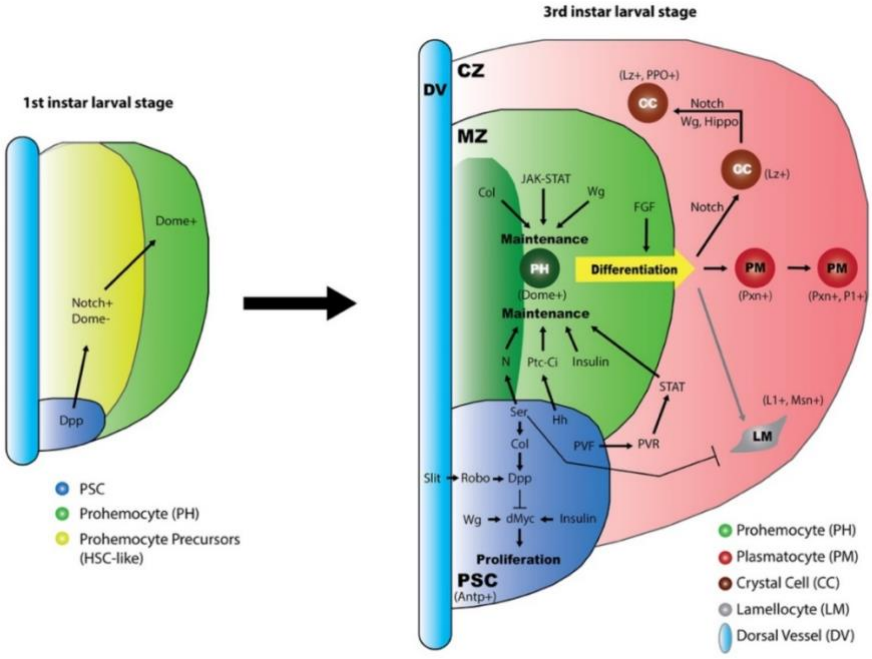

Figure 5. Markers of *Drosophila* lymph gland zones and blood cell types.
Early progenitor markers during 1st instar larval stage and various signaling proteins defining the different cell types during lymph gland development at 3rd instar larval stage, adapted from (63).

1.5 Cell types in Drosophila hematopoietic system

1.5.1 Medullary zone progenitor cells

The MZ progenitor cells are round cells with a diameter of 4.8-7.4 μm (19). These cells give rise to all the mature blood cell types (62,66,95,104,105). The progenitor cell homeostasis is regulated by multitude of factors originating from the progenitor themselves in the medullary zone, from the neighbouring cells of cortical zone and PSC, and systemic signals emanating from other tissue and extracellular environment (Fig. 5). The proliferation of progenitors is under tight regulation during development and this regulation is essential for the medullary zone cells to maintain their multipotency and quiescence. Progenitor cells are maintained by an "equilibrium signal" ie. a signal from the PSC niche cells as well as a signal coming from the surrounding differentiating cells. Loss of either of these signal leads to lose of progenitor multipotency (65,74,106). The progenitor cell pool in primary lobe of lymph gland is divided into four sub-populations: both Tep4 and Dome expressing core progenitors, only Dome expressing distal, Dome and a low level of Eater expressing distal committed progenitors, and Dome, Eater, and Hml expressing intermediary progenitors (107,108). Additional subpopulations of cells expressing multiple trajectories from progenitors to differentiated cells have been characterized recently in the single cell analysis studies done by (109,110). These studies indicate cell type heterogeneity in the lymph gland compartment and have shown the existence of various overlapping cell types and zones in the primary lobe of lymph gland. The differentiation of progenitors into hemocytes is majorly temporally restricted, and is primarily observed from the mid-second instar larval stage to the mid-third instar larval stage (74). The differentiation potential gets significantly reduced after the mid-third instar larval stage and during metamorphosis all the blood progenitors differentiate into mature hemocytes, that form the circulatory blood cell pool in adult flies (74,111).

1.5.2 Differentiated blood cell types

1.5.2.1 The plasmatocytes

Plasmatocytes are the mature hemocytes, with cell diameter ranging from 8-10 μm and constitute 90-95% of total blood cells in *Drosophila* (Fig. 6A) (19,62). Plasmatocytes show plasticity in their cell shape, from large round cells to cells with substantial cytoplasmic processes, known as filopodia (19). The morphological variations are

associated with the diversity of function carried out by plasmatocytes in various tissues and developmental stages (112). Ultrastructural analyses have shown that, plasmatocytes are macrophage like cells with presence of a large number of phagocytic vacuoles, primary and secondary lysosomes, and endoplasmic reticulum (19). Glial-Cells-Missing (Gcm) and Glial-Cells-Missing 2 (Gcm2) specifies the plasmatocytes fate during terminal differentiation of the progenitor cells (13,20,113,114). JAK-STAT signaling and the GATA factor Pannier are other essential factors responsible for the plasmatocytes maturation and development (91). Surface receptors and molecules including early differentiation marker hemolectin (Hml, (62,87), peroxidasin (Pxn, (89) and Eater (115), Croquemort (Crq, an ortholog of 19 vertebrate CD36 scavenger receptor) (116), and Nimrod C1 (P1 antigen, (117) are important phagocytic markers of plasmatocytes (1,118). Plasmatocytes are contributed from both primitive and definitive wave of hematopoiesis (62). Mature plasmatocytes perform a wide array of functions, can proliferate and actively migrate (62,95,119). Plasmatocytes, akin to vertebrate macrophages, recognize and engulf invading microorganisms, dead tissues, cell debris, and apoptotic cells (120). Additionally, plasmatocytes play important role in humoral immune response by promoting antimicrobial peptides (AMPs) production from the fat bodies and by directly secreting AMPs such as Cecropin A1 upon bacterial infection (118,121). Other functions of plasmatocytes include, rapid tissue remodelling during embryogenesis and morphogenesis by clearing cell debris and apoptotic cells (116,119,122,123), secretion of ECM proteins such as collagen protein Viking and Laminin (12,85,124).

1.5.2.2 The crystal cells

Crystal cells are 2-5% of the total hemocytes population in *Drosophila* and these are big spherical cells with crystalline inclusions and a diameter ranging from 10-12.2 μm (Fig. 6B) (19,125). Unlike plasmatocytes, crystal cells are non-proliferative and mitotically inactive. BrdU incorporation studies in crystal cell show that, these cells undergo endoreplication rather than cell proliferation (95). These cells originate from both primitive and definitive wave of hematopoiesis and do not show the migration behaviour. Due to presence of multiple tyrosine-rich crystalline inclusions, these cells are termed as crystal cells (19,20). Crystal cell specification, differentiation, and maturation is regulated by complex regulatory mechanisms, involving various transcription factors and signaling proteins (1). The transcription factors Lozenge, Serpent, and U-shaped act synergistically to specify crystal cells (29,30,126–129) and

Wnt/Wg, Hippo/Yorkie pathways regulate the crystal cells number within the lymph gland (71,130). Crystal cell differentiation and maintenance is mediated by Notch pathway (45,66), and transcription factor Sima (ortholog of the hypoxia inducible factor-1 α, Hif1α, (131). Prophenoloxidase (ProPO) are the enzymes found within the crystalline inclusions in mature crystal cells and are necessary for catalysing melanisation reactions (125,132–134), these are encoded by the genes PPO1, PPO2 and PPO3. Their expression in crystal cell is regulated by Serpent and Lozenge (133,135). Crystal cells can be marked utilizing antibodies or reporters proteins such as, Hindsight (Hnt), Lozenge, ProPO, and PPO1 (1,62,136). Crystal cells are important in wound healing and melanisation reaction during injury responses and thus share functional similarity to mammalian platelets. These cell form a black or dark brown clot-like structure around the wound site following injury, which is due to melanin that is formed by the melanisation reaction (133,137,138). This reaction, initiated by the ProPO enzyme in the crystalline inclusions, converts phenol to quinones that further polymerizes to form melanin and produces reactive oxygen species (ROS) as a by-product that help in neutralizing invading bacteria (139,140). Consistent with their gene expression profile, as described in the recent single-cell analyses, crystal cells also regulate the hypoxia stress response in *Drosophila* (141).

1.5.2.3 The lamellocytes

Lamellocytes are large, flat cells with a diameter ranging from 16-24 μm and a surface area exceeding 400 μm^2 (Fig. 6C) (19,20,142). These cells are rarely present in healthy larvae and are predominantly formed in response to parasite wasp infections or injury to the larval cuticle (143). Ultrastructure analyses have revealed that lamellocytes have irregular cell margins, numerous cytoplasmic processes, and an organelle-free cortical cytoplasm (19). However, lamellocytes possess numerous primary lysosomes and phagocytic vacuoles compared to plasmatocytes, despite the absence of phagocytic activity (19). Lamellocytes are labelled by various markers including Misshapen (Msn, a JNK activator), L1 antigen (encoded by antilla), α-PS (PS4 integrin α chain), and β-PS integrin (encoded by the gene myospheriod) (109,118,136,144). Several hymenopteran wasp species (such as *L.boulardi*, *L.heterotoma*) deposit their eggs into *Drosophila* larvae through oviposition and injection (145). This triggers the rapid differentiation of lamellocytes from the progenitor cells and trans differentiation from plasmatocytes to protect the animal against parasitic infestation. These cells encapsulate

the wasp eggs and eliminates approximately 40% of the wasp larvae (146). Parasitic wasp infection leads to lamellocyte formation in the lymph gland, which are released into the larval haemolymph and thus causes rupturing of the lymph gland (64,102). Multiple signaling pathways and proteins regulate lamellocyte specification and differentiation. Lamellocytes derived from the progenitor cells or lamelloblasts (only Msn) show different marker expression as compared to the lamellocytes transdifferentiated from plasmatocytes (both Msn and plasmatocytes marker such as P1, eater) and are thus labelled as Type I and Type II lamellocytes (146). The specification and formation of functional lamellocytes in the lymph gland is regulated by JNK/Basket (147), Toll (148), NF-κB (57), Notch, JAK/STAT, ROS (149), ecdysone and EGFR signaling (93,102,150,151). Ectopic activation of the Toll or JNK signaling, or hyperactivation of JAK-STAT pathway dramatically induces lamellocyte differentiation without parasitic wasp infections (148,152). β-PS integrin, a mature lamellocyte marker, dispensable for lamellocyte differentiation is essential for the encapsulation process (153). Apart from the signaling in progenitor cell, lymph gland-derived lamellocyte induction is also mediated by the increased ROS levels within the PSC niche. The increased oxidative stress activates Toll and NF-κB pathways leading to a massive production of lamellocytes and rupturing of lymph gland (149). Lamellocyte induction is also regulated by various metabolic inputs, which is described in the proceeding sections.

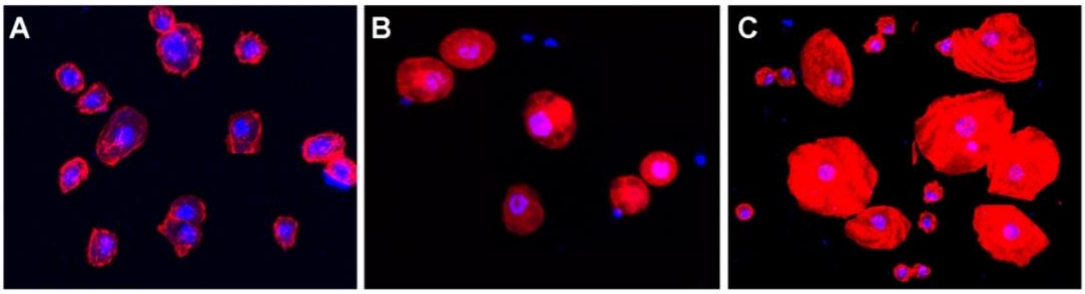

Figure 6. Confocal images of *Drosophila* blood cell types.
(A) Plasmatocytes, (B) crystal cells in homeostatic conditions and (C) lamellocytes after wasp-infection.

1.6 Regulation of lymph gland development

Homeostatic development of a tissue or organ involves various regulatory mechanisms that work synergistically to have a coordinated growth. Lymph gland is an organ with different type of cells ranging from the signaling niche cells, progenitor cells and differentiated cells (1,63,154). Therefore, a plethora of regulatory signaling and

metabolic pathways control lymph gland development. These include autonomous mechanisms, originating from the progenitor itself (autocrine), non-autonomous mechanisms, originating from the neighbouring cells of PSC, CZ and cardiac tube (paracrine) and systemic (nutritional and environmental control) (Fig. 7) (1,155,156).

1.6.1 Autonomous regulation of progenitor development

Key molecular events that control autonomous progenitor proliferation and differentiation include extracellular matrix (ECM) proteins. During lymph gland development, progenitor cells are densely packed during early development and later E-cad loss in the progenitor cells causes differentiation, whereas overexpression of E-cad promotes progenitor maintenance (157–159). Wingless protein also functions in the MZ progenitor cells to repress premature differentiation of progenitors (71). Similarly, Colier is expressed at low levels in the core progenitors of MZ cells and regulate the progenitor differentiation. Its loss leads to premature differentiation and overexpression of *col* leads to progenitor proliferation and MZ expansion (79,160). During immune response conditions, downregulation of *col* in the MZ progenitor is important to induce lamellocyte formation (64). JAK/STAT activity within the MZ assist in maintaining progenitor identity and it prevents differentiation (62,95,161). JAK/STAT pathway receptor domeless (dome) is a predominant marker for the MZ progenitor cells (Fig. 7) (62,162,163). Another factor that maintain MZ progenitor cells is Asrij, *Drosophila* homolog of Ociad1, a hematopoietic stem cell marker (101,164). Asrij loss leads to reduction in the number of progenitor and PSC (niche) cells and increased numbers of differentiated cells, with a corresponding decrease in E-cad within the medullary zone (101). Dopamine is synthesized by lymph gland progenitor cells and regulate progenitor development via controlling different phases of cell cycle mediated by synthesis and signaling modules of the neurotransmitter (165). FGF pathways works autonomously to control MZ proliferation and loss of FGF in the progenitor cells leads to excessive differentiation to all the three cell types (166). MZ progenitor cells show elevated levels of Reactive oxygen species (ROS) and these are important to prime the progenitors towards differentiation cues. Loss of ROS in the progenitor causes dampened differentiation and increased levels of ROS causes increased differentiation of the progenitor cells by mechanisms involving JNK and polycomb group proteins (72).

1.6.2 Non-Autonomous regulation of Progenitor development

Signaling cues emanating from PSC and CZ regulate homeostatic development of medullary zone progenitor cells, by paracrine mechanisms. PSC acts as a signaling centre for the progenitor maintenance, thus sends a variety of signals controlling both progenitor proliferation and differentiation. PSC also send signal to CZ, which further maintain an equilibrium signal in the MZ (1). Pvf1, one of the ligands of Pvr is secreted by PSC and sensed by PDGV/VEGF receptor, PVR in the CZ cells. This leads to secretion of AdgfA (Adenosine deaminase growth factor-A), which control progenitor quiescence and differentiation by regulating adenosine levels (65,74). Another signaling entity Dpp, produced by the PSC is sensed by the pre-progenitor cells of early lymph gland and drives Notch expression in them to facilitate its proliferation and transition into $Dome^{+}$ progenitor cells (Fig. 5 and Fig. 7) (66). Hh signal from PSC binds to the patched (ptc) receptor in the progenitor cells of MZ. Additionally, Hh signal in PSC is trapped by Relish (Rel), which maintains cytoskeletal architecture and thus impedes progenitor maintenance by regulating Hh transfer to MZ cells (65,167). In addition to the niche, the cardiac tube also regulate progenitor maintenance through FGF/Bnl signaling, acting as a niche for progenitor cells (168). Branchless (bnl) signal is secreted from the cardiac tube cells and leads to activation of its receptor breathless (btl) in progenitor cells and maintains calcium levels in the MZ by activating PLCγ. Moreover, blockage of this interaction leads to differentiation of progenitor cells. The involvement of mechanosensitive mechanisms of blood flow by vascular niche cells of cardiac tube is also shown to impact hematopoietic progenitor maintenance (169).

1.6.3 *Systemic control of progenitor development*

Drosophila blood cells respond to a variety of nutritional and sensory cues originating from nutritional status (75,170,171), odors (172) and environmental CO_2 or O_2 (173). These signals are transduced to the lymph gland progenitor cells via a multiorgan, hormone-dependent signaling cascade. Interestingly, disruption of these pathways or sensing mechanisms give rise to distinct hematopoietic defects indicating the involvement of different regulatory mechanisms. Amino acid levels within the hemolymph control progenitor maintenance via insulin and its receptor (InR), PI3K, Akt, and TOR (170,171,174). This is controlled by secretion of dilp2 from the brain which is sensed by InR in the progenitor cells. The amino acid transporter slimfast (slif), present on the progenitor cells also sense the amino acids and therefore collectively

regulate progenitor maintenance through TOR and Wg mediated mechanisms (Fig. 7) (171,175). Other nutritional inputs such as sugars and fatty acids regulate progenitor maintenance and differentiation via JNK and JAK/STAT pathways and triggers immune response (176,177).

Environmental odors and gases such as CO_2/O_2 detected by gustatory receptors trigger a series of signaling cascades involving diverse sensory organ, which relay downstream signal to brain and lymph gland to regulate progenitor development (Fig. 7). During development, low levels of CO_2 through a multi-organ crosstalk impacts Serrate (Ser) expression in the intermediate zone, resulting in crystal cell differentiation (173,178).

Odor sensing triggers γ-aminobutyric acid (GABA) secretion from the neurosecretory cells in brain into the haemolymph. Circulating GABA regulates progenitor maintenance in the lymph gland by GABA receptor mediated calcium signaling (172). In an immune perspective, GABA released from the brain is internalized as a metabolite by blood-progenitors and GABA catabolism mediated succinate conversion induce lamellocyte differentiation. The GABA catabolic pathway in the progenitor cells, converts internalized GABA into succinate and stabilizes sima, which is required for lamellocyte differentiation (94). Developmentally, GABA catabolism derived succinate regulate tricarboxylic acid (TCA) cycle activity to moderate ROS levels in the progenitor cells and supports lymph gland growth (179) (Fig. 7).

Altogether, lymph gland progenitor cells regulate their specification, proliferation and differentiation through a combination of intrinsic and extrinsic mechanisms.

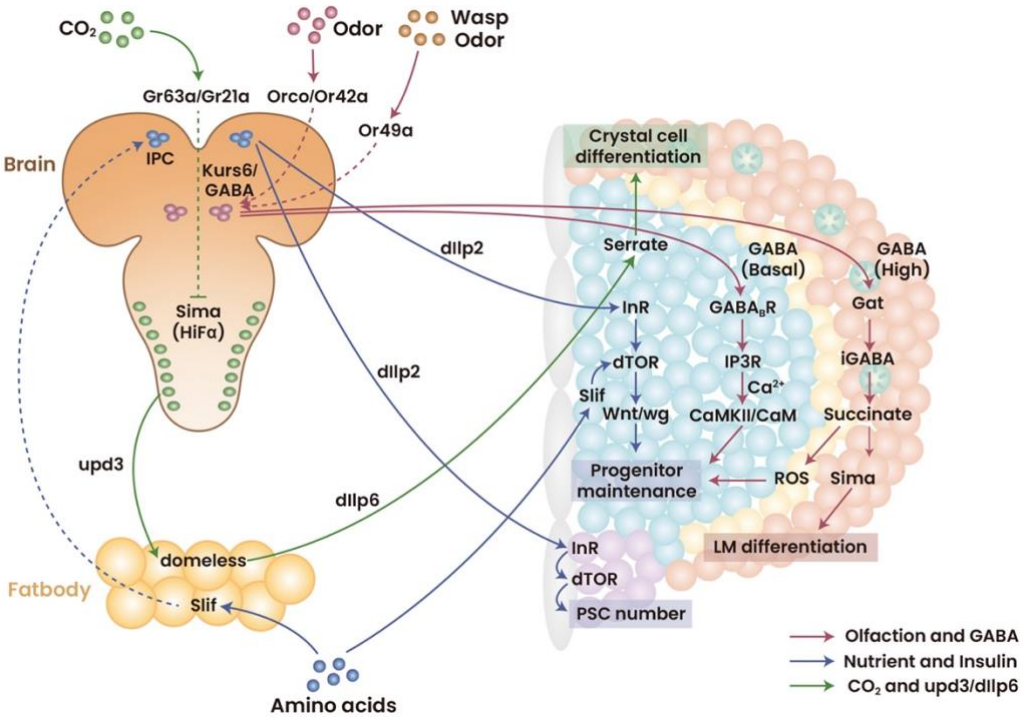

Figure 7. Regulation of lymph gland development**.**
Various intrinsic and extrinsic factors involved in *Drosophila* hematopoietic development (180).

1.7 Reactive oxygen species and blood progenitor development

1.7.1 What are reactive oxygen species (ROS)?

ROS are free radicals generated from molecular oxygen. These majorly include the superoxide ($O2^{-}$), hydrogen peroxide (H_2O_2), and hydroxyl radicals ($OH^{\bullet}$). Oxygen undergo electron transfer reactions and reduction to produce superoxide radical anions ($O2^{-}$). Playing the role of an oxidant as well reductant, superoxide anions give rise to other forms of free radicals. Reactive oxygen species are mostly produced in mitochondria, where electron leakage during oxidative phosphorylation and reduction of molecular oxygen cause ROS formation. ROS are a stress signal in the cell and damage cellular proteins, lipids and DNA. ROS mediated oxidative stress induce various pathological conditions ranging from neurodegenerative disorders cardiovascular diseases, respiratory diseases and cancers. Unfolded protein response, DNA breaks, necrosis are the major damages caused at cellular level. Nonetheless, ROS are also essential for some of the cellular functions, ROS acts as signaling molecule and impact cellular proliferation, differentiation and other functions.

1.7.2 Sources of ROS

The major site of ROS generation is mitochondria, and it occurs at various metabolic points in the cell (Fig. 8).

1.7.2.1 ETC as source of ROS

One of the prime sources of ROS production in cellular spaces is electron escape during the respiratory chain. The leakage of electron leads to ROS generation in the cell (181–187). Inner mitochondrial membrane is the site for multiprotein complexes (complexes I–IV) that form the electron transport chain. These complexes houses a range of redox catalysts such as pyridine flavoproteins, nucleotides, ubiquinone, iron sulphur proteins, and cytochromes cause electron leakage and ROS generation. ETC utilizes FADH/NADH transferred from glycolysis and the tricarboxylic acid (TCA) cycle and generate ATP as energy source by the process of oxidative phosphorylation, OXPHOS (188,189). The multiprotein complexes of ETC are the major sites for superoxide radical generation. Mechanistically, transfer of electrons from complex I (NADH dehydrogenase) or complex II (Succinate dehydrogenase, SDH) cause conversion of coenzyme Q to coenzyme Q (QH2). The regeneration of coenzyme Q from QH2 occurs forms an unstable intermediate semiquinone anion (•Q) in this process, known as Q-cycle. This oxidation-reduction reaction transfer electrons to oxygen and leads to superoxide radical production. Mutations in complex II subunits C and D elevates Superoxide ($O2^{-}$) and H_2O_2 formation leading to cancer and genome instability (190–193).

TCA cycle fluxes into ETC, thus act as an indirect source of ROS. The TCA metabolites not only fuel energy into the cell, but also act as source of ROS generation. For example, pyruvate dehydrogenase (PDH) and α-ketoglutarate dehydrogenase (αKDH) enzymes of TCA cycle produce significant amounts of O_2^{-} radicals and H_2O_2. Inter-mitochondrial oxidoreductase protein, p66Shc, and outer mitochondrial membrane enzyme, monoamine oxidase are other sources of mitochondrial ROS generation (194) (Fig. 8).

1.7.2.2 Nicotinamide adenine dinucleotide phosphate (NADPH) oxidases (NOXs)

NOXs are the other leading cause of intracellular ROS generation. These are homologs of the phagocyte NOX (e.g., Phox or NOX2) and were first identified in neutrophils (195,196). NOXs I-V, DUOX1, and DUOX2 comprise the NOX family of enzymes. These diversified class of redox signaling proteins, transfer electrons from NAD(P)H

to molecular oxygen and form superoxide radicals and hydrogen peroxide performing significant physiological and pathophysiological functions (197).

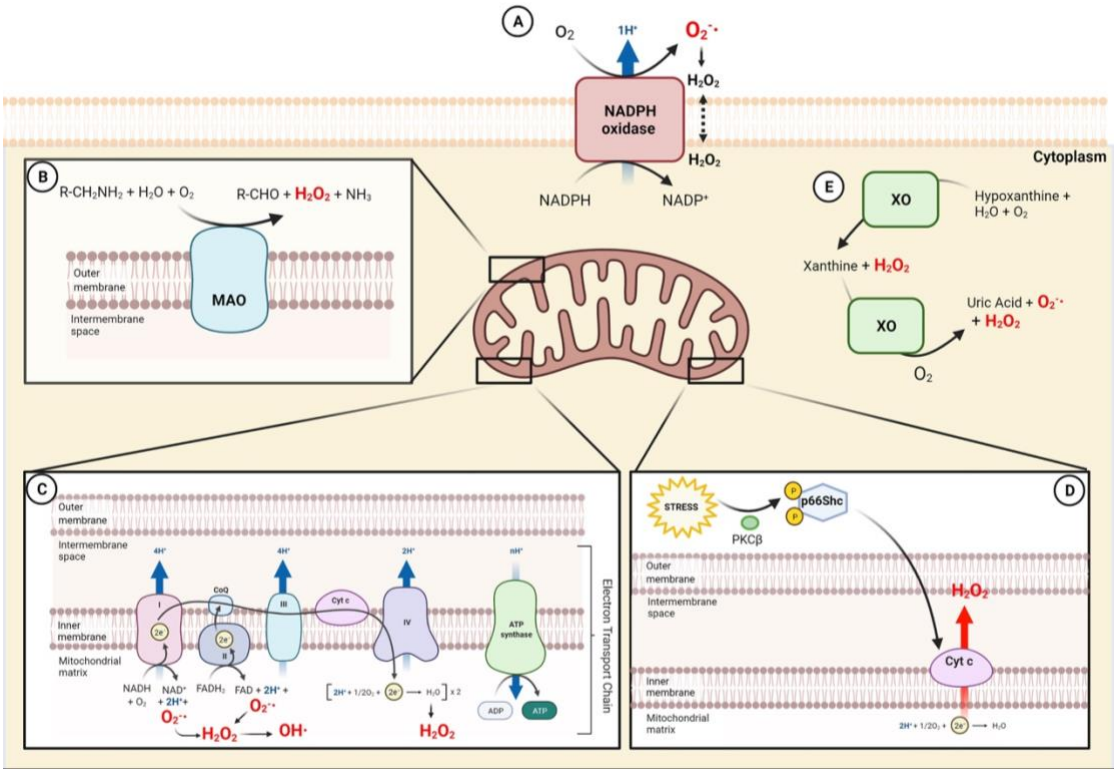

Figure 8. Sources of ROS.
(A) Superoxide radicals are generated in the cellular membrane by NADPH oxidases, **(B)** monoamine oxidases catalyse the production of hydrogen peroxide in outer mitochondrial membrane, **(C)** O_2 radicals, H_2O_2 and OH. generation in inner mitochondrial membrane from ETC, **(D)** p66Shc activation by CytC leads to H_2O_2 production in inner mitochondrial membrane, **(E)** H_2O_2 and O_2 radical production by xanthine metabolism in the cytoplasm (198).

Peroxisomes and endoplasmic reticulum are other important sites of ROS generation in cell. In peroxisomal respiratory pathway, transfer of electrons from diverse metabolites to the oxygen causes H2O2 formation (199) and this process is independent of energy generation, but form heat. Fatty acids β-oxidation in peroxisomal generate H_2O_2. In endoplasmic reticulum, enzymes such as cytochrome p-450, diamine oxidase and b5 enzymes lead to the generation of ROS (200).

1.7.3 ROS Scavenging: antioxidants and antioxidant enzymes

An effective mechanism for scavenging reactive oxygen species (ROS) is in place to regulate the formation of ROS. It is made up of molecules that counteract ROS directly through various neutralization reactions. The ROS generation and antioxidant scavenging equilibrium in cellular redox homeostasis control both physiological and pathological cellular processes. An intricate group of natural and nutritional

compounds, and molecules comprise the antioxidant system. Glutathione (GSH) is a major antioxidant, involved in the reduction of oxidized proteins and peroxides through diverse mechanisms such as Grx and Trx. The natural antioxidant enzymes system include superoxide dismutases (SOD), catalases, glutathione S-transferases, glutathione reductases and peroxidases, and small nutritional molecules, ascorbic acid and α-tocopherols (Fig. 9) (187,201–203).

1.7.3.1 Superoxide dismutase (SOD) and Catalase

Superoxide dismutase and catalases are the major anti-oxidant enzymes present intracellularly in all the organisms utilizing O_2. SOD enzymes catalyse the dismutation of superoxide ($O2^-$) and hydrogen peroxide (H_2O_2) (204). Dismutation reactions catalysed by SOD are extremely efficient (205). SOD enzymes regulate the levels of a variety of ROS and reactive nitrogen species (RNS) by neutralizing their radical, thus limit their potential toxicity and maintain their homeostatic levels for diverse signaling functions (206). Catalase is another important antioxidant enzyme and present in all aerobic organisms. Catalase breakdown hydrogen peroxide molecules into oxygen and water in a two-step process (207). Maintenance of optimum level of H_2O_2 in the cell is essential for a multiple cellular signaling processes (208).

1.7.3.2 Glutathione (GSH)

Glutathione (GSH) is the most abundant thiol compound and a non-protein tripeptide existing in the cells. GSH (γ-glutamyl-cysteinyl-glycine), a major and potent intracellular redox buffer, is produced *de novo* in two sequential enzymatic reactions, which are ATP-dependent. First, cysteine and glutamate combine to form γ-glutamylcysteine. Catalysed by the γ-glutamylcysteine synthase (γ-GCS), this step is the rate-limiting step in GSH synthesis and is regulated by availability of cysteine in the cell. Glutathione synthase (GS) catalyses the second step, where γ-glutamyl-cysteine is linked to glycine via covalent bonding to complete GSH production (209). The redox-active thiol (-SH) group of cysteine residue determines the antioxidant function of GSH, as it gets oxidized when GSH reduces target molecules such as H_2O_2 and organic hydroperoxides (210). The oxidized form, GSSG regenerates reduced form of GSH utilizing electrons from NADPH by involvement of glutathione reductase enzyme (Fig. 9). Another ROS scavenging function of GSH include detoxification of electrophiles produced during oxidative stress, these conjugation reactions are catalysed by glutathione transferase enzymes (211,212).

GSH distributes in different compartments, including both mitochondria and cytosol, While it is synthesized exclusively in the cytoplasm. As mitochondria play a central role in the activation and cell death, mitochondrial GSH has been shown to critically regulate these processes and maintain cellular homeostasis (213).

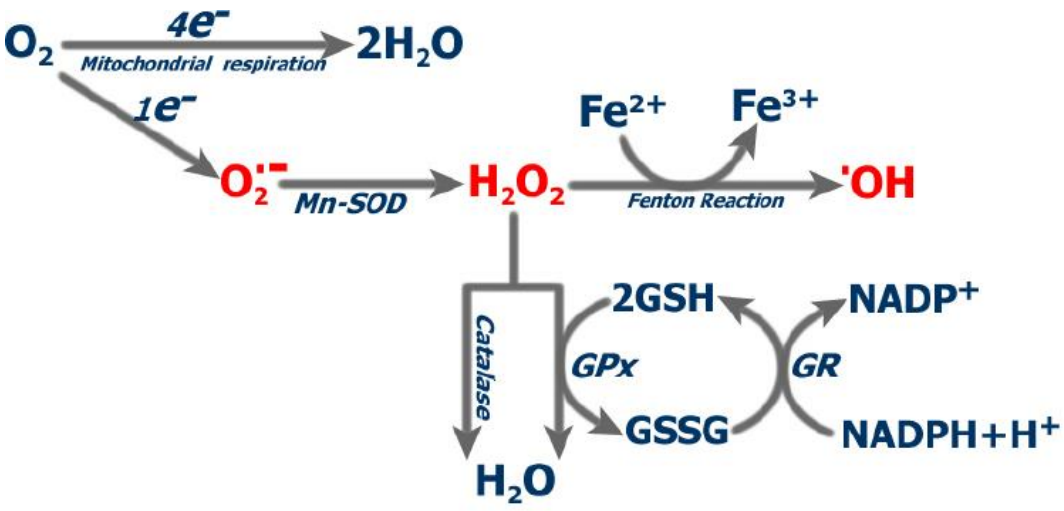

Figure 9. ROS scavenging mechanisms.
Various ROS scavenging enzymes and compounds contributing to ROS homeostasis of the cell (214).

1.7.4 ROS in cellular signaling

Reactive oxygen species play important role in cellular signaling apart from acting as the stress signal (215). This area of ROS regulation is known as Redox Biology and has implications on cellular homeostasis (216). A threshold levels of ROS are required to perform such functions and ROS requirement varies across different cellular stages ranging from stem cells, progenitors and differentiated cells (Fig. 10) (217,218). It is predominantly clear that manipulation of metabolic pathways and ROS affect stem cell fate, including their proliferation, quiescence and differentiation (219–221). ROS is tightly coupled to metabolic pathways, as any change in metabolic pathways leads to alteration in ROS levels. Since, ROS molecules can directly affect various proteins, including transcription resulting in affected cellular dynamics and function (222–224).

Reversely, ROS can also impact metabolic enzymes and various signaling proteins responsible for nutrient-sensing to impact the metabolic flux (225–227). These functions and properties of ROS molecules highlight them as emerging key mediator of stem cell fate decisions.

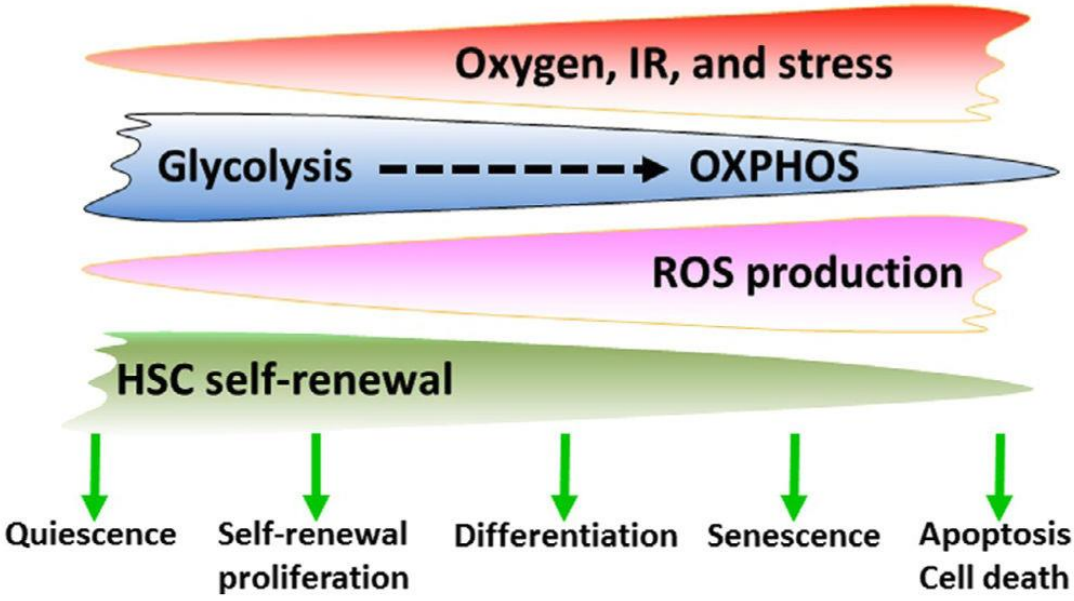

Figure 10. Role of ROS in cellular signaling.
Low levels of ROS is important for hematopoietic stem cells quiescence and self-renewal, while elevation of ROS levels lead to HSC senescence and cell death (197).

1.7.5 ROS in HSC and blood progenitor development

ROS has been implicated in myriad of cell fate decisions. Common myeloid progenitors (CMPs) possess higher levels of ROS and it is associated with the blood-progenitor proliferation and differentiation. ROS regulates cell cycle progression resulting in increased progenitor proliferation (228). Consistently, elevated ROS leads to myeloproliferation in Foxo3 mutant mouse and is the cause for myeloproliferative neoplasm progression (229,230).

Unlike myeloid progenitors, HSCs present in bone marrow niche have reduced levels of ROS and any elevation in ROS in the bone-marrow compartment leads to retardation in hematopoietic stem cell activity (Fig. 10) (228). Similarly, genetic ablation of DNA-damage checkpoint kinase ataxia telangiectasia mutated kinase (Atm) in mice, knockdown of Foxo3 (Forkhead box O), have high levels of ROS in HSCs, which retarded their repopulation capacity (Fig. 11) (231–234). Further, antioxidant supplementation, N-acetylcysteine (NAC) rescued the HSC proliferation phenotype caused by ATM knockdown, depicting the regulation of ROS on stem cell proliferation. Moreover, it was found that reduced expression of ROS scavenging enzymes catalase and SOD2 resulted in elevated ROS levels in Foxo3-/- HSCs (231–235). Surprisingly, mice with a SOD2 mutation do not show any HSC defects highlighting potential functional redundancy between enzymes of the antioxidant system (236).

Regulation of ROS on cellular fate decision occurs through different regulator mechanisms. While the ATM-/- retarded HSC activity is via ROS-mediated activation of p16Ink4a, a retinoblastoma gene product pathway (231), ROS-induced p53 tumour suppressor activation (234) or of p38-MAPK activation (232) causes HSC defects in Foxo3 mutant conditions (Fig. 11).

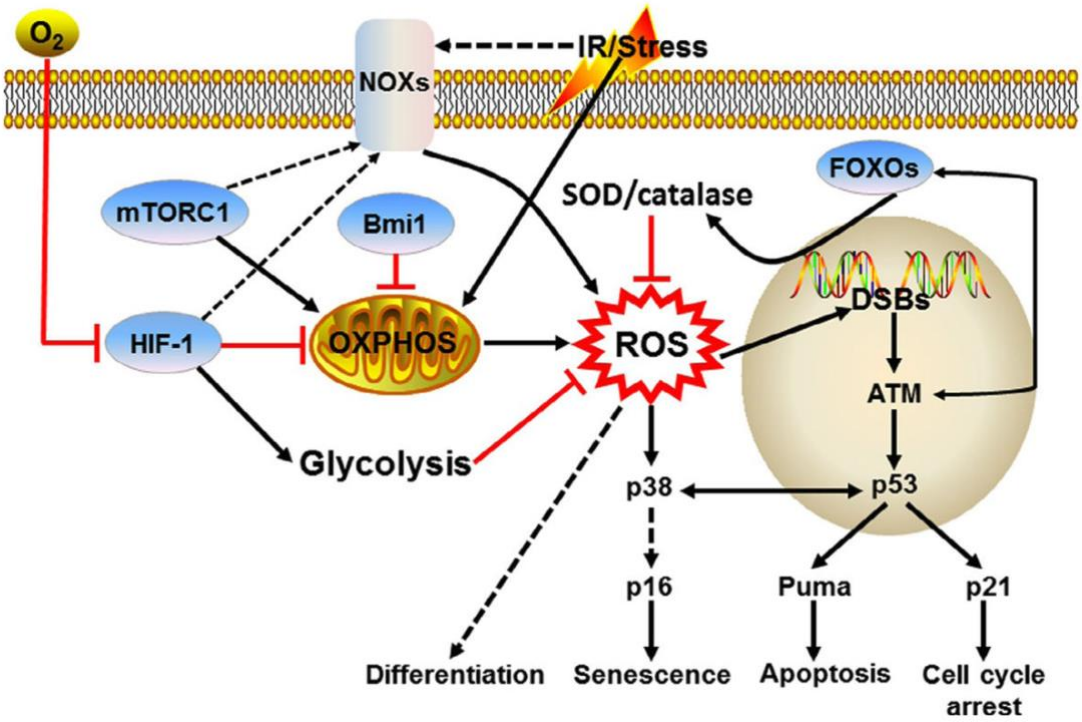

Figure 11. ROS in hematopoietic stem cells and blood-progenitor development.
ROS regulates HSC development through different signaling and metabolic mechanisms (197).

In *Drosophila*, multipotent blood progenitors akin to mammalian common myeloid progenitors (CMPs) maintain elevated levels of ROS under physiological scenarios, this is important to prime progenitor differentiation (Fig. 12) (72). The progenitor cells of lymph gland have higher levels of ROS, which decline as these differentiate. Any further increase in ROS levels impairs progenitor homeostasis and leads to precocious differentiation. Overexpression of antioxidant enzymes such as superoxide dismutase (SOD2) lowers the ROS levels in lymph gland progenitor cells and retards mature blood cell formation. Mechanistically, ROS mediated blood-progenitor proliferation and differentiation is controlled by JNK and FoxO activation along with downregulation of Polycomb group proteins, confirming that ROS play a signaling role in controlling hematopoietic progenitor fate (72).

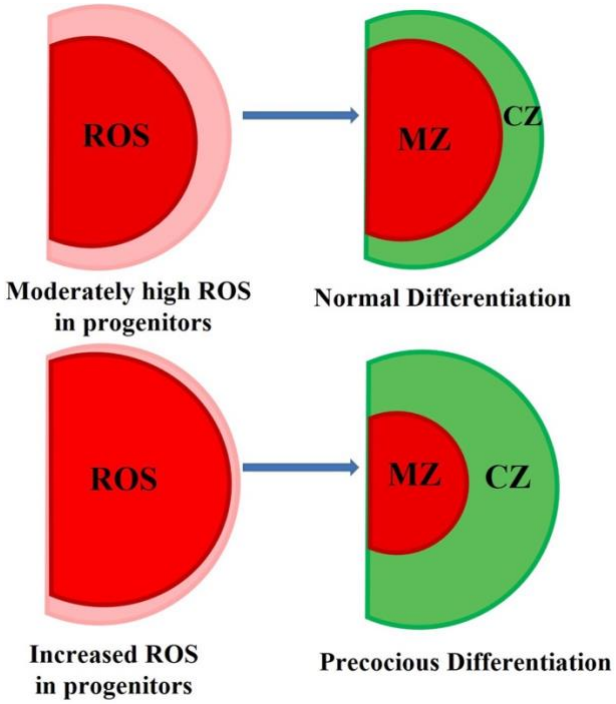

Figure 12. ROS primes blood-progenitors for differentiation.
Moderate levels of ROS are required for progenitor differentiation, however any increase in ROS levels in the progenitor compartment leads to precocious differentiation (72).

1.8 GABA: canonical and non-canonical functions

1.8.1 GABA: a neurotransmitter

γ-aminobutyric acid, commonly known as GABA was first discovered in 1950 as a predominant amine in brain and it was found that GABA is synthesized from another amino acid, glutamic acid (237). It is a four-carbon non-protein amino acid and exists in the free amino acid form in most prokaryotic and eukaryotic organisms (Fig. 13). Later reports delineated the function of this monoamine in regulating neuronal physiology, acting as inhibitory neurotransmitter (238). However, GABA is also shown to act as an excitatory neurotransmitter during embryonic development. GABA is one of the first active neurotransmitter within the developing brain that regulate neuronal progenitor cells proliferation (239,240). Physiologically, in adult brain, GABA modulates the inhibitory neurotransmission in the neurons. Any perturbations of GABAergic (GABA producing neurons) inhibition results in seizures and GABA is a prime target in treatment of many disorders such as epilepsy (241). Many other diseases such as psychiatric (242), stiff-person syndrome (243) and schizophrenia (244) have been associated with dysfunctional GABAergic neurons in the brain.

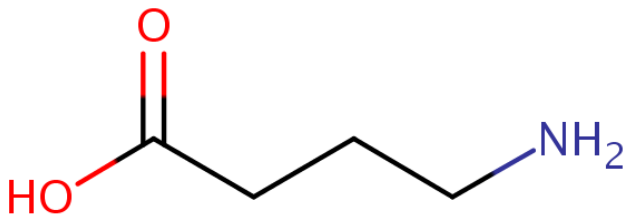

Figure 13. GABA: a neurotransmitter

1.8.2 GABA neurotransmission

GABA is majorly known as a signaling molecule and it regulates ionic channel flow in the neurons. In GABAergic neurons, GABA is synthesized from glutamate, a reaction catalysed by glutamate decarboxylase (GAD) enzymes (245). Synthesized GABA is transported to the neuronal terminals via vesicular neurotransmitter transporter, such as VGAT (246) and released into the synaptic cleft, where it is sensed by the GABA receptors assembled on the post-synaptic neurons. Two types of receptors ionotropic receptors $GABA_A$, (247) and $GABA_c$ (248) and metabotropic receptors $GABA_B$ (249) have been characterized, that sense GABA and regulate downstream signaling. $GABA_A$, and $GABA_c$ receptors are ligand gate ion channels and regulated by the influx of Cl^- to the postsynaptic neurons. $GABA_B$ receptor are G protein coupled receptor and has two Subunits, B1 and B2, these function during later stages of development and as slow constituent of inhibitory transmission. $GABA_B$ receptors are present both presynaptically and postsynaptically. $GABA_B$ receptor activation is coupled with K^+ and/or $Ca2^+$ channels by a G-protein mediated pathway (250–252). The neurotransmitter signaling is terminated by GABA reuptake into surrounding glial cells or nerve terminals. GABA uptake is carried out by SLC class of GABA transporters (GATs) present on plasma membrane of the cell (253). Internalized, GABA is converted into succinic semialdehyde, a reaction catalysed by GABA transaminase (GABA-T). Further, succinic semialdehyde is either catabolized into succinate by succinic semialdehyde dehydrogenase (254) or gamma-hydroxybutyric acid (GHB), catalysed by succinic semialdehyde reductase (255) (Fig. 14).

GABA has a variety of cellular functions and is crucial for numerous organ systems. Deficits in GABA signaling have important ramifications for various physiological systems and ailments in animals reviewed in (256) and GABA receptor expression is seen in diverse organ systems, including, pancreas, muscle, fat, liver and hematopoietic progenitors (257–259).

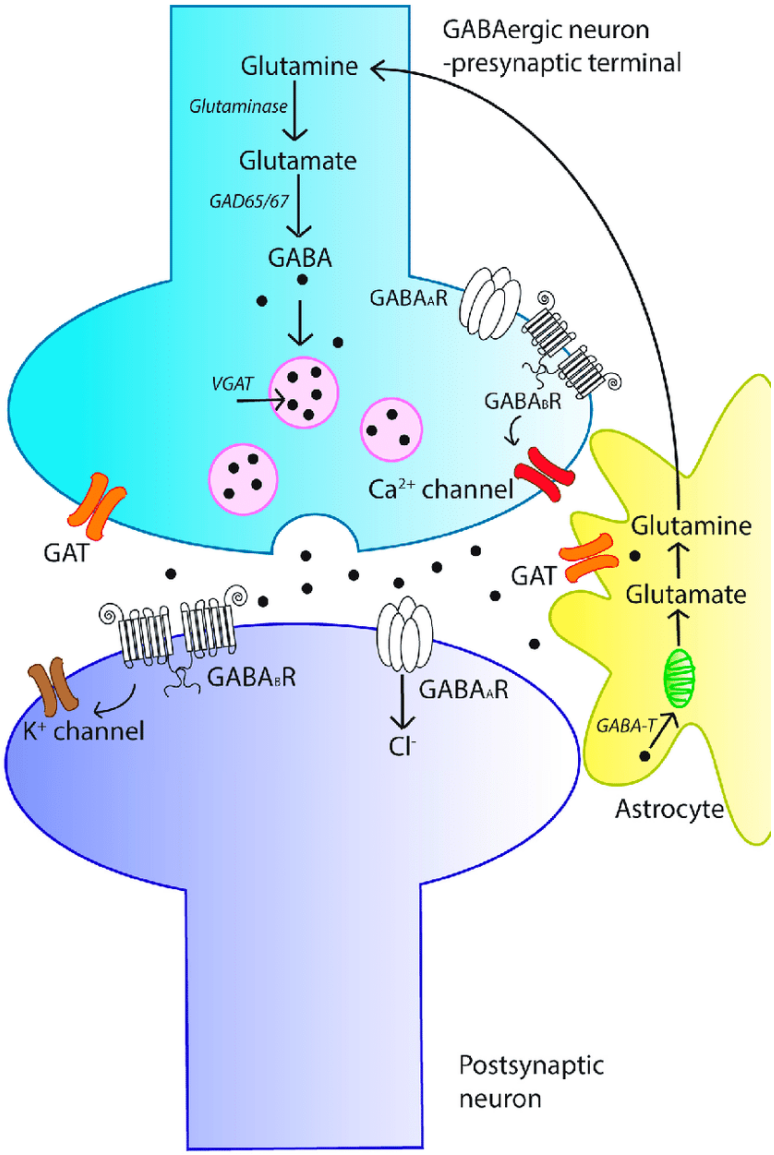

Figure 14. GABA synthesis and signaling.
GABA is synthesized from glutamine and glutamate in a two step-process via enzymes glutaminase and GAD respectively and it is released from the pre-synaptic neurons, where it is sensed by the GABA receptors present on the post-synaptic neurons or internalized by GABA transporter present on the neighboring cells, where it is catabolized into downstream metabolites (260).

1.8.3 GABA signaling in HSC development

In addition, GABA signaling influences hematopoietic stem cell (HSC) outcomes during division and could be implicated in nervous system and blood system communication (261). HSCs and megakaryocyte progenitors express GABA receptor, GABRR1, GABA A type rho-subunit receptor. Overexpression of GABRR1 or agonist therapy led to an increase in the formation of megakaryocytic lineage and inhibition of GABRR1 signaling by genetic deletion or antagonists dramatically inhibited megakaryocyte and platelet differentiation (261). The GABA B type receptor, GABBR1, is also a crucial functional regulator of both human and mouse hematopoietic

progenitors and maintain their homeostasis. Hematopoietic stem cells (HSCs) in the bone marrow niche express GABBR1. Mass-spectrometry imaging analysis showed presence of GABA in bone-marrow niche and interestingly, it was found that B-lymphocytes are the source of GABA, as they express GABA synthesizing enzyme GAD. GABA is sensed by the blood progenitor cells and regulate their proliferation and B-cell differentiation (Fig. 15) (262). Activated-B cells secretes GABA, which inhibits the formation of cytotoxic T cells and macrophages (263). GABA produced by B cells stimulates monocyte differentiation into interleukin-10 (IL-10) secreting anti-inflammatory macrophages which inhibit the cytotoxic CD8+ T cells function by $GABA_A$ receptor mediated signaling. B-cells derived GABA release induce anti-inflammatory responses and facilitates pro-tumour microenvironment by targeting multiple immune cell types (263).

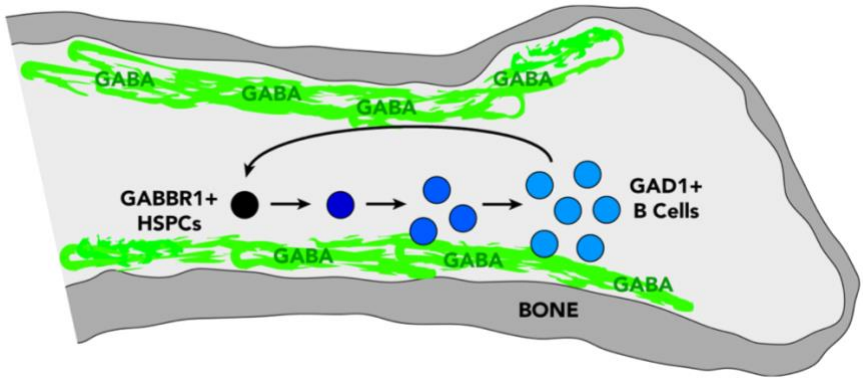

Figure 15. GABA in HSC development
GABA synthesized from B cells regulate HSCs proliferation and differentiation potential (262).

Nervous system derived hematopoietic regulation has been an active area of research and is reported in multiple metazoan organisms (264–266). The impact of neuronal cues on hematopoietic development is not limited to mammalian system and is characterised in other model systems such as *Drosophila*. Interestingly, in *Drosophila*, olfactory stimulation induce GABA secretion from a small subset of neurosecretory cells in the brain. GABA release into the haemolymph and sensing by the blood-progenitor cells promote their maintenance (172). *Drosophila* blood-progenitor cells express metabotropic $GABA_B$ receptor, which sense extracellular GABA from haemolymph. GABA sensing induce elevated Ca2+ levels in the cytosol and thus promote progenitor maintenance. Any perturbation of GABA signaling and $Ca2^+$/CamKII axis leads to loss of progenitor maintenance and heightened differentiation. Thus, blood-progenitors use GABA as a ligand to activate $GABA_BR$ signaling and regulation of intra-cellular calcium homeostasis to maintain their undifferentiated state (Fig. 16) (172).

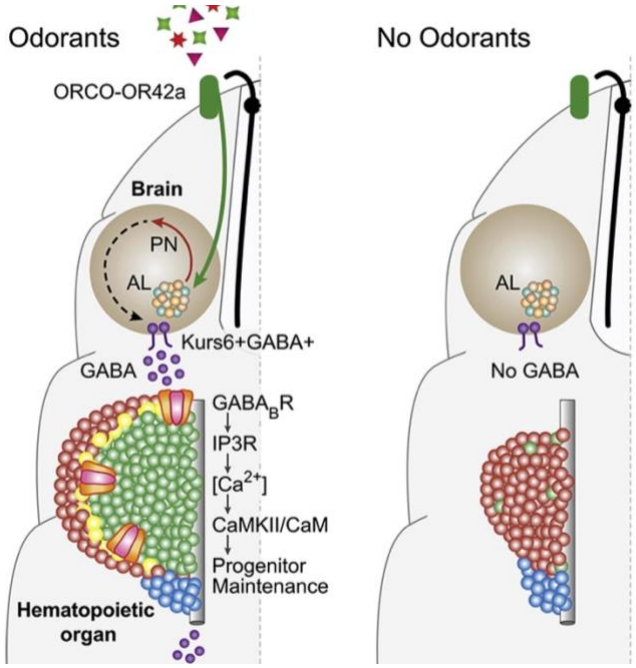

Figure 16. Olfaction derived GABA release and signaling in blood-progenitor control their maintenance (172).

1.8.4 GABA metabolism in Blood-progenitor development

GABA is also shown to have a notable impact on metabolism at the cellular level of multiple organ systems (Fig. 17). GABA is placed at the nexus of various metabolic pathways regulating development and disease. GABA is synthesized from glutamate, which is formed either from glutamine or as a result of TCA cycle anaplerosis from α-Ketoglutarate. Glutamate dehydrogenase (GDH) catalyses the reversible conversion of glutamate to αKG and uses ammonia and NAD^+ or $NADP^+$ as coenzymes (267). GABA can be transported from the cellular microenvironment through GABA transporters (GAT) and is catabolized into succinate and GHB (γ-hydroxybutyrate) through "GABA shunt" pathway. The end product of GABA catabolism ie. succinate which is also a component of TCA cycle and complex II of ETC regulate myriad of cellular functions ranging from epigenetics, signal transduction, tumorigenesis, hypoxia response, endo- and paracrine modulation, ROS homeostasis and inflammation reviewed in (268,269). GABA metabolism is closely connected to cellular metabolism and is regulator for a variety of cellular functions including fate decisions.

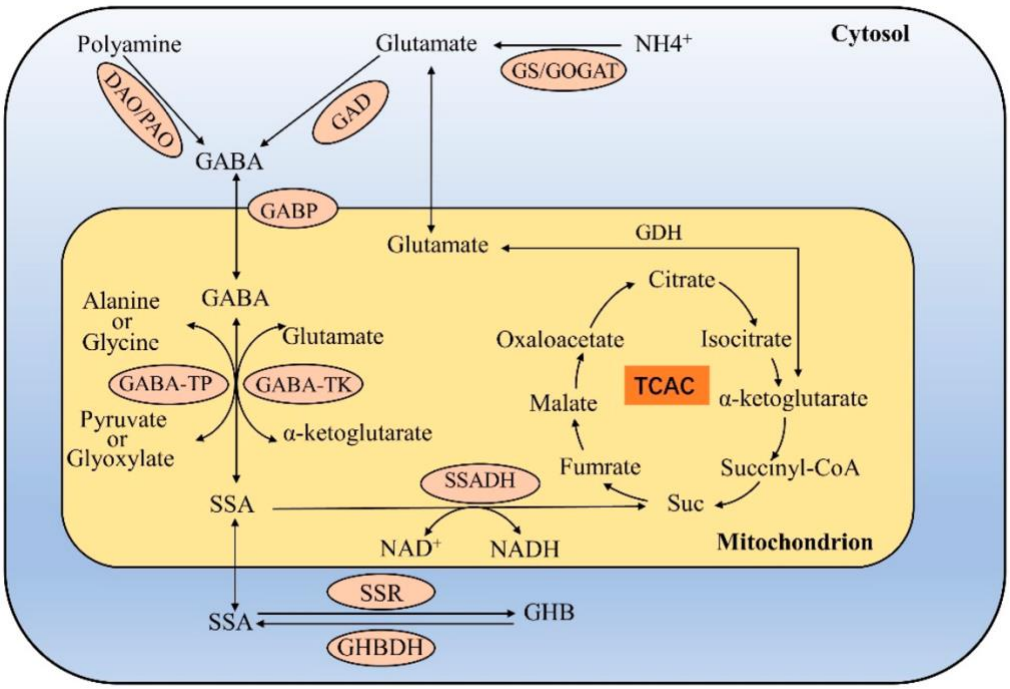

Figure 17. GABA metabolism in the cell.
GABA is synthesized from glutamate in the cells and it is metabolized into succinate via GABA shunt pathway (270).

In Drosophila blood-progenitor cells, GABA catabolic pathway regulate blood-cell development. GABA is released by neurosecretory cells in the brain and is taken up by progenitor cells via the GABA transporter (GAT). A two-step mechanism then catabolizes the GABA into succinate. GABA shunt pathway derived succinate regulate sima (Hif1α) stabilization through inhibition of hyrodxyl prolyl hydroxylases (hph, PHD domain enzyme complexes). Sima stabilization causes transcriptional upregulation of *Ldh*, a crucial enzyme controlling the reversible conversion of pyruvate to lactate, which triggers the glycolytic shift. This GABA catabolism derived sima stabilization is essential for lamellocyte formation in the lymph gland. Utilization of GABA as a metabolite by progenitor cells and its catabolism to succinate is necessary to mount a successful immune response (Fig. 18) (94).

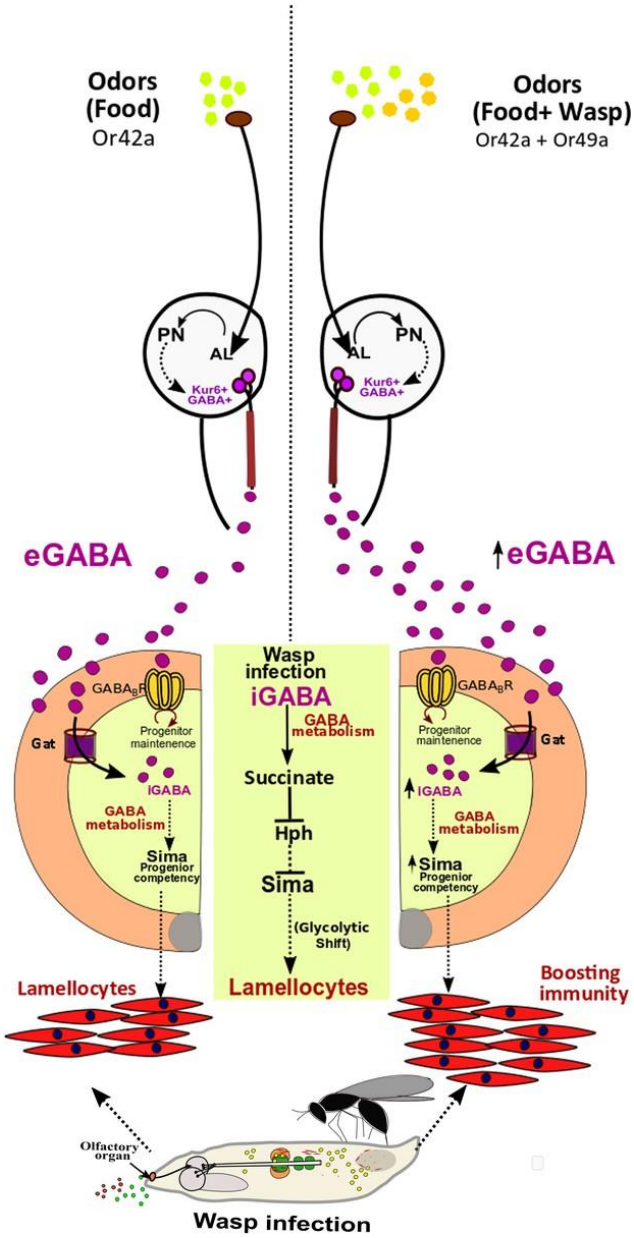

Figure 18. Olfaction derived GABA release and catabolism regulates *Drosophila* immune competency (94).

Moreover, the GABA release from the brain is under olfactory control and odor-sensing by the developing animal establishes a long-range olfactory-immune axis to regulate progenitor development and maintenance, immunological priming and blood progenitor competency towards differentiation (94,172).

1.9 Neuronal Control of organismal homeostasis

Neuronal modulation of hematopoiesis is mediated by both distant signals via neurotransmitters and neurohormones to the HSPCs (271,272), as well as direct peripheral nerve innervations to niche areas (273). Numerous elements of hematopoiesis, such as HSPC proliferation, migration and homing, circadian rhythm

modulation, and others, are regulated by this neural control (274–276). These findings demonstrate the significance of a neuronal-immune link during development. Furthermore, studies aimed at comprehending the regulation of neurons during immunological challenge and stress situations will be valuable to gain a grasp of the physiological relevance and potential of this well-established neuro-immune crosstalk. Olfaction, the sensory cue of smell, stimulates neuronal behaviour and various aspects of organismal homeostasis including, metabolic sensing, obesity, diabetes, and development of hematopoietic compartment.

1.9.1 Role of olfaction in development and disease

It has been demonstrated that in fasting mice, the mere appearance of food (rather than its consumption) has an identical effect on neuronal activity in the arcuate nucleus (ARC) as does the presence of nutrients or hormones associated with food intake in the bloodstream (277). Olfactory system play a novel bidirectional function in energy homeostasis in response to hormonal and sensory signals. Conditional deletion of the IGF1 receptor in OSNs improves mice's ability to smell by increased OSN neurogenesis and results in increased adiposity and insulin resistance (278).

In *Drosophila* hematopoietic development regulation, GABA accumulation in haemolymph is originated from a subset of Kurs6^{+} neurosecretory cells in the brain (Fig. 16). These Kurs6+ neurosecretory cells are under olfactory control and input from olfactory receptor neurons via ORN-PN signaling results in GABA synthesis in these cells. Food odors sensing by Or42a receptors (279) relays information to additional circuitry involving the PNs and deeper brain regions, controlling GABA release from Kurs6^{+} neurosecretory cells in the brain to influence hematopoiesis. Genetic ablation of the olfactory component or growing the *Drosophila* larvae in odor-free environment results in loss of GABA secretion from the Kurs6+ neurosecretory cells and subsequently, haemolymph GABA. This leads to loss of $GABA_B$ metabotropic receptors activation in the progenitor compartment and impedes their maintenance (172). Not only does odor sensing affect this component of organismal homeostasis, but it also controls immunological priming. Another type of olfactory receptor called Or49a is involved in the detection of predatory wasp volatiles. It also controls the release of GABA from Kurs6+ neurosecretory cells by modulating an as-yet-unidentified circuitry of projection neurons and higher brain centres. Increased haemolymph GABA levels in a predatory setting allow blood progenitor cells to internalize GABA, which triggers a

metabolic switch and causes the development of lamellocytes. The loss of olfactory perception results in a decrease in GABA release into the haemolymph, which impedes the progenitor cells GABA catabolic pathway, preventing the production of lamellocytes and thwarting the immunological response (Fig. 18) (94).

1.9.2 Drosophila olfactory system

Olfactory system of *Drosophila* is primarily located in the head region. The four unique anatomical features that make up the *Drosophila* larval olfactory system are the antennal lobes, the paired dorsal organs (DO) at the anterior tip of the larvae, the mushroom body (MB) calyx, and the lateral horn, inside the brain (Fig. 19) (280). *Drosophila* larval olfactory system comprises 21 ORNs (Olfactory Receptor Neurons) per hemisphere in the larva, and they all express different receptor types and innervate different glomeruli in the larval antennal lobe (LAL) (279,281). The dendritic terminals of olfactory receptor neurons (ORNs) in the DO area are home to olfactory receptors (ORs), which are expressed on their membrane and have an affinity for binding volatile chemicals known as odorants (282–286). In total 25 olfactory receptors (ORs) exist in the larval olfactory system, where OR83b, commonly known as Orco, dimerizes with other olfactory receptors and function as co-receptor to these receptors (287,288). LAL harbours 21 subunits, equivalent to adult glomeruli for ORNs innervation (289) and innervates several olfactory projection neurons (PNs) and local neurons (LNs), transmitting the olfactory information to the higher brain centres, mushroom body, MB and the lateral horn (LH) (290).

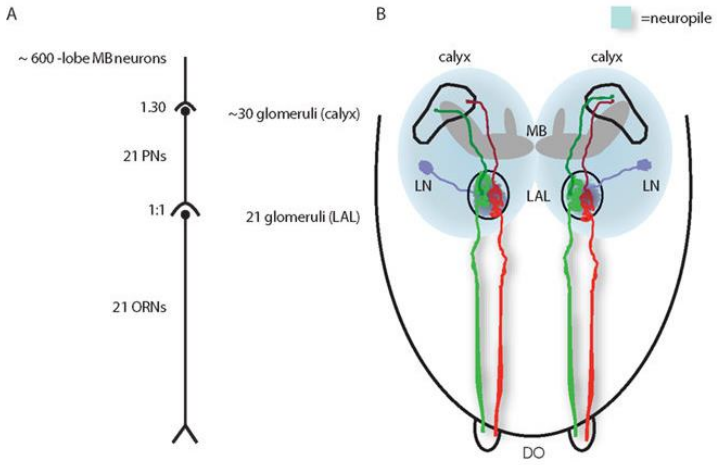

Figure 19. *Drosophila* larval olfactory system.
(A) 21 ORNs connected to twenty-one glomeruli in larval antennal lobe, and via PNs target mushroom body glomeruli in the calyx and MB neurons, **(B)** Schematic representation of the anatomical structure showing individual ORNs (green/red), which form synapse with a single PN each (dark green/red). PNs further project to the MB calyx and LNs interconnect with glomeruli of LAL (291).

2 Aims and Objectives

The importance of ROS levels in myeloid cell development and function is well-established. Central theme of the work undertaken in this study is based on the understanding that ROS as a signaling entity is critical for blood stem-progenitor development and maintenance reported both in invertebrates and vertebrates (292–297). However, to sustain its developmental role, mechanisms controlling ROS levels that are critical towards its functioning in myeloid progenitor cells remain to be characterized. Myeloid-like blood progenitor cells of the *Drosophila* larvae reside in a specialized hematopoietic organ called the lymph gland and these cells maintain elevated levels of ROS. Various signaling cues have been shown to regulate lymph gland development, and recent studies shed light on the involvement of metabolic pathways in myeloid development. Progenitor cells rely on GABA, which is neuronally derived upon olfactory stimulation and is sensed by blood cells both as a signaling entity and as a metabolite. GABA signaling via $GABA_BR$ in lymph gland progenitor cells controls their maintenance (172), while its utilization as a metabolite regulates progenitor differentiation potential (94). Any understanding of intracellular metabolic or signaling events that enable the sustenance of this fine redox balance and blood-progenitor development remains obscure.

The current thesis work aims to understand the odor mediated control of blood progenitor homeostasis and development via redox regulation.

2.1 Understand the metabolic control of olfaction derived GABA catabolic pathway in blood-progenitor homeostasis and development.

a. Investigate the function of GABA catabolic pathway in lymph gland growth control.
b. Understand the mechanistic basis of lymph gland growth control by GABA catabolism and its involvement in blood-progenitor differentiation.
c. Mapping the physiological importance of GABA catabolism mediated ROS regulation and lymph gland growth control.

2.2 Investigate the regulation of ROS scavenging mechanisms (glutathione, GSH) by olfaction derived GABA catabolism in the blood-progenitor cells.

2.3 Establish the protocol for ^{13}C-isotopic labelling and metabolic flux analysis from Drosophila lymph gland blood-progenitor cells.

2.1 Understand the metabolic control of olfaction derived GABA catabolic pathway in blood-progenitor homeostasis and development.

a. *Drosophila* larval blood-progenitors rely on GABA catabolism to regulate ROS homeostasis and control lymph gland growth. GABA breakdown into succinate in the progenitor cells activates pyruvate dehydrogenase kinase (PDK), which controls inhibitory phosphorylation of pyruvate dehydrogenase (PDH). PDH is the rate-limiting enzyme that connects pyruvate to the TCA cycle and to oxidative phosphorylation. Thus, GABA catabolism via PDK activation maintains TCA activity and blood progenitor ROS homeostasis, and supports normal lymph gland growth. Consequently, any perturbations in GABA catabolism lead to heightened TCA activity and impaired ROS homeostasis, which leads to lymph gland growth retardation. Our work shows TCA cycle activity and ROS as one of the prime regulator of lymph gland growth (179).

b. GABA catabolism mediated restriction on TCA cycle activity is important for progenitor homeostasis and immune response. We have shown that perturbation of GABA transporter and GABA catabolism leads to appearance of double positive cells with both progenitor (dome) and differentiation markers (Plasmatocytes, P1), and GABA-TCA regulation is important to maintain proper identity of the cells in homeostatic conditions. Increase in TCA activity led to reduction in lamellocyte formation upon parasitic wasp-infections and reduction in TCA activity significantly increased the lamellocytes formation. Detailed investigation showed the importance of TCA activity regulation by GABA catabolism in lamellocyte formation upon wasp-infections (179).

c. Sense of smell stimulates blood-progenitor ROS homeostasis and lymph gland growth. Previous studies (94,172) have shown the importance of odor-sensing and downstream systemic GABA release in blood-progenitor development in homeostatic and immune-response conditions. We found that odor-sensing is important to maintain blood-progenitor ROS homeostasis. Animals that fail to smell, fail to sustain TCA

activity and ROS levels in the blood-progenitor cells, and consequently leads to retarded lymph gland growth (179).

2.2 Investigating the function of GABA catabolism in glutathione (GSH) synthesis. We show that olfaction derived GABA catabolism in lymph gland progenitor cells restricts pyruvate metabolism to control GSH synthesis. Our immunohistochemistry and metabolomic data show that cysteine is the limiting component towards GSH synthesis in progenitor cells. GABA catabolism control serine levels in the progenitor cells, which contribute to cysteine and downstream GSH synthesis and thus maintain progenitor ROS homeostasis via dual axis of ROS generation and ROS scavenging control.

2.3 Metabolite measurement of the lymph gland cells to decipher the role of metabolic pathways in growth and differentiation. This part of the thesis deals with standardizing and utilizing the mass-spectrometry based approach for ^{13}C-isotope labelling and metabolic flux analysis in the lymph gland blood-progenitor cells. We have standardized various LC/MS/MS based methods for analysing TCA cycle metabolites, amino acids, GSH:GSSG, NAD:NADH in lymph glands.

3 Olfaction derived GABA catabolic pathway control blood-progenitor homeostasis and development via redox regulation

3.1 Introduction

The utilization of reactive oxygen species (ROS) as a developmental signal in immune progenitor development and fate decisions is apparent both in vertebrates and invertebrates (292). The developmental roles for ROS are reliant on its threshold levels, as any aberrant generation of ROS can alter immune progenitor-cell development at the level of their maintenance, differentiation or function (72,170). Thus, mechanisms underlying ROS homeostasis during hematopoietic development comprise an integral component of redox signaling. In this context, an understanding of metabolic programs that enable blood-progenitor cells to co-ordinate their ROS levels are still limited and forms the central focus of our investigation.

Drosophila larval blood-progenitors akin to the mammalian common-myeloid progenitors (CMP), reside in a hematopoietic organ termed the lymph gland. These progenitor cells maintain elevated levels of ROS whose homeostasis is necessary for their development. While physiological levels of ROS sensitizes progenitor-cells to differentiation cues, any excessive ROS production causes oxidative stress leading to precocious differentiation and loss of progenitor homeostasis (72,170). In addition to ROS, factors governing progenitor maintenance includes signaling proteins and metabolites emanating from the local niche (posterior signaling centre, PSC) differentiating hemocytes and systemic cues derived from the brain and fat body (reviewed in (1). With these intrinsic features of metabolic and signaling requirements, the lymph gland offers a perfect developmental model to gain a comprehensive view of programs controlling progenitor ROS homeostasis during blood development.

A key source of ROS in cells is carbon cycling or the tricarboxylic acid cycle (TCA) (298,299). TCA generates multiple intermediates and also controls mitochondrial oxidative phosphorylation (OXPHOS) leading to ROS generation (298,300–302). Pyruvate, which is end-product of glycolysis, and is also derived from additional sources in the cellular cytoplasm, is ultimately destined for transport into mitochondria as a master fuel input driving the TCA cycle and oxidative phosphorylation (188,189,303). Pyruvate is converted to acetyl-CoA via pyruvate dehydrogenase enzyme (PDH), the key enzyme linking glycolysis to TCA. Its activity is regulated by post-translational modifications, which involves phosphorylation driven by pyruvate

dehydrogenase kinase (PDK) which inactivates PDH. The dephosphorylation event by pyruvate dehydrogenase phosphatase (PDP) activates the enzyme fuelling the TCA cycle (304,305).

Our past work has implicated olfaction and its downstream neuronally-derived GABA in progenitor maintenance (172) and immune response (94). Systemic GABA is sensed by blood cells both as a signaling entity and as a metabolite. Utilization of GABA as a metabolite by progenitor-cells and its catabolism to succinate is necessary to mount a successful immune response (94). In this study, we explore the importance of GABA metabolic pathway in governing progenitor ROS homeostasis. We find that in homeostatic conditions, the fuelling of pyruvate into the TCA-cycle and activation of mitochondrial complex II protein, succinate dehydrogenase (SDH), a key TCA enzyme, leads to ROS generation in progenitor cells. However, elevation in TCA activity and excessive ROS generation limits overall growth of the lymph gland tissue and loss of progenitor maintenance. Thus, to maintain TCA activity, progenitor cells adopt the GABA catabolic pathway to limit pyruvate's entry into the TCA. Specifically, GABA catabolism into succinate maintains active PDK function. This suppresses PDH enzymatic activity leading to lower TCA rate and homeostatic control of ROS generation. Finally, we also find that animals utilize environmental odors to moderate progenitor TCA activity and consequently redox balance as a means to coordinate lymph gland growth. Overall, the work presented here describes the use of a systemically-derived metabolite in blood-progenitor metabolic homeostasis and growth control with the underlying physiology driving the long-range cross-talk.

3.2 GABA metabolism in blood-progenitor cells control overall size of the lymph gland

Drosophila lymph gland blood-progenitor cells internalize systemic GABA (eGABA) via GABA transporter (Gat) and catabolize it into succinate via GABA catabolic pathway (Fig. 1A) (94). Succinic-semialdehyde dehydrogenase (Ssadh), the last and the rate-limiting step of GABA catabolism (306) is responsible for generation of succinate in progenitor cells.

We observed that loss of components of this GABA catabolic pathway (Fig. 20A) from blood-progenitor cells led to a significant reduction in the overall size of the lymph gland (Fig. 20B-D, H). While, defects in lymph gland growth and progenitor homeostasis were evident in our previous study (94), the mechanism underlying the

growth defect remained unaddressed. In this study, using the RNA*i* mediated genetic knock-down approach, we down-regulated each respective component of the GABA catabolic pathway in blood-progenitor cells. Using blood-progenitor specific drivers (*domeMeso>GFP* and *TepIV>mCherry*) we assessed the role for this pathway in homeostatic conditions. We blocked: a) progenitor cell *Gat* function to perturb GABA uptake (Fig. 20C, H and Ap. Fig. 1A, B) *Ssadh* to perturb its breakdown into succinate (Fig. 20D, H and Ap. Fig. 1A, B). In these conditions, a significant reduction in lymph gland size was noticed. On the other hand, differentiating Hemolectin^{+} (Hml^{+}) blood cells, with comparatively lower expression of Gat protein than progenitors (Ap. Fig. 1C, D), blocking their GABA uptake, showed no growth defect (Ap. Fig. 1E-G). This implied a specific function for GABA breakdown in progenitor cells for lymph gland size control.

The final metabolic output of GABA breakdown is succinate (Fig. 20A) and when larvae expressing Gat^{RNAi} or $Ssadh^{RNAi}$ in blood-progenitor cells were reared on food supplemented with succinate, they showed a significant restoration of lymph gland sizes (Fig. 20E-H). They were almost comparable to sizes detected in control animals reared on regular diet (Fig. 20F, G, H). Furthermore, controls raised on succinate diet also showed a twenty percent increase in lymph gland size in comparison to controls raised on regular diet (Fig. 20E, H). This implied a role for succinate in moderating lymph gland size downstream of the GABA metabolic pathway and led us to investigate the downstream mechanism by which this pathway controlled lymph gland growth.

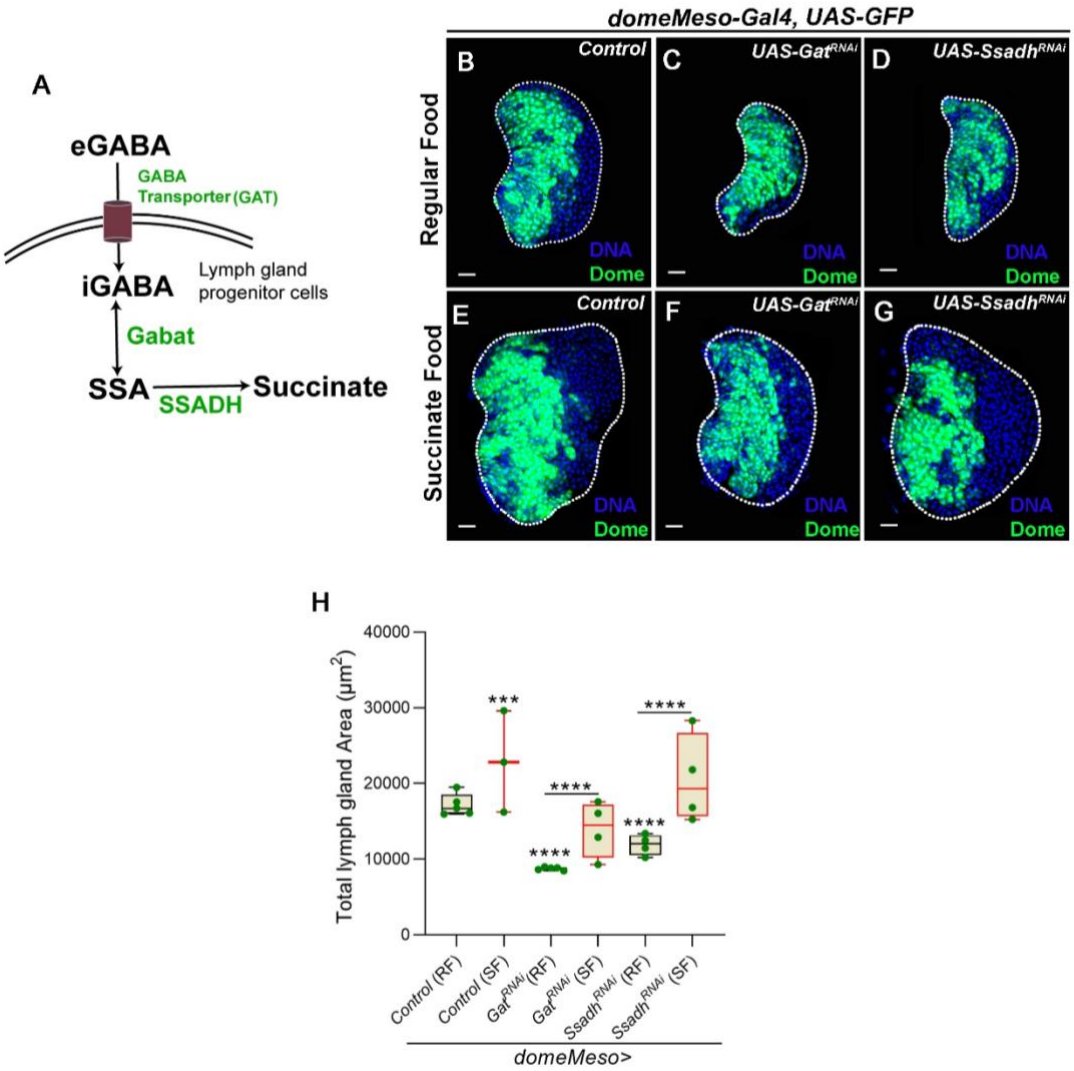

Figure 20. GABA catabolism in *Drosophila* blood-progenitor cells control lymph gland growth.
(A) Schematic representation of the GABA catabolic pathway. Uptake of extra-cellular GABA (eGABA) via GABA Transporter (GAT) in blood-progenitor cells and its intracellular catabolism (iGABA) into succinic-semialdehyde (SSA) by GABA-transaminase (Gabat) and into final product, succinate by succinic semi-aldehyde dehydrogenase (SSADH), the rate limiting step of GABA catabolic pathway. **(B-G)** Representative images showing lymph gland size **(B)** *control* (RF, *domeMeso-Gal4,UAS-GFP/+*), expressing **(C)** Gat^{RNAi} (RF, *domeMeso-Gal4,UAS-GFP;UAS-*Gat^{RNAi}) and **(D)** $Ssadh^{RNAi}$ (RF, *domeMeso-Gal4,UAS-GFP;UAS-*$Ssadh^{RNAi}$) leads to reduction in lymph gland size, **(E-G)** feeding succinate to **(E)** *control* (SF, *domeMeso-Gal4,UAS-GFP/+*), **(F)** Gat^{RNAi} (SF, *domeMeso-Gal4,UAS-GFP;UAS-*Gat^{RNAi}) and **(G)** $Ssadh^{RNAi}$ (SF, *domeMeso-Gal4,UAS-GFP;UAS-*$Ssadh^{RNAi}$) leads to increase in lymph gland size as compared to (**B, C, D)** respectively**.** For quantifications, refer to **H. (H)** Quantification of lymph gland area in *domeMeso>GFP/+*(*control*, RF, n=48) *domeMeso>GFP/+*(SF, n=48, p=0.0422), *domeMeso>GFP/*Gat^{RNAi} (RF, n=53, p<0.0001), *domeMeso>GFP/*Gat^{RNAi} (SF, n=38, p<0.0001), *domeMeso>GFP/*$Ssadh^{RNAi}$ (RF, n=33, p=0.0002) and *domeMeso>GFP/*$Ssadh^{RNAi}$ (SF, n=32, p<0.0001). RF is regular food; SF is succinate food. Data is presented as median plots (*p<0.05; **p<0.01; ***p<0.001; ****p<0.0001), two-way ANOVA, Tukey's multiple comparisons test. Scale bar: 20µm.'n'=lymph gland lobes. DAPI marks DNA. Comparisons for significance are with control values, unless marked by horizontal lines for other respective comparisons.

3.3 GABA catabolism in blood-progenitor cells controls their ROS levels

The progenitor cells of the lymph gland, exhibit elevated levels of ROS in them (Fig. 21A), which is necessary for their maintenance and differentiation (72). We observed that blocking *Gat* or *Ssadh* function in blood-progenitor cells led to elevation of lymph gland ROS (Fig. 21A-C, G). This implicated intracellular GABA uptake and its breakdown in blood-progenitor ROS homeostasis. As the metabolic output of GABA breakdown, we tested the involvement of succinate in progenitor ROS modulation. Here as well, like the growth phenotype, mutant lymph glands expressing Gat^{RNAi} or $Ssadh^{RNAi}$ when reared on food supplemented with succinate showed a significant down-regulation of ROS levels (Fig. 21D-G). Importantly, control animals raised on the succinate diet, showed further reduction in progenitor ROS levels when compared to ROS detected in animals reared on regular food (Fig. 21D, G). These data implied that succinate derived from GABA metabolism was sufficient in moderating ROS in progenitor cells and suggested an underlying connection between GABA breakdown, succinate generation and ROS levels in lymph gland growth control.

To address, if elevated ROS detected in GABA metabolic mutants was indeed the reason for lymph gland growth retardation, we asked if increasing progenitor ROS through independent means impacted lymph gland size. For this, we expressed RNA*i* against ROS scavenging enzymes, *Catalase* and *Superoxide dismutase 2 (Sod2)* in progenitor cells. Similar to *Gat* and *Ssadh* loss of function, knockdown of these scavenging enzymes demonstrated an elevation in ROS (Fig. 21H, K and Ap. Fig. 2A, B, G) with a concomitant reduction in lymph gland size (Fig. 21L, M, Q and Ap. Fig. 2H). This implied that conditions leading to elevated progenitor ROS negatively affected lymph gland growth. Therefore, we undertook experiments to scavenge ROS in *Gat* and *Ssadh* mutant conditions and asked if this was sufficient to recover their growth defect. For this, we fed larvae expressing *Gat* and *Ssadh* RNA*i* with N-acetylcysteine (NAC), a known antioxidant (307,308). This led to restoration of ROS levels in the mutant conditions (Ap. Fig. 2C-G) and significant recovery of lymph gland size (Ap. Fig. 2H, I). We undertook genetic means to scavenge ROS in Gat^{RNAi} condition and this was undertaken by over-expressing ROS scavenging enzyme, *Catalase*, in progenitor cells co-expressing Gat^{RNAi}. Although over-expression of *Catalase* on its own in progenitor cells led to down-regulation in ROS levels (Fig. 21I,

K), it did not alter lymph gland size (Fig. 21N, Q). Co-expressing *UAS-Catalase* in Gat^{RNAi} condition demonstrated a significant reduction in ROS (Fig. 21J, K) and its sufficiency in recovering lymph gland size phenotype (Fig. 21N-Q and Ap. Fig. 3A). These data suggested that lowering ROS over and above the basal threshold did not lead to any further growth advantage. However, in GABA loss condition the recovery of lymph gland growth by scavenging ROS, demonstrated that elevation in ROS above the physiological levels led to the growth defect. The recoveries seen in these genetic combinations were not a consequence of any impact on *Gal4* activity or its dilution. This was assessed by quantifying the level of GFP expression in these lymph glands as its expression (*UAS-GFP*) in these genetic backgrounds was also under the control of same *domeMeso-Gal4*. Hence, as the read out of *Gal4* activity, we measured GFP levels, which remained comparable across all genetic conditions (Ap. Fig. 3B). This further strengthened the rescues detected and the mechanism for progenitor ROS homeostasis via GABA in lymph gland growth control was investigated next.

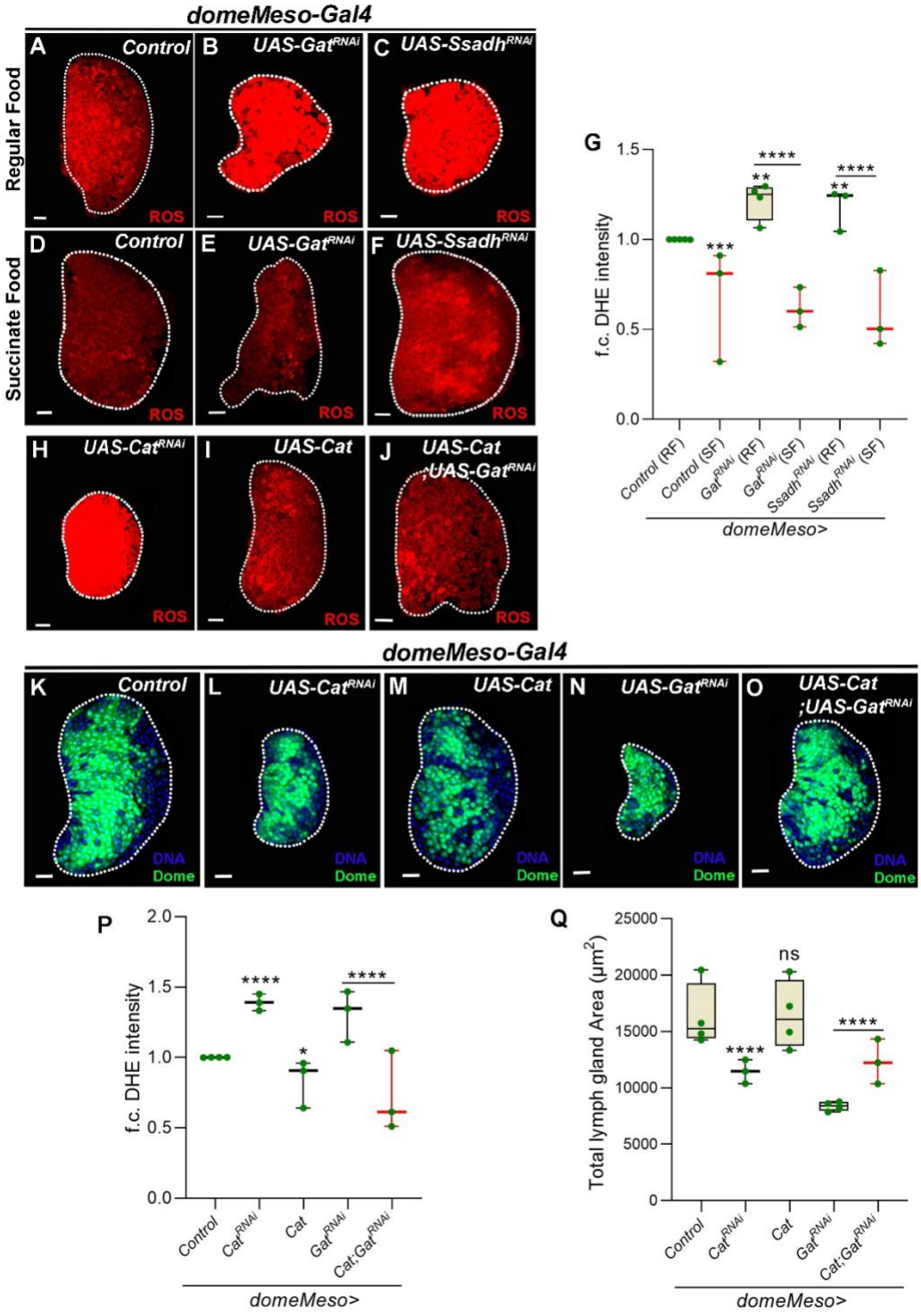

Figure 21. ROS regulation by GABA shunt pathway in *Drosophila* blood-progenitors is important for lymph gland growth.

(A) *Control* (RF, *domeMeso-Gal4,UAS-GFP/+*) lymph gland showing higher ROS levels in the blood-progenitor cells (dome^{+}), as compared to the differentiating cells, **(B)** expressing *Gat^{RNAi}* (RF, *domeMeso-Gal4,UAS-GFP;UAS-Gat^{RNAi}*) and **(C)** *Ssadh^{RNAi}* (RF, *domeMeso-Gal4,UAS-GFP;UAS-Ssadh^{RNAi}*) leads to increase in ROS levels as compared to **(A)** *control* on regular food, (**D-F)** succinate supplementation to **(D)** *control* (SF, *domeMeso-Gal4,UAS-GFP/+*) **(E)** *Gat^{RNAi}* (SF, *domeMeso-Gal4,UAS-GFP;UAS-Gat^{RNAi}*) and (**F)** *Ssadh^{RNAi}* (SF, *domeMeso-Gal4,UAS-GFP;UAS-Ssadh^{RNAi}*) leads to reduction in ROS

levels as compared to **(A, B, C)** respectively. For quantifications, refer to **G**. **(G)** Relative fold change in lymph gland ROS (DHE) levels in *domeMeso>GFP/+* (*control*, RF, n=60), *domeMeso>GFP/+* (SF, n=27, p=0.0210), *domeMeso>GFP/Gat^{RNAi}* (RF, n=30, p=0.0006), *domeMeso>GFP/Gat^{RNAi}* (SF, n=22, p<0.0001), *domeMeso>GFP/Ssadh^{RNAi}* (RF, n=28, p=0.0009) and *domeMeso>GFP/Ssadh^{RNAi}* (SF, n=25, p<0.0001). **(H-J)** Expressing **(H)** *Catalase^{RNAi}* (*domeMeso-Gal4,UAS-GFP;UAS-Cat^{RNAi}*) leads to increase in ROS levels, over-expressing **(I)** *Catalase* (*domeMeso-Gal4,UAS-GFP;UAS-Cat*) shows reduction in ROS levels as compared to (**A)** *control*, over-expressing **(J)** *Catalase* in *Gat^{RNAi}* (*domeMeso-Gal4,UAS-GFP;UAS-Cat;UAS-Gat^{RNAi}*) rescues lymph gland ROS defect of (**B)** *Gat^{RNAi}***.** For quantifications, refer to **K. (K)** Relative fold change in lymph gland ROS (DHE) levels in *domeMeso>GFP/+* (*control*, n=34), *domeMeso>GFP/Cat^{RNAi}* (n=30, p<0.0001), *domeMeso>GFP/Cat* (n=29, p=0.0394), *domeMeso>GFP/Gat^{RNAi}* (n=27, p=0.0382) and *domeMeso>GFP/Cat;Gat^{RNAi}* (n=23, p<0.0001). **(L-P)** Representative images showing lymph gland size, **(L)** *control* (*domeMeso-Gal4,UAS-GFP/+*), expressing **(M)** *Cat^{RNAi}* in blood progenitors (*domeMeso-Gal4,UAS-GFP;UAS-Cat^{RNAi}*) shows reduction in lymph gland size, over-expressing **(N)** *Catalase* (*domeMeso-Gal4,UAS-GFP;UAS-Cat*) shows no change in lymph gland size as compared to **(L)** control, over-expressing **(P)** *Catalase* in *Gat^{RNAi}* (*domeMeso-Gal4,UAS-GFP;UAS-Cat;UAS-Gat^{RNAi}*) leads to rescue of lymph gland size defect as compared to **(O)** *Gat^{RNAi}*. For quantifications, refer to **Q**. **(Q)** Quantification of lymph gland area in domeMeso>GFP/+(control, n=40), domeMeso>GFP/Cat^{RNAi} (n=45, p<0.0001), *domeMeso>GFP/Cat* (n=37, p>0.9999), *domeMeso>GFP/Gat^{RNAi}* (n=37, p<0.0001) and *domeMeso>GFP/Cat;Gat^{RNAi}* (n=37, p=0.0001). RF is regular food; SF is succinate food. Data is presented as median plots (*p<0.05; **p<0.01;***p<0.001; ****p<0.0001, n.s.=non-significant), two-way ANOVA, Tukey's multiple comparisons test. f.c.= fold change. Scale bar: 20µm.'n'=lymph gland lobes. DAPI marks DNA. Comparisons for significance are with control values, unless marked by horizontal lines for other respective comparisons.

3.4 TCA activity, a prime producer of ROS in blood-progenitor cells

We explored the source of developmental ROS in these cells. TCA cycle and its intermediates driving mitochondrial oxidative phosphorylation (OXPHOS), is a significant centre for ROS production (189,298). Thus, we investigated TCA activity in lymph gland progenitor cells. For this, as a proxy for measuring TCA activity, we assessed expression levels of enzymes PDK and PDH, using antibodies that detected their total levels along with active and inactive forms respectively (Fig. 22). PDH enzyme converts pyruvate to acetyl-CoA and drives the TCA cycle (188,189). PDH activity is regulated at the level of its phosphorylation, where the phosphorylated form (pPDH) marks inactive enzymatic state and represses TCA activity. Phosphorylation of PDH is mediated by PDK, whose phosphorylated form (pPDK), marks active PDK state and hence, decreased TCA activity (Fig. 22A).

Immuno-histochemical analysis of third instar larval lymph glands against PDK^{total}, PDH^{total}, active pPDK, and inactive pPDH was undertaken. PDK^{total} showed uniform expression in all cells of a 3rd instar larval lymph gland (Fig. 22B, B', F) and PDH^{total} showed mild increase in dome+ progenitors (Fig. 22C, C', G). Compared to this, levels of pPDK and pPDH was specifically elevated in dome^{+} progenitor cells in comparison to their levels detected in dome^{-} differentiating cells (Fig. 22D-E', H, I). These data suggested that in homeostasis, blood-progenitor cells maintained substantial fraction of

PDH in an inactive state (pPDH). The increased threshold of active PDK (pPDK) in progenitor cells highlighted PDK's regulation to limit PDH function and suggested moderation of TCA activity in these cells.

We employed genetic means to perturb *Pdh* and *Pdk* enzymes by employing RNA*i* against them and assessed for changes in progenitor ROS generation and consequently blood-progenitor development. First, we confirmed the specificity of the RNA*i* lines by undertaking analysis of pPDH and PDH^{total} in lymph glands expressing *Pdha*^{RNAi} and *Pdk*^{RNAi} (Ap. Fig. 4). A striking down-regulation of PDH^{total} (Ap. Fig. 4A, B, G) and pPDH (Ap. Fig. 4D, E, H) was seen in *Pdha*^{RNAi} expressing lymph glands. In *Pdk*^{RNAi} expressing lymph glands, PDH^{total} remained unaffected (Ap. Fig. 4C, G), but the levels of phosphorylated form (pPDH) was reduced (Ap. Fig. 4F, H). Together, these data confirmed the specificity of the RNA*i* lines. The specific loss of pPDH in *Pdk*^{RNAi} condition also showed that the phosphorylation of PDH in progenitor cells was reliant on Pdk function.

RNA*i* mediated knock-down of *Pdha* expression in blood-progenitor cells, led to a 50% reduction in ROS in comparison to levels detected in control lymph glands (Fig. 22J, K, N). Importantly, loss of progenitor *Pdha* expression did not impede lymph gland growth and they remained comparable to control conditions (Fig. 22O). These data were consistent with *Catalase* over-expression results (Fig. 21K, Q) and further strengthened the notion that lowering progenitor ROS than the physiological levels did not lead to any growth advantage. On the other hand, blocking *Pdk* expression in blood-progenitor cells, using two-independent RNA*i* lines led to almost 1.5-fold increase in ROS levels (Fig. 22L, N and Ap. Fig. 4I) and growth defect (Fig. 22O and Ap. Fig. 4J). These data were consistent with loss of *Gat, Ssadh, Cat* or *Sod2* conditions, where an increase in ROS accompanied the reduction in lymph gland size (Fig. 21Q and Ap. Fig. 2G, H). Taken together, *Pdha* loss-of-function data implied PDH function in facilitating production of ROS in progenitor cells and the *Pdk* loss-of-function data implied PDK activity in controlling progenitor ROS levels necessary for normal lymph gland growth.

Consistent with TCA involvement in OXPHOS, progenitor cell specific down-regulation of TCA cycle enzyme, *Succinate dehydrogenase A (SdhA)*, also a component of Complex II of the mitochondrial electron transport chain (ETC), lowered progenitor ROS levels (Fig. 22M, N). In this genetic condition, lymph gland sizes remained unaffected (Fig. 22O). The *SdhA* loss of function data were consistent with phenotypes

detected with *Pdh* loss in progenitor cells, that functioned upstream in the TCA cycle. The data showed that in homeostatic conditions, PDH dependent entry of pyruvate into the TCA and the subsequent oxidation and activation of mitochondrial ETC via SDH caused ROS production in blood-progenitor cells. Lowering ROS and TCA function was however not necessary for lymph gland growth, but the regulatory step via PDK, implicated in moderating PDH activity to limit excessive TCA activity and ROS generation.

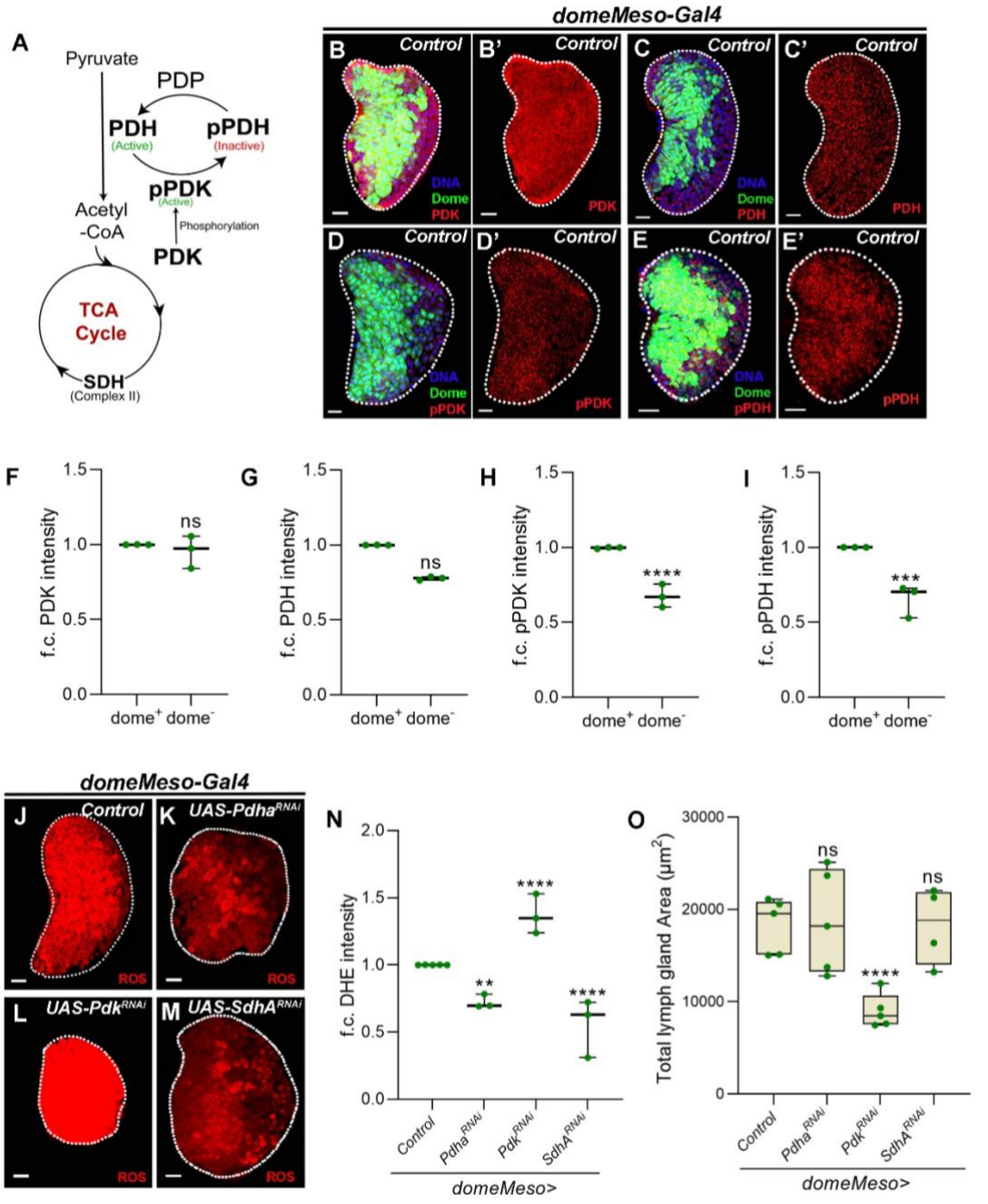

Figure 22. TCA cycle activity contributes to blood-progenitor ROS levels and regulates lymph gland growth.

(A) Schematic representation showing regulation of pyruvate entry and conversion to acetyl-CoA by PDH enzyme (active). PDH enzyme is phosphorylated by pPDK, which makes it inactive, and PDP dephosphorylates pPDH (inactive) to PDH (active), which converts pyruvate into acetyl-CoA and fuels the TCA cycle. **(B-C')** Representative lymph gland images showing PDK (red) and PDH (red) in *control* lymph gland (*domeMeso-Gal4,UAS-GFP/+*), **(B,B')** shows PDK expression in the dome$^+$ overlap (green) and without dome$^+$ overlap respectively, no alteration in PDK levels in the dome$^+$ and dome$^-$ cells is observed, **(C,C')** shows PDH expression in the dome$^+$ overlap (green) and without dome$^+$ overlap respectively, dome$^+$ cells show more PDH levels as compared to dome$^-$ cells. For quantifications, refer to **F, G. (D-E')** Representative lymph gland images showing pPDK (red) and pPDH (red) in *control* lymph gland (*domeMeso-Gal4,UAS-GFP/+*), **(D,D')** shows pPDK in the dome$^+$ overlap (green) and without dome$^+$ overlap respectively, and **(E, E')** shows pPDH in the dome$^+$ overlap (green) and without dome$^+$ overlap respectively, where dome$^+$ cells show more pPDK and pPDH as compared to dome$^-$ cells. For quantifications, refer to **H, I. (F)** Relative fold change in PDK levels in *domeMeso>GFP/+* in the dome$^+$ (n=15) and dome$^-$ region (n=15, p=0.5949), **(G)** PDH levels in *domeMeso>GFP/+* in the dome$^+$ (n=15) and dome$^-$ region (n=15, p=0.0141), **(H)** pPDK levels in *domeMeso>GFP/+* in the dome$^+$ (n=17) and dome$^-$ region (n=17, p<0.0001) and **(I)** pPDH levels in *domeMeso>GFP/+* in the dome$^+$ (n=18) and dome$^-$ region (n=18, p=0.0004). **(J-M)** Representative lymph gland images showing ROS levels, compared to **(J)** *control* (*domeMeso-Gal4,UAS-GFP/+*), expressing **(K)** *Pdha^{RNAi}* (*domeMeso-Gal4,UAS-GFP;UAS-Pdha^{RNAi}*) leads to reduction in ROS levels, **(L)** *Pdk^{RNAi}* (*domeMeso-Gal4,UAS-GFP;UAS-Pdk^{RNAi}*) elevates ROS levels and **(M)** *SdhA^{RNAi}* (*domeMeso-Gal4,UAS-GFP;UAS-SdhA^{RNAi}*) leads to reduction in ROS levels as compared to **(J)** *control*. For quantifications, refer to **N**. **(N)** Relative fold change in lymph gland ROS (DHE) levels *in domeMeso>GFP/+* (*control*, n=43), *domeMeso>GFP/Pdha^{RNAi}* (n=32, p<0.0001), *domeMeso>GFP/Pdk^{RNAi}* (n=36, p<0.0001) and *domeMeso>GFP/SdhA^{RNAi}* (n=24, p<0.0001). **(O)** Quantifications of lymph gland size in *domeMeso>GFP/+* (*control*, n=52), *domeMeso>GFP/Pdha^{RNAi}* (n=54, p=0.4219), *domeMeso>GFP/Pdk^{RNAi}* (n=51, p<0.0001) and *domeMeso>GFP/SdhA^{RNAi}* (n=53, p=0.0796). dome$^+$ (green) marks the lymph gland blood progenitor cells and dome$^-$ region marks the differentiating cells. Data is presented as median plots (*p<0.05; **p<0.01; ***p<0.001; ****p<0.0001, n.s.=non-significant), two-way ANOVA, Tukey's multiple comparisons test. f.c.= fold change. Scale bar: 20µm.'n'=lymph gland lobes. DAPI marks DNA.

If modulation of TCA enzymes also affected progenitor homeostasis or immune response was examined. Homeostatic response was addressed by assessment of progenitor population by analysing their dome-GFP reporter expression and staining lymph glands for differentiation markers PPO1 to mark crystal cells (Fig. 23A-E) and P1 to mark plasmatocytes (Fig. 24) (95). Infection responses were assessed by analysing formation of lamellocytes using Myospheroid marker in response to parasitic wasp-infection (78). Lamellocyte numbers were assessed in the lymph glands and in circulation at 24 hours (Fig. 23F-L) at 48 hours (Fig. 23M) post-infection, respectively.

In control lymph glands, 60-70% area of lymph gland was dome$^+$, 15-20% area was dome$^-$ but P1$^+$ and remaining 20-25% was negative for both the markers (dome$^-$P1$^-$) (Fig. 24A-A",E). Loss of *Pdha* (low TCA) from progenitor cells, did not alter progenitor homeostasis or their differentiation and remained comparable to controls (Fig. 23B, F and 24B-B", E). Like *Pdha* loss of function, *SdhA^{RNAi}* did not show any dramatic changes in progenitor or differentiation status, except a mild reduction in progenitor population (Fig. 23C, F and Fig. 24C-C", E). When assessed for immune

response, loss of TCA function did not impede lamellocyte formation. Contrarily a significant increase in lamellocyte numbers was detectable in lymph glands lacking *Pdha* or *SdhA* expression (Fig. 23H, I, L, M). These data revealed an unexpected role for TCA regulation in immune response while being largely dispensable for normal hematopoiesis and downregulation of *Pdha* (Ap. Fig. 4K-L) or *SdhA* (94) in lymph gland blood-progenitors in homeostatic (uninfected) conditions did not affect lamellocyte formation. In Pdk^{RNAi} condition (increased TCA), changes were however more dramatic.

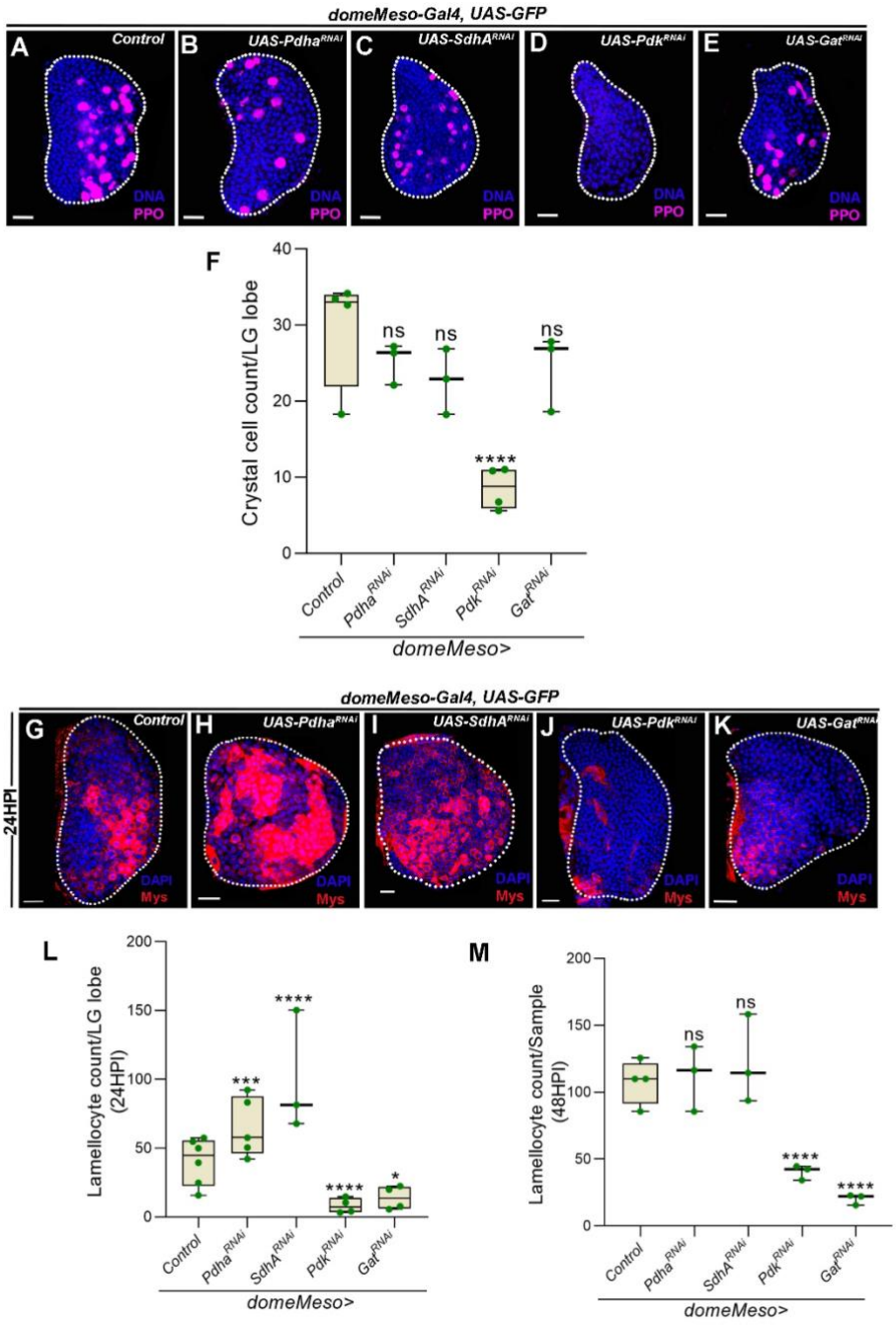

Figure 23. Modulations in TCA activity affects blood progenitor differentiation in homeostasis and immune response upon wasp-infection.
(A-E) Representative images showing lymph gland crystal cell status, **(A)** *control* (*domeMeso-Gal4,UAS-GFP/+*) showing **(A)** crystal cells, **(B)** expressing $Pdha^{RNAi}$ (*domeMeso-Gal4,UAS-GFP;UAS-*$Pdha^{RNAi}$) and **(C)** expressing $SdhA^{RNAi}$ (*domeMeso-Gal4,UAS-GFP;UAS-*$SdhA^{RNAi}$) does not affect crystal cell number, expressing **(D)** Pdk^{RNAi} in progenitor cells (*domeMeso-Gal4,UAS-GFP;UAS-*Pdk^{RNAi}) leads to a decrease in crystal cell number and **(F)** expressing Gat^{RNAi} (*domeMeso-Gal4,UAS-GFP;UAS-*Gat^{RNAi}) does not show any change in crystal cell number as compared to *control* **(A)**. For quantifications, refer to **F**. **(F)** Quantifications of crystal cell count per lymph gland lobe in *domeMeso>GFP/+* (*control*, N=4, n=63), *domeMeso>GFP/*$Pdha^{RNAi}$ (N=3, n=32, p=0.8486), *domeMeso>GFP/*Pdk^{RNAi} (N=4, n=45, p<0.0001), *domeMeso>GFP/*$SdhA^{RNAi}$ (N=3, n=44, p=0.2574) and *domeMeso>GFP/*Gat^{RNAi} (N=3, n=30, p=0.341). **(G-K)** Representative images showing lymph gland lamellocyte status at 24HPI, **(A)** *control* (*domeMeso-Gal4,UAS-GFP/+*) showing **(G)** lamellocyte at 24HPI, **(H)** expressing $Pdha^{RNAi}$ (*domeMeso-Gal4,UAS-GFP;UAS-*$Pdha^{RNAi}$) and **(I)** expressing $SdhA^{RNAi}$ (*domeMeso-Gal4,UAS-GFP;UAS-*$SdhA^{RNAi}$) leads to a dramatic increase in lamellocyte number post-infection, expressing **(J)** Pdk^{RNAi} in progenitor cells (*domeMeso-Gal4,UAS-GFP;UAS-*Pdk^{RNAi}) leads to a decrease in lamellocyte number and **(K)** expressing Gat^{RNAi} (*domeMeso-Gal4,UAS-GFP;UAS-*Gat^{RNAi}) show a reduction in lamellocyte number at 24HPI as compared to *control* **(G)**, For quantifications, refer to **L**. **(L)** Quantifications of lamellocyte count per lymph gland lobe at 24HPI in *domeMeso>GFP/+* (control, N=6, n=66), *domeMeso>GFP/*$Pdha^{RNAi}$ (N=5, n=60, p=0.0002), *domeMeso>GFP/*Pdk^{RNAi} (N=4, n=43, p=0.0002), *domeMeso>GFP/*$SdhA^{RNAi}$ (N=3, n=11, p<0.0001) and *domeMeso>GFP/*Gat^{RNAi} (N=4, n=46, p=0.0167). **(M)** Quantifications of lamellocyte count in circulation at 48HPI in *domeMeso>GFP/+* (*control*, N=4, n=54), *domeMeso>GFP/*$Pdha^{RNAi}$ (N=3, n=30, p=0.9948), *domeMeso>GFP/*Pdk^{RNAi} (N=3, n=71, p<0.0001), *domeMeso>GFP/*$SdhA^{RNAi}$ (N=3, n=22, p=0.9435) and *domeMeso>GFP/*Gat^{RNAi} (N=3, n=22, p<0.0001). Data is presented as median plots (*p<0.05; **p<0.01; ***p<0.001; ****p<0.0001, n.s.=non-significant), two-way ANOVA, Tukey's multiple comparisons test and f.c.= fold change. MZ=Medullary Zone. Scale bar: 20µm.'n'=lymph gland lobes and number of animals analysed for **M**. 'N'= number of experimental repeats (green dot). DAPI marks DNA. HPI indicates hours post-infection.

An increase in $dome^+$ population alongside an increase in $P1^+$ population and a reduction in $dome^-P1^-$ population was detected (Fig. 24D-E). Importantly, in Pdk^{RNAi} condition, we observed a subset of $dome^+$ cells overlapping with $P1^+$ cells (Fig. 24D-E) which was undetectable in control lymph glands in homeostasis. A reduction in crystal cell formation was also evident in Pdk^{RNAi} condition (Fig. 23D, F). When assessed for cellular immune response, loss of *Pdk* function severely abrogated lamellocyte formation (Fig. 23J, L, M). These data implied a role for PDK in progenitor maintenance and proper differentiation in homeostasis and upon infection. The Pdk^{RNAi} immune phenotypes were comparable to phenotypes described for GABA function in blood-progenitor cells (94). A careful assessment of Gat^{RNAi} expressing progenitors with the markers described in this study showed a significant overlap of $dome^+$ cells with $P1^+$ marker (Fig. 24E and Fig. 27B-B"). This implied functional overlap between GABA catabolism and PDK activity in regulating lymph gland growth, progenitor differentiation and immune response.

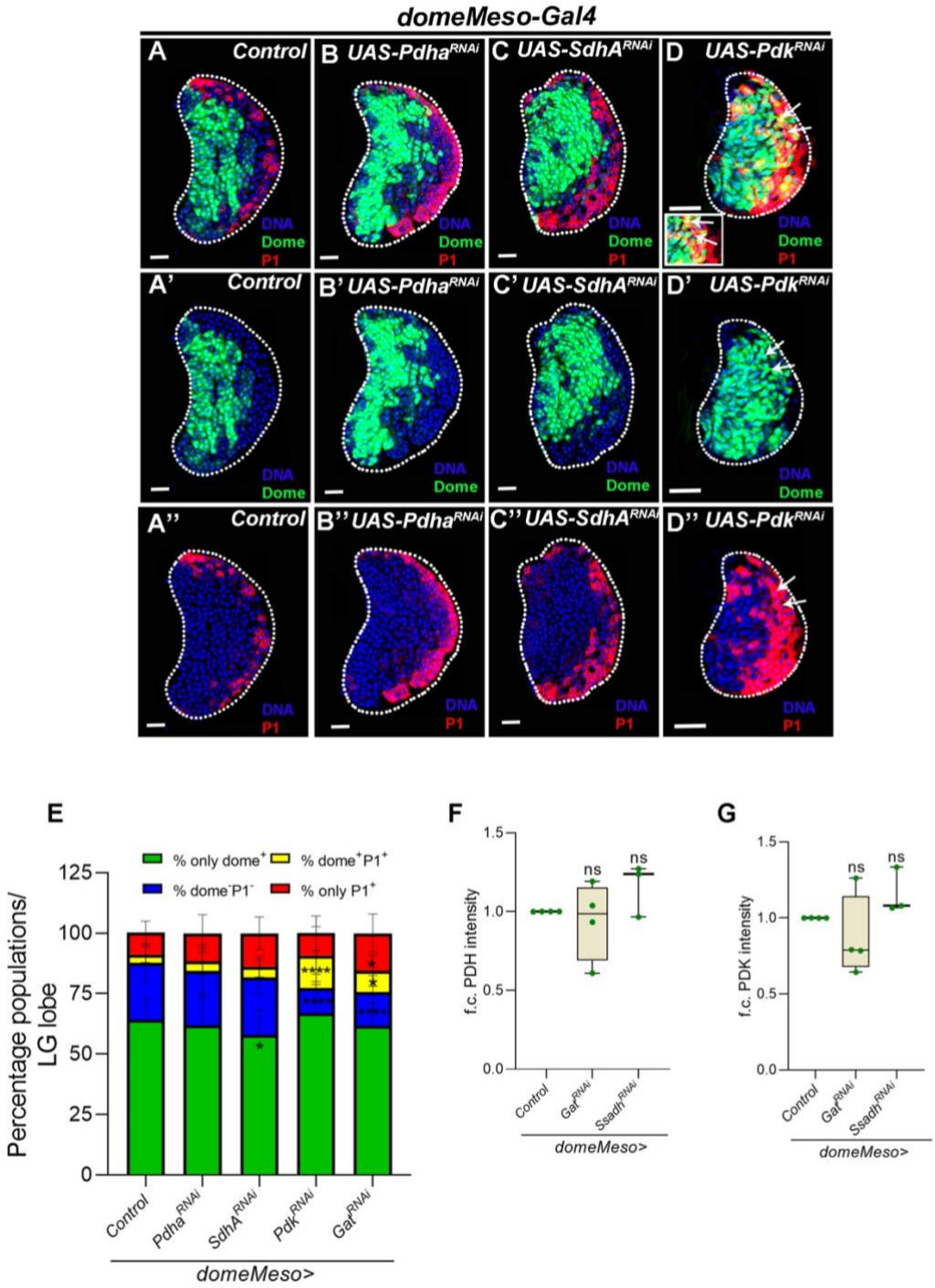

Figure 24. Modulations in TCA activity affects blood progenitor differentiation in homeostasis.
(A-D") Representative images showing lymph gland growth and differentiation status, **(A-A")** *control* (*domeMeso-Gal4,UAS-GFP/+*) showing **(A)** dome^{+} (green) and P1^{+} (red), **(A')** dome^{+}(green) and **(A")** P1^{+} (red), **(B-B")** expressing *Pdha^{RNAi}* (*domeMeso-Gal4,UAS-GFP;UAS-Pdha^{RNAi}*) and **(C-C")** expressing *SdhA^{RNAi}* (*domeMeso-Gal4,UAS-GFP;UAS-SdhA^{RNAi}*) does not show any major defect in lymph gland differentiation status, expressing **(D-D")** *Pdk^{RNAi}* in progenitor cells (*domeMeso-Gal4,UAS-GFP;UAS-Pdk^{RNAi}*) leads to small lymph gland size and appearance of **(D)** dome^{+}p1^{+} overlap population (shown in inset and by white arrows). For quantifications, refer to **E**. **(E)** Quantifications of lymph gland differentiation status shown as percentage of only dome^{+}(green), dome^{-}P1^{-}(blue), dome^{+}P1^{+}(yellow) and only P1^{+}(red) populations per lymph gland lobe. p-values are presented in the preceding order. *domeMeso>GFP/+* (*control*, n=30), *domeMeso>GFP/Pdha^{RNAi}* (n=30, p=0.6970, 0.9647, 0.9976, 0.5921), *domeMeso>GFP/SdhA^{RNAi}* (n=30, p=0.0135, 0.9999, 0.9649, 0.0890), *domeMeso>GFP/Pdk^{RNAi}*

(n=30, p=0.5046, <0.0001, <0.0001, 0.9999) and *domeMeso>GFP/Gat*^{RNAi} (n=26, p=0.6528, <0.0001, 0.0456, 0.0139). **(F-G)** Relative fold change in lymph gland MZ **(F)** PDH levels in *domeMeso>GFP/+* (*control*, N=4, n=40), *domeMeso>GFP/Gat*^{RNAi} (N=4, n=33, p=0.6817), and *domeMeso>GFP/Ssadh*^{RNAi} (N=3, n=30, p=0.1197) and **(G)** PDK levels in *domeMeso>GFP/+* (*control*, N=4, n=47), *domeMeso>GFP/Gat*^{RNAi} (N=4, n=41, p=0.1101), and *domeMeso>GFP/Ssadh*^{RNAi} (N=3, n=30, p=0.3347). Data is presented as median plots (*p<0.05; **p<0.01; ***p<0.001; ****p<0.0001, n.s.=non-significant), two-way ANOVA, Tukey's multiple comparisons test and Dunnett's multiple comparison test for G (mean±SD). f.c.= fold change. MZ=Medullary Zone. Scale bar: 20µm.'n'=lymph gland lobes. 'N'= number of experimental repeats (green dot). DAPI marks DNA.

3.5 GABA catabolism regulates TCA activity by regulating PDK function and moderates ROS generation in blood-progenitor cells.

Based on the phenotypic similarities between GABA and *Pdk* loss of function data, we hypothesized that an increase in TCA activity in GABA catabolic mutants, led to the small lymph gland and differentiation phenotypes. We investigated the levels of PDH^{total}, PDK^{total}, inactive form of PDH (phospho-PDH, pPDH) and active PDK (pPDK) in GABA metabolic pathway mutants (Fig. 24 and Fig. 25). PDH^{total} and PDK^{total} expression upon loss of progenitor *Gat* and *Ssadh* remained comparable to controls (Fig. 24F, G and Fig. 25A-F). This showed that changes in GABA metabolism did not alter the production of these enzymes. However, we observed specific down-regulation in the levels of pPDH (inactive PDH, Fig. 25G-I, Q) and pPDK (active PDK, Fig. 25J-L, R) upon loss of *Gat* and *Ssadh* expression in progenitor cells. The reduction in pPDH, implied increased fraction of active PDH enzyme and implied enhanced TCA activity in GABA metabolic mutants.

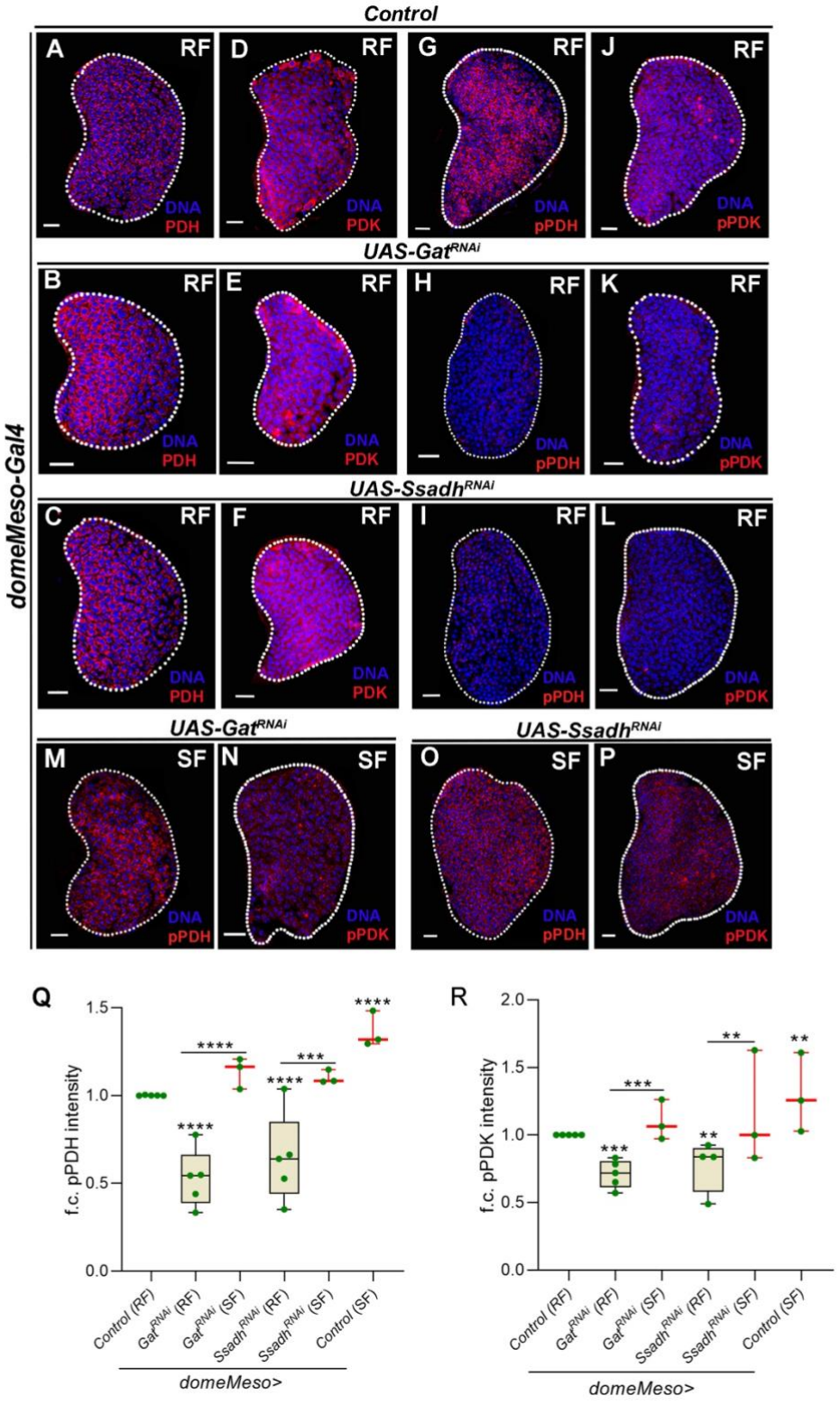

Figure 25. GABA catabolism via PDK activity regulates TCA cycle in blood-progenitor cells and coordinates overall lymph gland growth.
(A-F) Representative lymph gland images showing PDH and PDK levels **(A, D)** *control* (*domeMeso-Gal4,UAS-GFP/+*) showing **(A)** PDH and **(D)** PDK levels**,** expressing **(B, E)** *Gat*^{RNAi} (*domeMeso-Gal4,UAS-GFP;UAS-Gat*^{RNAi}) and **(C, F)** *Ssadh*^{RNAi} (*domeMeso-Gal4,UAS-GFP;UAS-Ssadh*^{RNAi}) in progenitor cells does not show reduction in **(B, C)** PDH and **(E, F)** PDK levels as compared to **(A, D)** *control* respectively. For quantifications, refer to **Fig. 24F, G**. **(G-I)** Representative lymph gland images showing pPDH on RF, **(G)** *control* (*domeMeso-Gal4,UAS-GFP/+*) showing pPDH**,** expressing **(H)**

Gat^{RNAi} (*domeMeso-Gal4,UAS-GFP;UAS-Gat*^{RNAi}) and **(I)** *Ssadh*^{RNAi} (*domeMeso-Gal4,UAS-GFP;UAS-Ssadh*^{RNAi}) leads to reduction in pPDH levels as compared to **(G)** *control*. For quantifications, refer to **U**. **(J-L)** Representative lymph gland images showing RF, **(J)** *control* (*domeMeso-Gal4,UAS-GFP/+*) showing pPDK**,** expressing **(K)** *Gat*^{RNAi} (*domeMeso-Gal4,UAS-GFP;UAS-Gat*^{RNAi}) and **(L**) *Ssadh*^{RNAi} (*domeMeso-Gal4,UAS-GFP;UAS-Ssadh*^{RNAi}) leads to reduction in pPDK levels as compared to **(J)** *control*. For quantifications, refer to **V**. **(M-P)** Succinate supplementation (SF) in (**M, N)** *Gat*^{RNAi} (*domeMeso-Gal4,UAS-GFP;UAS-Gat*^{RNAi}) and **(O, P)** *Ssadh*^{RNAi} (*domeMeso-Gal4,UAS-GFP;UAS-Ssadh*^{RNAi}) rescues **(H, I)** pPDH and **(K, L)** pPDK levels of **(H, I)** *Gat*^{RNAi} and **(K, L)** *Ssadh*^{RNAi} on RF respectively. For quantifications, refer to **Q, R**. **(Q)** Relative fold change in lymph gland MZ pPDH levels in *domeMeso>GFP/+* (RF, *control*, n=51), *domeMeso>GFP/Gat*^{RNAi} (RF, n=30, p=0.0002), *domeMeso>GFP/Gat*^{RNAi} (SF, n=24, p<0.0001), *domeMeso>GFP/Ssadh*^{RNAi} (RF, n=47, p<0.0001), *domeMeso>GFP/Ssadh*^{RNAi} (SF, n=23, p=0.0022) and *w*^{1118} (SF, n=38, p<0.0001, pPDH compared to *w*^{1118}, RF, n=47). **(R)** Relative fold change in lymph gland MZ pPDK levels in *domeMeso>GFP/+* (RF, *control*, n=38), *domeMeso>GFP/Gat*^{RNAi} (RF, n=32, p=0.0003), *domeMeso>GFP/Gat*^{RNAi} (SF, n=20, p=0.0091), *domeMeso>GFP/Ssadh*^{RNAi} (RF, n=35, p<0.0001), *domeMeso>GFP/Ssadh*^{RNAi} (SF, n=20, p=0.0102) and *w*^{1118} (SF, n=30, p=0.0100, pPDK compared to *w*^{1118}, RF, n=30). RF is regular food; SF is succinate food. Data is presented as median plots (*p<0.05; **p<0.01; ***p<0.001; ****p<0.0001, n.s.=non-significant), two-way ANOVA, Tukey's multiple comparisons test. f.c.= fold change. Scale bar: 20µm.'n'=lymph gland lobes. DAPI marks DNA. MZ= medullary zone. Comparisons for significance are with control values, unless marked by horizontal lines for other respective comparisons.

The specific reduction in pPDK, suggested GABA function in maintaining active PDK state in progenitor cells to limit PDH activity and suppress TCA. We investigated this by down-regulating components of the TCA cycle in *Gat*^{RNAi} condition and assessed for changes in lymph gland ROS and growth phenotypes. Interestingly, down-regulation of *Pdha* or *SdhA* expression in *Gat*^{RNAi} expressing progenitor cells corrected both lymph gland elevated ROS phenotype almost comparable to levels detected in controls (Fig. 26A-E) and growth defect (Fig. 26F). This suggested that increased TCA activity in GABA metabolic mutants was the key source of elevated ROS generation leading to the growth defect. These genetic combinations were also sufficient to recover the differentiation and immune defects seen in *Gat*^{RNAi} condition (Fig. 27 and Fig. 28).

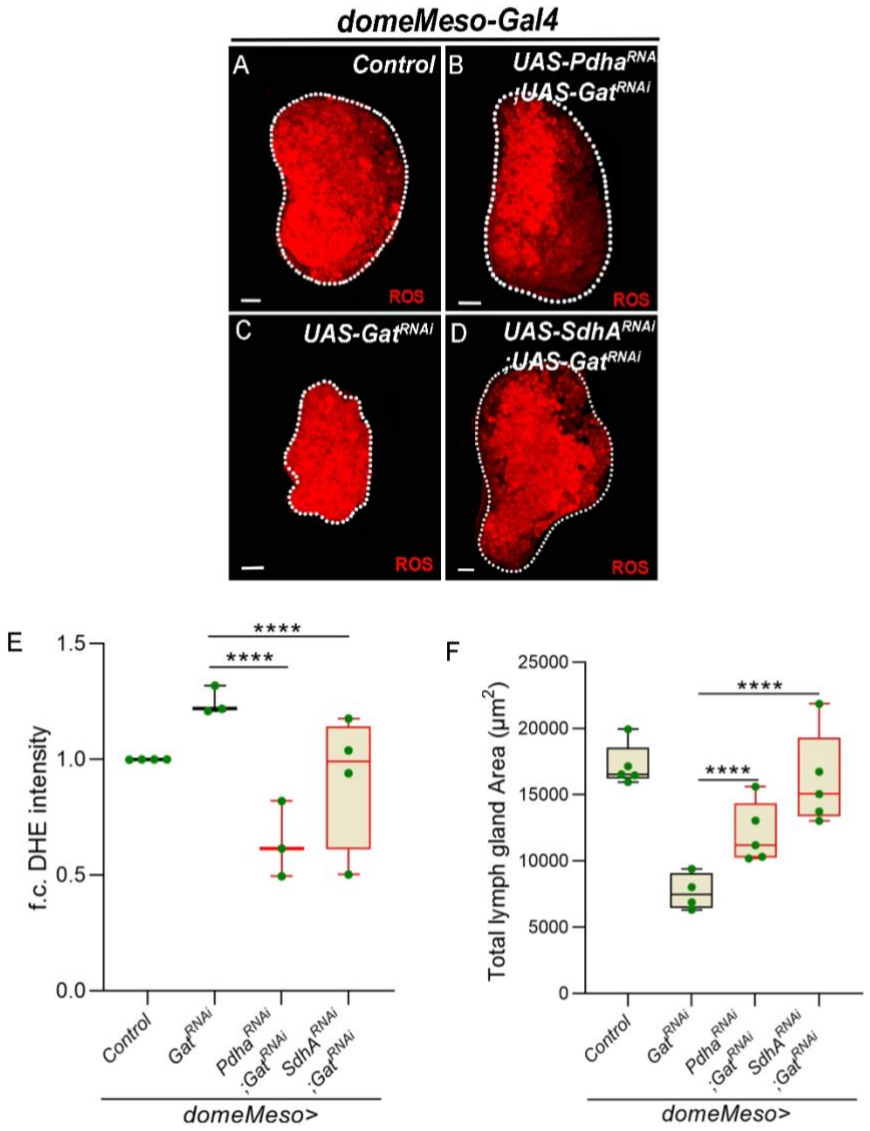

Figure 26. GABA catabolism via PDK activity regulates TCA cycle in blood-progenitor cells and coordinates overall lymph gland growth.
(A-D) Representative lymph gland images showing ROS levels in the **(A)** *control* (*domeMeso-Gal4,UAS-GFP/+*), **(B)** expressing Gat^{RNAi} (*domeMeso-Gal4,UAS-GFP;UAS-*Gat^{RNAi}) leads to elevation in ROS levels, expressing **(C**) $Pdha^{RNAi}$;Gat^{RNAi} (*domeMeso-Gal4,UAS-GFP;UAS-*$Pdha^{RNAi}$;*UAS-*Gat^{RNAi}) and **(D**) $SdhA^{RNAi}$;Gat^{RNAi} (*domeMeso-Gal4,UAS-GFP;UAS-*$SdhA^{RNAi}$;*UAS-*Gat^{RNAi}) rescues the increased ROS phenotype of **(N)** Gat^{RNAi}. For quantifications, refer to **E**. **(E)** Relative fold change in lymph gland ROS (DHE) levels in *domeMeso>GFP/+* (*control*, n=35), *domeMeso>GFP/*Gat^{RNAi} (n=22, p=0.0014), *domeMeso>GFP/*$Pdha^{RNAi}$;Gat^{RNAi} (n=19, p<0.0001) and *domeMeso>GFP/*$SdhA^{RNAi}$;Gat^{RNAi} (n=26, p=0.0004). **(F)** Quantifications of lymph gland size in *domeMeso>GFP/+* (*control*, n=44), *domeMeso>GFP/*Gat^{RNAi} (n=33, p<0.0001), *domeMeso>GFP/*$Pdha^{RNAi}$;Gat^{RNAi} (n=50, p=0.0006), and *domeMeso>GFP/*$SdhA^{RNAi}$;Gat^{RNAi} (n=41, p<0.0001). Data is presented as median plots (*p<0.05; **p<0.01; ***p<0.001; ****p<0.0001, n.s.=non-significant), two-way ANOVA, Tukey's multiple comparisons test. f.c.= fold change. Scale bar: 20µm.'n'=lymph gland lobes. DAPI marks DNA. MZ= medullary zone. Comparisons for significance are with control values, unless marked by horizontal lines for other respective comparisons.

While the overall hematopoietic profile of Gat^{RNAi} lymph glands was comparable to controls (Fig. 27E and Fig. 28E), the dome^{+}P1^{+} double positive cells detected in Gat^{RNAi}

condition were no longer detectable in *Pdha*^{RNAi};*Gat*^{RNAi} or in *SdhA*^{RNAi};*Gat*^{RNAi} condition (Fig. 27A-E).

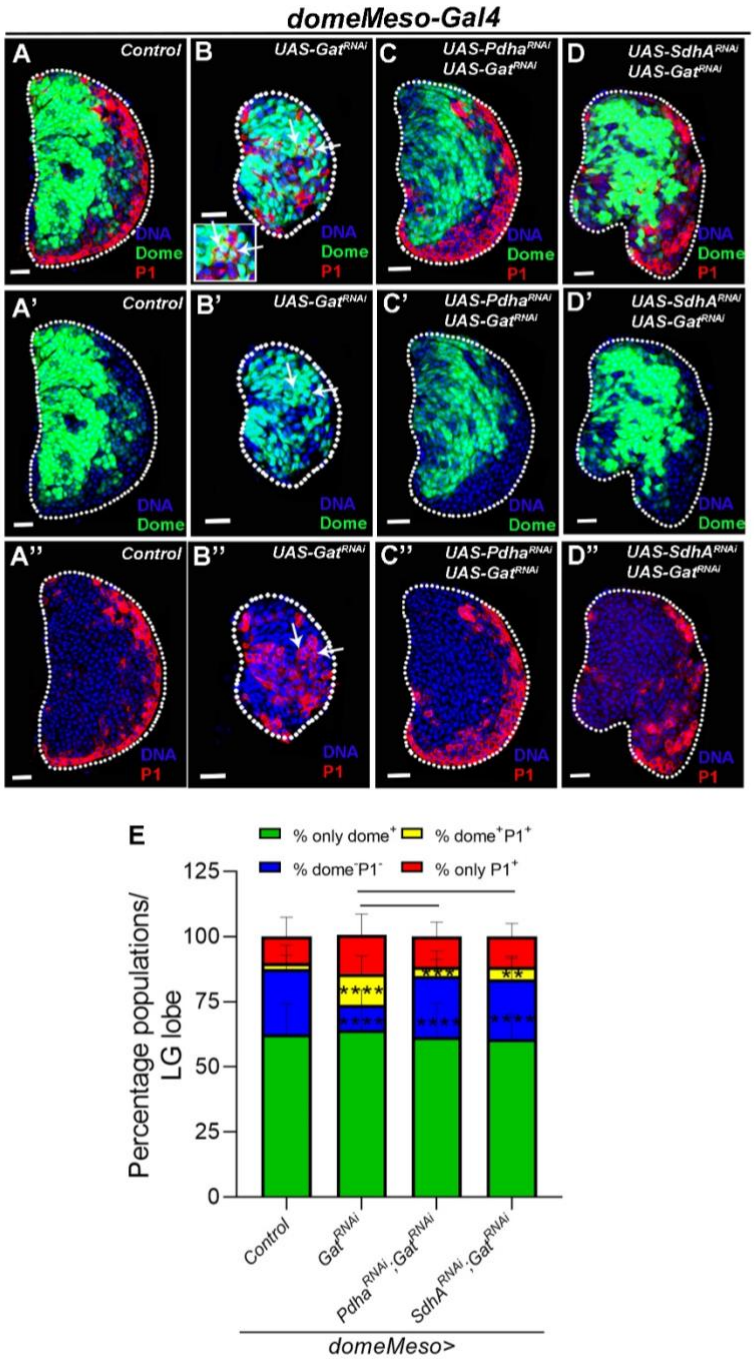

Figure 27. GABA catabolism dependent control of TCA activity maintains blood progenitor homeostasis. **(A-D")** Representative images showing lymph gland growth and differentiation status, **(A-A")** *control* (*domeMeso-Gal4,UAS-GFP/+*) **(A)** dome$^+$ (green) and P1$^+$ (red), **(A')** dome$^+$(green) and **(A")** P1$^+$ (red), **(B-B")** expressing *Gat*^{RNAi} in progenitor cells (*domeMeso-Gal4,UAS-GFP;UAS-Gat*^{RNAi}) leads to small lymph gland size and appearance of **(B)** dome$^+$p1$^+$ overlap population (shown in inset and by white arrows) along with an increase in **(B")** P1 population, expressing **(C-C")** *Pdha*^{RNAi} in *Gat*^{RNAi} (*domeMeso-Gal4,UAS-GFP;UAS-Pdha*^{RNAi};*UAS-Gat*^{RNAi}) and **(D-D")** *SdhA*^{RNAi} in *Gat*^{RNAi} (*domeMeso-Gal4,UAS-GFP;UAS-SdhA*^{RNAi};*UAS-Gat*^{RNAi}) rescues the lymph gland growth and differentiation defect of **(B-B")** *Gat*^{RNAi}. For quantifications, refer to **E**. **(E)** Quantifications of lymph gland differentiation status shown as percentage of only dome$^+$(green), dome$^-$P1$^-$(blue), dome$^+$P1$^+$(yellow) and only P1$^+$(red) populations

per lymph gland lobe. p-values are presented in the preceding order. *domeMeso>GFP/+* (control, n=36) and *domeMeso>GFP/Gat^{RNAi}* (n=20, p=0.7812, <0.0001, <0.0001, 0.0889), *domeMeso>GFP/Pdha^{RNAi};Gat^{RNAi}* (n=34, p=0.4635, <0.0001, 0.0005, 0.2920), and *domeMeso>GFP/SdhA^{RNAi};Gat^{RNAi}* (n=31, p=0.2428, <0.0001, 0.0045, 0.3084). Data is presented as median plots (*p<0.05; **p<0.01; ***p<0.001, ****p<0.0001, n.s.=non-significant), two-way ANOVA and Dunnett's multiple comparison test for **E** (mean± SD). f.c.= fold change. MZ=Medullary Zone. Scale bar: 20µm.'n'=lymph gland lobes. 'N'= number of experimental repeats (green dot). DAPI marks DNA. Comparisons for significance are with control values, unless marked by horizontal lines for other respective comparisons and red bars represent rescue combinations.

The lamellocyte formation defect seen in GABA metabolic mutants (Fig. 28G, L, M) was significantly restored upon co-expression of *Pdha* or *SdhA* RNA*i* in them (Fig. 28 H, I, L, M). These data suggested that GABA function in progenitor cells via regulating PDK activity, controlled PDH dependent pyruvate entry into TCA and OXPHOS and controlled excessive ROS generation. This regulation supported growth and proper differentiation of progenitor cells in homeostasis. Given the striking recovery of lamellocyte response with loss of TCA components in *Gat^{RNAi}* condition, we tested the involvement of ROS. But unlike the growth rescues that were restored by over-expression of *Catalase*, the lamellocyte defects were not restored in this genetic context (Fig. 28J-M). Which implied that excessive TCA activity in *Gat^{RNAi}* condition blocked lamellocyte formation, but this inhibition was not due to the excessive ROS and suggested a ROS independent connection between TCA activity and GABA metabolism in moderating immune response.

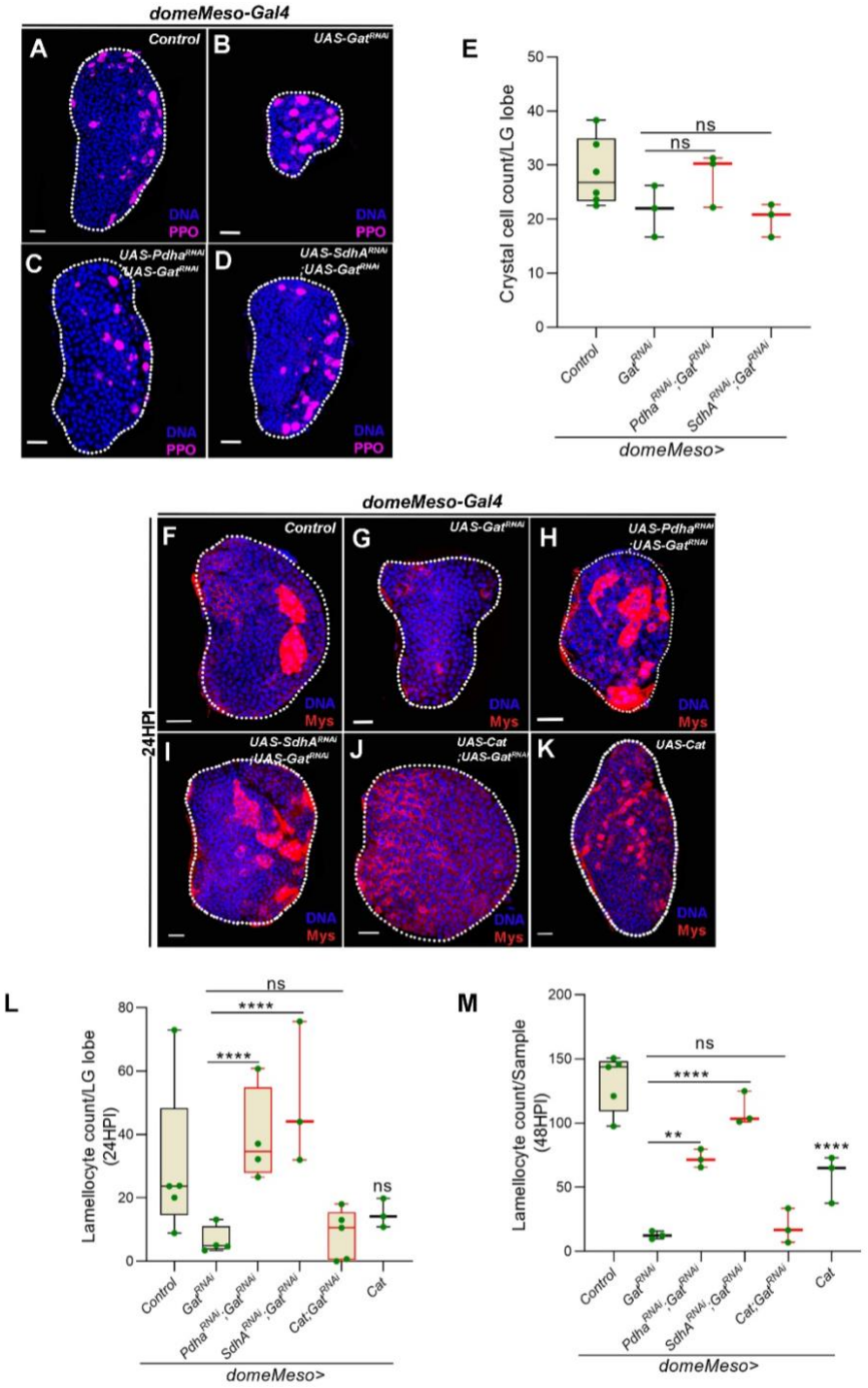

Figure 28. GABA catabolism dependent control of TCA activity maintains blood progenitor homeostasis and immune response upon wasp-infection.
(A-D) Representative images showing lymph gland crystal cell status, **(A)** *control* (*domeMeso-Gal4,UAS-GFP/+*), **(B)** expressing Gat^{RNAi} in progenitor cells (*domeMeso-Gal4,UAS-GFP;UAS-*Gat^{RNAi}) did not show any change in crystal cell number, expressing **(C)** $Pdha^{RNAi}$ in Gat^{RNAi} (*domeMeso-Gal4,UAS-GFP;UAS-*$Pdha^{RNAi}$*;UAS-*Gat^{RNAi}) and **(D)** $SdhA^{RNAi}$ in Gat^{RNAi} (*domeMeso-Gal4,UAS-GFP;UAS-*$SdhA^{RNAi}$*;UAS-*Gat^{RNAi}) did not affect crystal cell formation. For quantifications, refer to **E**. **(E)** Quantifications of crystal cell count per lymph gland lobe in *domeMeso>GFP/+* (*control*, N=6, n=63) and *domeMeso>GFP/*Gat^{RNAi} (N=3, n=20, p=0.8298), *domeMeso>GFP/*$Pdha^{RNAi}$*;*Gat^{RNAi} (N=3, n=37, p=0.4133), and *domeMeso>GFP/*$SdhA^{RNAi}$*;*Gat^{RNAi} (N=3, n=32, p=0.9671). **(F-K)** Representative images showing lymph gland lamellocyte status post wasp-infection at 24HPI, **(F)** *control* (*domeMeso-*

Gal4,UAS-GFP/+), **(G)** expressing Gat^{RNAi} in progenitor cells (*domeMeso-Gal4,UAS-GFP;UAS-*Gat^{RNAi}) leads to reduction in lamellocytes number, expressing **(H)** $Pdha^{RNAi}$ in Gat^{RNAi} (*domeMeso-Gal4,UAS-GFP;UAS-*$Pdha^{RNAi}$*;UAS-*Gat^{RNAi}) and **(I)** $SdhA^{RNAi}$ in Gat^{RNAi} (*domeMeso-Gal4,UAS-GFP;UAS-*$SdhA^{RNAi}$*;UAS-*Gat^{RNAi}) rescues the reduced lamellocyte phenotype of **(G)** Gat^{RNAi} and **(J)** over-expressing *Catalase* in Gat^{RNAi} (*domeMeso>GFP/Cat;*Gat^{RNAi}) does not rescues the lamellocyte defect, while **(K)** over-expressing *Catalase* leads to a reduction in lymph gland lamellocyte count post wasp-infection. For quantifications, refer to **L**. **(L)** Quantifications of lamellocyte count per lymph gland lobe at 24HPI in *domeMeso>GFP/+* (*control*, N=5, n=58) and *domeMeso>GFP/*Gat^{RNAi} (N=4, n=38, p=0.0426), *domeMeso>GFP/*$Pdha^{RNAi}$*;*Gat^{RNAi} (N=4, n=52, p<0.0001), *domeMeso>GFP/*$SdhA^{RNAi}$*;*Gat^{RNAi} (N=3, n=28, p<0.0001), *domeMeso>GFP/Cat;*Gat^{RNAi} (N=5, n=32, p=0.9966) and *domeMeso>GFP/Cat* (N=3, n=18, p=0.7201). **(M)** Quantifications of lamellocyte count in circulation at 48HPI in *domeMeso>GFP/+* (*control*, N=5, n=49) and *domeMeso>GFP/*Gat^{RNAi} (N=3, n=29, p<0.0001), *domeMeso>GFP/*$Pdha^{RNAi}$*;*Gat^{RNAi} (N=3, n=26, p=0.0064), *domeMeso>GFP/*$SdhA^{RNAi}$*;*Gat^{RNAi} (N=3, n=29, p= p<0.0001), *domeMeso>GFP/Cat;*Gat^{RNAi} (N=3, n=36, p=0.9998) and *domeMeso>GFP/Cat* (N=3, n=27, p<0.0001). Data is presented as median plots (*p<0.05; **p<0.01; ***p<0.001, ****p<0.0001, n.s.=non-significant), two-way ANOVA, Tukey's multiple comparisons test and f.c.= fold change. MZ=Medullary Zone. Scale bar: 20µm.'n'=lymph gland lobes and number of animals analysed for **M**. 'N'= number of experimental repeats (green dot). DAPI marks DNA. HPI indicates hours post-infection. Comparisons for significance are with control values, unless marked by horizontal lines for other respective comparisons and red bars represent rescue combinations.

3.6 GABA-catabolism via succinate controls PDK activity necessary for ROS homeostasis in blood-progenitor cells

The mechanism by which GABA catabolic pathway regulated pPDK levels was next explored. The restoration of ROS and lymph gland growth defect with succinate supplemented diet implied regulation of TCA activity via succinate (Fig. 20 and Fig. 21A-G). We examined levels of pPDH and pPDK in succinate supplemented conditions. Compared to pPDH and pPDK detected in *Gat* and *Ssadh* RNA*i* expressing animals raised on regular food (Fig. 25G-L and Q, R), we observed that succinate supplemented diet restored levels of pPDH (Fig. 25M, O compared to H,I respectively and Q) and pPDK (Fig. 25N, P compared to K,L respectively and R) to control levels and showed that GABA derived succinate regulated PDK activity to suppress TCA. Therefore, we propose that in progenitor cells, succinate derived from GABA metabolism activates PDK function and suppresses PDH activation. This lowers TCA activity and moderates ROS generation. This succinate is independent of the TCA-derived succinate which via SdhA and mitochondrial ETC promotes OXPHOS and ROS production. We speculate the existence of distinct pools of succinate which serve independent roles and is consistent with our previous findings (94). How succinate is compartmentalized to control distinct developmental decisions remains unclear.

Our previous findings have implicated GABA catabolism derived succinate in the inhibition of hydroxy prolyl hydroxylase activity (Hph) necessary for cellular immune response to wasp-infection. We have shown that in conditions with low progenitor cell

GABA metabolism, reduction in succinate causes increased Hph activity and abrogation of cellular immune response. Contrarily, increased progenitor-cell GABA metabolism causes reduction of Hph activity leading to superior immune responses (94). If GABA and succinate functioned via moderating Hph activity to control lymph gland growth was assessed.

For this, gain and loss-of-function approaches to moderate Hph expression in progenitor cells were undertaken. We observed that, gain of Hph activity led to reduction in lymph gland size (Fig. 29P), elevation in ROS (Fig.29A, D, Q) and reduction in pPDH (Fig. 29B, E, R) and pPDK levels (Fig. 29C, F, S). Total levels of PDH or PDK however remained unaffected (Ap. Fig. 5A, B). This implied that although total levels of these proteins did not change, increased Hph expression caused a reduction in the levels of pPDK (Fig. 29F, S) and subsequently pPDH (Fig. 29E, R). This suggested sufficiency of increased Hph activity in increasing TCA rate leading to heightened ROS generation and lymph gland growth defect. Reduction in progenitor-cell *Hph* expression, however failed to show any effect on lymph gland size (Fig. 29P), ROS levels (Fig. 29G, Q) or PDH activity as pPDH levels remained unchanged (Fig. 29H, R) even though an increase in pPDK levels (Fig. 29I, S) was apparent. We also assessed for total PDH and PDK levels and they remained unchanged (Ap. Fig. 7A, B). These data are unlike gain of Hph function and suggested that, in homeostasis, *Hph* function in progenitor cells was not necessary to moderate TCA activity or lymph gland growth.

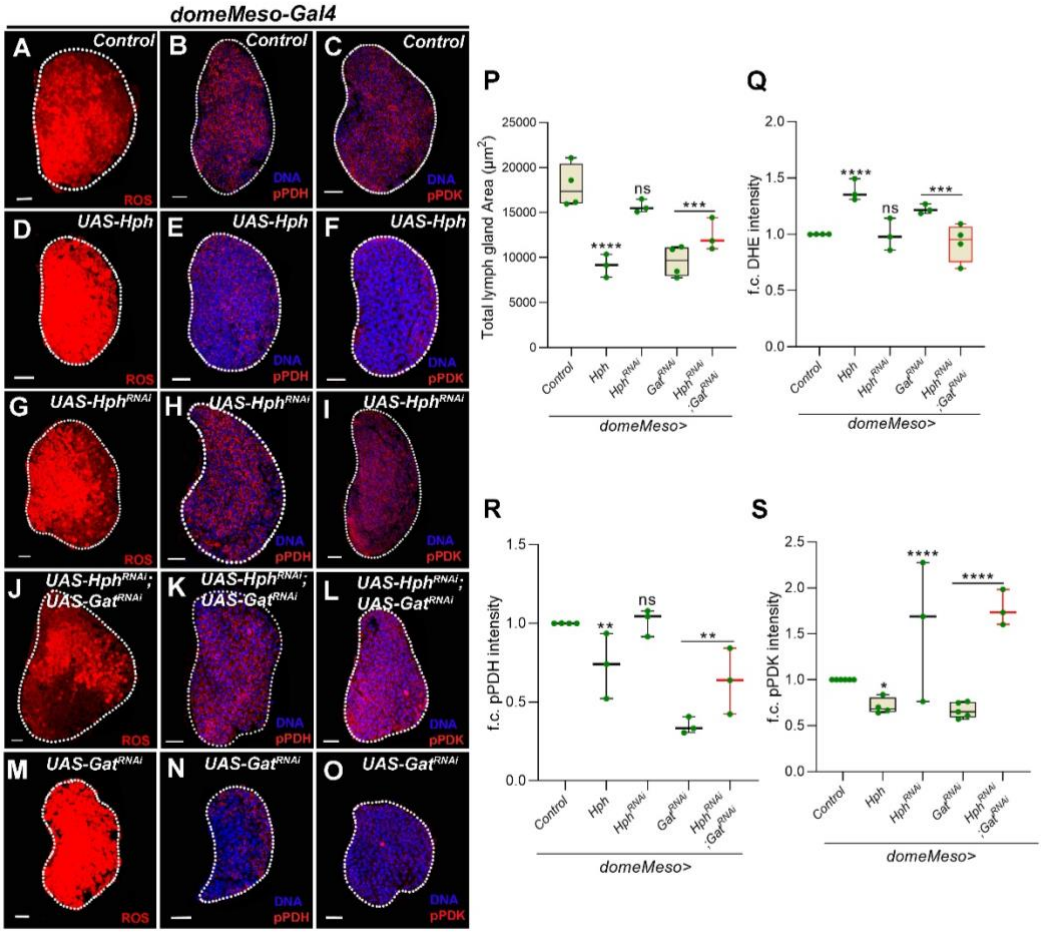

Figure 29. GABA catabolism derived succinate inhibits Hph function to maintain PDK activity and limit TCA cycle which sustains lymph gland growth.
(A-C) Representative lymph gland images showing **(A)** ROS **(B)** pPDH and **(C)** pPDK in *control* (*domeMeso-Gal4,UAS-GFP/+*). **(D-F)** Over-expressing *Hph* (*domeMeso-Gal4,UAS-GFP;UAS-Hph*) leads to **(D)** significant increase in ROS levels**,** reduction in **(E)** pPDH and **(F)** pPDK levels in the progenitor cells. (**G-I)** Expressing Hph^{RNAi} (*domeMeso-Gal4,UAS-GFP;UAS-*Hph^{RNAi}) did not show any change in **(G)** ROS levels and **(H)** pPDH levels, a significant increase in **(I)** pPDK levels is observed in the progenitor cells. For quantifications, refer to **Q, R, S. (J-O)** Expressing Hph^{RNAi} in Gat^{RNAi} (*domeMeso-Gal4,UAS-GFP;UAS-*Hph^{RNAi}*;UAS-*Gat^{RNAi}) leads to **(J)** reduction in lymph gland ROS levels as compared to Gat^{RNAi} **(M),** an increase in **(K)** pPDH and **(L)** pPDK levels is evident in the progenitor cells as compared to **(N, O)** Gat^{RNAi} (*domeMeso-Gal4,UAS-GFP;UAS-*Gat^{RNAi}) respectively. For quantifications, refer to **Q, R, S. (P)** Quantifications for lymph gland area in *domeMeso>GFP/+* (*control*, n=40), *domeMeso>GFP/Hph* (n=40, p<0.0001), *domeMeso>GFP/*Hph^{RNAi} (n= 40, p>0.9999), *domeMeso>GFP/*Gat^{RNAi} (n=40, p<0.0001) and *domeMeso>GFP/*Hph^{RNAi}*;*Gat^{RNAi} (n=40, p=0.0011), **(Q)** Relative fold change in lymph gland ROS (DHE) levels in *domeMeso>GFP/+* (*control*, n=36), *domeMeso>GFP/Hph* (n=32 p=0.0002), *domeMeso>GFP/*Hph^{RNAi} (n=24, p>0.9999), *domeMeso>GFP/*Gat^{RNAi} (n=14, p=0.0189) and *domeMeso>GFP/*Hph^{RNAi}*;*Gat^{RNAi} (n=31, p<0.0001), **(R)** MZ pPDH levels in *domeMeso>GFP/+* (*control*, n=43), *domeMeso>GFP/Hph* (n=39, p=0.0025), *domeMeso>GFP/*Hph^{RNAi} (n=37, p>0.9999), *domeMeso>GFP/*Gat^{RNAi} (n=19, p<0.0001) and *domeMeso>GFP/*Hph^{RNAi}*;*Gat^{RNAi} (n=32, p=0.0003) and **(S)** MZ pPDK levels in *domeMeso>GFP/+* (control, n=46), *domeMeso>GFP/Hph* (n=30, p=0.0071), *domeMeso>GFP/*Hph^{RNAi} (n=41, p=0.0059), *domeMeso>GFP/*Gat^{RNAi} (n=23, p=0.0415) and *domeMeso>GFP/*Hph^{RNAi}*;*Gat^{RNAi} (n=36, p<0.0001). Data is presented as median plots (*p<0.05; **p<0.01; ***p<0.001; ****p<0.0001, n.s.=non-significant), two-way ANOVA, Tukey's multiple comparisons test. f.c.= fold change. Scale bar: 20µm.'n'=lymph gland lobes. DAPI marks DNA. MZ= medullary zone. Comparisons for significance are with control values, unless marked by horizontal line for other respective comparisons.

Given the phenotypic similarities between *Hph* gain of function and GABA catabolic mutants, we hypothesized that in the absence of GABA, the growth defect could be due to increased Hph activity. To test this, we co-expressed Hph^{RNAi} in progenitor cells also expressing Gat^{RNAi}. This led to a significant recovery of lymph gland size (Fig. 29P) , ROS (Fig. 29J compared to M, Q), pPDH (Fig. 29K compared to N, R) and pPDK levels (Fig. 29L compared to O, S). These data therefore implied that in the absence of GABA metabolism, the gain in *Hph* function over and above the basal threshold, could lead to growth defect by the down-regulation of pPDK levels leading to increased TCA activity and elevated ROS generation. However, if GABA also inhibited Hph activity in homeostasis to maintain TCA and redox balance remains unclear. The data reflect a complex role for Hph which may be a consequence of the different isoforms (309) and our current findings with the approaches utilized (either the RNA*i* or *UAS-Hph*) are limited in this aspect. The involvement of the specific isoform/s in blood development and their regulation remains to be completely addressed.

Succinate via inhibition of hydroxy prolyl hydroxylase (Hph) activity, stabilizes Sima protein in progenitor cells. Sima functions orthologous to mammalian Hifα, where prolyl hydroxylase activity of Hph marks Sima protein for proteasomal mediated degradation. In the presence of GABA, blood progenitor cells stabilize Sima protein, whose downstream target lactate dehydrogenase (Ldh) is known to capacitates blood cells with differentiation potential necessary to respond to parasitic wasp-infections (94). We observed that loss of *Sima* and *Ldh* in the progenitor cells led to reduction in lymph gland size (Ap. Fig. 7C-F), however corresponding elevation in lymph gland ROS levels upon downregulation of *Sima* in the progenitor cells was not seen (Ap. Fig. 7G-I). This indicated that Hph function in progenitor cells in the context of ROS regulation was independent of Sima. This notion was further supported by pPDH and pPDK expression levels in $sima^{RNAi}$ expressing progenitor cells whose levels did not change (Ap. Fig. 7J-O) and corroborated with the independence of ROS detected in $sima^{RNAi}$. This further reinforced alternative mechanisms employed by Sima to coordinate lymph gland growth. Based on involvement of Ldh in regulating lymph gland growth in the study, we propose Sima function in activating Ldh dependent glycolytic program in progenitor cells that supports growth of the blood tissue. Our study demonstrates that the breakdown of GABA into succinate inhibits Hph function, this maintains PDK activity in progenitor cells and consequently lower TCA activity and progenitor ROS generation.

3.7 Physiological regulation of GABA in lymph gland growth

The GABA detected by the lymph gland progenitor cells is derived upon olfactory stimulation (94,172), Fig. 30A). As animals sense environmental odors, the olfactory input derived upon activation of specific olfactory receptors, stimulates neuronal production and release of GABA which is sensed by blood-progenitor cells both as a signaling ligand and as a metabolite. Our recent findings have implicated GABA's metabolic role in specification of cells necessary to respond to wasp-infections (94). If the odor sensing/GABA axis in normal physiological conditions moderated hematopoietic growth was therefore investigated. For this, we first assessed the impact of anosmia on lymph gland growth and TCA/ROS homeostasis. We employed genetic means to ablate olfactory receptor neurons as done previously (94,172), by expressing the pro-apoptotic gene *Hid* in all olfactory neurons using *Orco-Gal4* as the driver. We observed that this genetic manipulation led to a stark reduction in lymph gland size (Fig. 30B) with a dramatic increase in their ROS levels (Fig. 30C, D, G). We also observed that olfactory dysfunction (*Orco>Hid*) led to significant reduction in the levels of pPDH (Fig. 30E, H, J) and pPDK (Fig. 30F, I, K) in lymph glands without altering expression levels of total PDH or PDK (Ap. Fig. 6 M, N). These data were similar to progenitor *Gat* and *Ssadh* loss of function and implied that loss of olfaction most likely via reduction in systemic GABA levels led to dysregulation of lymph gland PDK activity. This resulted in elevation in TCA activity, increased ROS generation and consequently leading to retardation in lymph gland size. The data showed that during homeostasis lymph gland growth was sensitive to animal odor-sensing and this axis was also necessary to control progenitor redox balance.

As animals rearing in conditions with predisposition to predatory wasp-odors co-opt the olfaction/systemic GABA axis to stimulate superior immune response when infected (94), we asked, if this pre-conditioning moderated hematopoietic growth. We therefore reared *Drosophila* larvae in the wasp-odor condition (WOF) and assessed their lymph gland size in homeostatic un-infected conditions. Interestingly, these animals presented a significant increase in lymph gland size (Fig. 30O). The lymph gland ROS was significantly lower than detected in control animals raised in regular odor-condition (Fig. 30L, P). The level of TCA enzymes remained comparable to controls (Fig. 30M, N, Q, R and Ap. Fig. 6E, F) although, a mild but significant increase in pPDH (Fig. 30M, Q) was apparent in WOF animals. If the growth advantage manifested in WOF was due to an increase in progenitor GABA levels, was also assessed. For this lymph

gland growth in animals over-expressing *Gat* in progenitor cells, as a means to allow more GABA uptake by blood-progenitor was investigated. Like WOF, *Gat* over-expression phenocopied lymph gland size expansion (Ap. Fig. 6G) along with reduction in progenitor ROS (Ap. Fig. 6H-J) and TCA activity (Ap. Fig. 6K-R).

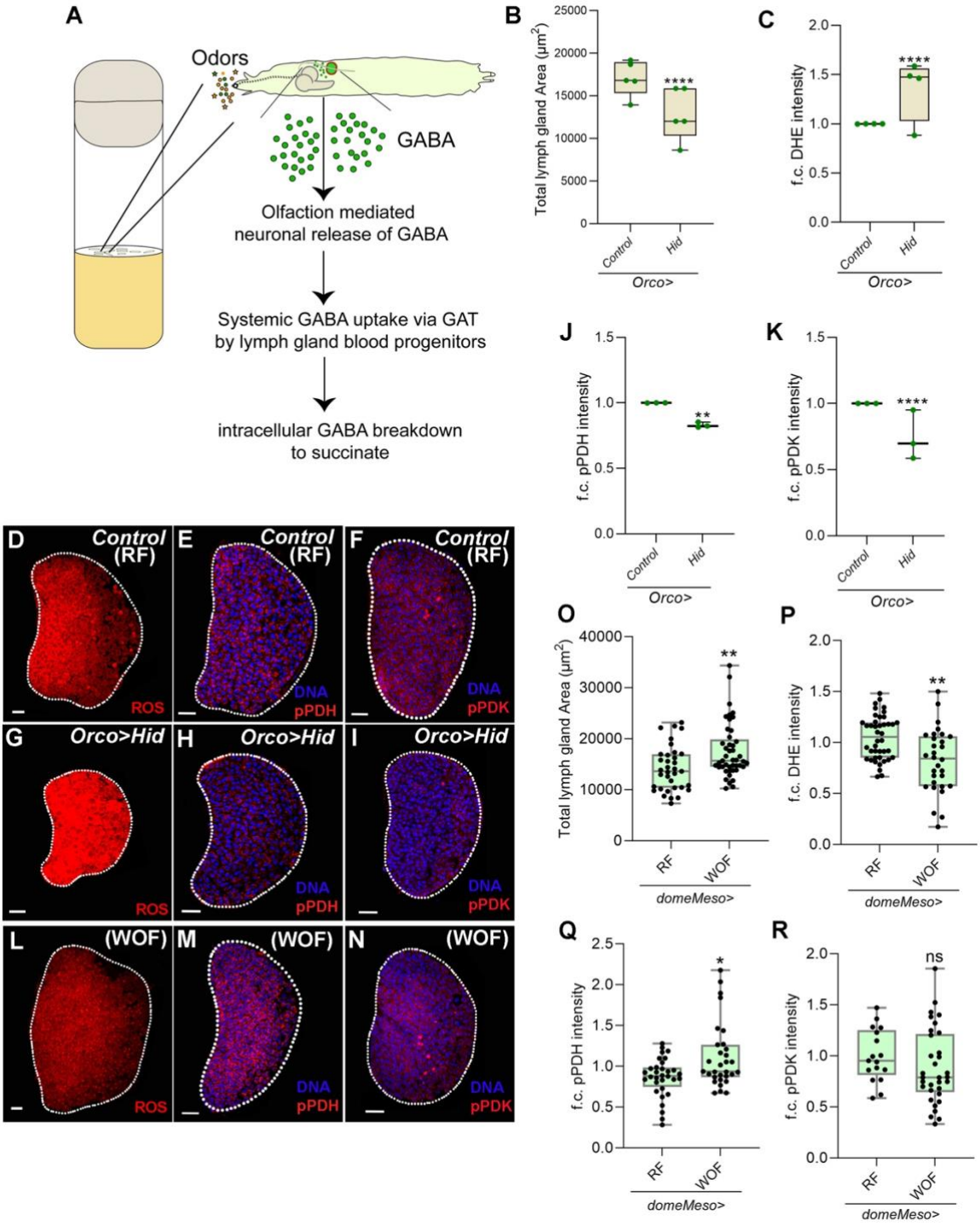

Figure 30. Olfactory regulation of lymph gland growth and ROS homeostasis.

(A) A schematic representation showing larvae rearing in a food medium (shown in the vial) where the exposure of the animal to environmental odors stimulates the release of GABA from the larval brain. This extracellular GABA is sensed by blood-progenitor cells of the lymph gland and is thereafter catabolized into succinate via the GABA catabolic pathway. **(B)** Quantifications of lymph gland size in *Orco>/+* (*control*, N=5, n=74) and *Orco>/Hid* (N=5, n=76, p<0.0001). **(C)** Relative fold change in lymph gland ROS (DHE) levels in *Orco>/+* (*control*, N=4, n=32) and *Orco>/Hid* (N=4, n=30, p<0.0001). **(D-I)** Representative lymph gland images showing **(D)** ROS **(F)** pPDH and **(H)** pPDK in control (*Orco-Gal4/+*)**, (E, G, I)** Over-expressing Hid in olfactory receptor neurons (*Orco-Gal4;UAS-Hid*) leads to **(E)** increase in ROS levels, reduction in **(G)** pPDH and **(I)** pPDK levels as compared to **(D, F, H)** control respectively. For quantifications, refer to **C, J, K. (J)** Relative fold change in lymph gland pPDH levels in *Orco>/+* (control, N=3, n=35) and *Orco>/Hid* (n=29, N=3 p=0.0053) and **(K)** pPDK levels in *Orco>/+* (control, N=3, n=30) and *Orco>/Hid* (N=3, n=33, p<0.0001). **(L-N)** Representative lymph gland images showing **(L)** ROS **(M)** pPDH and **(N)** pPDK in *control* (*domeMeso-Gal4,UAS-GFP/+*) on wasp odor food, WOF. For quantifications, refer to **P,Q,R**. **(O)** Quantifications of lymph gland size in *domeMeso>GFP/+*(RF, control, n=35), and *domeMeso>GFP/+*(WOF, n=45, p=0.0029). **(P)** Relative fold change in lymph gland ROS (DHE) levels *domeMeso>GFP/+*(RF, control, n=42), *domeMeso>GFP/+*(WOF, n=30, p=0.0011), **(Q)** pPDH levels *domeMeso>GFP/+*(RF, control, n=32), *domeMeso>GFP/+*(WOF, n=31, p=0.0248) and **(R)** pPDK levels *domeMeso>GFP/+*(RF, control, n=17), *domeMeso>GFP/+*(WOF, n=33, p=0.1360). Data is presented as median plots (*p<0.05;**p<0.01;***p<0.001,****p<0.0001, two-way ANOVA, Tukey's multiple comparisons test. Mann-Whitney test for **O-R.** f.c.= fold change. Scale bar: 20µm.'n'=lymph gland lobes. 'N'= number of experimental repeats (green dot). DAPI marks DNA.

Overall, these data suggested that pre-sensing of predatory wasp-odors most-likely via up-regulation of systemic and consequently progenitor GABA levels enabled further growth of the lymph glands and also moderated their TCA activity/ROS homeostasis. The growth advantage seen in WOF or high GABA conditions, however, appears to be independent of the TCA/ROS axis and remains to be deciphered.

To summarize, we propose that *Drosophila* larvae rely on GABA derived from environmental odor-sensing as a means to moderate blood progenitor TCA cycle activity and ROS balance to maintain normal lymph gland growth and development including lamellocyte potential during immune response conditions (Fig. 31).

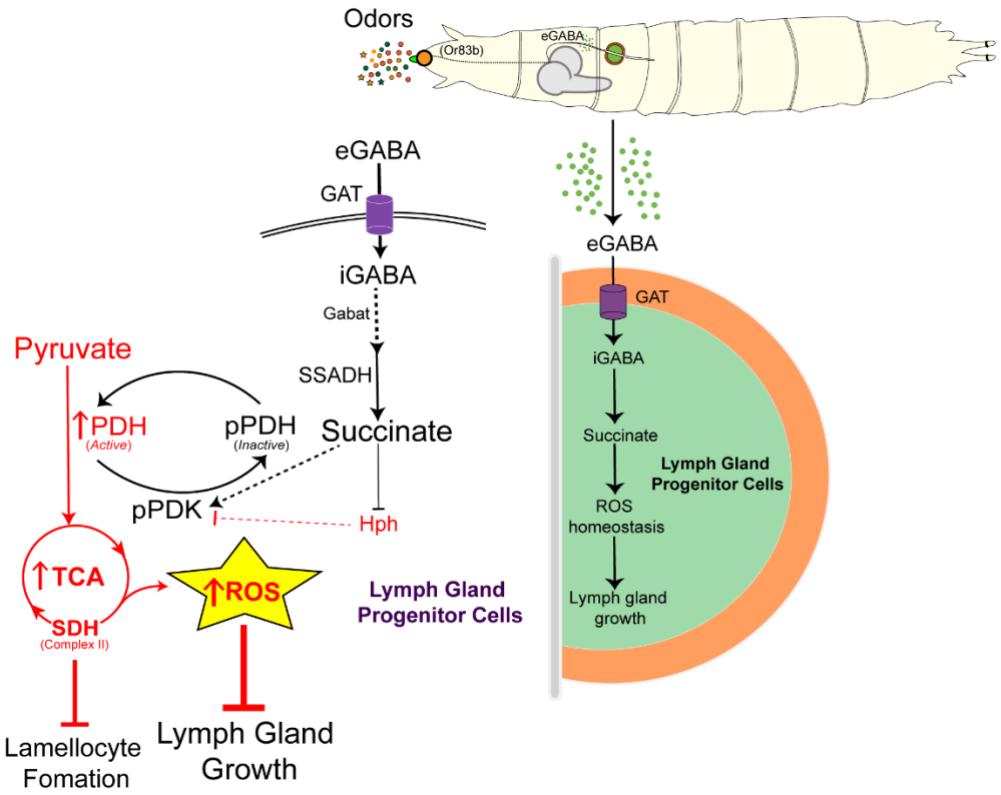

Figure 31. Olfaction-derived systemic GABA in lymph gland ROS homeostasis and growth control. The model describes the importance of olfaction-derived GABA metabolism in lymph gland growth control and lamellocytes formation. All elements that repress growth are shown in red, while positive regulators of growth are shown in black. Blood progenitor cells of the *Drosophila* larval lymph gland maintains ROS in them which is derived from the TCA cycle. However, heightened, or uncontrolled TCA activity leading to increased ROS production in progenitor cells abrogates lymph gland growth, development and lamellocyte potential. Thus, to moderate progenitor TCA activity and ROS levels, *Drosophila* larvae rely on olfaction-derived systemic GABA (eGABA). Sensing of extracellular GABA (eGABA) via blood-progenitor cells and its subsequent metabolism through the GABA catabolic pathway into succinate promotes maintenance of pPDK, which is the active form of PDK. PDK phosphorylates PDH (pPDH) and inactivates it, a key rate-limiting enzyme of the TCA-cycle, whose activation drives TCA activity. Thus, GABA metabolism in progenitor cells via activating PDK limits TCA cycle and subsequently maintains ROS homeostasis in them. This metabolic state supports normal lymph gland growth and development. In the absence of any olfactory input, or loss of blood progenitor GABA utilization, the lack of succinate in progenitor cells leads to increased Hph function which blocks PDK activation that consequently leads to heightened TCA activity and ROS generation leading to lymph gland growth retardation.

4 GABA catabolism regulates pyruvate cycling to control GSH formation and Redox homeostasis in Drosophila blood-progenitors

4.1 Introduction

Drosophila blood progenitors, residing in the hematopoietic organ, lymph gland have been shown to possess higher ROS levels as compared to the surrounding differentiated cells (72). In the progenitor cells, ROS levels are maintained at a specific threshold level which primes these progenitor cells toward differentiation. Any increase or decrease in ROS levels affect the progenitor differentiation capacity, therefore maintenance of ROS levels in these progenitor cells is of prime importance. This demands specific requirement of ROS regulatory mechanisms in the progenitor cells. Our previous work has revealed the mechanism of ROS generation regulation in the progenitor cells. We have shown that olfaction derived GABA catabolism regulates phosphorylation of pyruvate dehydrogenase kinase (PDK) and pyruvate dehydrogenase (PDH), which regulates TCA cycle activity and results in ROS generation regulation (179). Here, we asked if lymph gland progenitor cells express the components of ROS scavenging mechanisms. Previous studies have shown the presence of ROS scavenging regulatory mechanism in progenitor homeostasis (72) and lymph gland growth control (179). But how the components of ROS scavenging in the blood-progenitor are maintained remains unclear. Glutathione a tripeptide, γ-L-glutamyl-L-cysteinyl-glycine is a potent anti-oxidant in the cells and it serves several vital functions in the cell. Glutathione naturally exists in two forms; the thiol-reduced (GSH) and disulphide-oxidized (GSSG) forms, of which GSH is the predominant form and accounts for >98% of total glutathione (209). Here, for the first time with the help of immunostaining we have shown the presence of glutathione reservoirs in the blood progenitor cells. We have used the glutathione antibody which stains both oxidised and reduced form of glutathione, marking the availability of total glutathione levels in the progenitor blood cells. Moreover, we investigated the role of olfaction derived GABA catabolism derived succinate at the level of ROS scavenging regulation.

4.2 Antioxidant glutathione is present in the blood-progenitors

ROS scavenging in various cells and tissues is mediated by antioxidant molecules and enzymes, such as glutathione, catalase and superoxide dismutase. Single cell analysis studies in *Drosophila* lymph gland progenitor cells have shown the presence of GST-rich clusters, indicating the requirement of different regulatory mechanisms to control

GSH synthesis in the progenitor cells (109). But the studies showing GSH regulation are sparse and do not specifically demonstrate the regulation of glutathione synthesis. To understand the mechanism of GSH synthesis in the progenitor cells, first, we checked the presence of this antioxidant in the lymph gland progenitor cells with an antibody based approach, which also provided the information about the spatial localization of GSH in the different zones of the lymph gland (Fig. 32). Previous studies have shown that MZ progenitor cells have higher levels of ROS as compared to the CZ cells (72) (Fig. 32A-A"). Here, in the current work glutathione levels were checked with an antibody targeting total glutathione in the cells, which does not specifically mark the oxidized or reduced form. Interestingly, our analysis showed that progenitor cells have higher level of glutathione expression as compared to their differentiated counter parts (Fig. 32B-B"). Although, glutathione (GSH) levels were seen in both the progenitor and differentiated cells, but increased expression of GSH in progenitor cells was intriguing. The existence of higher levels of ROS and its scavenging proteins such as GSH depicts the existence of tight regulatory mechanisms to control redox homeostasis. This shows that ROS regulation is not limited to its generation control (179), but also involves the regulation of ROS-scavenging mechanisms in the progenitor cells. This led us to ask, how glutathione levels are maintained in the progenitor cells.

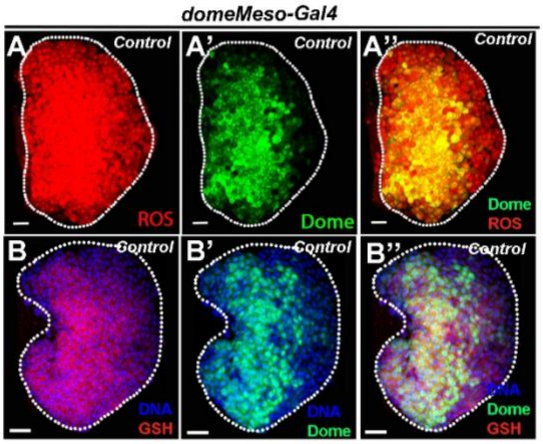

Figure 32. Lymph gland blood-progenitor cells show higher expression of glutathione (GSH).
(A-A") Representative images showing ROS levels in the lymph gland progenitor cells, **(A)** *control* (*domeMeso-Gal4,UAS-GFP/+*) showing ROS (stained with DHE) in red, **(A')** *control* (*domeMeso-Gal4,UAS-GFP/+*) showing dome (progenitor cells) expression in green and **(A")** merge image of A and A' showing higher ROS levels in the progenitor cells. **(B-B")** Representative images showing GSH levels in the lymph gland progenitor cells, **(B)** *control* (*domeMeso-Gal4,UAS-GFP/+*) showing GSH levels in red, **(B')** *control* (*domeMeso-Gal4,UAS-GFP/+*) showing dome (progenitor cells) expression in green and **(B")** merge image of B and B' showing higher GSH levels in the progenitor cells. DAPI marks DNA in **B-B".**

4.3 Glutathione levels in the blood-progenitor cells are controlled by GABA catabolism

Our previous research has demonstrated that olfactory-derived GABA catabolism controls the production of reactive oxygen species (ROS) via phosphorylating pyruvate dehydrogenase kinase (PDK) and pyruvate dehydrogenase (PDH), which in turn controls the activity of the TCA cycle (179). We speculated the involvement of GABA catabolic pathway in the ROS scavenging regulation as well and checked for GSH levels in the genetic backgrounds, where GABA catabolic pathway components are specifically downregulated in the progenitor cells.

GABA secreted from the Kurs6+ neuroendocrine cells (172) is internalized by GABA transporter (Gat) in the progenitor cells, which is catabolized into succinate by two-step process, catalysed by Gabat and Ssadh respectively (94). The second step of GABA catabolic pathway, where succinic semialdehyde dehydrogenase (Ssadh) converts succinic semi-aldehyde (SSA) to succinate is the rate limiting step of this pathway (Fig. 33A) (306). We knocked-down GABA transporter (Gat) and GABA catabolic enzymes (Ssadh) in the blood-progenitor cells utilizing progenitor specific driver *domeMeso-Gal4* (Fig. 33B-D, G). Downregulation of *Gat* (Fig. 33C) and *Ssadh* (Fig. 33D) in the progenitor cells led to reduction in lymph gland glutathione (GSH) levels, indicating the involvement of GABA catabolic pathway in controlling glutathione levels in the progenitor cells (Fig. 33G). Reduction of GSH in the progenitor cells in GABA mutant background is the result from reduction in GABA catabolism derived succinate was checked next. As, the metabolic product of GABA catabolic pathway is succinate, we supplemented *domeMeso>Gat*^{RNAi} (Fig. 33E) and *domeMeso>Ssadh*^{RNAi} (Fig. 33F) larvae with succinate and checked if succinate supplementation rescues blood-progenitor glutathione levels. Indeed, we found that succinate supplementation to these genetic backgrounds rescued their reduced glutathione phenotype (Fig. 33E, F, H) and confirmed that GABA catabolism derived succinate is involved in regulating glutathione levels in the progenitor cells. Our findings show that, GABA catabolic pathway is playing dual role in regulation of ROS homeostasis, by both ROS generation regulation (179) and ROS scavenging mechanisms. We next explored the mechanism of GSH regulation by GABA catabolic pathway.

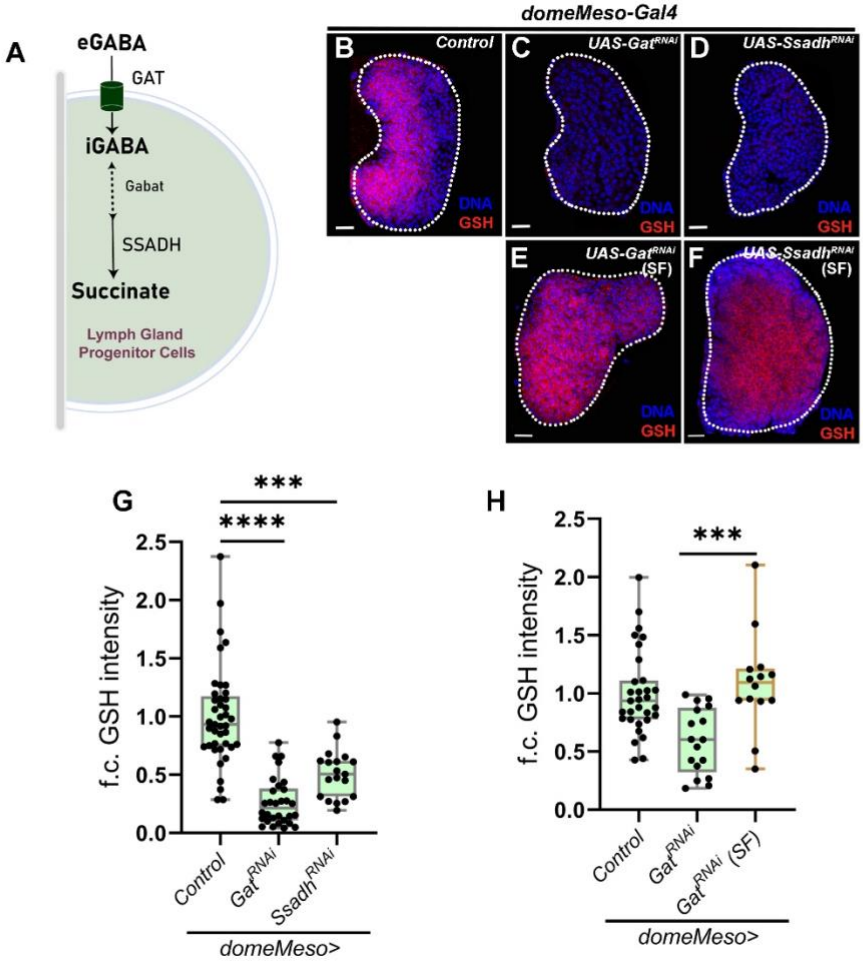

Figure 33. GABA catabolic pathway in *Drosophila* blood-progenitor cells control their GSH levels. **(A)** Schematic representation of the GABA catabolic pathway. Uptake of extra-cellular GABA (eGABA) via GABA Transporter (GAT) in blood-progenitor cells and its intracellular catabolism (iGABA) into succinic-semialdehyde (SSA) by GABA-transaminase (Gabat) and into final product, succinate by succinic semi-aldehyde dehydrogenase (SSADH), the rate limiting step of GABA catabolic pathway. **(B-F)** Representative images showing GSH expression in lymph gland progenitor cells **(B)** *control* (RF, *domeMeso-Gal4,UAS-GFP/+*) show higher GSH levels in the progenitor-cells, expressing **(C)** Gat^{RNAi} (RF, *domeMeso-Gal4,UAS-GFP;UAS-*Gat^{RNAi}) and **(D)** $Ssadh^{RNAi}$ (RF, *domeMeso-Gal4,UAS-GFP;UAS-*$Ssadh^{RNAi}$) leads to reduction in lymph gland progenitor-cells GSH levels, **(E-F)** feeding succinate to **(E)** Gat^{RNAi} (SF, *domeMeso-Gal4,UAS-GFP;UAS-*Gat^{RNAi}) and **(F)** $Ssadh^{RNAi}$ (SF, *domeMeso-Gal4,UAS-GFP;UAS-*$Ssadh^{RNAi}$) leads to increase in GSH levels as compared to (**C** and **D)** respectively**.** For quantifications, refer to **G** and **H. (G)** Quantification of GSH levels in *domeMeso>GFP/+* (control, RF, n=41), *domeMeso>GFP/*Gat^{RNAi} (RF, n=30, p<0.0001) and *domeMeso>GFP/*$Ssadh^{RNAi}$ (RF, n=19, p=0.0003). **(H)** Quantification of GSH levels in *domeMeso>GFP/+* (control, RF, n=31), *domeMeso>GFP/*Gat^{RNAi} (RF, n=17, p=0.0023) and *domeMeso>GFP/*Gat^{RNAi} (SF, n=14, p=0.0005, in comparison to Gat^{RNAi}, RF). RF is regular food; SF is succinate food. Data is presented as median plots (*p<0.05; **p<0.01; ***p<0.001, ****p<0.0001), Kruskal-Wallis test, Dunn's multiple comparisons test. Scale bar: 20µm.'n'=lymph gland lobes. DAPI marks DNA.

4.4 Regulation of glutathione synthesis by GABA catabolic pathway

Since, the antibody employed for GSH detection labels for total glutathione, reduction in GSH levels in GABA catabolic mutants hinted towards regulation at the level of GSH synthesis or degradation. The regulation at the synthesis level was explored first and to

understand if GSH synthesis is affected in the progenitor cells, presence of individual components of GSH synthesis pathway was analysed in GABA catabolic mutant backgrounds. Glutathione is a non-protein thiol, comprising cysteine, glutamate and glycine (Fig. 34A). Cysteine and glutamate combine to form γ -glutamyl cysteine, this is the rate-limiting step of GSH synthesis reaction and is catalysed by enzyme cysteine glutamyl lyase. The next step is catalysed by enzyme glutathione synthetase, where glycine addition results in GSH formation (209). We found that, perturbation of GABA transporter (*Gat*) and GABA catabolism (*Ssadh*) did not significantly affect glutamate levels in the lymph gland (Fig. 34B-F). Levels of glycine also remain unchanged upon downregulation of *Gat* and *Ssadh* in the progenitor cells (Fig. 34G). This showed that glutamate and glycine are dispensable amino acids in GABA catabolism mediated GSH regulation.

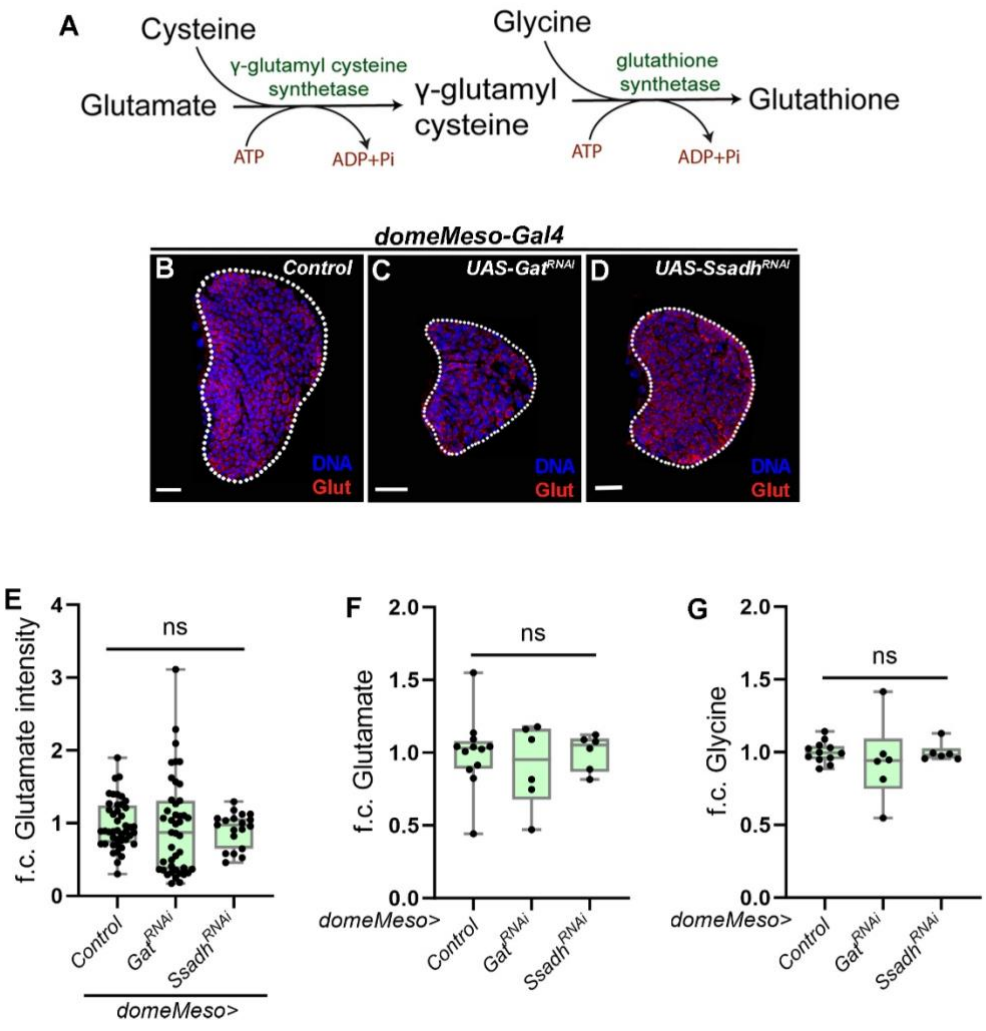

Figure 34. GABA catabolic pathway does not control levels of glutamate and glycine to regulate GSH synthesis.

(A) Schematic representation of the GSH synthesis from cysteine, glutamate and glycine. GSH synthesis is two-step process, glutamate and cysteine combine to form γ-glutamyl cysteine, a reaction catalysed by enzyme y-glutamyl cysteine synthetase. γ-glutamyl cysteine combines with glycine to form the final product glutathione, GSH. This step is catalysed by enzyme glutathione synthetase. The first step of γ-glutamyl cysteine synthesis catalysed by enzyme γ-glutamyl cysteine synthetase is the rate limiting step. **(B)** Representative images showing glutamate expression in lymph gland progenitor cells **(B)** control (RF, *domeMeso-Gal4,UAS-GFP/+*) lymph gland showing glutamate levels in the progenitor-cells, expressing **(C)** Gat^{RNAi} (*domeMeso-Gal4,UAS-GFP;UAS-*Gat^{RNAi}) and **(D)** $Ssadh^{RNAi}$ (*domeMeso-Gal4,UAS-GFP;UAS-*$Ssadh^{RNAi}$) in the progenitor cells does not affect lymph gland progenitor-cells glutamate levels. For quantifications, refer to **E. (E)** Quantification of glutamate levels in *domeMeso>GFP/+* (control, RF, n=44), *domeMeso>GFP/*Gat^{RNAi} (RF, n=43, p=0.6455) and *domeMeso>GFP/*$Ssadh^{RNAi}$ (RF, n=19, p>0.9999). **(F)** Relative steady state amount (fold change, f.c.) of glutamate in *domeMeso>GFP/+* (control, RF, n=12), *domeMeso>GFP/*Gat^{RNAi} (RF, n=6, p>0.9999) and *domeMeso>GFP/*$Ssadh^{RNAi}$ (RF, n=6, p>0.9999). **(G)** Relative steady state amount (fold change, f.c.) of glycine in *domeMeso>GFP/+* (control, RF, n=12), *domeMeso>GFP/*Gat^{RNAi} (RF, n=6, p=0.2396) and *domeMeso>GFP/*$Ssadh^{RNAi}$ (RF, n=6, p>0.9999). RF is regular food, SF is succinate food. Data is presented as median plots (*p<0.05; **p<0.01; ***p<0.001, ****p<0.0001), Kruskal-Wallis test, Dunn's multiple comparisons test. ns=non-significant. Scale bar: 20μm.'n'=lymph gland lobes. DAPI marks DNA.

However, when analysed for cysteine levels in the progenitor cells utilizing an antibody against cysteine, a significant reduction was seen in progenitor specific loss of *Gat* and *Ssadh* conditions (Fig. 35A-C, F). This showed that GABA catabolic pathway regulates GSH synthesis in the lymph gland progenitor cells and it is mediated by controlling cysteine levels in the lymph gland.

Effect of GABA catabolic pathway on cysteine levels was confirmed by supplementing the *domeMeso>*Gat^{RNAi} and *domeMeso>*$Ssadh^{RNAi}$ larvae with succinate and a subsequent analysis for cysteine in these genetic backgrounds (Fig. 35D-F). Succinate supplementation significantly rescued the reduced cysteine phenotype of Gat^{RNAi} and $Ssadh^{RNAi}$ corroborating with the glutathione rescue seen upon succinate supplementation in *domeMeso>*Gat^{RNAi} and *domeMeso>*$Ssadh^{RNAi}$ conditions and confirmed that GABA catabolism mediated cysteine regulation is controlling GSH synthesis in the progenitor cells.

Further, the effect of cysteine analog N-acetylcysteine (NAC) supplementation was analysed in the *domeMeso>*Gat^{RNAi} and *domeMeso>*$Ssadh^{RNAi}$ conditions. N-acetylcysteine is an important anti-oxidant in the cells regulating ROS homeostasis and also acts as a substitute to cysteine (308). NAC supplementation in the conditions, where *Gat* and *Ssadh* are downregulated in the progenitor cells, rescued the reduce GSH phenotype of Gat^{RNAi} and $Ssadh^{RNAi}$ observed in regular food conditions (Fig. 35G-L). This demonstrated that cysteine is the limiting component in the GABA catabolic mutant backgrounds, and leading to GSH synthesis in the lymph gland progenitor cells.

The mechanism of cysteine synthesis regulation by GABA catabolic pathway was explored next.

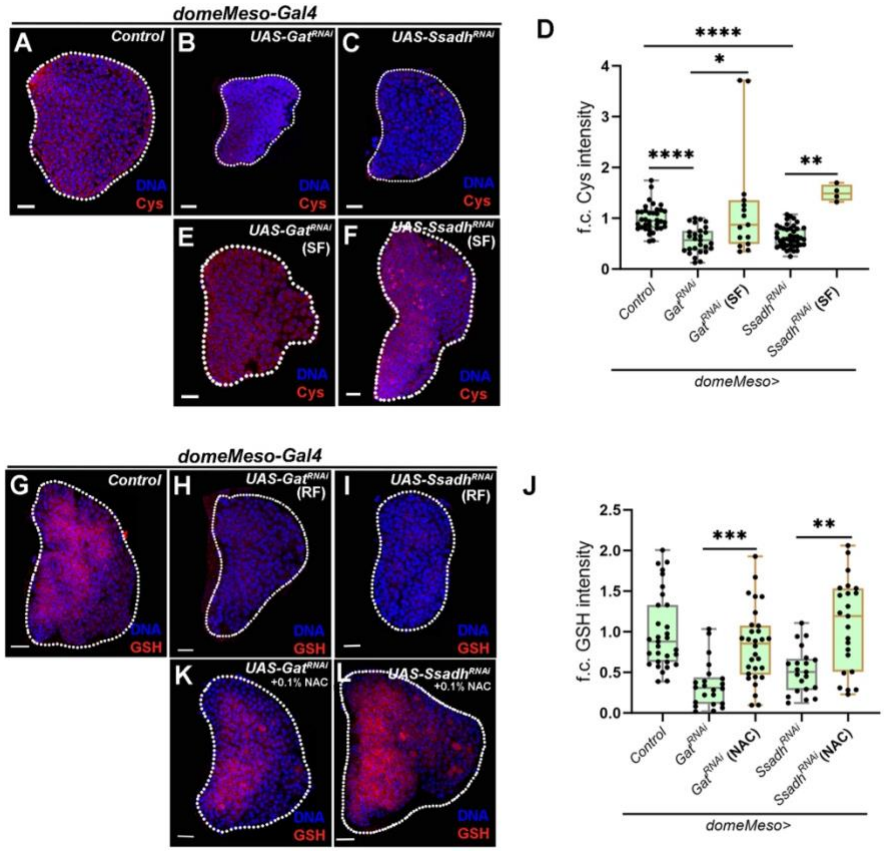

Figure 35. GABA catabolic pathway control levels of cysteine to regulate GSH synthesis.
(A-E) Representative images showing cysteine expression in lymph gland progenitor cells **(A)** control (RF, *domeMeso-Gal4,UAS-GFP/+*) lymph gland showing glutamate levels in the progenitor-cells, expressing **(B)** Gat^{RNAi} (RF, *domeMeso-Gal4,UAS-GFP;UAS-Gat^{RNAi}*) and **(C)** *Ssadh^{RNAi}* (RF, d*omeMeso-Gal4,UAS-GFP;UAS-Ssadh^{RNAi}*) leads to reduction in cystine levels in the progenitor cells, **(D-E)** succinate supplementation to **(D)** *Gat^{RNAi}* (SF, *domeMeso-Gal4,UAS-GFP;UAS-Gat^{RNAi}*) and **(E)** *Ssadh^{RNAi}* (SF, *domeMeso-Gal4,UAS-GFP;UAS-Ssadh^{RNAi}*) leads to rescue of cysteine levels as compared to (**B** and **C**) respectively**.** For quantifications, refer to **F. (F)** Quantification of Cysteine levels in *domeMeso>GFP/+* (control, RF, n=36), *domeMeso>GFP/Gat^{RNAi}* (RF, n=27, p<0.0001), *domeMeso>GFP/Ssadh^{RNAi}* (RF, n=43, p<0.0001), *domeMeso>GFP/Gat^{RNAi}* (SF, n=15, p=0.0344 in comparison to *Gat^{RNAi}*, RF) and *domeMeso>GFP/Ssadh^{RNAi}* (SF, n=4, p=0.0015 in comparison to *Ssadh^{RNAi}*, RF). **(G-K)** Representative images showing GSH expression in lymph gland progenitor cells **(G)** control (RF, *domeMeso-Gal4,UAS-GFP/+*) lymph gland showing GSH levels in the progenitor-cells, expressing **(H)** *Gat^{RNAi}* (RF, *domeMeso-Gal4,UAS-GFP;UAS-Gat^{RNAi}*) and **(I)** *Ssadh^{RNAi}* (RF, *domeMeso-Gal4,UAS-GFP;UAS-Ssadh^{RNAi}*) leads to reduction in GSH levels in the progenitor cells, **(J-K)** N-acetyl cysteine (NAC) supplementation to **(J)** *Gat^{RNAi}* (SF, *domeMeso-Gal4,UAS-GFP;UAS-Gat^{RNAi}*) and **(K)** *Ssadh^{RNAi}* (SF, *domeMeso-Gal4,UAS-GFP;UAS-Ssadh^{RNAi}*) leads to rescue of GSH levels as compared to (**H** and **I)** respectively**.** For quantifications, refer to **L. (L)** Quantification of GSH levels in domeMeso>GFP/+ (control, RF, n=31), *domeMeso>GFP/Gat^{RNAi}* (RF, n=22, p<0.0001), *domeMeso>GFP/Ssadh^{RNAi}* (RF, n=30, p=0.0065), *domeMeso>GFP/Gat^{RNAi}* (NAC, n=21, p=0.0009 in comparison to *Gat^{RNAi}*, RF) and *domeMeso>GFP/Ssadh^{RNAi}* (NAC, n=23, p=0.0068 in comparison to *Ssadh^{RNAi}*, RF). RF is regular food; SF is succinate food and NAC is N-acetyl cysteine supplemented food. Data is presented as median plots (*p<0.05; **p<0.01; ***p<0.001, ****p<0.0001), Kruskal-Wallis test, Dunn's multiple comparisons test. Scale bar: 20µm.'n'=lymph gland lobes. DAPI marks DNA.

4.5 Mechanism of Cysteine synthesis regulation by GABA catabolic pathway

Cysteine is a non-essential amino acid and is metabolized in the cells via a conserved pathway for metabolism of sulfur-amino acids termed transsulfuration pathway (TSP) (Fig 36A). In TSP, methionine converts into cysteine involving an intermediate step of cystathionine formation (310). This process is catalysed by two enzymes, first step involves CβS (cystathionine β-synthase), and catalyses the formation of cystathionine from homocysteine and serine, and second reaction is catalysed by CGL (cystathionine γ-lyase), which forms cysteine from cystathionine (311). To understand the role of GABA catabolic pathway in cysteine synthesis regulation, we undertook a metabolomics based approach and amino acid analysis from *control* and *domeMeso>Gat*^{RNAi} lymph glands was performed (Fig. 36B, Ap. Fig. 7 and Appendix Table 1). Interestingly, our analysis showed the reduction of amino acid serine in *Gat*^{RNAi} mutant lymph glands (Fig. 36B), while majority of other amino acids levels were unaltered (Ap. Fig. 7 and Appendix Table 1). A significant reduction in the levels of branched chain amino acids were seen, which could be the resulting from some independent function of GABA catabolic pathway. Our current method, employed for LC/MS bases amino acid analysis could not detect for methionine and cysteine in the lymph glands provided the unstable nature of these amino acids. Nonetheless, a reduction in serine levels upon progenitor specific knock-down of *Gat* led us to hypothesize about metabolic contribution of serine via GABA catabolic pathway in GSH synthesis regulation in the progenitor cells.

To understand the metabolic regulation of GABA catabolic pathway on GSH synthesis, we undertook amino acid supplementation in the *Gat*^{RNAi} mutant backgrounds and supplemented *Gat*^{RNAi} larvae with methionine and serine, as both these amino acids are the prime components of transsulfuration pathway. Concomitant with our amino acid analysis, serine supplementation to the *domeMeso>Gat*^{RNAi} larvae rescued reduced GSH phenotype of blood-progenitor cells (Fig 36C-F). Surprisingly, methionine supplementation could not rescue the reduced GSH phenotype of *Gat*^{RNAi} lymph glands (Fig. 36F-I) and demonstrated the methionine independent regulation of GSH synthesis by GABA catabolic pathway. Furthermore, cysteine levels were analysed post serine supplementation to *domeMeso>Gat*^{RNAi} lymph glands and showed a rescue of cysteine levels with serine supplementation as compared to progenitor specific loss of Gat (*domeMeso>Gat*^{RNAi}) on regular food (Fig. 36J-M). These data concluded that serine acts as the intermediate in GABA catabolism mediated GSH synthesis regulation.

How GABA catabolism regulates serine synthesis to control GSH formation and redox homeostasis of blood-progenitors was unclear.

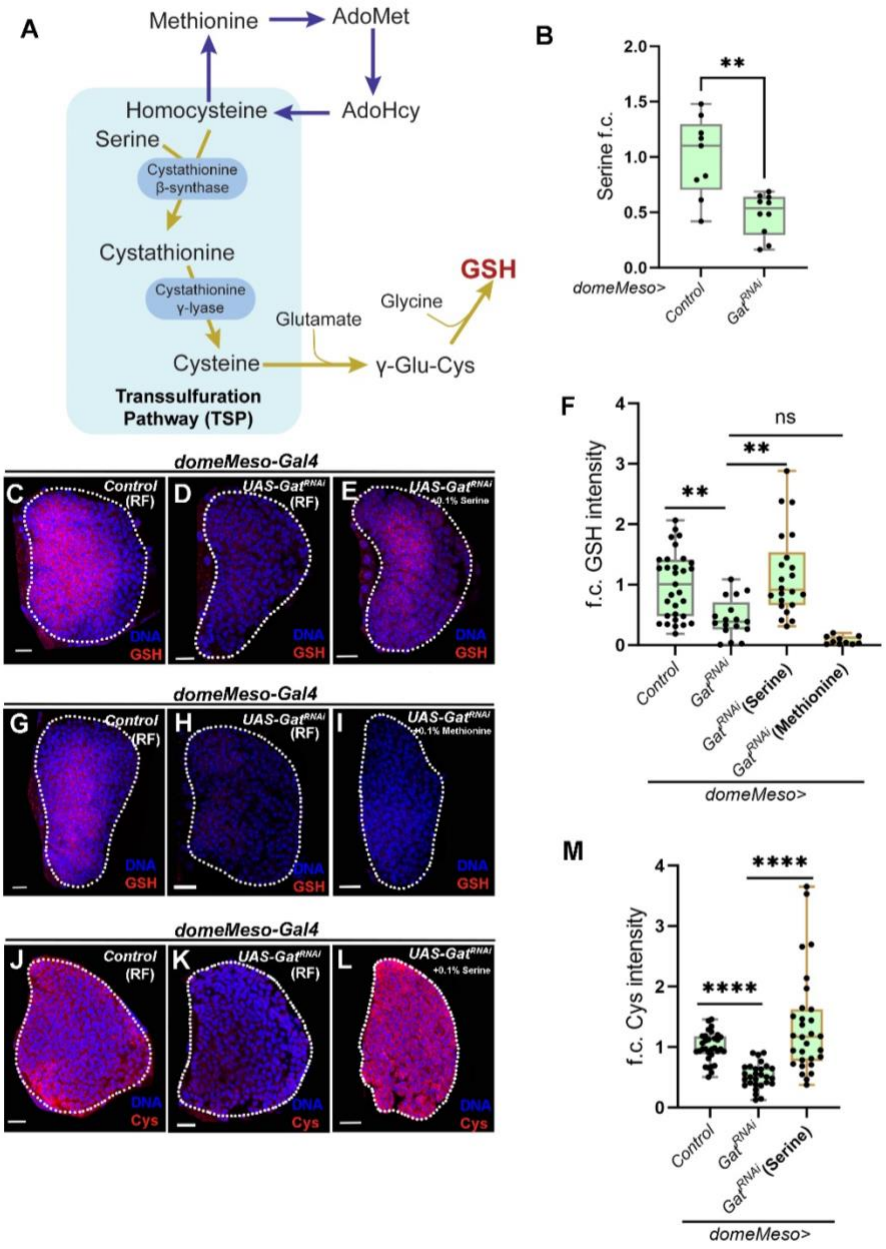

Figure 36. Serine is the limiting amino acid, leading to GABA catabolism regulated GSH formation. **(A)** Schematic representation of the cysteine and GSH synthesis by transsulfuration pathway (TSP). Methionine, the sulphur amino acid undergoes methionine cycle to form homocysteine. Homocysteine combines with serine to form cystathionine and cysteine in two subsequent reactions, catalysed by enzymes cystathionine-β-synthase and cystathionine-γ-lyase respectively. Cysteine further combines with glutamate and glycine to form glutathione (GSH). **(B)** Relative steady state amount (fold change, f.c.) of serine in *domeMeso>GFP/+* (*control*, RF, n=9) and *domeMeso>GFP/Gat^{RNAi}* (RF, n=10, p=0.0030). *Gat^{RNAi}* in the progenitor cells leads to reduction in lymph gland serine levels as compared to control. **(C-E)** Representative images showing GSH expression in lymph gland progenitor cells **(C)** *control* (RF, *domeMeso-Gal4,UAS-GFP/+*) lymph gland showing GSH levels in the progenitor-cells, expressing **(D)** Gat^{RNAi} (RF, *domeMeso-Gal4,UAS-GFP;UAS-Gat^{RNAi}*) leads to reduction in GSH levels in the progenitor cells, **(E)** methionine supplementation to **(E)** *Gat^{RNAi}* (Methionine, *domeMeso-Gal4,UAS-GFP;UAS-Gat^{RNAi}*) does not rescue GSH levels of *Gat^{RNAi}* on RF (**D).** For quantifications, refer to **F. (F)** Quantification of GSH levels in *domeMeso>GFP/+* (*control*, RF, n=31), *domeMeso>GFP/Gat^{RNAi}* (RF, n=17, p=0.0056), *domeMeso>GFP/Gat^{RNAi}* (Methionine, n=10, p=0.1054

in comparison to *Gat*^{RNAi}, RF) and *domeMeso>GFP/Gat*^{RNAi} (Serine, n=22, p=0.0018 in comparison to *Gat*^{RNAi}, RF). **(G-I)** Representative images showing GSH expression in lymph gland progenitor cells **(G)** *control* (RF, *domeMeso-Gal4,UAS-GFP/+*) lymph gland showing GSH levels in the progenitor-cells, expressing **(H)** *Gat*^{RNAi} (RF, *domeMeso-Gal4,UAS-GFP;UAS-Gat*^{RNAi}) leads to reduction in GSH levels in the progenitor cells, **(E)** Serine supplementation to **(I)** *Gat*^{RNAi} (Serine, *domeMeso-Gal4,UAS-GFP;UAS-Gat*^{RNAi}) leads to rescue of GSH levels of *Gat*^{RNAi} on RF (**H).** For quantifications, refer to **F. (J-L)** Representative images showing cysteine expression in lymph gland progenitor cells **(J)** *control* (RF, *domeMeso-Gal4,UAS-GFP/+*) lymph gland showing cysteine levels in the progenitor-cells, expressing **(K)** *Gat*^{RNAi} (RF, *domeMeso-Gal4,UAS-GFP;UAS-Gat*^{RNAi}) leads to reduction in cysteine levels in the progenitor cells, **(L)** Serine supplementation to **(L)** *Gat*^{RNAi} (Serine, *domeMeso-Gal4,UAS-GFP;UAS-Gat*^{RNAi}) leads to rescue of cysteine levels of *Gat*^{RNAi} on RF (**K).** For quantifications, refer to **M. (M)** Quantification of cysteine levels in *domeMeso>GFP/+* (*control*, RF, n=32), *domeMeso>GFP/Gat*^{RNAi} (RF, n=28, p<0.0001), and *domeMeso>GFP/Gat*^{RNAi} (Serine, n=30, p<0.0001). RF is regular food. Data is presented as median plots (*p<0.05; **p<0.01; ***p<0.001, ****p<0.0001), Kruskal-Wallis test, Dunn's multiple comparisons test and Mann-Whitney test for **B**. Scale bar: 20µm.'n'=lymph gland lobes. DAPI marks DNA.

4.6 Pyruvate fueling to different metabolic outputs control GSH synthesis and lymph gland ROS homeostasis

Metabolic underpinnings coupling GABA catabolic pathway to GSH synthesis were explored next. Our previous work has shown that GABA catabolic pathway regulates Pdha, the entry step of pyruvate to acetyl-CoA to control TCA cycle activity in the lymph gland and consequent ROS generation (179). Moreover, it is known that pyruvate shuttling to the gluconeogenic arm leads to serine formation in cells (312,313) (Fig. 37A). We hypothesized the existence of such regulation on pyruvate shuttling towards different metabolic pathways by GABA catabolism to control GSH formation in lymph gland progenitor cells. Therefore, we checked for the glutathione levels in conditions where pyruvate entry to TCA cycle was perturbed, we downregulated the enzyme catalysing entry of pyruvate into TCA, *Pdha*. Our analysis showed that blocking the flux of pyruvate into TCA lead to increased GSH levels in the lymph glands (Fig. 37B, C, F). Further, we knocked-down *Pdha* in *Gat*^{RNAi} conditions and assessed for GSH levels. When we checked for GSH levels in these genetic backgrounds, interestingly, we found that, inhibiting pyruvate entry into TCA cycle by downregulating pyruvate dehydrogenase (*Pdha*), along with *Gat*^{RNAi} in the progenitor cells rescued the reduced GSH phenotype of *Gat*^{RNAi} (Fig. 37D-F). This showed that GABA catabolic pathway regulates GSH levels in the blood-progenitor cells by controlling pyruvate entry into TCA cycle and subsequent, TCA activity. We extended our analysis to check cysteine levels in these genetic backgrounds and found that downregulation of TCA entry enzyme *Pdha* in GABA mutant backgrounds (*Gat*^{RNAi}) also rescued the reduced cysteine phenotype of *Gat*^{RNAi} (Fig. 37G-K). Further, we checked for serine levels in *PdhA*^{RNAi}*;Gat*^{RNAi} and a rescue in serine levels was observed as compared to *Gat*^{RNAi}

alone (Ap. Fig. 8A). While the regulation of TCA cycle activity by GABA catabolic pathway to control GSH synthesis is evident from our above experiments, TCA cycle activity is not directly controlling GSH synthesis in the progenitor cells, as downregulating *Pdha* inhibitory enzyme pyruvate dehydrogenase kinase (*Pdk*), which inhibits the function of enzyme *Pdha* by inhibitory phosphorylation and thus leads to increased flux of pyruvate to TCA did not lead to reduction in lymph gland GSH levels (Ap. Fig. 8B, C), indicating the existence of complex metabolic rewiring between these pathways which are controlled by GABA catabolism to maintain redox homeostasis of the blood-progenitor cells. To delineate this, we undertook a 13C-isotope based isotopic-labelling analysis approach to understand the metabolic dynamics involving glutathione synthesis in lymph glands.

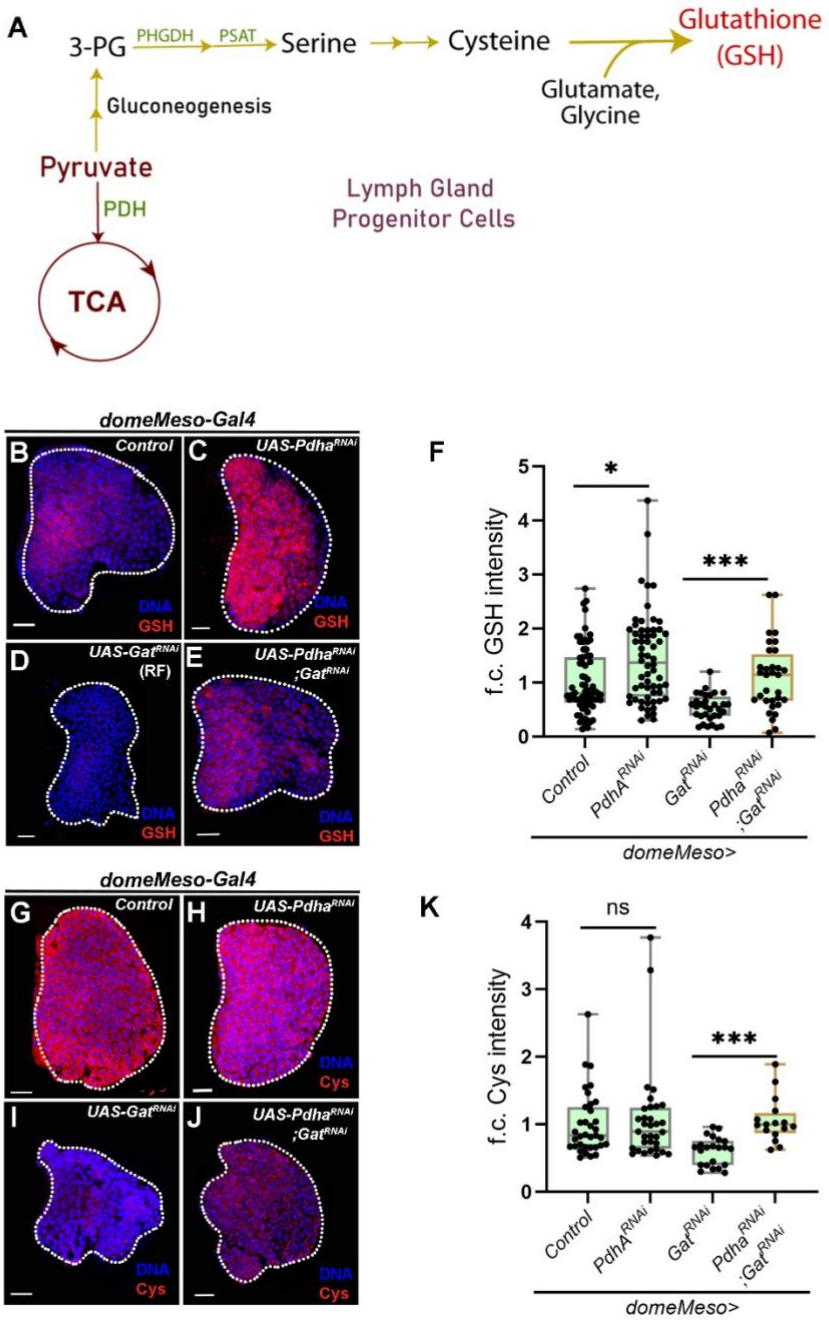

Figure 37. GABA catabolism derived PDH regulation is central to control glutathione levels in the lymph gland progenitor cells.

(A) Schematic representation of the serine, cysteine and GSH synthesis from pyruvate by the involvement of gluconeogenic arm. Pyruvate forms 3-phosphoglycerate (3-PG, a gluconeogenic intermediate), which converts to serine by two step process involving enzymes PHGDH and PSAT (aay). Serine undergoes transsulfuration reaction (TSP) to form cysteine, which further combines with glutamate and glycine to form glutathione (GSH). **(B-E)** Representative lymph gland images showing GSH levels in the **(B)** *control* (*domeMeso-Gal4,UAS-GFP/+*), expressing **(C)** $Pdha^{RNAi}$ (*domeMeso-Gal4,UAS-GFP;UAS-*$Pdha^{RNAi}$) leads to an increase in blood-progenitor GSH levels**,** expressing **(D)** Gat^{RNAi} (*domeMeso-Gal4,UAS-GFP;UAS-*Gat^{RNAi}) leads to a reduction in blood-progenitor GSH levels, expressing **(E)** $Pdha^{RNAi}$;Gat^{RNAi} (*domeMeso-Gal4,UAS-GFP;UAS-*$Pdha^{RNAi}$;*UAS-*Gat^{RNAi}) rescues the reduced GSH phenotype of **(D)** Gat^{RNAi}. For quantifications, refer to **F. (F)** Quantification of GSH levels in *domeMeso>GFP/+* (control, RF, n=71), *domeMeso>GFP/*$Pdha^{RNAi}$ (n=62, p=0.0102), *domeMeso>GFP/*Gat^{RNAi} (RF, n=32, p=0.0007), and *domeMeso>GFP/*$Pdha^{RNAi}$;Gat^{RNAi} (n=32,

p=0.0008 in comparison to *Gat*^{RNAi}). **(G-J)** Representative lymph gland images showing cysteine levels in the **(G)** control (*domeMeso-Gal4,UAS-GFP/+*), expressing **(H)** *Pdha*^{RNAi} (*domeMeso-Gal4,UAS-GFP;UAS-Pdha*^{RNAi}) leads to a slight increase in blood-progenitor cysteine levels**,** expressing **(I)** *Gat*^{RNAi} (*domeMeso-Gal4,UAS-GFP;UAS-Gat*^{RNAi}) leads to a reduction in blood-progenitor cysteine levels, expressing **(J)** *Pdha*^{RNAi}*;Gat*^{RNAi} (*domeMeso-Gal4,UAS-GFP;UAS-Pdha*^{RNAi}*;UAS-Gat*^{RNAi}) rescues the reduced cysteine phenotype of **(I)** *Gat*^{RNAi}. For quantifications, refer to **K. (K)** Quantification of cysteine levels in *domeMeso>GFP/+* (control, RF, n=35), *domeMeso>GFP/Pdha*^{RNAi} (n=33, p>0.9999), *domeMeso>GFP/Gat*^{RNAi} (RF, n=22, p=0.0016), and *domeMeso>GFP/Pdha*^{RNAi}*;Gat*^{RNAi} (n=16, p=0.0003 in comparison to Gat^{RNAi}). RF is regular food. Data is presented as median plots (*p<0.05; **p<0.01; ***p<0.001, ****p<0.0001), Kruskal-Wallis test, Dunn's multiple comparisons test. Scale bar: 20µm.'n'=lymph gland lobes. DAPI marks DNA.

4.7 Metabolic pathway fluxes in wandering 3rd instar larval lymph glands

13C-based isotopic labelling analysis is an approach utilised to unravel the metabolic pathway activity and metabolite flux into different metabolic arms. To understand the dynamics of metabolic pathways in the blood-progenitor cells, we undertook a 13C-isotope based metabolic analysis in wandering 3rd instar larval lymph glands. For our analysis, we utilized U^{13}C-pyruvate labelling and dissected lymph glands were incubated in 10mM of 13C-pyruvate label for 30 minutes and post incubation 13C label incorporation in downstream metabolites were checked in the lymph glands. Pyruvate is at the nexus of various metabolic pathways, including TCA cycle, gluconeogenesis, lactate formation and fatty acid synthesis (Fig. 38A).

Pyruvate is a 3 carbon acid, that contribute two carbons to the TCA cycle through the pyruvate dehydrogenase (PDH) dependent generation of acetyl-CoA, which combines with oxaloacetate to form citrate and other TCA metabolites. Alternatively, pyruvate can fuel its full 3 carbons to the TCA cycle by generating oxaloacetate through the activity of pyruvate carboxylase (PC) (314). We followed 13C label in the TCA metabolites and performed the analyses for different isotopic combinations of labelled carbon (13C) such as percentage content of m+2, m+3, m+4. m+2 label provided the information about carbon label derived from PDH mediated TCA to acetyl-CoA conversion and further metabolism and higher carbon labels indicated about the overall TCA activity in the lymph glands. m+2 label in oxaloacetate is derived from PDH, while m+3 label incorporation is mediated by PC, which directly converts pyruvate to oxaloacetate by decarboxylation reaction and thus contribute to 3 carbons in OAA. As various steps of TCA cycle are reversible and also feeds cyclically, 3 carbon label (m+3) is contributed from PC derived OAA conversion and m+2 label is contributed from PDH derived acetyl-CoA conversion in TCA metabolites and leading to higher 13C incorporation as the cycle continues. Our analysis showed that in control lymph glands

13C-pruvate label incorporation in citrate and other TCA metabolites increased with time (Fig. 38B), whereas OAA showed almost 40% label incorporation (m+3) even at 5 min. incubation time point (Fig. 38C). These data indicated that pyruvate conversion to acetyl-CoA via PDH (m+2) (Fig. 38B) happens at relatively lower rate, while, pyruvate majorly converts into OAA by PC (m+3) (Fig. 38C). Nonetheless, the incorporation for higher label 13C in citrate and αKG was observed, which increases with a corresponding increase in incubation time till 2 hrs (Fig. 38 and Ap. Fig. 9), this indicated an overall flux of pyruvate towards TCA cycle. Pyruvate converts into lactate in the reversible reaction catalysed by Ldh and thus 13C incorporation could be seen for all the 3C of lactate (Ap. Fig. 9G, H). However, pyruvate flux towards lactate was seen at relatively lower rate as compared to pyruvate flux towards TCA cycle. These data confirmed that in control homeostatic conditions, lymph glands TCA activity is relatively high as compared to lactate formation. However, the possibility of lactate being shunted out from the lymph gland system cannot be ignored and could be the reason of lower relative label observed in our analysis.

Since, the isotopic labelling analysis showed dynamics of pyruvate shuttling towards different metabolic arms, the regulation of pyruvate shuttling in controlling GSH synthesis by GABA catabolic pathway was explored further.

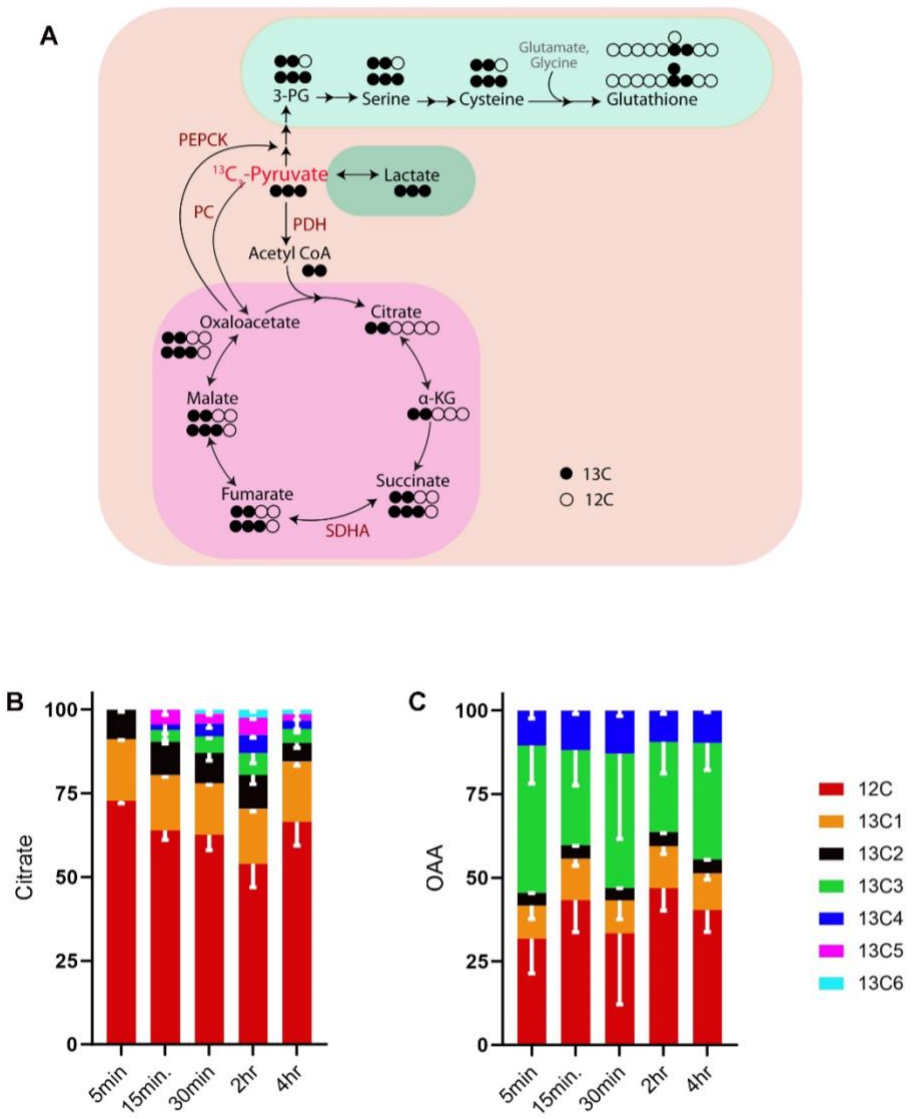

Figure 38. Metabolic pathways activity during homeostatic lymph gland development.
(A) Schematic representation of the U^{13}C-pyruvate isotopic labelling in TCA metabolites, lactate, gluconeogenic components, serine, cysteine and GSH. U_{13}C-pyruvate contributes two 13C carbons to TCA metabolites via PDH and labels three carbons (13C) via PC mediated metabolism. Since, TCA is a cyclic pathway and many of the TCA steps are reversible, higher carbon label occurs in TCA metabolites in the subsequent series of reactions. U_{13}C-pyruvate labels all the three carbons of lactate, which is a reversible reaction. Following the gluconeogenic arm, U_{13}C-pyruvate labels either two or three carbons of serine and cysteine. GSH is a ten-carbon compound and U_{13}C-pyruvate labels GSH carbons differently based on the metabolic pathways followed and the intermediates utilized. **(B-C)** U_{13}C-pyruvate labelling analysis in wandering 3rd instar control lymph glands showing the label incorporation, **(B)** Citrate is a TCA metabolite, which is synthesized from the acetyl-CoA and oxaloacetate, a reaction catalysed by enzyme citrate synthase (CS). Over a period of 5 min. to 4hr. an increase in label incorporation was observed, as the higher C label (13C4, 13C5 and 13C6) appears over time and gradually with increase in incubation time a decrease in label incorporation is seen at 4 hr. time point, indicating the flux of pyruvate towards TCA metabolites, **(C)** oxaloacetate (OAA), shows label incorporation from both PC (13C3, blue) and PDH (13C2, black) derived metabolism. Interestingly, the 13C3 (green) label incorporation in OAA occurs at much higher rate as compared to 13C2 (black), PDH derived label incorporation. At 5 min. time point around 40% of 13C3 (green) label is observed, indicating the higher flux of pyruvate to OAA via PC in wandering 3rd instar larval lymph glands as compared to PDH derived 13C2 (black) label.

4.8 GABA catabolism controls pyruvate fueling to different metabolic pathways to maintain redox homeostasis of blood-progenitor cells

We extended our 13C based flux analysis in *Gat*^{RNAi} lymph glands and analysed for label incorporation in TCA cycle metabolites and lactate. Due to technical limitations and experimental complexity, the label incorporation analysis in serine from lymph glands could not be done and is currently under standardization. Upon U^{13}C-pyruvate label incorporation analysis for TCA metabolites and lactate in *Gat*^{RNAi} lymph glands (Fig. 39 and Ap. Fig. 10), we found that label incorporation was increased for higher isotopic carbons in citrate and αKG in *domeMeso>Gat*^{RNAi} condition compared to control (Fig. 39A, C, D and Ap. Fig. 10A, B, E-G). Further, Label incorporation in lactate was decreased upon downregulation of *Gat*^{RNAi} in the progenitor cells (Ap. Fig. 10D, H). Pyruvate to lactate conversion mediated glycolytic switch and decreased TCA activity is central to lamellocyte formation during the immune-response scenarios (94,179) and our isotopic labelling analysis strengthened the metabolic control of GABA catabolic pathway on pyruvate shuttling into lactate and TCA activity which governs the lamellocyte formation potential of progenitor cells during immune response conditions. Interestingly, in *domeMeso>Gat*^{RNAi} the m+3 label incorporation for OAA, which was PC derived was less as compared to the control lymph glands (Fig. 39B, E), which showed another contribution of GABA catabolic pathway in controlling the metabolic homeostasis of blood-progenitors. Taken together, our flux analysis showed the dynamics of TCA cycle via PC and Pdh in *Gat*^{RNAi} and control lymph glands.

Isotopic labelling analysis alluded to the fact that GABA catabolism positively regulates PC derived OAA metabolism and inhibits PDH derived TCA cycle activity. As demonstrated by our earlier research (179), GABA catabolism inhibits PDH to regulate TCA activity and subsequent ROS generation. The positive control of the GABA catabolic pathway at the level of PC metabolism is highly intriguing. This shows that GABA catabolism functions as a critical regulator for pyruvate metabolism to govern ROS homeostasis and blood-progenitor growth.

Since, PC derived OAA generation is the reaction occurring at relatively higher rate in the progenitor-cells and GABA catabolism (*Gat*^{RNAi}) downregulation led to deceased PC derived OAA generation, we checked for GSH levels in progenitor specific downregulation of PC. Our data showed that progenitor specific loss of PC (*domeMeso>PC*^{RNAi}), indeed led to decreased GSH levels in the lymph glands progenitor cells along with a corresponding reduction in lymph gland size (Ap. Fig. 8D)

implementing the importance of PC derived pyruvate metabolism in blood-progenitor ROS homeostasis and lymph gland development. Thus, GABA catabolic pathway act as a central regulator of pyruvate metabolism towards metabolic arms of PC, PDH and Ldh to control blood-progenitor ROS homeostasis and consequently, its development.

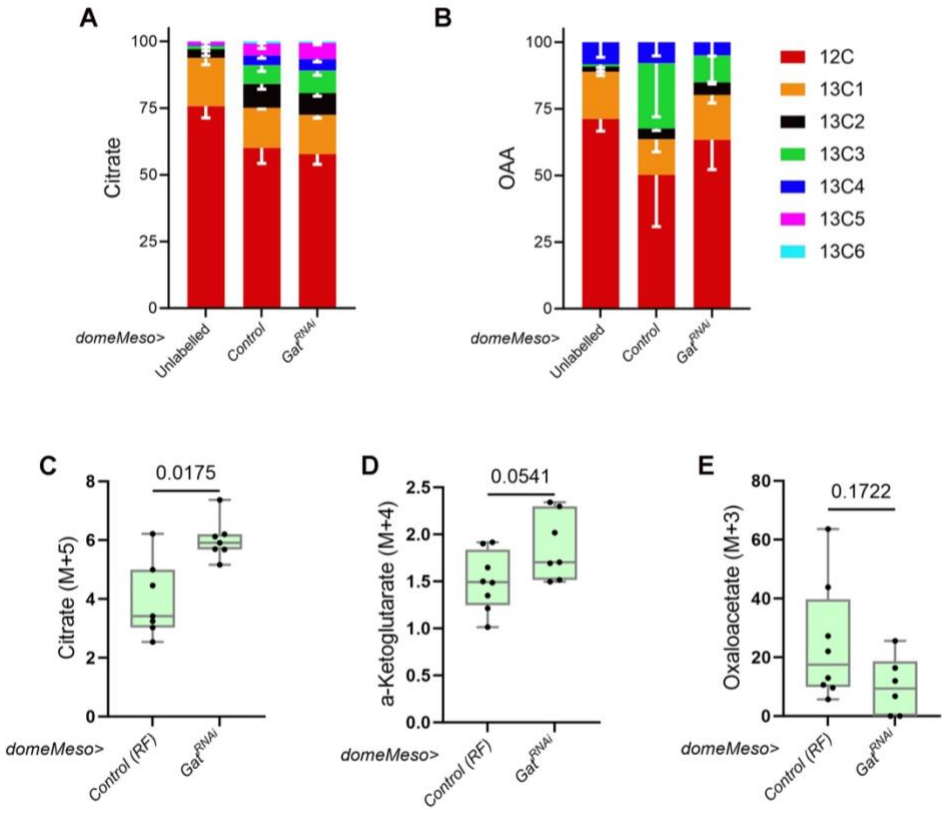

Figure 39. GABA catabolic pathway regulates metabolic pathways activity in the lymph gland. **(A-B)** Wandering 3rd instar *control* and *domeMeso>Gat^{RNAi}* lymph glands showing the label incorporation after U^{13}C-pyruvate label incubation in **(A)** citrate and **(B)** oxaloacetate (OAA), **(A)** in citrate, increased label incorporation is seen for higher 13C in *Gat^{RNAi}* lymph glands as compared to control and **(B)** relative label incorporation for OAA is less for 13C in Gat^{RNAi} lymph glands as compared to control. **(C)** U_{13}C-pyruvate label incubation in *domeMeso>Gat^{RNAi}* (n=7, p=0.0175) lymph glands show an increase in relative label incorporation for 13C5 (m+5) in citrate as compared to *control* (n=7). **(D)** U_{13}C-pyruvate label incubation in *domeMeso>Gat^{RNAi}* (n=7, p=0.0541) lymph glands show an increase in relative label incorporation for 13C4 (m+4) in α-ketoglutarate (αKG) as compared to *control* (n=8). **(E)** U_{13}C-pyruvate label incubation in *domeMeso>Gat^{RNAi}* (n=6, p=0.1722) lymph glands show a reduction in relative label incorporation for 13C3 (m+3) in oxaloacetate (OAA) as compared to *control* (n=8). Data is presented as median plots (*p<0.05; **p<0.01; ***p<0.001, ****p<0.0001), Mann-Whitney test is applied.

4.9 Olfactory control of blood-progenitor metabolism and GSH synthesis regulation

GABA detected by lymph gland progenitor cells is under olfactory control and is released by the Kurs6+ neurosecretory cells upon olfactory stimulation (172). Our previous studies (94,179) have shown that perturbation of olfactory activity leads to impaired lamellocyte formation in the lymph glands, affect blood-progenitor ROS homeostasis and development. We have shown that olfactory ablation leads to heightened PDK and PDH phosphorylation resulting in increased TCA activity and

hence, ROS generation (179). Elevation in lymph gland ROS levels leads to retardation of lymph gland growth. Previously, we have shown that wasp odor sensing (WOF) leads to immune benefit to the animals and results in increased lamellocyte formation due to elevated GABA levels and its catabolism (94). Along with providing immune benefit to the animals, WOF sensitized animals also showed a reduction in blood-progenitor ROS levels and significant increase in lymph gland growth (Fig.30L, O, P). Here, we explored the role of olfaction in regulation of blood-progenitor metabolic pathway activity by employing $U^{13}C$-Pyruvate based isotopic labelling in WOF and GABA supplementation conditions. Upon $U^{13}C$-Pyruvate incubation, label incorporation was checked in TCA metabolites, lactate and glutathione. We found decreased 13C label incorporation for higher carbons in TCA metabolites, citrate and αKG in olfactory sensitized condition of WOF and GABA supplementation (Fig. 40 and Ap. Fig. 11). This ascertained that wasp odor sensing leads to decreased TCA activity, corroborating with our previous analysis where increased pPDH was observed in WOF condition as compared to the control (Fig. 30M, Q). Similarly, label incorporation was found to be increased towards lactate as compared to control in WOF condition (Ap. Fig. 11D, J), which is in line with the requirement of more lactate for bringing the glycolytic switch needed for lamellocyte formation upon parasitic wasp-infections (94,179), however GABA supplementation did not show an increase in lactate m+3 label incorporation (Ap. Fig. 11D, J) either due to more labelled lactate being shunted out from the system or the systemic effect of GABA supplementation on the blood-progenitor compartment. When we checked for m+3 label incorporation in OAA, a measure for PC derived metabolism, an increase in label incorporation was observed in WOF conditions (Fig. 40B, E), indicating the requirement of this regulation in GSH synthesis. Similar to less label seen in lactate (m+3) in GABA supplementation, OAA m+3 label was also less indicating the existence of some systemic effect of GABA supplementation on lymph glands, as lowering of GABA internalization by *Gat* downregulation led to a decrease in pyruvate to OAA flux which is supported by an increase in flux of pyruvate towards OAA (m+3) seen in WOF conditions. Moreover, olfactory perturbation, where olfactory neurons were genetically killed by overexpressing the pro-apoptotic gene, *hid*, led to increased label from $U^{13}C$-Pyruvate in citrate and αKG (Fig. 40A, C, D and Ap. Fig. 11A-C, E-I), similar to genetic ablation of *Gat* in the progenitor cells. Likewise, less label incorporation in lactate (m+3, Ap. Fig. 11D, J) and OAA (m+3, Fig. 40B, E) was observed in *Orco>hid* condition. Overall, these data showed that metabolic

rewiring derived by GABA catabolic pathway is under olfactory control and odor sensing is important to control metabolic pathway activity to regulate redox homeostasis of blood-progenitor cells and maintenance of blood-progenitor development.

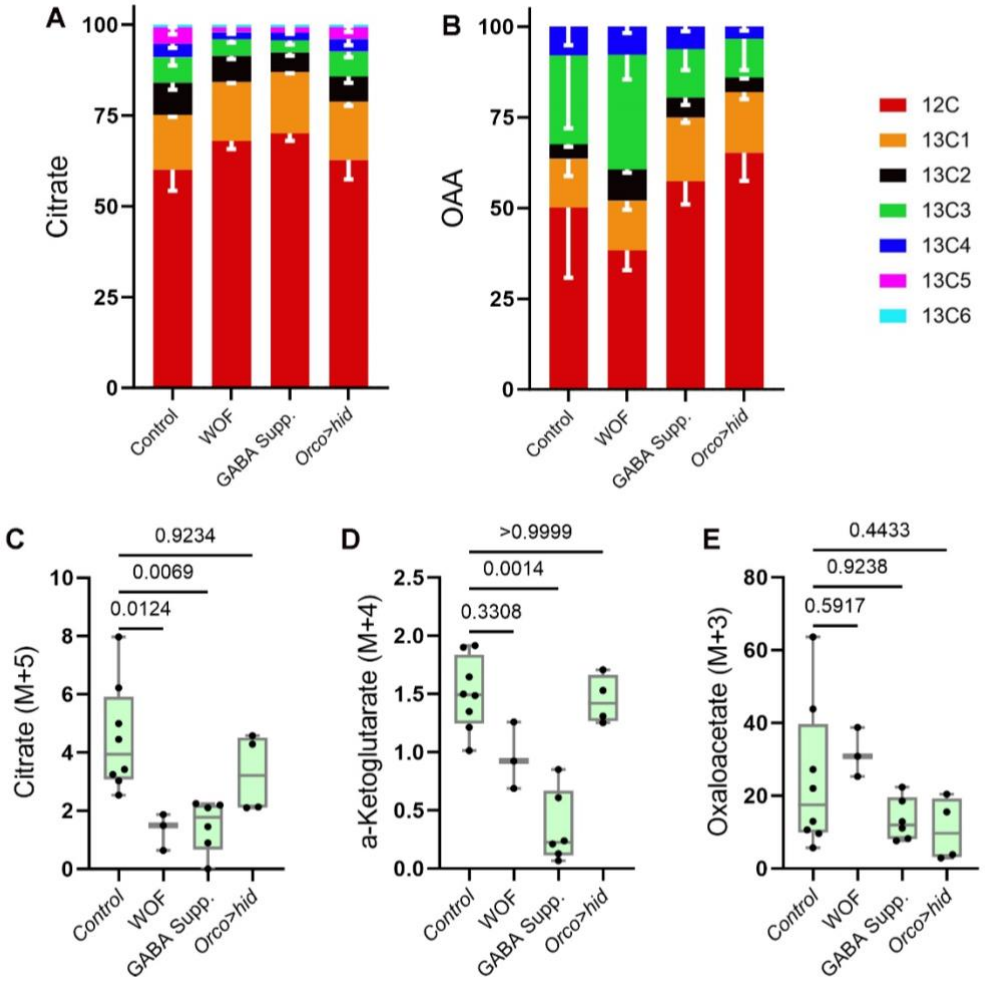

Figure 40. Olfactory control of metabolic pathways activity in the lymph gland.
(A-B) Wandering 3rd instar *control*, wasp odor food (WOF), GABA supplementation and olfactory perturbation (*Orco>hid*) lymph glands showing the label incorporation after U^{13}C-pyruvate label incubation in **(A)** citrate and **(B)** oxaloacetate (OAA), **(A)** in citrate, relatively lower label incorporation is seen for higher 13C in WOF and GABA Supp. lymph glands as compared to *control* and on the other hand, *Orco>hid* does not show any significant change in label incorporation for higher 13C isotopes **(B)** relative label incorporation for OAA increases for 13C isotope in WOF lymph glands, GABA Supp. Did not show much change, however a slight reduction was observed, and *Orco>hid* leads to a decrease in relative label incorporation for 13C isotope as compared to *control*. **(C)** U^{13}C-pyruvate label incubation in WOF (n=3, p=0.0124) and GABA Supp. (n=6, p=0.0069) lymph glands lead to a decrease in relative label incorporation and *Orco>hid* (n=4, p=0.9234) lymph glands do not show any change in relative label incorporation for 13C5 (m+5) in citrate as compared to *control* (n=8). **(D)** U^{13}C-pyruvate label incubation in WOF (n=3, p=0.3308) and GABA Supp. (n=6, p=0.0014) lymph glands lead to a decrease in relative label incorporation and *Orco>hid* (n=4, p>0.9999) lymph glands does not show any change in relative label incorporation for 13C4 (m+4) in α-ketoglutarate (αKG) as compared to *control* (n=8). **(E)** U$_{13}$C-pyruvate label incubation in WOF (n=3, p=0.5917) lymph glands leads to an increase in relative label incorporation, GABA Supp. (n=6, p=0.9238) show a mild decrease in relative label incorporation and *Orco>hid* (n=4, p=0.4433) lymph glands show a reduction in relative label incorporation for 13C3 (m+3)

in oxaloacetate (OAA) as compared to *control* (n=8). Data is presented as median plots (*p<0.05; **p<0.01; ***p<0.001, ****p<0.0001), Kruskal-Wallis test, Dunn's multiple comparisons test is applied.

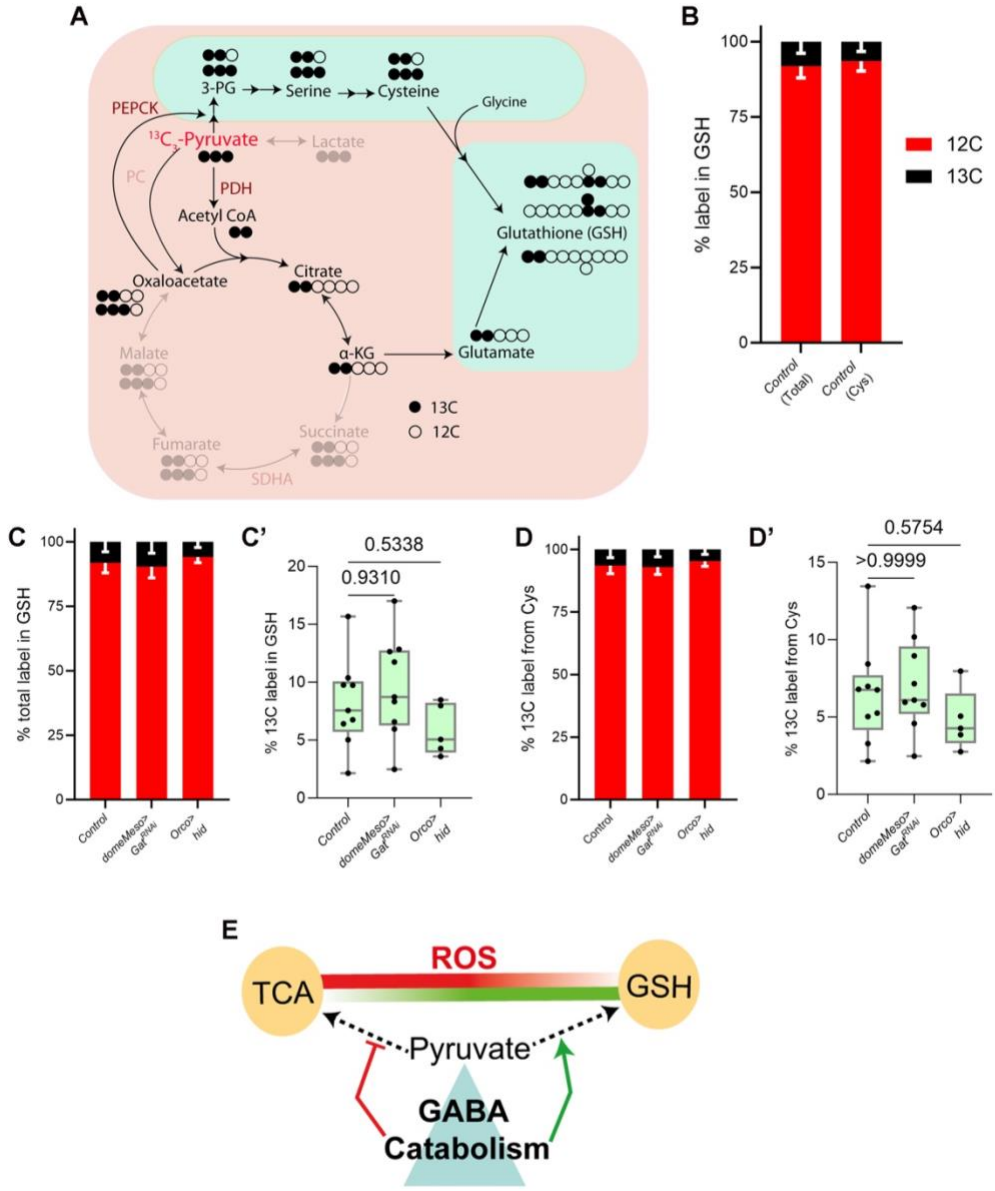

Figure 41. Metabolic dynamics of glutathione (GSH) synthesis in the *Drosophila* lymph gland.
(A) Glutathione labelling pattern with U^{13}C pyruvate isotope incorporation, pyruvate labels GSH via cysteine, glutamate as well as glycine. Depending upon the fragmentation pattern used, labelling in GSH can be derived from either cysteine or glycine and glutamate or all of its constituents, **(B)** 13C label incorporation analysis in GSH from control lymph glands, labelling from glutamate, cysteine, glycine (first bar, black) is comparatively higher than the 13C label incorporation from cysteine (second bar, black) alone, **(C)** Total 13C label incorporation analysis in GSH from *control*, *domeMeso>Gat^{RNAi}* and *Orco>hid* lymph glands, **(C')** U^{13}C-pyruvate label incubation in *domeMeso>Gat^{RNAi}* (n=8, p=0.9310) lymph glands show mild increase in relative total 13C label incorporation in GSH and *Orco>hid* (n=6, p=0.5338) lymph glands lead to a mild decrease in relative total 13C label incorporation in GSH as compared to *control* (n=9**), (D)** 13C label incorporation analysis specifically from cysteine in GSH from *control*, *domeMeso>Gat^{RNAi}* and *Orco>hid* lymph glands, **(D')** U^{13}C-pyruvate label incubation in *domeMeso>Gat^{RNAi}* (n=8, p>0.9999) and *Orco>hid* (n=6, p=0.5754) lymph glands lead to a mild decrease in relative label incorporation 13C from cysteine in GSH as compared to *control* (n=9). These data showed the decrease flux of pyruvate towards GSH synthesis in *domeMeso>Gat^{RNAi}* and *Orco>hid* conditions, **(E)** Schematic representation highlighting the control of GABA catabolism on ROS

homeostasis, where TCA activity leads to ROS generation and GSH leads to ROS scavenging. GABA catabolism balances ROS in the cell by controlling TCA activity and GSH levels.

$U^{13}C$-pyruvate based isotopic labelling analysis was further extended to check the label incorporation in glutathione (GSH). Glutathione is a ten carbon peptide, constituted from five carbons contributed from glutamate, three carbons from cysteine and two from glycine $U^{13}C$-pyruvate labelling in GSH leads to various combination of isotopic possibilities as pyruvate can form glutamate, glycine, and cysteine by following different routes and the number of 13C incorporated from each of these amino acids varies under different conditions or tissues, which makes it difficult to predict the fragments contributions. However, utilization of specific combination of LC/MS parameters can provide the information on incorporation of carbon from pyruvate via different intermediates in GSH (Fig. 41A).

Our $U^{13}C$-Pyruvate based isotopic labelling analysis for glutathione could differentiate among the carbon derived from the amino acid components that finally contributes to GSH formation due to different fragmentation parameters used in the analysis (Fig. 41A, B). In control lymph glands, labelling from glutamate, glycine and cysteine was observed as pyruvate contributes to all the three amino acids components of GSH (Fig. 41B) and specifically the 13C label contribution from cysteine was also seen (Fig. 41B). These data confirmed that indeed in *Drosophila* lymph glands pyruvate contributes to GSH formation via cysteine. Interestingly, when analysed for the label contribution in GSH from *domeMeso>Gat*^{RNAi} and *Orco>hid* lymph glands (Fig. 41C-D'), dynamics of 13C label contribution in GSH as compared to label incorporation in TCA was observed (Fig. 41C-F). Although, total 13C label incorporation (Fig. 41C, C') and labelling from cysteine in GSH (Fig. 41D, D') in the *domeMeso>Gat*^{RNAi} and *Orco>hid* conditions did not show dramatic change as compared to *control*, the dynamics in the extent of labelling as compared to the labelling seen in TCA cycle (Fig. 39 and Fig. 40) was seen. Pyruvate shuttles proportionally towards TCA cycle and glutathione synthesis in control conditions and relative increase in flux of pyruvate towards TCA cycle in the *domeMeso>Gat*^{RNAi} and *Orco>hid* conditions revealed an overall change in the pyruvate metabolism, which leads to ROS imbalance in the lymph gland progenitor cells (Fig. 41E). Taken together, these data showed that olfaction mediated GABA catabolic pathway regulates pyruvate shuttling to different metabolic pathways to control lymph gland ROS homeostasis and consequently, blood development (Fig. 42).

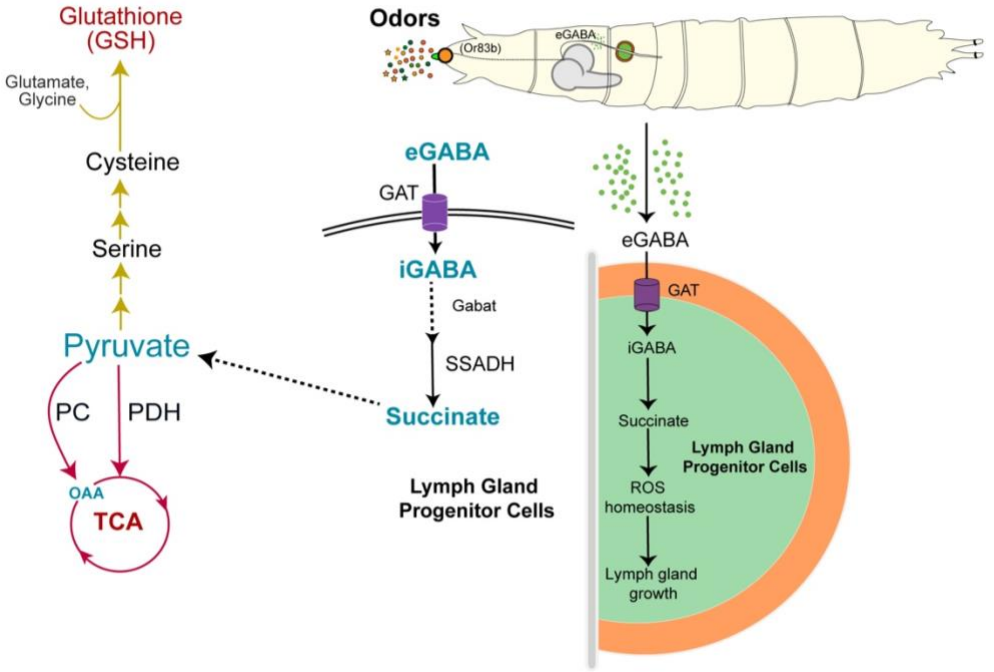

Figure 42. Olfactory control of glutathione (GSH) synthesis in the *Drosophila* lymph gland.
Odor sensing controls metabolic pathway activity and GSH synthesis in the lymph glands. Olfaction leads to GABA release from the neurosecretory cells in brain (172), which gets internalized by GABA transporter in the progenitor cells. GABA metabolism and its conversion to succinate controls pyruvate shuttling to different metabolic pathways to control progenitor homeostasis. GABA catabolism derived succinate directs pyruvate towards serine synthesis via controlling PDH activity and thus regulates GSH synthesis in the progenitor cells. This is important to maintain the ROS balance of the hematopoietic compartment, which regulates homeostatic development of blood-progenitor cells.

4.10 Olfactory neuron metabolic status impact lymph gland homeostasis and development

Understanding the intricate interaction between distinct ORNs and their corresponding glomeruli, as well as how they regulate PN activity, is starting to emerge. This is particularly true for specialized ORNs like Or49a, whose signaling mechanism is distinct (315). Early Or49a activation during larval development is thought to be a stress response that benefits the animal by enhancing its immunological capabilities. Larval Or49a is designed to identify the volatiles that *Leptopilina* wasps exclusively create, known as iridomyrmecin (316). The development of olfactory glomeruli, which are key in this crosstalk, is influenced by interactions between various cell types, including ORNs, glial cells, and mitral/tufted cells (317). The nuclear aggregation of olfactory receptor genes, as observed in mouse olfactory neurons, further contributes to the monogenic expression of these genes (318). The differential effects of specific olfactory receptors on epidermal proliferation and differentiation also highlight the diverse functions of these receptors in non-olfactory tissues (319).

Role of olfaction in *Drosophila* blood-progenitor development is undoubtedly obvious. The olfactory dysfunction leads to loss of progenitor maintenance, smaller lymph glands, elevated ROS levels and dysregulated differentiation both in homeostasis as well as during immune response conditions (94,172,179). There are 21 ORNs in *Drosophila* larvae, which sense specific volatiles and relay the signals to downstream higher brain centers (279). It has been shown that Or42a is food-sensing olfactory receptor neuron (ORN) and controls progenitor homeostasis and basal immune response in *Drosophila* larvae (172), whereas Or49a, which is wasp-odor sensing ORN, provide immune response advantage and lamellocyte formation potential under pre-exposed predatory conditions such as WOF (Wasp odor food), though its requirement is dispensable for basal immune response (94). These studies allude to the existence of specific olfactory signaling and metabolic influences, that govern blood-progenitor development.

We undertook progenitor maintenance and differentiation analysis in homeostatic as well as immune response conditions upon metabolic alterations of olfactory receptor neurons. To understand the metabolic dynamics of these ORNs affecting blood progenitor development specifically amino acid sensing was perturbed in olfactory neuronal subsets.

4.10.1 Effect of ORNs metabolic dynamics on blood progenitor development in homeostasis

During homeostatic development of blood-progenitors, olfactory receptor neurons mediated GABA release from Kurs6+ neurosecretory cells in brain and its downstream sensing and GABA receptor derived signaling in the progenitor cells is important for blood-progenitor homeostatic development (172). Moreover, GABA metabolism in the progenitor cells control lymph gland growth and blood-progenitor ROS homeostasis (179). The physiological control of olfaction on hematopoietic development is intriguing and olfactory mechanisms harnessing this control remains unknown. To understand the mechanisms of olfactory regulation of blood development, we explored the effect of metabolic state change of olfactory receptor neurons on blood-development. Specifically, the amino acid transporter, slimfast (slif) was downregulated in the entire subset of ORNs (Orco) and the effect of metabolic state change of ORNs was investigated. To achieve this olfactory receptor co-receptor (*Orco*) *Gal4* was utilized and amino acid transport in the ORNs was perturbed using slimfast antisense ($slif^{As}$). Interestingly, in homeostatic conditions, perturbation of amino-acid transport in ORNs led to a decrease in lymph gland growth (Fig. 42). The lymph glands were significantly smaller in $Orco>slif^{As}$ condition as compared to control. We checked for the progenitor differentiation status in amino-acid sensing perturbation condition of ORNs and found that amino acid sensing in ORNs indeed control progenitor differentiation. $Orco>slif^{As}$ led to an increase in plasmatocytes differentiation marker, P1 (Fig. 42A, B). However, the progenitor/early differentiation marker PXN levels remain unchanged (Fig. 42C, D). Previous studies have shown that GABA signaling and metabolism in the progenitor cells regulate progenitor maintenance and differentiation. To understand the mechanism of this regulation, GABA levels were checked in $Orco>slif^{As}$ genetic background and a reduction in GABA levels was observed (Fig. 42E, F). This data showed that amino acid sensing by ORNs control lymph gland size and progenitor differentiation through mechanisms involving GABA. However, the complete understanding of the involvement of ORNs amino acid sensing mechanisms in blood-progenitor development control remains unclear and warrants further investigation.

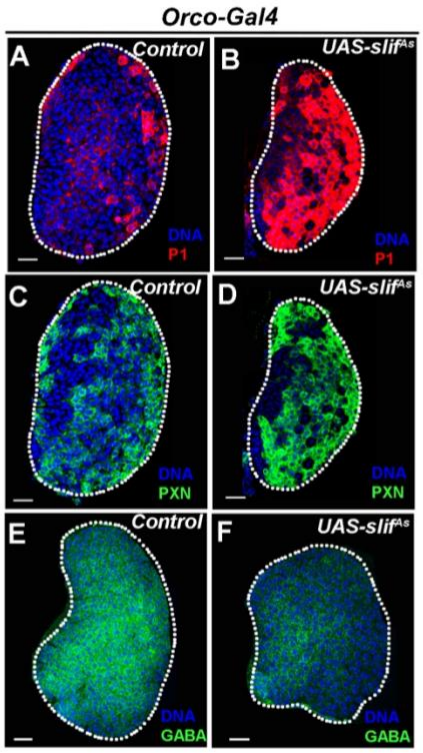

Figure 43. Olfactory neurons metabolic status regulates blood progenitor development.
(A, B) Downregulation of amino-acid transporter **(B)** *slimfast* (*Orco-Gal4;UAS-slif*^{As}) in olfactory receptor neurons leads to a decrease in lymph gland size and increase in plasmatocytes differentiation, P1 as compared to **(A)** *control* (*Orco-Gal4;/+*)**, (C, D)** expressing **(D)** *slif*^{As} in (*Orco-Gal4;UAS-slif*^{As}) in olfactory receptor neurons does not change PXN status as compared to **(C)** *control* (*Orco-Gal4;/+*), **(E, F)** downregulation of amino-acid transporter **(F)** *slimfast* (*Orco-Gal4;UAS-slif*^{As}) in olfactory receptor neurons leads to a decrease lymph gland GABA levels as compared to **(E)** *control* (*Orco-Gal4;/+*).

4.10.2 Effect of ORNs Metabolic dynamics on blood progenitor development in immune-response conditions

Olfactory sensing mediated GABA catabolism in blood-progenitor cells is a critical regulator of *Drosophila* larval immune potential (94). Olfactory receptor neurons (ORNs) ablation leads to a weakened immune response and such animals are not able to form the lamellocytes. To understand olfactory mechanisms controlling lamellocyte formation upon parasitic wasp infection, dynamics of lamellocyte production upon amino-acid sensing perturbation in ORNs was assessed. Surprisingly, downregulation of amino acid sensing in ORNs led to heightened immune response post parasitic wasp infections. We found that *Orco>slif*^{As} had elevated immune potential as it showed a significant increase in lamellocyte formation at 24HPI in the lymph glands (Fig.43A, B). Increased lamellocyte formation upon amino acid sensing perturbation of ORNs indicated the role of metabolic dynamics of ORNs in blood-progenitor differentiation in immune-response scenarios as well.

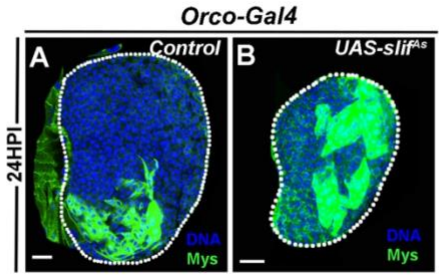

Figure 44. Olfactory neurons metabolic status regulates blood progenitor differentiation during wasp-infection conditions.
(A, B) Downregulation of amino-acid transporter **(B)** *slimfast* (*Orco-Gal4;UAS-slif^As*) in olfactory receptor neurons leads to an increase in lymph gland lamellocyte formation as compared to **(A)** *control* (*Orco-Gal4;/+*) at 24HPI. HPI indicates hours post infection.

As, it has been shown previously that distinct ORN subset control the lamellocyte potential differently, ie. Or42a is required for basal lamellocyte formation, whereas Or49a is involved during the sensitized immune response conditions of wasp odor infusion (94). Therefore, we checked for the effect of amino acid sensing in these separate subsets of ORNs on lamellocyte formation upon wasp infections. Surprisingly, these receptor neurons showed distinct responses. Ablation of amino acid sensing in Or42a (*Or42a>slif^As*) neurons did not affect lamellocyte formation and no significant change was observed (Fig. 44A, B). On the contrary, downregulation of amino acid sensing in Or49a (*Or49a>slif^As*) neuronal subset led to a significant elevation in lamellocyte formation potential of the lymph gland progenitor cells (Fig. 44C, D). However, the increase in lamellocyte formation was much more heightened upon amino acid sensing perturbation in entire subset of olfactory receptor neurons (*Orco>slif^As*).

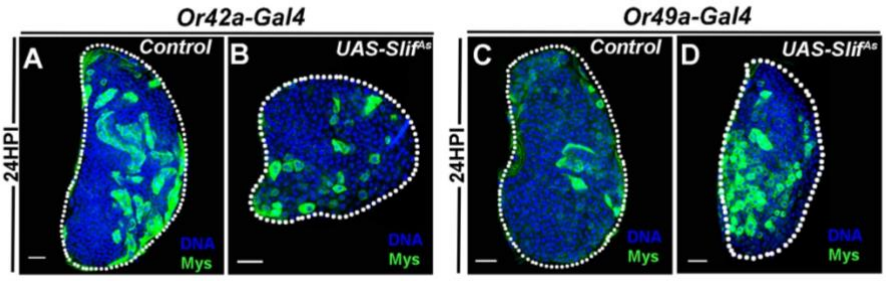

Figure 45. Distinct subset of olfactory receptor neurons metabolic status impact blood progenitor differentiation during wasp-infection conditions.
(A, B) Downregulation of amino-acid transporter **(B)** *slimfast* (*Or42a-Gal4;UAS-slif^As*) in olfactory receptor neurons (Or42a) does not change lymph gland lamellocyte formation as compared to **(A)** *control* (*Or42a-Gal4;/+*) at 24HPI**, (C, D)** downregulation of amino-acid transporter **(C)** *slimfast* (*Or49a-Gal4;UAS-slif^As*) in olfactory receptor neurons (Or49a) leads to an increase in lymph gland lamellocyte formation as compared to **(C)** *control* (*Or49a-Gal4;/+*) at 24HPI. HPI indicates hours post infection.

These data show that the metabolic status of olfactory receptor neurons is important for deciding the fate of progenitor cells, however, these metabolic states of specific subset of ORNs affect the blood-progenitor development in association with other subset of ORNs, while some of these olfactory neuronal subsets might be dispensable for blood-progenitor development.

5 Metabolite measurement of the lymph gland cells to decipher the role of metabolic pathways in growth and differentiation.

This chapter of the thesis deals with standardization of metabolite analysis protocols utilizing liquid chromatography-mass-spectrometry (LC/MS) technique from *Drosophila* larval lymph glands. These protocols were also applied to another *Drosophila* larval tissues to understand the dynamics of metabolic pathways.

Following methods are standardized for the metabolite analysis from *Drosophila* larval lymph glands.

5.1 Steady State Metabolite analysis

a. OBHA derivatization for TCA metabolite analysis
b. HILIC method for amino acid analysis
c. T3 column method for GSH:GSSG and cysteine analysis
d. BEH amide column method for CoA analysis
e. NAD:NADH analysis

Sr. No.	**Method**	**Column**	**Buffer**	**Metabolites**
a	OBHA	C18/C8	A: Water, 0.1% FA, B: ACN, 0.1% FA	TCA metabolites, Lactate, Glutamate, Glycine
b	HILIC-AA	Imtakt # WAA25, Intrada Amino Acid, 2.0x150mm, 3um	A: ACCN+0.3% FA, B: ACCN:100mM Ammonium Formate (20/80 v/v)	Amino Acids
c	T3	HSS T3	A: Water, 0.1% FA, B: ACN, 0.1% FA	GSH, GSSG, Cys, NAC
d	BEH amide	Acquity BEH Amide	A: 95% LCMS H2O, + 5% ACN and 20mM Ammonium Acetate +20mMNH4OH, B: ACN	Acetyl-CoA, Malonyl CoA
e	NAD: NADH	HSS-T3	A: 100% Water, B: 100% ACN	NAD, NADH

Table 1. Different methods for metabolite analysis

5.1.1 OBHA derivatization for TCA metabolite analysis

Steps:

1. Cells/Tissue Extraction in ice-cold methanol only or Chloroform: Methanol extraction (if need to collect lipid and proteins) and store the samples O/N at minus 80 degrees and speed vac dry.
2. OBHA-EDC derivatization and speed vac dry.

Note: Speed vac dry of samples is faster at stage 2 takes around 2 hrs depending upon the instrument and step 1 takes longer around 4-6 hrs. Do not leave samples O/N in the speedvac. It will not affect much the metabolites but will affect samples for lipidomic analysis.

Other important points:

- Prepare a minimum of 4 biological replicate per sample.
- For Normalization purpose, Save the protein layer (middle layer) from Chloroform: Methanol extraction for protein estimation (BCA) of samples.
- Prepare 80% methanol (LCMS grade) with LC/MS water and keep at minus 80 degrees for 4-6 hours and store at 4 degrees for later use.

1a. Cells/Tissue Extraction in ice-cold methanol only

1. Add 200 µL of 80% ice-cold methanol to samples (cells/tissue).
2. Vortex/shake according to tissue type. For cells, a gentle vortex works.
3. Centrifuge at 13000 RPM for 10 min. at 4 degrees.
4. Transfer the supernatant to fresh tube.
5. Repeat step 1-3. ie. again add 200 µL of 80% ice-cold methanol to the tube with sample and vortex, centrifuge.
6. Transfer the supernatant to fresh tube and store at -80 degrees.

1b. Chloroform: Methanol extraction (Store the samples O/N at minus 80 degrees)

1. Add 400 µL of 80% ice-cold methanol to samples (cells/tissue). Vortex/shake according to tissue type. For cells, a gentle vortex works.
2. Add 200 µL of ice-cold LCMS grade water.
3. Incubate at 4 degrees/ice for 30 min.
4. Add 300 µL of Chloroform.
5. Vortex well
6. Centrifuge at 13000 RPM for 10 min. at 4 degrees.
7. Top layer= metabolite, bottom= lipid and middle layer for protein estimation.
8. Stores the samples at this stage in -80 degrees for at least 1 hr. or O/N

The metabolite layer (top) will be processed for EDC-OBHA derivatization.

2. OBHA-EDC Derivatization: Processing of samples for derivatization

1. For derivatization, add 50 µL of LC/MS grade water to speed-vac dried samples.

2. Take TCA metabolite and lactate standard/the analyte standard (10ng) for derivatization in 50 µL LC/MS grade water. Also consider, having a LCMS H_2O blank for a derivatization.
3. Sonicate for 5 minutes.
4. Add 50 µL of 1M EDC (in Pyridine buffer).
5. Keep samples on a thermomixer for 10 min. at room temperature.
6. Add, 100 µL of 0.5 M OBHA (in Pyridine buffer).
7. Incubate the samples again for 1.5 hours on the thermomixer at 25°C.
8. Add 300 µL of ethyl acetate to extract metabolites and keep the samples on thermomixer/shaker for ten minutes.
9. Carefully Collect the top layer in a new Eppendorf tube.
10. Repeat the step 7 and 8 thrice.
11. Dry down the samples in a Vacufuge plus speed-vac at room temperature.
12. Store at -80°C until run or shipment for LC/MS analysis.

Pyridine Buffer: Pyridine buffer was prepared by combining 540 µL of conc. HCl (12.1 M), 860 µL of pyridine, and 8.6 ml of water. The pH was measured with pH paper to be around 5.0. (Pyridine-Solvent, dry Box), Pyridine Buffer: Store at -20 degrees.

EDC: 1-ethyl-3 (3-dimethylaminopropyl) carbodiimide (powder, storage -20)

OBHA: O-benzylhydroxylamine (Powder, storage-Dry Box, RT)

This method is adapted from (320,321). For R_T and Q1/Q3, refer to Appendix Table 2.

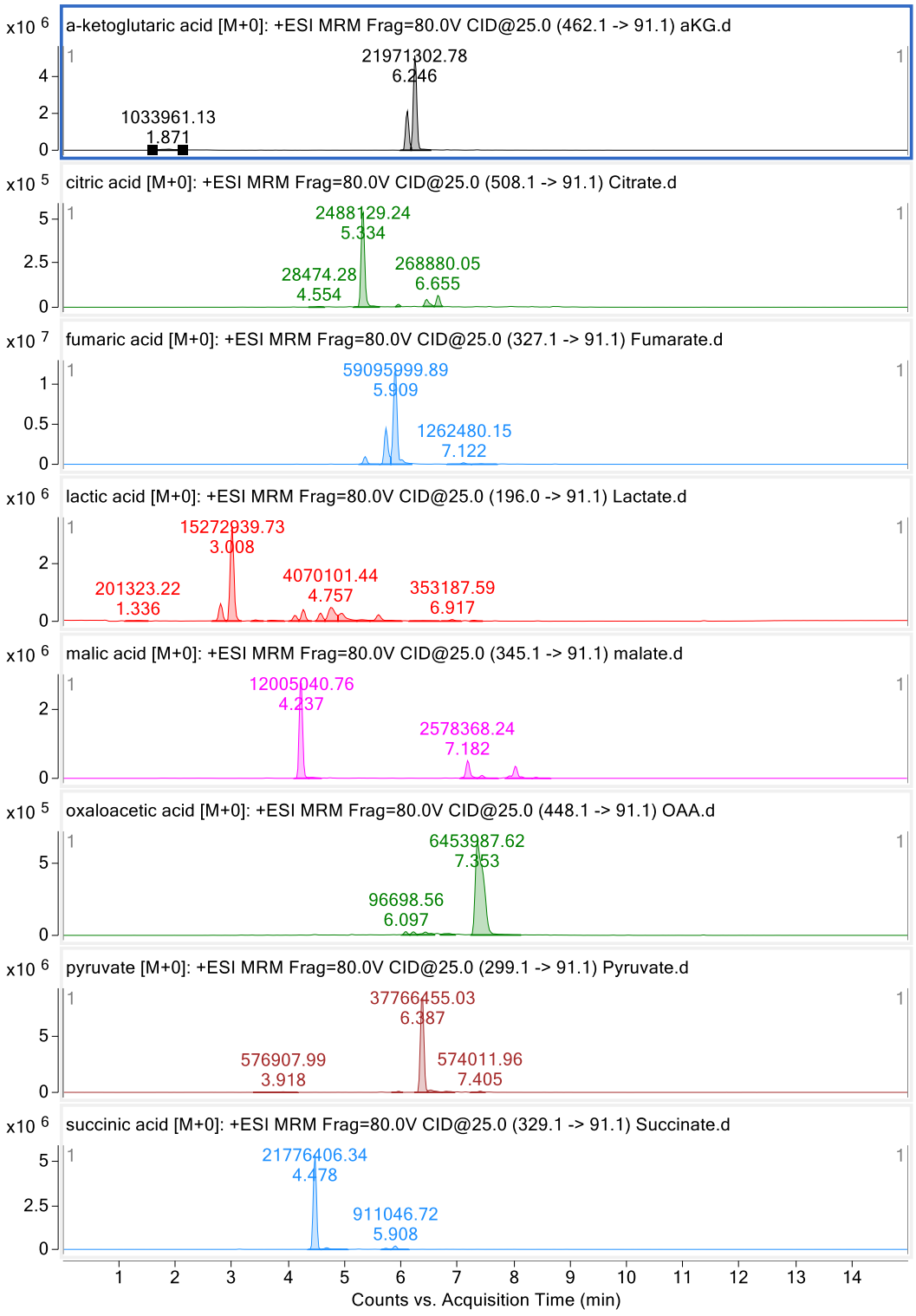

Figure 46. Peak areas and RT for TCA standards with OBHA-EDC derivatization.

For OBHA analysis, in majority of the experiments, a significant change in peak areas for fumarate and succinate was not observed across different experiments. If succinate and Fumarate are primary metabolites that need to be tested, please consider using other methods. The method works well for other metabolites.

5.1.2 HILIC method for amino acid analysis

1. Precipitate protein with 100% TCA solution, then mix Solution with organic for HILIC separation.
2. Take tissues in 200 µL of PBS (adjust depending upon the sample size)
3. Add 10ug ABA ISTD (1ug/µL x 10µL spike)
4. Add 40µL of 100% TCA solution (500mg/350µL water), Note: For 200µL of sample volume 40µL of TCA is used and for 100ul, use 25µL of TCA solution.
5. Incubate for 10 min. at 4C.
6. Centrifuge at 13000 RPM for 10 min
7. Collect Solution and store at -80 degrees.
8. Just prior to analysis, mix 50% by volume Solution with 100% ACN for HILIC separation.

Note: Cysteine and methionine were not detectable in lymph gland samples with this method, although the peaks in aa standard were resolved well.

For R_T and Q1/Q3, refer to Appendix Table 3.

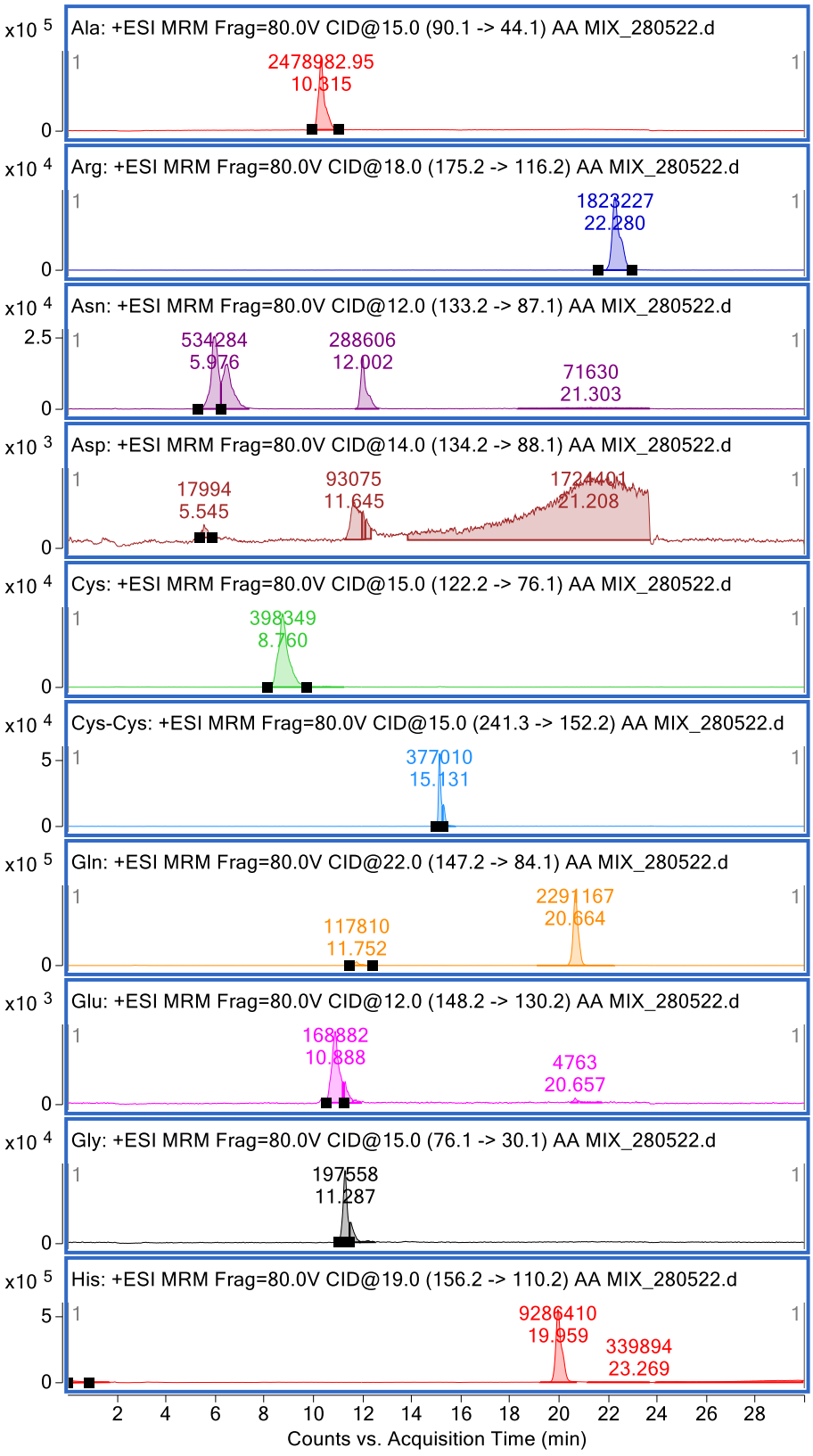
x10 5
Ala: +ESI MRM Frag=80.0V CID@15.0 (90.1 -> 44.1) AA MIX_280522.d
2478982.95
10.315
x10 4
Arg: +ESI MRM Frag=80.0V CID@18.0 (175.2 -> 116.2) AA MIX_280522.d
1823227
22.280
x10 4
Asn: +ESI MRM Frag=80.0V CID@12.0 (133.2 -> 87.1) AA MIX_280522.d
534284
5.976
288606
12.002
71630
21.303
x10 3
Asp: +ESI MRM Frag=80.0V CID@14.0 (134.2 -> 88.1) AA MIX_280522.d
17994
5.545
93075
11.645
1724401
21.208
x10 4
Cys: +ESI MRM Frag=80.0V CID@15.0 (122.2 -> 76.1) AA MIX_280522.d
398349
8.760
x10 4
Cys-Cys: +ESI MRM Frag=80.0V CID@15.0 (241.3 -> 152.2) AA MIX_280522.d
377010
15.131
x10 5
Gln: +ESI MRM Frag=80.0V CID@22.0 (147.2 -> 84.1) AA MIX_280522.d
2291167
20.664
117810
11.752
x10 3
Glu: +ESI MRM Frag=80.0V CID@12.0 (148.2 -> 130.2) AA MIX_280522.d
168882
10.888
4763
20.657
x10 4
Gly: +ESI MRM Frag=80.0V CID@15.0 (76.1 -> 30.1) AA MIX_280522.d
197558
11.287
x10 5
His: +ESI MRM Frag=80.0V CID@19.0 (156.2 -> 110.2) AA MIX_280522.d
9286410
19.959
339894
23.269
2 4 6 8 10 12 14 16 18 20 22 24 26 28
Counts vs. Acquisition Time (min)

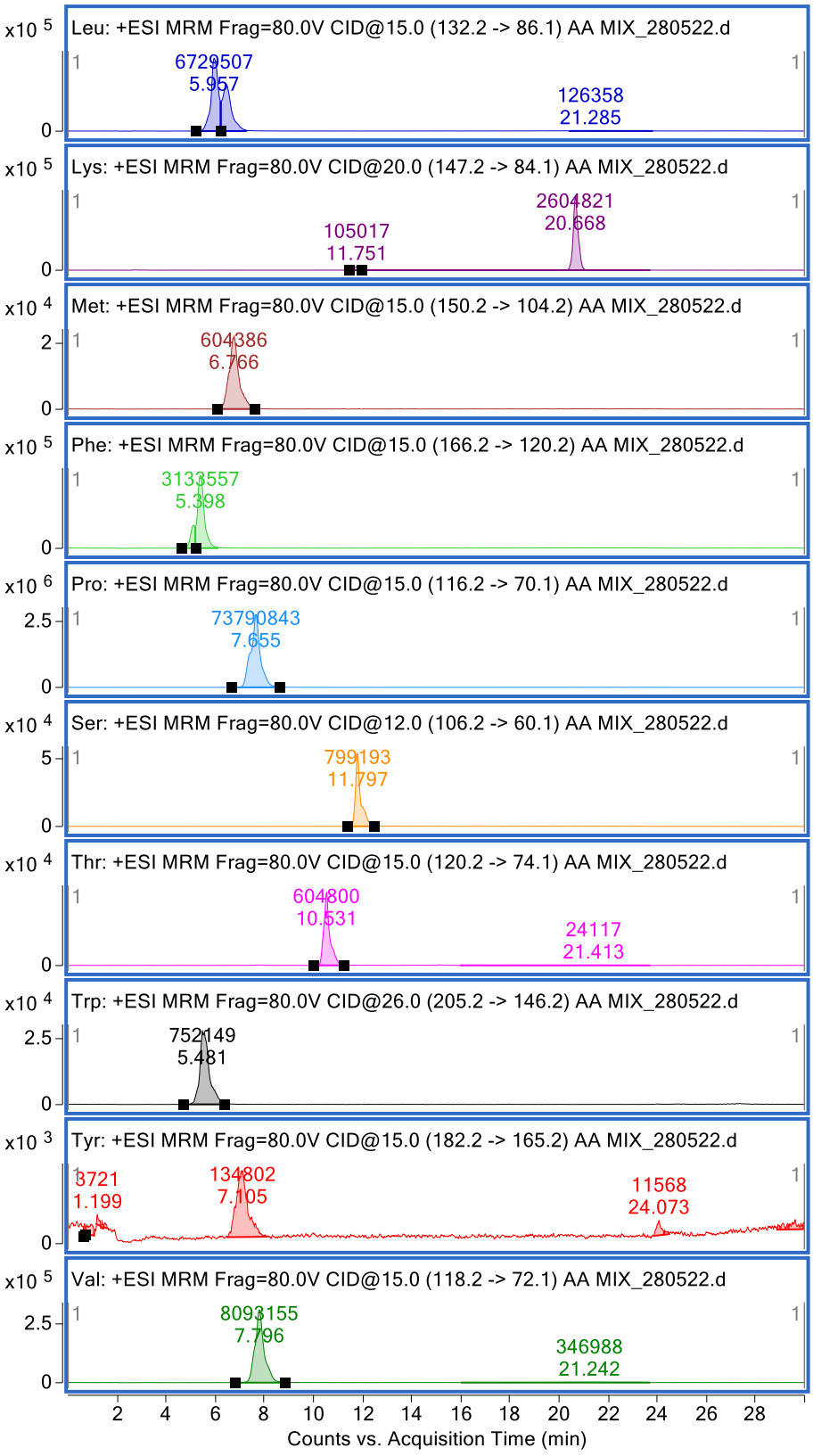

Figure 47. Peak areas and RT for amino acid standard with TCA precipitation (HILIC).

5.1.3 GSH: GSSG and Cysteine analysis

1. Buffer and ISTD preparation

a. Prepare GSH: GSSG buffer by dissolving 3mg EDTA, 5mg NaHCO3 to pH to ~7.5 into 2mL of 3/2 water/MeOH and Mix well.

b. Add 250mM NEM (62.5mg in 2mL vol) to the buffer just before the sample preparation.

c. For GSH-NEM/GSSG ISTD: Use GSSG "as is" in water at 10ng/µL conc. Make fresh GSH NEM by mixing 200µL of GSH (+TCEP) @ 20ng/µL with 200µL of 5M NEM. Final conc is 10ng/uL.

2. Sample Preparation:

a. Take 200 µL of buffer with NEM and add to the dissected tissues or cells.

b. Add the GSH, GSSG ISTD at 10ng/µL (10µL volume) to the prepared samples.

c. Quickly store the samples at -80 degrees until further processing.

3. For TCA precipitation and extraction, Thaw, vortex if need to mix:

a. Add 40µL of TCA (0.5g/mL solution in water)

b. Vortex and centrifuge 13000rpm/10min

c. Collect Solution.

d. Add 100µL of water and 500µL of DCM.

e. Vortex to remove excess NEM.

f. Centrifuge at 13000rpm/10min.

g. Collect Aq. Fraction.

h. Dry in speedvac.

i. Store -20C or resuspend in 100µL of water for LC/MS analysis.

Note: This method can also be utilized for Cysteine, homocysteine and NAC analysis. For R_T and Q1/Q3, refer to Appendix Table 4. This method is adapted and modified from (322).

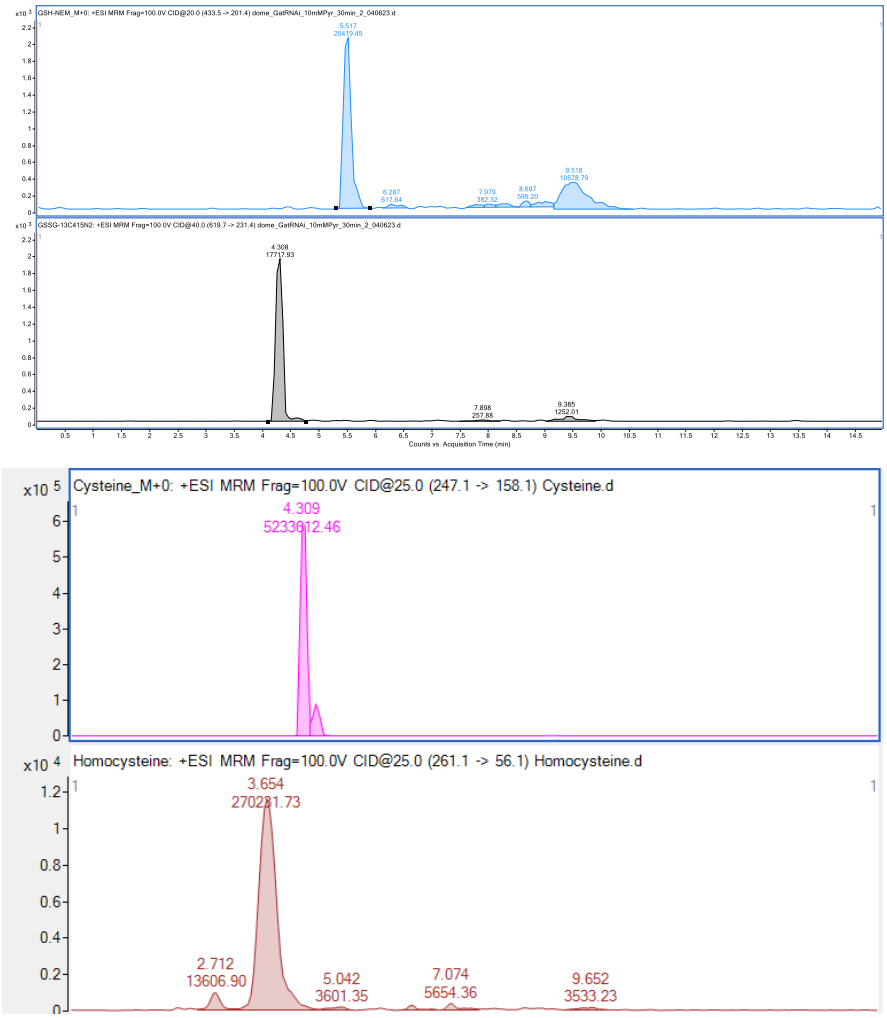

Figure 48. Peak areas and RT for GSH, GSSG, cysteine and NAC standard.

5.1.4 NAD:NADH analysis

1. Collect tissues into 200µL of MeOH.
2. Add d4-MeNAM as ISTD (~10ng).
3. Homogenize and Centrifuge at 5000 rpm for 1min.
4. Collect Solution.
5. Dry in speedvac ~2 hr at RT.
6. Resuspend in 50µL of T3 buffer.
7. Analysis on LC/MS with HSS T3 column.

For R_T and Q1/Q3, refer to Appendix Table 4.

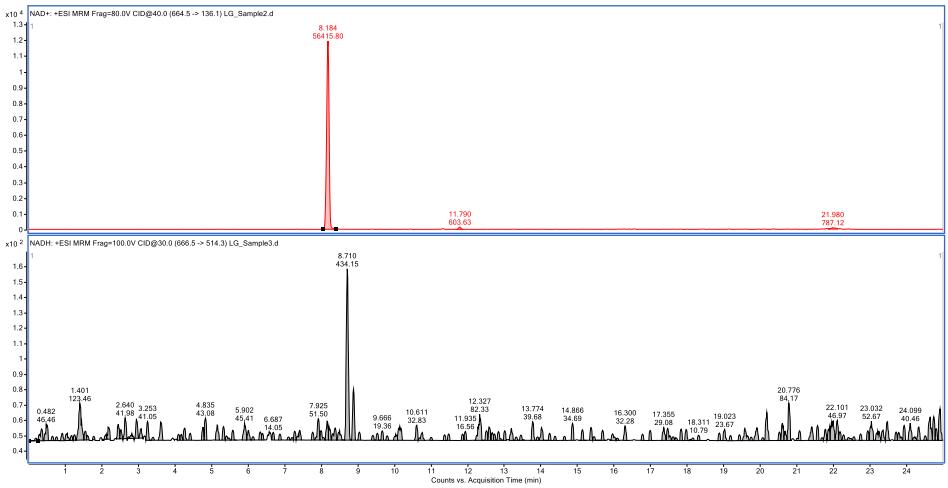

Figure 49. Peak areas and RT for NAD, NADH from lymph glands.

5.1.5 BEH-Amide column method for CoA analysis

For sample preparation: Chloroform: Methanol extraction (Store the samples O/N at minus 80 degrees)

1. Add 400 µL of 80% ice-cold methanol to samples (cells/tissue). Vortex/shake according to tissue type. For cells, a gentle vortex works.
2. Add 200 µL of ice-cold LCMS grade water.
3. Incubate at 4 degrees/ice for 30 min.
4. Add 300µL of Chloroform.
5. Vortex well.
6. Centrifuge at 13000 RPM for 10 min. at 4 degrees.
7. Top layer= metabolite, bottom= lipid and middle layer for protein estimation. Stores the samples at this stage in -80 degrees or directly prepares the samples in 80% MeOH if protein quantification is not required.

Note: No derivatization is needed for CoA analysis.

8. Dissolve the speed-vac dried samples in 70% MeOH and run on LC/MS.

For R_T and Q1/Q3, refer to Appendix Table 4. This method is adapted from (323).

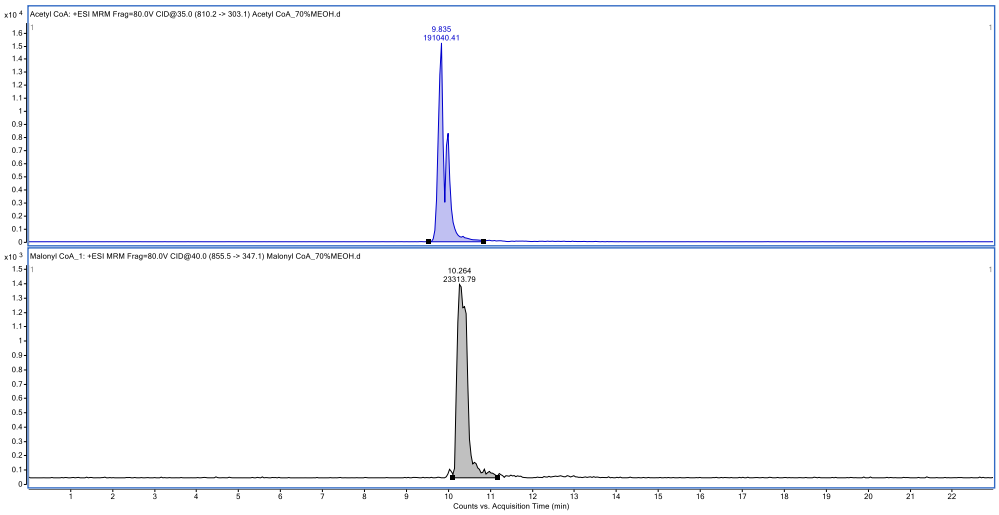

Figure 50. Peak areas and RT for Acetyl-CoA and Malonyl-CoA standard.

For LC/MS reagents, refer to Appendix Table 5.

5.1.6 Steady state analysis

For relative quantification between control and sample, ideally two types of normalization are needed:

1. Protein estimation, (BCA assay): is a read-out for sample size normalization, which is done for tissue samples, and cell-count can be done for normalization when cells are used.
- For protein estimation, either use the protein layer extracted during $CHCl_3$:MeOH preparation or prepare a duplicate sample for each condition with same number of cells or tissue weight.
- Or normalization with the cell count, if possible.

2. Total ion count or internal standards (ISTD): Either total ion count for each MS data or an ISTD need to be added to MS samples. The sample peak areas need be normalized against peak areas of ISTD in each sample.

MassHunter Quant software is used for peak area correction and then the area values are normalized to protein content and TIC/ISTD as mentioned above for relative quantification.

5.2 13C isotopic labelling Analysis

A non-radioactive, naturally occurring carbon 13 (13C) isotopomer in which all or specific carbons are 13C. It allows the detailed quantification of all intracellular fluxes in the central metabolism of an organism.

The process of 13C-isotopomer analysis by LC/MS (QQQ) comprises of following steps:

a. 13C-isotopic labelling of sample
b. Sample preparation/extraction
c. LC/MS run and data acquisition.
d. Data analysis

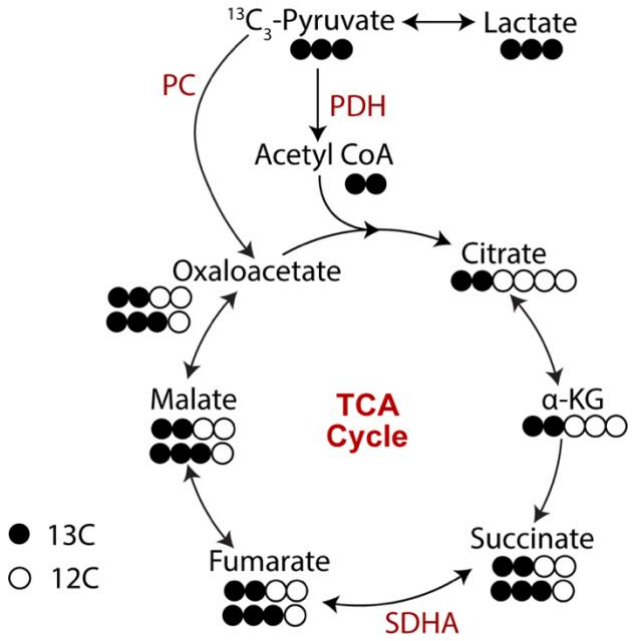

Figure 51. 13C-isoptoic labelling pattern for TCA cycle and lactate.
(2C label happens from PDH derived conversion and 3C label happens from PC derived conversion).

5.2.1 13C incubation of sample

Either universal 13C or specific (e.g. 2,3) 13C labelled isotope are used and these can be procured from Cambridge Isotope Laboratories (CIL). $U_{13}C$ Pyruvate is utilized in the below description.

1. Cells or tissue samples are incubated in 10mMof 13C Pyruvate for 30 min. in 1X PBS. PBS is prepared in LC/MS grade water.
2. For standardization purpose, different conc of 13C Pyruvate, ie. 1mM, 10mM and 20mM were tried and 10mM was chosen as it gave the optimum labelling pattern.
3. Similarly, to draw a saturation analysis, 13C Pyr-10mM labelling was done at different time points ranging from 5 min.-4 hr. and 30 min. was used further.
4. The duration of label incubation might vary across different cell or tissue types.
5. 13C-incubation was done at room temperature.

Note:

1. Cell culture, custom-made media can also be used for 13C-isotope incubation depending upon cell or tissue types. Although, incubation in PBS also worked well.
2. It is better to have a minimum of 4 biological replicates per sample.
3. It is advisable to have an unlabeled control in each experiment to avoid the false labelling pattern upon 13C-incorporation. Ideally, the unlabeled control should not show the peaks for 13-C label incorporation, or these should be very small, compared to the labelling samples.

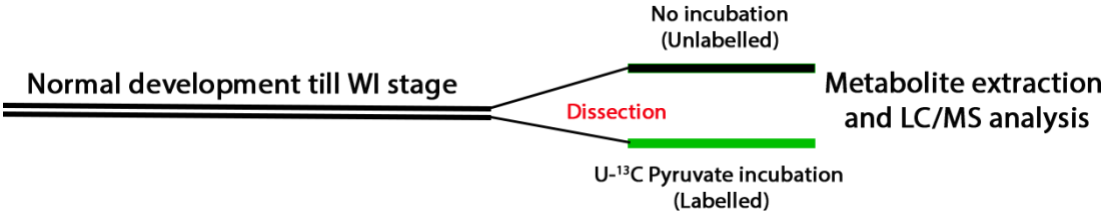

Figure 52. Timeline adopted for U13C-Pyr incubation and sample preparation from *Drosophila* tissues.

5.2.2 13C label incorporation analysis in TCA metabolites

OBHA-EDC method was followed for preparing the samples for TCA analysis for the labelling analysis like the steady-state analysis.

1. Tissues are quickly rinsed in LCMS water and transferred to ice-cold 80% methanol or the desired buffer for respective LC/MS analysis.
2. For sample preparation and LC/MS run the same protocol is followed, as mentioned in the steady-state analysis for OBHA-EDC derivatization.
3. The Q1/Q3 transitions for respective isotopes are added in the acquisition method.

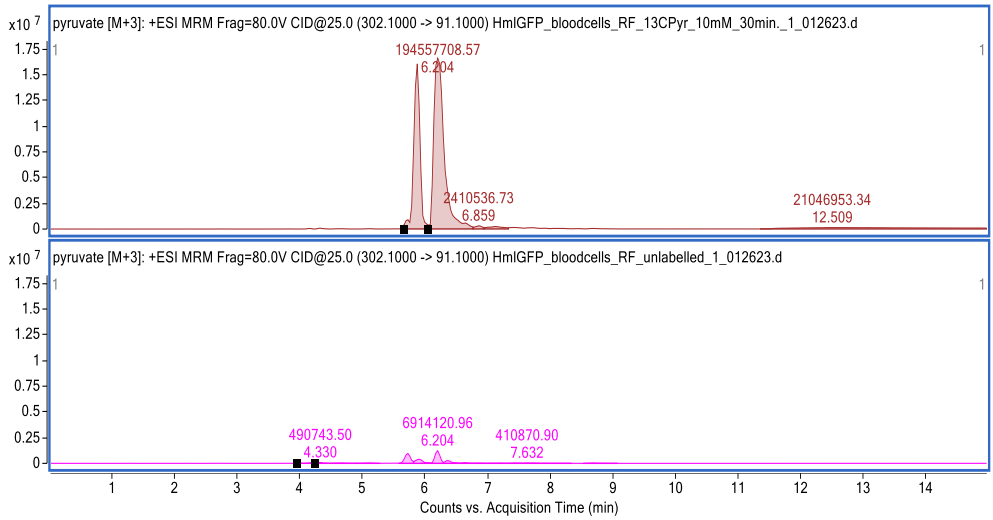

Figure 53. Peak areas and RT for U13C Pyruvate in labelled vs unlabelled condition.

C. For LC/MS QQQ run: The QQQ transitions for different isotopomer were added in the method section on MassHunter Acquisition software. All other parameters remain the same, as done for steady state analysis.

Q1/Q3 transitions will vary depending upon the label used. Since, in OBHA derivation Q3 remains 91.1 for each analyte it does not change for M+n, mass additions. But, for different analysis both Q1 and Q3 need to be checked carefully, depending upon the label incorporation and fragmentation pattern.

5.2.3 Data analysis

The following steps are followed for TCA metabolite data analysis. (Label incorporation in citrate is shown upon incubating the sample with 10mM U-^{13}C Pyruvate in 1X PBS for 30 min.)

1. The peak area for each isotope is checked and corrected for similar retention time and peak width in Mass Hunter Quant software and data is exported as excel file and below procedure is followed for data analysis.
2. Peak area data from acquired LC/MS data for each isotope of citrate from U-13C Pyr label.
3. Percentage of label in each isotope (for 6 carbons in citrate) from U-13C Pyr label.
4. Graph plotted from percentage data for percentage label in citrate from 10mM U-13C Pyr label for 30 min. in blood-cells.

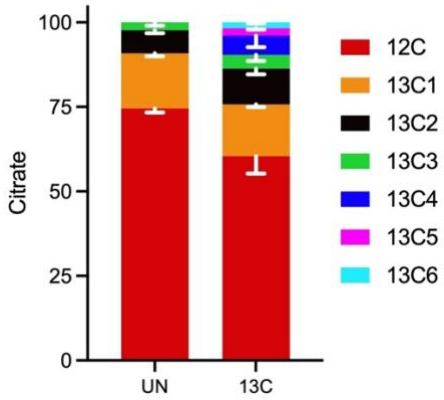

Figure 54. Representative image showing label incorporation in citrate.
Post U13C-pyruvate incubation in unlabeled and labeled conditions. First bar represents the percentage label in unlabeled condition, where U-13C Pyruvate was not added, and sample was incubated in only PBS without any label, and the second bar shows the percentage label incorporation in citrate from 10mM U-13C Pyr label for 30 min.

Note: Our analysis for TCA metabolites with OBHA-EDC derivatization show the peaks for M+1 in unlabeled control, and the peak area for higher isotopes are very small or negligible as compared to U^{13}C Pyruvate incubated samples.

For further analysis and natural-isotope abundance correction, INCA or any other MFA software can be used, depending upon the metabolite analysis in question.

5.3 Label incorporation analysis in GSH

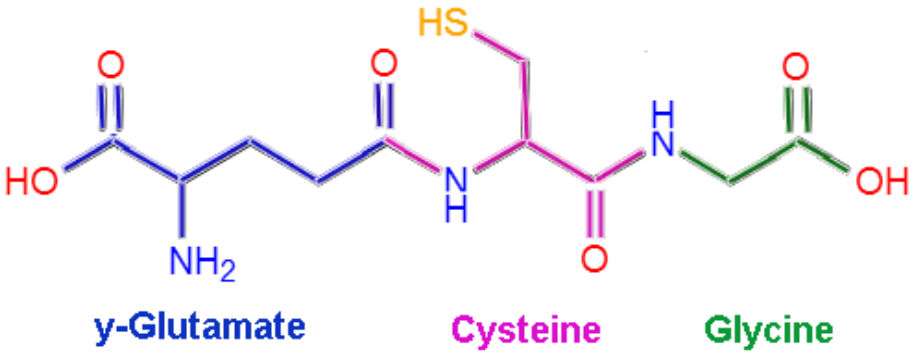

Figure 55. Chemical Formula of glutathione, GSH.

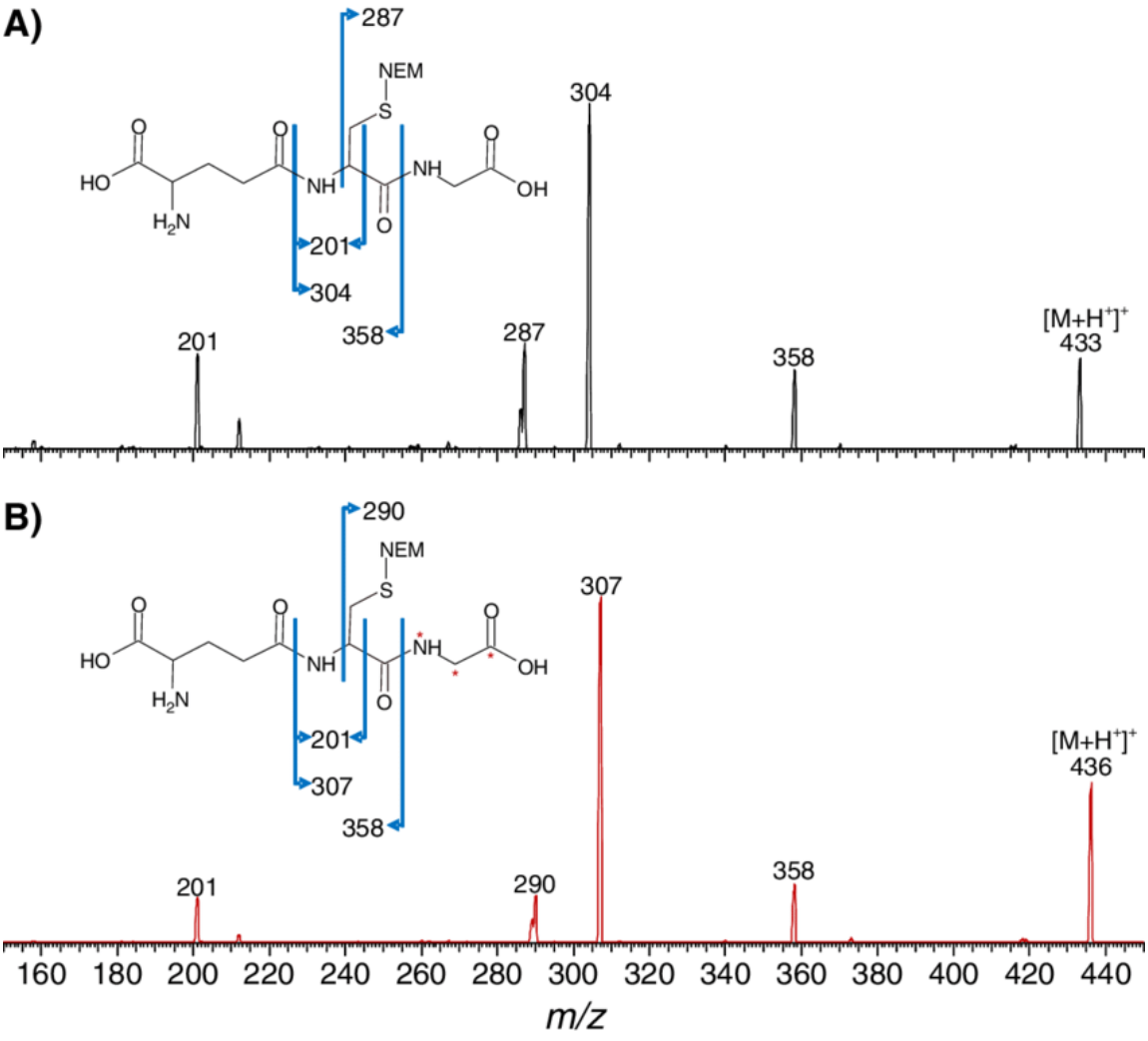

Figure 56. Different fragments of GSH upon ionization in the LC/MS.
GSH is composed of glutamate, cysteine and glycine and it is fragmented to different ions comprising the carbons contributed from different constituents (adapted from (324).

5.3.1 Fragment ion formation upon utilization of different isotopic labels

In case of label incorporation analysis in GSH, if a more complex condition like U^{13}C pyruvate is used for label incorporation analysis in GSH, it leads to various combination of Q1 and Q3 fragments, as pyruvate can form glutamate, glycine, and cysteine by following different routes and the number of 13C incorporated from each of these amino acids will vary under different conditions or tissues, which makes it difficult to predict the fragments. But utilization of specific combination of Q1 and Q3 fragments will give the information on flux of pyruvate towards GSH.

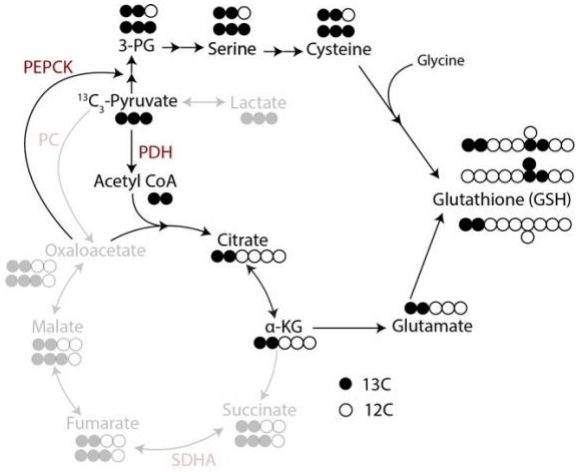

Figure 57. Glutathione labelling pattern with U-13C Pyruvate isotope incorporation

As, GSH comprises of 10 carbons and the different combinations of Q1/Q3 fragments can be utilized to understand the contribution of glutamate, glycine, or cysteine in GSH formation from pyruvate. Although, it is preferrable to use the terminal label isotopes e.g. cysteine, glycine, glutamate etc. for GSH to have a better understanding of contribution/flux and regulation of these individual components towards GSH.

Drosophila husbandry, stocks, and genetics

The following *Drosophila melanogaster* stocks were used in this study: w^{1118} (wild type, *wt*), *domeMeso-Gal4,UAS-GFP* and *TepIV-Gal4,UAS-mCherry* (Banerjee lab), *Hml$^{\Delta}$-Gal4, UAS-2xEGFP* (S. Sinenko), *Orco-Gal4* (BDSC 26818), *Or42a-Gal4* (BDSC 9969), *Or49a-Gal4* (BDSC 9985), *UAS-Hph* (C. Frei) and *UAS-Gat* (M. Freeman). The *RNAi* stocks were either obtained from VDRC (Vienna) or BDSC (Bloomington) *Drosophila* stock centres. The lines used in this study are: Gat^{RNAi} (BDSC 29422), $Ssadh^{RNAi}$ (VDRC 106637, BDSC 55683), $SdhA^{RNAi}$ (VDRC 330053), Hph^{RNAi} (VDRC 103382), $Pdha^{RNAi}$ (BDSC 55345), Pdk^{RNAi} (BDSC 28635, BDSC 35142), $Catalase^{RNAi}$ (Cat^{RNAi}, BDSC 43197), $Sod2^{RNAi}$ (BDSC 24489), $sima^{RNAi}$ (BDSC 33894), PC^{RNAi} (VDRC 105936), *UAS-Catalase* (*Cat*, BDSC 24621), *UAS-Hid* (BDSC 65403) and *UAS-slif*$^{\Delta s}$ (BDSC 52655).

All fly stocks were reared on corn meal agar food medium with yeast supplementation at 25°C incubator unless specified. Tight collections were done for 4-6 hours to avoid over-crowding and for synchronous development of larvae. The crosses involving RNA*i* lines were maintained at 29ºC to maximize the efficacy of the *Gal4/UAS RNAi* system. Controls correspond to *Gal4* drivers crossed with w^{1118}.

ROS (DHE) detection in lymph glands

Lymph glands dissected from the wandering 3rd instar larvae were stained for ROS levels following the protocol of (325). The dissected lymph gland tissues were stained in 1:1000 DHE (Invitrogen, Molecular Probes, D11347) dissolved in 1X PBS for 15 min in the dark. Tissues were washed in 1X PBS twice and fixed with 4% formaldehyde for 6-8 min. at room temperature in the dark. Tissues were again quickly washed in 1X PBS twice and then mounted in Vectashield (Vector Laboratories). The lymph glands were imaged immediately. A minimum of five animals were analysed per experiment and each experiment was repeated at least three times. One representative image (one lymph gland lobe) is shown in the figure panels.

Immunostaining and immunohistochemistry

Immunohistochemistry on lymph gland tissues were performed with the following primary antibodies: mouse-αP1 (I. Ando, 1:30), rabbit-αPPO (1:1000, H. M. Müller), mouse-αMys (1:100, DSHB, CF.6G11), mouse-αPDH (ab110334, 1:250), mouse-

αPDK (ab110025, 1:500), rabbit-αpPDK (TYR243, SAB #11597, 1:100), rabbit-αpPDH (S293, ab177461, 1:250), rabbit-αGat (1:2000, M. Freeman Lab), rabbit αGlutathione (1:100, abcam #5543), mouse αCysteine (1:20 # sc-69954), mouse-αGlutamate (1:100, #ab9440). The secondary antibodies Alexa Flour 488, 546 and 647 (Invitrogen) were used at 1:400 and Phalloidin (Invitrogen) at 1:100 dilutions. Nuclei were visualized using DAPI (Sigma). Samples were mounted with Vectashield (Vector Laboratories).

Lymph glands dissected from wandering 3rd instar larvae were stained following the protocol of (62). Lymph gland tissues from synchronized larvae of required developmental stage were dissected in cold PBS (1X Phosphate Buffer Saline, pH-7.2) and fixed in 4% Paraformaldehyde (PFA) for 40 min. at room temperature. Tissues were then washed thrice (15 min. each wash) in 0.3% PBT (0.3% triton-X in 1X PBS) for permeabilization and were further blocked in 5% NGS, for 45 min at RT. Tissues were next incubated in the respective primary antibodies with appropriate dilution in 5% NGS overnight at 4°C. After primary antibody incubation, tissues were washed thrice in 0.3% PBT for 15 min each. This was followed by incubation of tissues in respective secondary antibodies for 2-3 hrs at RT. After secondary antibody incubation, tissues were washed in 0.3% PBT for 15 min. following a DAPI+0.3% PBT wash for 15 min. Excess DAPI was washed off by a wash of 0.3% PBT for 15 min. Tissues were mounted in Vectashield (Vector Laboratories) and then imaged utilizing confocal microscopy. A minimum of five animals were analysed per experiment and each experiment was repeated at least three times. One representative image (one lymph gland lobe) is shown in the figure panels.

Image acquisition and processing

DHE stained (ROS) and immuno-stained lymph gland tissues images were acquired using Olympus FV3000 Confocal Microscopy 40X oil-immersion objective. Microscope settings were kept constant for each sample in every experiment. Specifically, for ROS the image acquisition settings were chosen to capture the difference between MZ and CZ ROS levels. Medullary zone containing the blood progenitor cells has elevated ROS than the differentiating cells of the cortical zone (72). The image acquisition settings were chosen to capture this difference in control lymph glands without causing saturation in majority of the pixels. This setting was thereafter kept constant for all other genotypes that were conducted in the corresponding

experimental batch and were processed for analysis and quantifications. Lymph gland images were processed using ImageJ (NIH) and Adobe Photoshop CS5 software.

Quantification of lymph gland phenotypes

All images were quantified using ImageJ (NIH) software and Microsoft Excel. Images were acquired as z-stacks and quantifications were done as described previously (326). For lymph gland area analysis, middle two z-stacks were merged, and total lymph gland area was marked using the free-hand tool of ImageJ and then analysed further for quantifications. The relative fold change in ROS levels and the intensities per lobe was calculated using mean fluorescence intensity values. ROS quantifications were done from the entire lymph gland lobe. The genetic backgrounds where progenitor specific knockdown was done, intensity quantifications was done only from the dome^{+} (blood progenitor cells) area and in other backgrounds entire lymph gland lobe was marked and then quantified. The area covering the entire lymph gland lobe or the dome^{+} region was marked, and mean fluorescence intensity was calculated. Background noise was quantified from the unmarked zones at four random regions (marked by equal sized square boxes) and subtracted from the mean intensity values. The relative fold change was calculated from the final mean fluorescence intensity values in Microsoft excel and graph plotting, and statistical data analysis was performed using GraphPad Prism software. For all intensity quantifications, the laser settings for each individual experimental set-up were kept constant and controls were analysed in parallel to the mutant conditions every time.

Lymph gland differentiation analysis

A single middle stack image was obtained from each lymph gland lobe from which areas of the respective populations was obtained by using the free hand tool on Image J to select areas in the respective channels. The images were marked accordingly to extract total lymph gland area (DAPI^{+} channel, C1), total dome^{+} area (Dome-GFP^{+} channel only, C2), total P1^{+} area (P1 channel only, C3) and total area covering all dome^{+} and P1^{+} regions (Dome-GFP^{+} channel merge with P1channel, C4). From here the percentage of Dome^{+}P1^{+} double positive cells was obtained by subtracting the area of all dome^{+} and P1^{+} region (C4) with combined areas from the individually marked Dome^{+} (C2) and P1^{+} (C3) regions. This was then represented as percentage with respect to total lymph gland area (C1, Dome^{+}P1^{+} double positive = (C2+C3)-C4/C1*100). To calculate percentage Dome^{-}P1^{-} area, dome^{+}P1^{+} area (C4) was subtracted from total

lymph gland area (C1, Dome^{-}P1^{-} = C1-C4/C1*100).

Wasp culture and infection

Leptopilina boulardi wasps were maintained as previously described (145). For wasp infections, protocol of (327) was followed. Early 3rd instar larvae were exposed to 10-15 females and 5-8 male *L. boulardi* wasps for a duration of 6 hrs at 25°. After removing wasps, the infected *Drosophila* larvae were kept back to 29° until respective analyses i.e., 24hrs for lymph gland lamellocyte analyses and 48hrs for circulation lamellocyte analyses.

Crystal cells and lamellocytes count

For crystal cells analysis, lymph glands were stained with PPO1 to mark the crystal cells. The stained tissues were then imaged, and z-stacks were acquired. Crystal cells were counted manually from entire z-stacks per lymph gland lobe utilizing ImageJ.

For lamellocyte count at 24HPI, the lymph gland tissues were stained with Myospheroid to mark the lamellocytes and imaged to obtain z-stacks. Lamellocytes were then manually counted as done for crystal cells. For circulating lamellocytes count at 48HPI, individual larvae were bled on Teflon printed microscopic slides (Immuno-Cell Int., one larva per well), then counterstained with phalloidin and lamellocytes were counted manually based on their large flattened morphology under the microscope as described previously (94).

Metabolite supplementation

Succinate (Sodium succinate dibasic hexahydrate, Sigma, S9637), N-Acetyl-L-cysteine (NAC, Sigma, A7250), methionine (Sigma, M9625) serine (Sigma, S4500) and GABA (Sigma, A2129) enriched diets were prepared by supplementing regular fly food with weight/volume measures of succinate and NAC to achieve 3% (Succinate) and 0.1% (NAC, methionine and serine) concentrations, respectively. Eggs were transferred in these supplemented diets and reared until analysis of the respective tissues (lymph gland).

Wasp odor stimulation

Wasp odor food (WOF) was prepared as described previously in (94). Sealed dialysis tubing (Spectra/Por Dialysis Membrane) containing *L. boulardi* wasps (15-20 females and 5–8 males) were kept in regular food media vials. This setup allowed odorant cues

to pass, without exposing the larvae to parasitic wasps. The food was freshly prepared each time and *Drosophila* eggs were transferred in these WOF vials and reared until analysis of the respective tissues (lymph gland).

TCA metabolite extraction and derivatization

For metabolite extraction, 5-10 lymph glands from wandering 3rd instar (WI) larvae were taken per sample in 300 µl of 80% ice-cold Methanol and samples were homogenized briefly. Then 100 µl of LC/MS grade water was added and the samples were incubated in ice for 30 min. After addition of 200 µl chloroform, samples were vortexed for 30 seconds and centrifuged at 15000 RPM for 10 min. at 4°C. The upper phase was transferred into a fresh tube, dried down in a Vacufuge plus speed-vac at room temperature and derivatized further with OBHA/EDC for metabolite analysis. The interphase was taken for protein estimation for normalization purpose. Proteins were resuspended in 5% SDS and heated at 37°C for 30 minutes. The protein concentration was determined using the Pierce BCA Protein Assay Kit Assay (ThermoFisher). For steady state analysis, the metabolite levels were normalized by per sample per total protein amount in µg.

For derivatization (328,329), the dried samples were dissolved in 50 µl of LC/MS grade water and 50 µl of 1M EDC (in Pyridine buffer, pH 5) was added. These samples were kept on a thermomixer for 10 min. at room temperature and 100 µl of 0.5M OBHA (in Pyridine buffer, pH 5) was added. The samples were incubated again for 1.5 hours on the thermomixer at 25°C, and metabolites were extracted by adding 300 µl of ethyl acetate and this step was repeated thrice. Samples were dried down in a Vacufuge plus speed-vac at room temperature and stored at -80°C until run for LC/MS analysis. A minimum of 3 biological replicates were taken per experiment.

^{13}C-isotopic labelling and stable isotope tracer analysis for TCA metabolite measurements

For isotopomer tracer analysis, wandering 3rd instar (WI) larvae were washed twice in PBS and lymph glands were dissected. Larval lymph glands were incubated in 10mM of U_{13}C-Pyruvate (Cambridge Isotope Laboratories, CLM-2440-0.5) in 1X PBS for 30 min. Samples were quickly rinsed in LC/MS grade water and processed for metabolite extraction and derivatization or amino acid extraction as done for steady state analysis.

Liquid chromatography-mass spectrometry (LC/MS/MS) analysis for TCA metabolites

The metabolite extract was separated using a Waters XBridge C18 Column (2.1 mm, 100 mm, 3.5 mm) on an Agilent QQQ 6470 system coupled to a Agilent 1290 UPLC system. The autosampler and column oven were kept at 4°C and 25°C, respectively. The buffers utilised for the analysis were, buffer A: Water plus 0.1% Formic Acid and buffer B 100% acetonitrile (ACN) plus 0.1% Formic Acid. A flow rate of 0.300 ml/minute was used for the chromatographic gradient as follows: 0 min- 10% B; 0.50 min: 10% B; 8 min: 100% B; 10 min: 10% B; 11 min: 10% B and at 16 min gradient was held at 10%B. MRM, positive ion mode was used for running the LC/MS and mass spectrometry detection was carried out on a QQQ Agilent 6470 system with ESI source attached to a UPLC system. For metabolite quantification, Peak areas were processed using MassHunter workstation (Agilent). Microsoft Excel 2016 and GraphPad Prism 9 software was used for statistical analysis.

Amino acid extraction and LC/MS/MS analysis from lymph glands

For amino acid analysis, TCA (trichloroacetic acid) precipitation method was utilized. Briefly, dissected lymph glands (5) were incubated in 200ul of 1X PBS (Gibco) and 40ul of TCA (100% TCA soln.) was added later. 10ul of ABA was added to each vial as an internal control. Samples were homogenized and incubated in ice for 10 minutes. After this, samples were centrifuged at 13000 RPM for 10 minutes at 4 degrees. Supernatant was transferred to fresh Eppendorf tubes and stored at -80 degrees until analysis. LC/MS/MS based analysis for amino acids was done utilizing HILIC column on Agilent UPLC-QQQ3 6470 system.

Targeted GSH:GSSG LC/MS/MS analysis

5 *Drosophila* larvae or 10 lymph glands per sample were dissected and kept in 200µl of GSH:GSSG buffer solution (62.5 mg NEM, 3 mg EDTA, 5 mg NaHO3 dissolved in 2 mL of 3:2 parts Water/MeOH (v/v)). Once all lymph glands were added to the buffer solution 10 µl of 100ng/ul of each internal standard was added 13C2-15N-GSH-NEM and 13C4-15N2-GSSG. Samples were homogenized using and stored at -80 degrees until further processing. TCA precipitation and extraction was done. Briefly samples were thawed, vortexed and centrifuged at 13000 RPM for 10 min. Solution was collected to new tubes and to this 100µl LC/MS grade water and 500µl of DCM (Dichloromethane) was added and vortexed to remove excess NEM. Samples were centrifuged again at 13000 RPM for 10 min. and aqueous fraction was collected, which

was speed-vac dried at room temperature. The dried samples were stored at -80 degrees until analysis (330).

LC/MS/MS analysis of GSH:GSSG was done on an Agilent 1290 Rapid Resolution liquid chromatography (UPLC) system coupled to an Agilent 6470 series QQQ mass spectrometer (MS/MS) (Agilent Technologies, Santa Clara, CA) and Waters T3 2.1 mm x 100 mm, 1.7 μm column was utilized for the LC separation (Water Corp, Milford, MA) (331). The autosampler and column oven were kept at 4°C and 25°C, respectively. The buffers utilised for the analysis were, buffer A: Water plus 0.1% Formic Acid and buffer B 100% acetonitrile (ACN) plus 0.1% Formic Acid. A flow rate of 0.300 ml/minute was used for the chromatographic gradient as follows: 0 min.: gradient 0% B; 2 min.: gradient 0% B; 8 min.: gradient 30% B; 9 min.: gradient 95% B; 9.1 min. gradient: 0% B; and at 15 min.: gradient 0% B. MRM, positive ion mode was used for running the LC/MS and mass spectrometry detection was carried out on a QQQ Agilent 6470 system with ESI source attached to a UPLC system. The other parameters for MS included jet stream ESI interface gas temperature of 350°C, gas flow rate at 9 L/min., nebulizer pressure 35 psi, sheath gas temp. 300°C, sheath gas flow rate at 9 L/min., capillary voltage was 4000V in positive ion mode, nozzle voltage of 1000V and ΔEMV voltage was kept 450V. For metabolite quantification, Peak areas were processed using MassHunter workstation (Agilent). Microsoft Excel 2016 and GraphPad Prism 9 software was used for statistical analysis.

Sample size and Statistical analyses

In all experiments "n" implies the total number of samples analysed which were obtained from multiple independent experimental repeats (N). All experiments have been repeated a minimum of three times and in each experimental setup, at least 5-10 animals were analysed. For *LC/MS based* steady-state and flux analysis five lymph glands per replicates were taken and each experiment included a minimum of three biological replicates. *Drosophila* are not limiting, therefore no power calculations were used to pre-determine sample size.

All statistical analyses and quantifications were performed using GraphPad Prism Nine and Microsoft Excel 2016. Graphs are plotted as median plots and non-parametric two tailed Mann-Whitney U test is employed for pairwise comparisons and Kruskal-Wallis test-Dunn's multiple comparison test is utilized for multiple comparisons to account for the variation between and within the experiments (332). Two-way ANOVA, Dunnett's

multiple comparison test is utilised for differentiation analysis and graphs are plotted as mean±SD plots. For LC/MS based data analysis is based on the methods of (314,333,334).

7 Discussion

The current thesis work has described the role of olfactory sensory in blood progenitor development which is achieved via regulation of redox homeostasis. In the first part of the study, we show that blood-progenitor cells of the lymph gland rely on TCA and OXPHOS to generate intracellular ROS. While its physiological levels do not control growth, its increased generation leads to retardation of lymph gland growth. Therefore, to control ROS production, the progenitor cells internalize olfaction-derived systemic GABA and via its breakdown into succinate, the cells activate PDK function. This facilitates PDH phosphorylation which limits TCA activity and consequently ROS production and supports lymph gland growth. In conditions with low progenitor GABA metabolism, the lack of succinate generation from this pathway promotes Hph function and reduction in PDK activation. This consequently leads to heightened TCA, increased ROS production and abrogation of lymph gland growth. Thus, conditions leading to block in progenitor GABA metabolism are susceptible to alterations in redox balance and subsequently hematopoietic growth defects. The second part of thesis describes the mechanism of glutathione synthesis regulation by GABA catabolic pathway. Glutathione, GSH is a potent antioxidant in the cells which regulate ROS scavenging by undergoing oxidation-reduction reactions. GABA catabolism derived succinate controls GSH synthesis in the blood-progenitor cells by controlling pyruvate metabolism. This regulation of GABA catabolic pathway on pyruvate flux is important to control cell fate decision including ROS homeostasis and lymph gland growth. GABA catabolic pathway controls serine synthesis, which is made in the cells from an intermediate step of glycolysis/gluconeogenic pathway. Serine further fuels cysteine formation which contributes to GSH formation and hence maintain glutathione levels in the progenitor cells. In this regard, animals with olfactory dysfunction that show a reduction in systemic GABA (172) have heightened ROS and smaller lymph glands. Taken together, we propose that *Drosophila* larvae rely on environmental odor-sensing derived GABA, as a means to moderate blood-progenitor TCA activity and ROS balance to maintain normal lymph gland growth and development.

7.1 GABA in myeloid development

A growing body of research has demonstrated that the mammalian nervous system controls innate immune responses via neuronal and hormonal pathways. Immune organs are directly innervated by the sympathetic and parasympathetic nervous systems,

whereas neuroendocrine variables regulate inflammation on a systemic scale. Moreover, the concept that the nervous system contributes to immunity is supported by the fact that immune cells express receptors for a variety of neuronal factors (335,336). Since the central nervous system is often assumed to suppress immunological responses, brain dysfunction, particularly some neurodegenerative illnesses, induces heightened immune responsiveness (337).

Recent findings have showcased the importance of GABA in myeloid immunity specifically with its role in metabolic-programming of myeloid cells during innate immune training (259,261–263). These studies indicate commonalities between the myeloid system of mammals and *Drosophila*. Our findings in the *Drosophila* hematopoietic system highlight the multiple developmental roles performed by GABA in myeloid development, progenitor homeostasis and immunity. The underlying crosstalk of GABA with other pathways to moderate such diverse functions (94,179) is also apparent. In homeostasis, the role of GABA as a ligand to activate $GABA_BR$ signaling and regulation of intra-cellular calcium homeostasis in progenitor-cells, maintains these cells in their undifferentiated state (172). In the context of immunity, GABA via its metabolism inhibits Hph and promotes Hifα/Sima stabilization to support a successful immune response (94). In this study, we show GABA as a necessary metabolite for hematopoietic growth. While the loss of GABA breakdown leads to hematopoietic growth retardation, its increase in blood cells is accompanied by a concomitant increase in lymph gland size. The regulation of PDK by GABA metabolism maintains homeostatic levels of progenitor ROS which supports normal lymph gland growth. The growth advantage provided by increased GABA as seen in *Gat* overexpression is via a TCA/ROS independent pathway which remains to be understood. In this study, we further find that GABA-mediated regulation of TCA activity is also necessary for proper lamellocyte induction during immune challenge. Together, the data reveal that in addition to promoting Sima (94), GABA via PDK inhibits TCA to bring about a successful immune response. Moreover, the requirement of GABA catabolism in regulation of GSH synthesis describes GABA as a central metabolic regulator in the blood-progenitor cells. GABA catabolism play dual role in control of ROS homeostasis of blood-progenitor compartment by both regulating ROS generation via controlling TCA activity and ROS scavenging by controlling GSH synthesis in the blood compartment. Thus, GABA in *Drosophila* myeloid-progenitor cells functions at the nexus of coordinating multiple intracellular signaling and

metabolic events that define cell fate decisions. The importance of GABA as a central regulator of myeloid development and function across systems including higher mammals is likely to emerge from such studies.

7.2 Regulators of blood-progenitor ROS

The central theme of the work undertaken in this study was based on the understanding that ROS as a signaling entity is critical for blood stem-progenitor development and maintenance as reported both in invertebrates and vertebrates (217,219,293,294,296,297). However, to sustain its developmental role, mechanisms controlling ROS levels that are critical towards its functioning in myeloid progenitor cells remain fairly uncharacterized. We show the importance of TCA activity and OXPHOS in the generation of ROS in progenitor-cells during homeostasis and the importance of pyruvate oxidation driving TCA activity. Loss of PDK function data proves PDK importance in the overall growth of the blood tissue. However, loss of either *Pdha* or *SdhA* function in progenitor cells, which resulted in further lowering of TCA and OXPHOS, failed to show any lymph gland growth phenotype. This implied that physiological levels of ROS did not contribute to lymph gland growth, it is only when ROS levels were over and above the basal threshold that it manifested a growth defect. The independence of physiological ROS in growth control is intriguing but needs a more thorough investigation. Additional sources of ROS, like Duox and NOx dependent mechanisms (338) or TCA derived succinate in reverse electron transport (RET) (339) are possibilities that have not been addressed. The regulation of ROS by catabolism of GABA derived succinate as opposed to TCA derived succinate that drives ROS generation, the data also reveal spatial localization and the availability of metabolites as distinct regulators of intracellular outcomes. Like the TCA, GABA breakdown also takes place in the mitochondria, but our data from the recent past and the current work highlights a distinct role for GABA-derived succinate in controlling cytosolic functions like Sima stabilization (94) and PDK enzyme activity. This raises the question of why TCA-derived succinate is not available to perform functions conducted by GABA-derived succinate? The TCA rate may be a limiting factor, or the two pathways contribute to spatially and temporally distinct pools of succinate that perform different functions. While this remains a speculation, metabolic flux analysis and spatial resolution of metabolites at a subcellular level are approaches that will address such fundamental questions.

Our work also describes the tight regulation on ROS scavenging mechanisms to maintain ROS homeostasis in the progenitor cells. We show that GABA catabolism derived succinate controls glutathione biosynthesis in the progenitor compartment and it is crucial not only to control ROS levels but is required for metabolic pathway homeostasis. It has been demonstrated that glutathione plays a crucial role in the development of blood progenitors, particularly in the context of red blood cell formation. Research has indicated that the production of glutathione is operative in leukocytes derived from preterm new-borns, implying its significance in preserving cellular glutathione concentrations (340). Glutathione is the predominant thiol found in red blood cells in embryonic mice, and its levels are kept constant at a particular ratio during development (341). Together, these results highlight the role that glutathione plays in the formation of blood progenitor cells. Here, we describe the mechanism of glutathione synthesis regulation in blood-progenitor cells. Glutathione (GSH) synthesis in blood-progenitors is tightly regulated, with key determinants being the availability of cysteine and the activity of the rate-limiting enzyme, glutamate cysteine ligase (GCL) (342,343). Indeed, our work show that cysteine is the limited amino acid that restricts glutathione formation in GABA mutant conditions. Furthermore, the production of glutathione is metabolically regulated, with different metabolic pathways being driven by pyruvate fuelling mediated by the GABA catabolic pathway.

Another unexpected finding from the study is the regulation of PDH and PDK function in ROS control by Hph, which is independent of Sima. In general, the inhibition of PDH activity is considered to be a downstream event of HIFα stabilization (344,345), which is mediated by the transcriptional induction of PDK expression. However, in our study loss of Sima from progenitor cells, a functional ortholog of mammalian Hifα, did not affect expression or activity of either PDH or PDK. On the contrary, our study identifies Hph function as a regulator of PDK activity in blood progenitor cells. Hifα independent functions of prolyl hydroxylases (Hph) are not unusual, but a mechanistic link between Hph and PDK independent of Hifα /Sima has not been described. The known Hifα independent function of prolyl hydroxylase, include regulation of transcriptional activity of NFκB (346) or Map organizer 1 (Morg1), a WD-repeat protein. Of these, NFκB activation via prolyl hydroxylase regulation is conducted by regulating activity of IKKβ, a kinase that in its non-hydroxylated form phosphorylates an inhibitory factor promoting NFκB activation. A similar mechanism for regulation of PDK activity by

Hph can be predicted, but a thorough understanding of this regulation requires further investigation.

7.3 Metabolic pathway dynamics in blood-development

The recent growth of metabolic studies in a developmental context has also shed light on increasing evidences that metabolic signals are involved in regulation of biological processes (347,348). Rather than merely running in the background, metabolism can shape developmental trajectories by participating in cellular signaling. Metabolites acting as direct signals or substrates for post-translational modifications, and 'moonlighting' metabolic enzymes have all been implicated in mediating the crosstalk between metabolism and developmental signaling (349–352).

Metabolic pathways play diverse role in maintenance and differentiation of blood-progenitor cells. HSC metabolism regulate their fate, it has been shown that loss of TCA inhibitory enzyme pyruvate dehydrogenase kinase (Pdk), responsible for inhibitory phosphorylation of PDH, an enzyme that converts pyruvate to acetyl CoA, leads to loss of HSC stemness capacity (295). PDK as a regulator of growth is evident in hypoxic conditions (295,353). PDK activity shunts pyruvate away from the citric acid cycle into lactate which keeps the hypoxic cell alive and growing (344). PDK activity in progenitor cells can be predicted as a central switch necessary for lymph gland growth and differentiation. Thus, regulation of PDK activity in progenitor cells can be envisaged as a core component whose regulation allows pyruvate availability for other processes contributing to growth. By directing pyruvate utilization into lactate via Ldh and other processes like the pentose phosphate pathway, lymph gland growth is supported. By invoking on PDK axis, GABA limits pyruvate's availability for its oxidation via the TCA. This sustains ROS homeostasis more efficiently and allows pyruvate availability for other metabolic arms necessary for lymph gland growth and progenitor maintenance.

Here, we demonstrate that pyruvate metabolism regulates blood-progenitor maintenance and differentiation by controlling their ROS levels. Pyruvate entry to TCA cycle is regulated by GABA catabolic pathway. Pyruvate is at the nexus of various metabolic pathways, it conversion to lactate is important for the glycolytic switch and thus mediate lamellocyte formation. Any increase in pyruvate conversion to acetyl-CoA and downstream TCA cycle leads to loss of ROS homeostasis and impairs lymph gland growth. Pyruvate feeding into gluconeogenic arm controls glutathione synthesis in the

progenitor cells and thus important for maintaining ROS homeostasis. The regulation of pyruvate flux in glutathione synthesis is a complex process involving various metabolic changes. (354) demonstrated that a decrease in pyruvate dehydrogenase (PDH) activity, which converts pyruvate to acetyl-CoA, can lead to a decrease in carbon flux from pyruvate to acetyl-CoA. This suggests a potential impact on the availability of acetyl-CoA for glutathione synthesis. The utilization of pyruvate and its conversion to glutamate, a precursor of glutathione, is also discussed by (355), providing further insight into the potential role of pyruvate in glutathione synthesis. Pyruvate metabolism is shown to impact stem cell homeostasis (356), pyruvate transport and its metabolism impacts intestinal stem cell homeostasis, where limiting pyruvate metabolism in the mitochondria is important to maintain stem cell homeostasis (357) and similarly, in context of adult neural stem cells, controlling pyruvate metabolism is important to regulate stem cell activation (358). Here, we have described the role of pyruvate in serine and downstream cysteine synthesis, which constitutes glutathione. Pyruvate availability and shunting to gluconeogenesis pathway in the blood-progenitor cells decides serine synthesis from 3-phosphoglycerate, which is a glycolytic intermediate. Thus, shunting of pyruvate towards other metabolic arms rather than TCA cycle maintain ROS homeostasis of blood progenitors and regulates homeostatic development of the lymph glands.

7.4 Olfactory mechanisms to control blood development

Olfaction is a central stress-sensing sensory input in animal. Research on a variety of systems has demonstrated the strong connection between immunity and smell (359). For example, mice with genetically altered olfactory systems exhibit elevated inflammatory signatures, reduced cellular immune function, and an inability to overcome an immune challenge (360). Certain odorants that are inhaled enhance the immune system's response to skin immunological reactions (361). This is achieved by modifying the activity of myeloid (362) and lymphoid (363) cells, which in turn reduces stress. These investigations demonstrate that there is pertinent interaction between immunity and olfaction. Research on the intricate physiological and mechanical foundations of this relationship is ongoing. We speculate the sensory module has perhaps also evolved to engage with the immune system to modulate its development as per environmental demands. Depending on the environmental context, odor-sensing and the types of odors sensed, relays information to the immune progenitor cells to

moderate their development or differentiation accordingly. When *Drosophila* larvae are dwelling in their food medium, the environmental odor conditions evolve from larval feeding stage to the wandering stage, when they leave the food medium and exposed to the external environment. During these time points, lymph gland transitions from being an actively growing and a proliferating organ, to an organ that has ceased its growth and embarks on a differentiation trajectory (20). When infested with predators, the olfaction axis is co-opted to enable improved hematopoietic growth and immune priming for the generation of successful immune responses. Thus, the importance of olfaction to enable the development of a competent immune system that functions superiorly when in need is a key point evident from this work as well. The results demonstrate that myeloid metabolism and ROS balance in them is sensitive to olfaction-derived GABA. This axis is necessary to maintain proper lymph gland growth and development. Whether the findings presented here are relevant for the development of blood-cells in higher organisms with complex lineages remains to be tested.

7.5 Significance of the study

Published literature has setup distinct metabolic demands of the myeloid progenitor development and differentiation (364,365). While recent evidences do point to distinct metabolic requirements of myeloid cells across systems ranging from mammals to invertebrates, a comprehensive study of this scale has not been attempted (21,366). Part of the problem is due to the developmental complexity seen in vertebrate model systems and general diversity seen in immune cell types, while in invertebrate systems the technical limitations have restricted the metabolic analysis. As a result the distinct metabolic process that regulate myeloid cell development and differentiation has been unexplored. In particular, metabolic and systemic effects on blood cell development are difficult to investigate *in vivo* in mammalian systems, and the *Drosophila* larval lymph gland presents an excellent genetically tractable model system to shed light on these complex issues, where an *in vivo* metabolic analysis can be performed. We have found that GABA catabolism in *Drosophila* blood progenitors regulates TCA cycle activity to control lymph gland growth (179). The function of neurotransmitters as signaling entities and metabolites in regulating myeloid progenitor development is quite intriguing. We show that, in homeostasis, myeloid-like blood progenitor cells of the Drosophila larvae, which reside in a specialized hematopoietic organ termed the lymph gland, use TCA to generate ROS. However, excessive ROS production leads to lymph

gland growth retardation. Therefore, to moderate blood progenitor ROS, *Drosophila* larvae rely on olfaction and its downstream systemic GABA. GABA internalization and its breakdown into succinate by progenitor cells activates pyruvate dehydrogenase kinase (PDK), which controls inhibitory phosphorylation of pyruvate dehydrogenase (PDH). PDH is the rate-limiting enzyme that connects pyruvate to the TCA cycle and to oxidative phosphorylation. Thus, GABA metabolism via PDK activation maintains TCA activity and blood progenitor ROS homeostasis, and supports normal lymph gland growth. Consequently, animals that fail to smell also fail to sustain TCA activity and ROS homeostasis, which leads to lymph gland growth retardation. Overall, this study describes the requirement of animal odor-sensing and GABA in myeloid ROS regulation and hematopoietic growth control.

Our findings also highlight a second important function of the olfactory derived GABA in lymph gland progenitor cells. GABA catabolism restricts pyruvate metabolism to control ROS scavenging by regulating glutathione (GSH) synthesis, a prime antioxidant. We found that GABA catabolism regulate cysteine synthesis by modulating serine levels in lymph gland, resulting from a regulation on pyruvate flux in the lymph gland blood-progenitor cells. This enables the blood progenitor cells with a capacity to generate, glutathione, a potent antioxidant. Together, this dual modality keeps ROS levels in the blood progenitor cells in check. Upon olfactory stimulation, neuronally derived systemic GABA is utilized by blood progenitors cells and metabolized. In animals with olfactory dysfunction the low GABA in them leads to, loss of ROS homeostasis. Taken together, these findings link animal odor-sensing to systemic moderation of blood progenitor metabolism and redox homeostasis.

Further, to decipher the role of metabolic pathways in lymph gland growth and differentiation, a more comprehensive metabolic analysis is undertaken. We have standardized and established the 13C-isotope based metabolic flux analysis from *Drosophila* larval lymph glands. Our analysis has shown the dynamics of various metabolic pathways that contribute to the homeostatic development and growth of the blood-progenitor compartment. As *Drosophila* blood progenitors are akin to vertebrate myeloid lineage, this analysis will indicate the existence of similar type of metabolic regulation in the vertebrate myeloid development.

7.6 Concluding remarks and future directions

Various studies have unveiled the distinct metabolic requirements of myeloid development across systems ranging from mammals to invertebrates. Diverse signaling cues have been shown to regulate blood progenitor development and the involvement of metabolic pathways in myeloid development is emerging. However, the distinct metabolic process that regulate myeloid cell development and differentiation has been unexplored. In the current work, we show that olfaction derived GABA release and its downstream catabolism in blood-progenitor cells regulate ROS homeostasis, blood-progenitor development and supports lymph gland growth. We undertook a comprehensive study of metabolic pathways and metabolites during blood cell development utilizing genetics, immunohistochemistry, microscopy and mass-spectrometry based approaches. Our analysis show that GABA catabolic pathway restricts pyruvate metabolism in blood-progenitor cells, and it determines the fate of pyruvate towards distinct metabolic pathways to control blood-progenitor maintenance and differentiation. Collectively, we show that olfaction derived GABA catabolism control blood progenitor development and homeostasis by regulating ROS generation and ROS scavenging mechanisms. We have identified the metabolic requirement of odor sensing and GABA in regulating redox homeostasis during *Drosophila* myeloid progenitor development, the relevance of which may be broadly conserved.

The present study raises a number of questions that require investigation and is presently being worked on. Understanding the importance of metabolic pathway dynamics in controlling blood-progenitor development lymph gland homeostasis is intriguing. Nonetheless, the current research work has outlined the several routes by which olfaction derived GABA regulation of pyruvate metabolism controls blood progenitor development and differentiation. More research is necessary to understand how this metabolic pathway, specifically, the TCA cycle builds up during blood development and regulate homeostasis. The current work also shows that the olfaction/GABA axis is required for the regulation of GSH synthesis; nevertheless, the role that GSH plays in regulating other cellular activities and fate specification, aside from controlling ROS homeostasis, is still unclear. Another area of active research is how the olfaction/GABA axis regulates metabolic pathways to generate a competent cell type like a lamellocyte. Olfactory cues affect GABA release and its detection by the blood-progenitors. Examining the mechanism of ORN regulation in mediating GABA release from brain is another question that demands further exploration. Our

initial research in this area highlights the significance of ORN metabolic status in triggering downstream controls that lead to blood formation. It is fascinating to see how the metabolic state of various ORNs control blood development under homeostatic and immune response scenarios. This will highlight the significance and mechanism of olfactory sensing in blood development. These findings call for further research into these mechanisms in more complex systems because they go beyond the context of invertebrate model systems and are not exclusive to *Drosophila* blood development.

8 References

1. Banerjee U, Girard JR, Goins LM, Spratford CM. Drosophila as a Genetic Model for Hematopoiesis. Genetics. 2019/02/09 ed. 2019;211(2):367–417.

2. Martinez-Agosto JA, Mikkola HKA, Hartenstein V, Banerjee U. The hematopoietic stem cell and its niche: a comparative view. Genes Dev. 2007 Dec 1;21(23):3044–60.

3. Jagannathan-Bogdan M, Zon LI. Hematopoiesis. Dev Camb Engl. 2013 Jun;140(12):2463–7.

4. Dzierzak E, Speck NA. Of lineage and legacy: the development of mammalian hematopoietic stem cells. Nat Immunol. 2008 Feb;9(2):129–36.

5. Paik EJ, Zon LI. Hematopoietic development in the zebrafish. Int J Dev Biol. 2010;54(6–7):1127–37.

6. Palis J, Yoder MC. Yolk-sac hematopoiesis: the first blood cells of mouse and man. Exp Hematol. 2001 Aug;29(8):927–36.

7. Orkin SH. Diversification of haematopoietic stem cells to specific lineages. Nat Rev Genet. 2000 Oct;1(1):57–64.

8. Orkin SH, Zon LI. Hematopoiesis: an evolving paradigm for stem cell biology. Cell. 2008 Feb 22;132(4):631–44.

9. Cumano A, Godin I. Ontogeny of the hematopoietic system. Annu Rev Immunol. 2007;25:745–85.

10. Dzierzak E. Embryonic Beginnings of Definitive Hematopoietic Stem Cells. Ann N Y Acad Sci. 1999 Apr;872(1):256–64.

11. Belyavsky A, Petinati N, Drize N. Hematopoiesis during Ontogenesis, Adult Life, and Aging. Int J Mol Sci. 2021 Aug 26;22(17):9231.

12. Tepass U, Fessler LI, Aziz A, Hartenstein V. Embryonic origin of hemocytes and their relationship to cell death in *Drosophila*. Development. 1994 Jul 1;120(7):1829–37.

13. Lebestky T, Chang T, Hartenstein V, Banerjee U. Specification of Drosophila hematopoietic lineage by conserved transcription factors. Science. 2000 Apr 7;288(5463):146–9.

14. Rizki MT, Rizki RM. Functional significance of the crystal cells in the larva of Drosophila melanogaster. J Biophys Biochem Cytol. 1959 Mar 25;5(2):235–40.

15. Galko MJ, Krasnow MA. Cellular and Genetic Analysis of Wound Healing in Drosophila Larvae. Alfonso Martinez Arias, editor. PLoS Biol. 2004 Jul 20;2(8):e239.

16. Rizki RM, Rizki TM. Selective destruction of a host blood cell type by a parasitoid wasp. Proc Natl Acad Sci. 1984 Oct;81(19):6154–8.

17. Holz A, Bossinger B, Strasser T, Janning W, Klapper R. The two origins of hemocytes in Drosophila. Dev Camb Engl. 2003 Oct;130(20):4955–62.

18. Rugendorff A, Younossi-Hartenstein A, Hartenstein V. Embryonic origin and differentiation of the Drosophila heart. Rouxs Arch Dev Biol. 1994 Mar;203(5):266–80.

19. Shrestha R, Gateff E. Ultrastructure and Cytochemistry of the Cell Types in the Larval Hematopoietic Organs and Hemolymph of Drosophila Melanogaster. (drosophila/hematopoiesis/blool cells/ultrastructure/cytochemistry). Dev Growth Differ. 1982 Feb;24(1):65–82.

20. Evans CJ, Hartenstein V, Banerjee U. Thicker Than Blood. Dev Cell. 2003 Nov;5(5):673–90.

21. Gold KS, Brückner K. Drosophila as a model for the two myeloid blood cell systems in vertebrates. Exp Hematol. 2014 Aug;42(8):717–27.

22. Letourneau M, Lapraz F, Sharma A, Vanzo N, Waltzer L, Crozatier M. *Drosophila* hematopoiesis under normal conditions and in response to immune stress. FEBS Lett. 2016 Nov;590(22):4034–51.

23. Fujiwara Y, Chang AN, Williams AM, Orkin SH. Functional overlap of GATA-1 and GATA-2 in primitive hematopoietic development. Blood. 2004 Jan 15;103(2):583–5.

24. Rehorn KP, Thelen H, Michelson AM, Reuter R. A molecular aspect of hematopoiesis and endoderm development common to vertebrates and Drosophila. Dev Camb Engl. 1996 Dec;122(12):4023–31.

25. Pevny L, Simon MC, Robertson E, Klein WH, Tsai SF, D'Agati V, et al. Erythroid differentiation in chimaeric mice blocked by a targeted mutation in the gene for transcription factor GATA-1. Nature. 1991 Jan;349(6306):257–60.

26. Shivdasani RA, Fujiwara Y, McDevitt MA, Orkin SH. A lineage-selective knockout establishes the critical role of transcription factor GATA-1 in megakaryocyte growth and platelet development. EMBO J. 1997 Jul 1;16(13):3965–73.

27. Ting CN, Olson MC, Barton KP, Leiden JM. Transcription factor GATA-3 is required for development of the T-cell lineage. Nature. 1996 Dec;384(6608):474–8.

28. Tsai FY, Keller G, Kuo FC, Weiss M, Chen J, Rosenblatt M, et al. An early haematopoietic defect in mice lacking the transcription factor GATA-2. Nature. 1994 Sep 15;371(6494):221–6.

29. Fossett N, Tevosian SG, Gajewski K, Zhang Q, Orkin SH, Schulz RA. The Friend of GATA proteins U-shaped, FOG-1, and FOG-2 function as negative regulators of blood, heart, and eye development in *Drosophila*. Proc Natl Acad Sci. 2001 Jun 19;98(13):7342–7.

30. Fossett N, Hyman K, Gajewski K, Orkin SH, Schulz RA. Combinatorial interactions of serpent, lozenge, and U-shaped regulate crystal cell lineage commitment during Drosophila hematopoiesis. Proc Natl Acad Sci U S A. 2003 Sep 30;100(20):11451–6.

31. Cantor AB, Katz SG, Orkin SH. Distinct domains of the GATA-1 cofactor FOG-1 differentially influence erythroid versus megakaryocytic maturation. Mol Cell Biol. 2002 Jun;22(12):4268–79.

32. Katz SG, Cantor AB, Orkin SH. Interaction between FOG-1 and the corepressor C-terminal binding protein is dispensable for normal erythropoiesis in vivo. Mol Cell Biol. 2002 May;22(9):3121–8.

33. Tsang AP, Visvader JE, Turner CA, Fujiwara Y, Yu C, Weiss MJ, et al. FOG, a multitype zinc finger protein, acts as a cofactor for transcription factor GATA-1 in erythroid and megakaryocytic differentiation. Cell. 1997 Jul 11;90(1):109–19.

34. Tsang AP, Fujiwara Y, Hom DB, Orkin SH. Failure of megakaryopoiesis and arrested erythropoiesis in mice lacking the GATA-1 transcriptional cofactor FOG. Genes Dev. 1998 Apr 15;12(8):1176–88.

35. Crispino JD, Lodish MB, Thurberg BL, Litovsky SH, Collins T, Molkentin JD, et al. Proper coronary vascular development and heart morphogenesis depend on interaction of GATA-4 with FOG cofactors. Genes Dev. 2001 Apr 1;15(7):839–44.

36. Svensson EC, Tufts RL, Polk CE, Leiden JM. Molecular cloning of FOG-2: a modulator of transcription factor GATA-4 in cardiomyocytes. Proc Natl Acad Sci U S A. 1999 Feb 2;96(3):956–61.

37. Tevosian SG, Deconinck AE, Cantor AB, Rieff HI, Fujiwara Y, Corfas G, et al. FOG-2: A novel GATA-family cofactor related to multitype zinc-finger proteins Friend of GATA-1 and U-shaped. Proc Natl Acad Sci. 1999 Feb 2;96(3):950–5.

38. Okuda T, van Deursen J, Hiebert SW, Grosveld G, Downing JR. AML1, the target of multiple chromosomal translocations in human leukemia, is essential for normal fetal liver hematopoiesis. Cell. 1996 Jan 26;84(2):321–30.

39. Sasaki K, Yagi H, Bronson RT, Tominaga K, Matsunashi T, Deguchi K, et al. Absence of fetal liver hematopoiesis in mice deficient in transcriptional coactivator core binding factor beta. Proc Natl Acad Sci U S A. 1996 Oct 29;93(22):12359–63.

40. Wang Q, Stacy T, Binder M, Marin-Padilla M, Sharpe AH, Speck NA. Disruption of the Cbfa2 gene causes necrosis and hemorrhaging in the central nervous system and blocks definitive hematopoiesis. Proc Natl Acad Sci U S A. 1996 Apr 16;93(8):3444–9.

41. Wang Q, Stacy T, Miller JD, Lewis AF, Gu TL, Huang X, et al. The CBFβ Subunit Is Essential for CBFα2 (AML1) Function In Vivo. Cell. 1996 Nov;87(4):697–708.

42. Rizki T, Rizki R. Alleles of lz as suppressors of the Bc-phene in Drosophila melanogaster. Genetics. 1981;97(Suppl 1):s90.

43. Allman D, Aster JC, Pear WS. Notch signaling in hematopoiesis and early lymphocyte development. Immunol Rev. 2002 Sep;187:75–86.

44. Duvic B, Hoffmann JA, Meister M, Royet J. Notch signaling controls lineage specification during Drosophila larval hematopoiesis. Curr Biol CB. 2002 Nov 19;12(22):1923–7.

45. Lebestky T, Jung SH, Banerjee U. A Serrate-expressing signaling center controls Drosophila hematopoiesis. Genes Dev. 2003 Feb 1;17(3):348–53.

46. Radtke F, Wilson A, Ernst B, MacDonald HR. The role of Notch signaling during hematopoietic lineage commitment. Immunol Rev. 2002 Sep;187:65–74.

47. Lindsell CE, Shawber CJ, Boulter J, Weinmaster G. Jagged: a mammalian ligand that activates Notch1. Cell. 1995 Mar 24;80(6):909–17.

48. Varnum-Finney B, Purton LE, Yu M, Brashem-Stein C, Flowers D, Staats S, et al. The Notch ligand, Jagged-1, influences the development of primitive hematopoietic precursor cells. Blood. 1998 Jun 1;91(11):4084–91.

49. Marshall CJ, Kinnon C, Thrasher AJ. Polarized expression of bone morphogenetic protein-4 in the human aorta-gonad-mesonephros region. Blood. 2000 Aug 15;96(4):1591–3.

50. Nishikawa M, Tahara T, Hinohara A, Miyajima A, Nakahata T, Shimosaka A. Role of the microenvironment of the embryonic aorta-gonad-mesonephros region in hematopoiesis. Ann N Y Acad Sci. 2001 Jun;938:109–16.

51. Bodmer R. The gene tinman is required for specification of the heart and visceral muscles in Drosophila. Dev Camb Engl. 1993 Jul;118(3):719–29.

52. Mandal L, Banerjee U, Hartenstein V. Evidence for a fruit fly hemangioblast and similarities between lymph-gland hematopoiesis in fruit fly and mammal aorta-gonadal-mesonephros mesoderm. Nat Genet. 2004 Sep 1;36(9):1019–23.

53. Cho NK, Keyes L, Johnson E, Heller J, Ryner L, Karim F, et al. Developmental Control of Blood Cell Migration by the Drosophila VEGF Pathway. Cell. 2002 Mar;108(6):865–76.

54. Ferrara N, Gerber HP, LeCouter J. The biology of VEGF and its receptors. Nat Med. 2003 Jun;9(6):669–76.

55. Gerondakis S, Grossmann M, Nakamura Y, Pohl T, Grumont R. Genetic approaches in mice to understand Rel/NF-κB and IκB function: transgenics and knockouts. Oncogene. 1999 Nov 22;18(49):6888–95.

56. Hou SX, Zheng Z, Chen X, Perrimon N. The Jak/STAT pathway in model organisms: emerging roles in cell movement. Dev Cell. 2002 Dec;3(6):765–78.

57. Lemaitre B, Meister M, Govind S, Georgel P, Steward R, Reichhart JM, et al. Functional analysis and regulation of nuclear import of dorsal during the immune response in Drosophila. EMBO J. 1995 Feb;14(3):536–45.

58. Rane SG, Reddy EP. JAKs, STATs and Src kinases in hematopoiesis. Oncogene. 2002 May 13;21(21):3334–58.

59. Kimelman D, Martin BL. Anterior-posterior patterning in early development: three strategies. Wiley Interdiscip Rev Dev Biol. 2012;1(2):253–66.

60. Brand AH, Perrimon N. Targeted gene expression as a means of altering cell fates and generating dominant phenotypes. Dev Camb Engl. 1993 Jun;118(2):401–15.

61. El Shatoury HH. The structure of the lymph glands ofDrosophila larvae. Wilhelm Roux Arch Entwicklungsmechanik Org. 1955 Jul;147(4–5):489–95.

62. Jung SH, Evans CJ, Uemura C, Banerjee U. The Drosophila lymph gland as a developmental model of hematopoiesis. Dev Camb Engl. 2005 Jun;132(11):2521–33.

63. Lan W, Liu S, Zhao L, Su Y. Regulation of drosophila hematopoiesis in lymph gland: From a developmental signaling point of view. Int J Mol Sci. 2020;21(15):1–15.

64. Crozatier M, Ubeda JM, Vincent A, Meister M. Cellular Immune Response to Parasitization in Drosophila Requires the EBF Orthologue Collier. Michael Levine, editor. PLoS Biol. 2004 Aug 17;2(8):e196.

65. Mandal L, Martinez-Agosto JA, Evans CJ, Hartenstein V, Banerjee U. A Hedgehog- and Antennapedia-dependent niche maintains Drosophila haematopoietic precursors. Nature. 2007 Mar 15;446(7133):320–4.

66. Dey NS, Ramesh P, Chugh M, Mandal S, Mandal L. Dpp dependent Hematopoietic stem cells give rise to Hh dependent blood progenitors in larval lymph gland of Drosophila. Elife [Internet]. 2016;5. Available from: https://www.ncbi.nlm.nih.gov/pubmed/27782877

67. Mikkola HKA, Orkin SH. The journey of developing hematopoietic stem cells. Dev Camb Engl. 2006 Oct;133(19):3733–44.

68. Krzemien J, Dubois L, Makki R, Meister M, Vincent A, Crozatier M. Control of blood cell homeostasis in Drosophila larvae by the posterior signalling centre. Nature. 2007;446(7133):325–8.

69. Luo F, Yu S, Jin LH. The Posterior Signaling Center Is an Important Microenvironment for Homeostasis of the Drosophila Lymph Gland. Front Cell Dev Biol. 2020;8:382.

70. Khadilkar RJ, Vogl W, Goodwin K, Tanentzapf G. Modulation of occluding junctions alters the hematopoietic niche to trigger immune activation. eLife. 2017 Aug 25;6:e28081.

71. Sinenko SA, Mandal L, Martinez-Agosto JA, Banerjee U. Dual role of wingless signaling in stem-like hematopoietic precursor maintenance in Drosophila. Dev Cell. 2009;16(5):756–63.

72. Owusu-Ansah E, Banerjee U. Reactive oxygen species prime Drosophila haematopoietic progenitors for differentiation. Nature. 2009 Sep 24;461(7263):537–41.

73. Small C, Ramroop J, Otazo M, Huang LH, Saleque S, Govind S. An unexpected link between notch signaling and ROS in restricting the differentiation of hematopoietic progenitors in Drosophila. Genetics. 2014 Jun;197(2):471–83.

74. Mondal BC, Mukherjee T, Mandal L, Evans CJ, Sinenko SA, Martinez-Agosto JA, et al. Interaction between differentiating cell- and niche-derived signals in hematopoietic progenitor maintenance. Cell. 2011 Dec 23;147(7):1589–600.

75. Benmimoun B, Polesello C, Waltzer L, Haenlin M. Dual role for Insulin/TOR signaling in the control of hematopoietic progenitor maintenance in Drosophila. Development. 2012 May 15;139(10):1713–7.

76. Ho KYL, An K, Carr RL, Dvoskin AD, Ou AYJ, Vogl W, et al. Maintenance of hematopoietic stem cell niche homeostasis requires gap junction–mediated calcium signaling. Proc Natl Acad Sci [Internet]. 2023 Nov 7;120(45). Available from: https://pnas.org/doi/10.1073/pnas.2303018120

77. Gueguen G, Kalamarz ME, Ramroop J, Uribe J, Govind S. Polydnaviral ankyrin proteins aid parasitic wasp survival by coordinate and selective inhibition of hematopoietic and immune NF-kappa B signaling in insect hosts. PLoS Pathog. 2013;9(8):e1003580.

78. Irving P, Ubeda JM, Doucet D, Troxler L, Lagueux M, Zachary D, et al. New insights into Drosophila larval haemocyte functions through genome-wide analysis. Cell Microbiol. 2005;7(3):335–50.

79. Benmimoun B, Polesello C, Haenlin M, Waltzer L. The EBF transcription factor Collier directly promotes *Drosophila* blood cell progenitor maintenance independently of the niche. Proc Natl Acad Sci. 2015 Jul 21;112(29):9052–7.

80. Hombría JCG, Brown S, Häder S, Zeidler MP. Characterisation of Upd2, a Drosophila JAK/STAT pathway ligand. Dev Biol. 2005 Dec 15;288(2):420–33.

81. Oyallon J, Vanzo N, Krzemień J, Morin-Poulard I, Vincent A, Crozatier M. Two Independent Functions of Collier/Early B Cell Factor in the Control of Drosophila Blood Cell Homeostasis. PloS One. 2016;11(2):e0148978.

82. Minakhina S, Steward R. Melanotic Mutants in Drosophila: Pathways and Phenotypes. Genetics. 2006 Sep 1;174(1):253–63.

83. Gao H, Wu X, Fossett N. Drosophila E-cadherin functions in hematopoietic progenitors to maintain multipotency and block differentiation. PloS One. 2013;8(9):e74684.

84. Asha H, Nagy I, Kovacs G, Stetson D, Ando I, Dearolf CR. Analysis of Ras-induced overproliferation in Drosophila hemocytes. Genetics. 2003 Jan;163(1):203–15.

85. Fessler LI, Nelson RE, Fessler JH. Drosophila extracellular matrix. Methods Enzymol. 1994;245:271–94.

86. Yasothornsrikul S, Davis WJ, Cramer G, Kimbrell DA, Dearolf CR. viking: identification and characterization of a second type IV collagen in Drosophila. Gene. 1997 Oct 1;198(1–2):17–25.

87. Goto A, Kumagai T, Kumagai C, Hirose J, Narita H, Mori H, et al. A Drosophila haemocyte-specific protein, hemolectin, similar to human von Willebrand factor. Biochem J. 2001 Oct 1;359(Pt 1):99–108.

88. Goto A, Kadowaki T, Kitagawa Y. Drosophila hemolectin gene is expressed in embryonic and larval hemocytes and its knock down causes bleeding defects. Dev Biol. 2003 Dec;264(2):582–91.

89. Nelson RE, Fessler LI, Takagi Y, Blumberg B, Keene DR, Olson PF, et al. Peroxidasin: a novel enzyme-matrix protein of Drosophila development. EMBO J. 1994 Aug;13(15):3438–47.

90. Vilmos P, Nagy I, Kurucz E, Hultmark D, Gateff E, Andó I. A rapid rosetting method for separation of hemocyte sub-populations of Drosophila melanogaster. Dev Comp Immunol. 2004 May 17;28(6):555–63.

91. Minakhina S, Tan W, Steward R. JAK/STAT and the GATA factor Pannier control hemocyte maturation and differentiation in Drosophila. Dev Biol. 2011 Apr;352(2):308–16.

92. Tan KL, Goh SC, Minakhina S. Genetic screen for regulators of lymph gland homeostasis and hemocyte maturation in Drosophila. G3 Bethesda Md. 2012 Mar;2(3):393–405.

93. Zettervall CJ, Anderl I, Williams MJ, Palmer R, Kurucz E, Ando I, et al. A directed screen for genes involved in *Drosophila* blood cell activation. Proc Natl Acad Sci. 2004 Sep 28;101(39):14192–7.

94. Madhwal S, Shin M, Kapoor A, Goyal M, Joshi MK, Ur Rehman PM, et al. Metabolic control of cellular immune-competency by odors in Drosophila. Lemaitre B, Akhmanova A, Dolezal T, Kacsoh BZ, editors. eLife. 2020 Dec 29;9:e60376.

95. Krzemien J, Crozatier M, Vincent A. Ontogeny of the Drosophila larval hematopoietic organ, hemocyte homeostasis and the dedicated cellular immune response to parasitism. Int J Dev Biol. 2010;54(6–7):1117–25.

96. Spratford CM, Goins LM, Chi F, Girard JR, Macias SN, Ho VW, et al. Intermediate progenitor cells provide a transition between hematopoietic progenitors and their differentiated descendants. Development [Internet]. 2021 Dec 15;148(24). Available from:

https://journals.biologists.com/dev/article/148/24/dev200216/273785/Intermediate-progenitor-cells-provide-a-transition

97. Morin-Poulard I, Destalminil-Letourneau M, Bataillé L, Frendo JL, Lebreton G, Vanzo N, et al. Identification of Bipotential Blood Cell/Nephrocyte Progenitors in Drosophila: Another Route for Generating Blood Progenitors. Front Cell Dev Biol [Internet]. 2022 Feb 14;10. Available from: https://www.frontiersin.org/articles/10.3389/fcell.2022.834720/full

98. Ghosh S, Singh A, Mandal S, Mandal L. Active hematopoietic hubs in Drosophila adults generate hemocytes and contribute to immune response. Dev Cell. 2015 May 26;33(4):478–88.

99. Rodrigues D, Renaud Y, Vijayraghavan K, Waltzer L, Inamdar MS. Differential activation of jak-stat signaling reveals functional compartmentalization in drosophila blood progenitors. eLife. 2021 Feb 1;10:1–77.

100. Kanwal A, Joshi PV, Mandal S, Mandal L. Ubx-Collier signaling cascade maintains blood progenitors in the posterior lobes of the Drosophila larval lymph gland. Wang H, editor. PLOS Genet. 2021 Aug 9;17(8):e1009709.

101. Kulkarni V, Khadilkar RJ, M. S. S, Inamdar MS. Asrij Maintains the Stem Cell Niche and Controls Differentiation during Drosophila Lymph Gland Hematopoiesis. Samakovlis C, editor. PLoS ONE. 2011 Nov 14;6(11):e27667.

102. Sorrentino RP, Carton Y, Govind S. Cellular Immune Response to Parasite Infection in the Drosophila Lymph Gland Is Developmentally Regulated. Dev Biol. 2002 Mar;243(1):65–80.

103. Stofanko M, Kwon SY, Badenhorst P. Lineage Tracing of Lamellocytes Demonstrates Drosophila Macrophage Plasticity. PLoS ONE. 2010 Nov 19;5(11):e14051.

104. Defaye A, Evans I, Crozatier M, Wood W, Lemaitre B, Leulier F. Genetic ablation of Drosophila phagocytes reveals their contribution to both development and resistance to bacterial infection. J Innate Immun. 2009;1(4):322–34.

105. Minakhina S, Steward R. Hematopoietic stem cells in Drosophila. Dev Camb Engl. 2010 Jan;137(1):27–31.

106. Mondal BC, Shim J, Evans CJ, Banerjee U. Pvr expression regulators in equilibrium signal control and maintenance of Drosophila blood progenitors. eLife. 2014 Sep 8;3:e03626.

107. Blanco-Obregon D, Katz MJ, Durrieu L, Gándara L, Wappner P. Context-specific functions of Notch in Drosophila blood cell progenitors. Dev Biol. 2020 Jun 1;462(1):101–15.

108. Ho KYL, Carr RL, Dvoskin AD, Tanentzapf G. Kinetics of blood cell differentiation during hematopoiesis revealed by quantitative long-term live imaging. eLife. 2023 Mar 31;12:e84085.

109. Cho B, Yoon SH, Lee D, Koranteng F, Tattikota SG, Cha N, et al. Single-cell transcriptome maps of myeloid blood cell lineages in Drosophila. Nat Commun. 2020 Dec 1;11(1).

110. Girard JR, Goins LM, Vuu DM, Sharpley MS, Spratford CM, Mantri SR, et al. Paths and pathways that generate cell-type heterogeneity and developmental progression in hematopoiesis. eLife [Internet]. 2021 Oct 29;10. Available from: https://elifesciences.org/articles/67516

111. Grigorian M, Mandal L, Hartenstein V. Hematopoiesis at the onset of metamorphosis: terminal differentiation and dissociation of the Drosophila lymph gland. Dev Genes Evol. 2011 Aug;221(3):121–31.

112. Coates JA, Brooks E, Brittle AL, Armitage EL, Zeidler MP, Evans IR. Identification of functionally distinct macrophage subpopulations in Drosophila. eLife. 2021 Apr 22;10:e58686.

113. Alfonso TB, Jones BW. gcm2 Promotes Glial Cell Differentiation and Is Required with glial cells missing for Macrophage Development in Drosophila. Dev Biol. 2002 Aug;248(2):369–83.

114. Bernardoni R, Vivancos V, Giangrande A. glide/gcm is expressed and required in the scavenger cell lineage. Dev Biol. 1997 Nov 1;191(1):118–30.

115. Kocks C, Cho JH, Nehme N, Ulvila J, Pearson AM, Meister M, et al. Eater, a Transmembrane Protein Mediating Phagocytosis of Bacterial Pathogens in Drosophila. Cell. 2005 Oct;123(2):335–46.

116. Franc NC, Dimarcq JL, Lagueux M, Hoffmann J, Ezekowitz RAB. Croquemort, A Novel Drosophila Hemocyte/Macrophage Receptor that Recognizes Apoptotic Cells. Immunity. 1996 May;4(5):431–43.

117. Kurucz É, Márkus R, Zsámboki J, Folkl-Medzihradszky K, Darula Z, Vilmos P, et al. Nimrod, a Putative Phagocytosis Receptor with EGF Repeats in Drosophila Plasmatocytes. Curr Biol. 2007 Apr;17(7):649–54.

118. Kurucz E, Váczi B, Márkus R, Laurinyecz B, Vilmos P, Zsámboki J, et al. Definition of Drosophila hemocyte subsets by cell-type specific antigens. Acta Biol Hung. 2007;58 Suppl:95–111.

119. Ratheesh A, Belyaeva V, Siekhaus DE. Drosophila immune cell migration and adhesion during embryonic development and larval immune responses. Curr Opin Cell Biol. 2015 Oct;36:71–9.

120. Rizki RM, Rizki TM. Cell Interactions in the Differentiation of a Melanotic Tumor in Drosophila. Differentiation. 1979 Feb;12(1–3):167–78.

121. Charroux B, Royet J. Elimination of plasmatocytes by targeted apoptosis reveals their role in multiple aspects of the *Drosophila* immune response. Proc Natl Acad Sci. 2009 Jun 16;106(24):9797–802.

122. Bunt S, Hooley C, Hu N, Scahill C, Weavers H, Skaer H. Hemocyte-Secreted Type IV Collagen Enhances BMP Signaling to Guide Renal Tubule Morphogenesis in Drosophila. Dev Cell. 2010 Aug;19(2):296–306.

123. Olofsson B, Page DT. Condensation of the central nervous system in embryonic Drosophila is inhibited by blocking hemocyte migration or neural activity. Dev Biol. 2005 Mar;279(1):233–43.

124. Martinek N, Shahab J, Saathoff M, Ringuette M. Haemocyte-derived SPARC is required for collagen-IV-dependent stability of basal laminae in Drosophila embryos. J Cell Sci. 2008 May 15;121(Pt 10):1671–80.

125. Lanot R, Zachary D, Holder F, Meister M. Postembryonic hematopoiesis in Drosophila. Dev Biol. 2001 Feb 15;230(2):243–57.

126. Moussalem D, Augé B, Di Stefano L, Osman D, Gobert V, Haenlin M. Two Isoforms of serpent Containing Either One or Two GATA Zinc Fingers Provide Functional Diversity During Drosophila Development. Front Cell Dev Biol. 2022 Feb 1;9:795680.

127. Muratoglu S, Garratt B, Hyman K, Gajewski K, Schulz RA, Fossett N. Regulation of Drosophila Friend of GATA gene, u-shaped, during hematopoiesis: A direct role for Serpent and Lozenge. Dev Biol. 2006 Aug;296(2):561–79.

128. Rizki TM, Rizki RM, Grell EH. A mutant affecting the crystal cells inDrosophila melanogaster. Wilhelm Rouxs Arch Dev Biol. 1980;188(2):91–9.

129. Waltzer L. Cooperation between the GATA and RUNX factors Serpent and Lozenge during Drosophila hematopoiesis. EMBO J. 2003 Dec 15;22(24):6516–25.

130. Milton CC, Grusche FA, Degoutin JL, Yu E, Dai Q, Lai EC, et al. The Hippo Pathway Regulates Hematopoiesis in Drosophila melanogaster. Curr Biol. 2014 Nov;24(22):2673–80.

131. Mukherjee T, Kim WS, Mandal L, Banerjee U. Interaction Between Notch and Hif-α in Development and Survival of Drosophila Blood Cells. Science. 2011 Jun 3;332(6034):1210–3.

132. Babcock DT, Brock AR, Fish GS, Wang Y, Perrin L, Krasnow MA, et al. Circulating blood cells function as a surveillance system for damaged tissue in *Drosophila* larvae. Proc Natl Acad Sci. 2008 Jul 22;105(29):10017–22.

133. Cerenius L, Lee BL, Söderhäll K. The proPO-system: pros and cons for its role in invertebrate immunity. Trends Immunol. 2008 Jun;29(6):263–71.

134. Gajewski KM, Sorrentino RP, Lee JH, Zhang Q, Russell M, Schulz RA. Identification of a crystal cell-specific enhancer of the black cells prophenoloxidase gene in drosophila. genesis. 2007 Apr;45(4):200–7.

135. Ferjoux G, Augé B, Boyer K, Haenlin M, Waltzer L. A GATA/RUNX cis-regulatory module couples Drosophila blood cell commitment and differentiation into crystal cells. Dev Biol. 2007 May;305(2):726–34.

136. Evans CJ, Liu T, Banerjee U. Drosophila hematopoiesis: Markers and methods for molecular genetic analysis. Methods San Diego Calif. 2014 Jun 15;68(1):242–51.

137. Bidla G, Lindgren M, Theopold U, Dushay M. Hemolymph coagulation and phenoloxidase in larvae. Dev Comp Immunol. 2005;29(8):669–79.

138. Binggeli O, Neyen C, Poidevin M, Lemaitre B. Prophenoloxidase Activation Is Required for Survival to Microbial Infections in Drosophila. Schneider DS, editor. PLoS Pathog. 2014 May 1;10(5):e1004067.

139. Nam HJ, Jang IH, You H, Lee KA, Lee WJ. Genetic evidence of a redox-dependent systemic wound response via Hayan protease-phenoloxidase system in Drosophila. EMBO J. 2012 Mar 7;31(5):1253–65.

140. Nappi AJ, Vass E, Frey F, Carton Y. Superoxide anion generation in Drosophila during melanotic encapsulation of parasites. Eur J Cell Biol. 1995 Dec;68(4):450–6.

141. Koranteng F, Cha N, Shin M, Shim J. The Role of Lozenge in Drosophila Hematopoiesis. Mol Cells. 2020 Feb 29;43(2):114–20.

142. Wan B, Belghazi M, Lemauf S, Poirié M, Gatti JL. Proteomics of purified lamellocytes from Drosophila melanogaster HopTum-l identifies new membrane proteins and networks involved in their functions. Insect Biochem Mol Biol. 2021 Jul;134:103584.

143. Rizki TM, Rizki RM. Lamellocyte differentiation in Drosophila larvae parasitized by Leptopilina. Dev Comp Immunol. 1992 Mar;16(2–3):103–10.

144. Balog JÁ, Honti V, Kurucz É, Kari B, Puskás LG, Andó I, et al. Immunoprofiling of Drosophila Hemocytes by Single-cell Mass Cytometry. Genomics Proteomics Bioinformatics. 2021 Apr;19(2):243–52.

145. Schlenke TA, Morales J, Govind S, Clark AG. Contrasting Infection Strategies in Generalist and Specialist Wasp Parasitoids of Drosophila melanogaster. Schneider DS, editor. PLoS Pathog. 2007 Oct 26;3(10):e158.

146. Anderl I, Vesala L, Ihalainen TO, Vanha-aho LM, Andó I, Rämet M, et al. Transdifferentiation and Proliferation in Two Distinct Hemocyte Lineages in Drosophila melanogaster Larvae after Wasp Infection. Schneider DS, editor. PLOS Pathog. 2016 Jul 14;12(7):e1005746.

147. Williams MJ, Wiklund ML, Wikman S, Hultmark D. Rac1 signalling in the Drosophila larval cellular immune response. J Cell Sci. 2006 May 15;119(Pt 10):2015–24.

148. Qiu P, Pan PC, Govind S. A role for the Drosophila Toll/Cactus pathway in larval hematopoiesis. Dev Camb Engl. 1998 May;125(10):1909–20.

149. Louradour I, Sharma A, Morin-Poulard I, Letourneau M, Vincent A, Crozatier M, et al. Reactive oxygen species-dependent Toll/NF-κB activation in the Drosophila hematopoietic niche confers resistance to wasp parasitism. eLife. 2017 Nov 1;6:e25496.

150. Kurucz E, Zettervall CJ, Sinka R, Vilmos P, Pivarcsi A, Ekengren S, et al. Hemese, a hemocyte-specific transmembrane protein, affects the cellular immune response in Drosophila. Proc Natl Acad Sci U S A. 2003 Mar 4;100(5):2622–7.

151. Sorrentino RP, Melk JP, Govind S. Genetic Analysis of Contributions of Dorsal Group and JAK-Stat92E Pathway Genes to Larval Hemocyte Concentration and the Egg Encapsulation Response in Drosophila. Genetics. 2004 Mar 1;166(3):1343–56.

152. Tokusumi T, Tokusumi Y, Brahier MS, Lam V, Stoller-Conrad JR, Kroeger PT, et al. Screening and Analysis of Janelia FlyLight Project Enhancer-Gal4 Strains Identifies Multiple Gene Enhancers Active During Hematopoiesis in Normal and Wasp-Challenged *Drosophila* Larvae. G3 GenesGenomesGenetics. 2017 Feb 1;7(2):437–48.

153. Irving P, Ubeda JM, Doucet D, Troxler L, Lagueux M, Zachary D, et al. New insights into Drosophila larval haemocyte functions through genome-wide analysis. Cell Microbiol. 2005 Mar;7(3):335–50.

154. Morin-Poulard I, Tian Y, Vanzo N, Crozatier M. Drosophila as a Model to Study Cellular Communication Between the Hematopoietic Niche and Blood Progenitors Under Homeostatic Conditions and in Response to an Immune Stress. Front Immunol. 2021;12:719349.

155. Alberts B, editor. Molecular biology of the cell. Hauptbd. 4. ed. New York: Garland; 2002.

156. Müller E, Wang W, Qiao W, Bornhäuser M, Zandstra PW, Werner C, et al. Distinguishing autocrine and paracrine signals in hematopoietic stem cell culture using a biofunctional microcavity platform. Sci Rep. 2016 Aug 18;6:31951.

157. Gao H, Wu X, Fossett N. Upregulation of the *Drosophila* Friend of GATA Gene *u-shaped* by JAK/STAT Signaling Maintains Lymph Gland Prohemocyte Potency. Mol Cell Biol. 2009 Nov 1;29(22):6086–96.

158. Gao H, Wu X, Fossett N. Drosophila E-cadherin functions in hematopoietic progenitors to maintain multipotency and block differentiation. PloS One. 2013;8(9):e74684.

159. Jung SH, Evans CJ, Uemura C, Banerjee U. The Drosophila lymph gland as a developmental model of hematopoiesis. Dev Camb Engl. 2005 Jun;132(11):2521–33.

160. Pennetier D, Oyallon J, Morin-Poulard I, Dejean S, Vincent A, Crozatier M. Size control of the *Drosophila* hematopoietic niche by bone morphogenetic protein signaling reveals parallels with mammals. Proc Natl Acad Sci. 2012 Feb 28;109(9):3389–94.

161. Ferguson GB, Martinez-Agosto JA. The TEAD family transcription factor Scalloped regulates blood progenitor maintenance and proliferation in Drosophila through PDGF/VEGFR receptor (Pvr) signaling. Dev Biol. 2017 May;425(1):21–32.

162. Brown S, Hu N, Hombría JC. Identification of the first invertebrate interleukin JAK/STAT receptor, the Drosophila gene domeless. Curr Biol CB. 2001 Oct 30;11(21):1700–5.

163. Ghiglione C, Devergne O, Georgenthum E, Carballès F, Médioni C, Cerezo D, et al. The *Drosophila* cytokine receptor Domeless controls border cell migration and epithelial polarization during oogenesis. Development. 2002 Dec 1;129(23):5437–47.

164. Sinha A, Khadilkar RJ, Vinay KS, Sinha AR, Inamdar MS. Conserved Regulation of the JAK/STAT Pathway by the Endosomal Protein Asrij Maintains Stem Cell Potency. Cell Rep. 2013 Aug 29;4(4):649–58.

165. Kapoor A, Padmavathi A, Madhwal S, Mukherjee T. Dual control of dopamine in Drosophila myeloid-like progenitor cell proliferation and regulation of lymph gland growth. EMBO Rep. 2022 Jun 7;23(6):e52951.

166. Dragojlovic-Munther M, Martinez-Agosto JA. Extracellular matrix-modulated Heartless signaling in Drosophila blood progenitors regulates their differentiation via a Ras/ETS/FOG pathway and target of rapamycin function. Dev Biol. 2013 Dec;384(2):313–30.

167. Ramesh P, Dey NS, Kanwal A, Mandal S, Mandal L. Relish plays a dynamic role in the niche to modulate Drosophila blood progenitor homeostasis in development and infection. eLife. 2021 Jul 22;10:e67158.

168. Destalminil-Letourneau M, Morin-Poulard I, Tian Y, Vanzo N, Crozatier M. The vascular niche controls Drosophila hematopoiesis via fibroblast growth factor signaling. eLife. 2021 Jan 4;10:e64672.

169. Tian Y, Morin-Poulard I, Liu X, Vanzo N, Crozatier M. A mechanosensitive vascular niche for Drosophila hematopoiesis. Proc Natl Acad Sci U S A. 2023 May 2;120(18):e2217862120.

170. Dragojlovic-Munther M, Martinez-Agosto JA. Multifaceted roles of PTEN and TSC orchestrate growth and differentiation of Drosophila blood progenitors. Dev Camb Engl. 2012 Oct;139(20):3752–63.

171. Shim J, Mukherjee T, Banerjee U. Direct sensing of systemic and nutritional signals by haematopoietic progenitors in Drosophila. Nat Cell Biol. 2012 Mar 11;14(4):394–400.

172. Shim J, Mukherjee T, Mondal BC, Liu T, Young GC, Wijewarnasuriya DP, et al. Olfactory control of blood progenitor maintenance. Cell. 2013 Nov 21;155(5):1141–53.

173. Cho B, Spratford CM, Yoon S, Cha N, Banerjee U, Shim J. Systemic control of immune cell development by integrated carbon dioxide and hypoxia chemosensation in Drosophila. Nat Commun. 2018 Jul 11;9(1):2679.

174. Kroeger PT, Tokusumi T, Schulz RA. Transcriptional regulation of *eater* gene expression in *Drosophila* blood cells. genesis. 2012 Jan;50(1):41–9.

175. Nässel DR, Liu Y, Luo J. Insulin/IGF signaling and its regulation in Drosophila. Gen Comp Endocrinol. 2015 Sep;221:255–66.

176. Woodcock KJ, Kierdorf K, Pouchelon CA, Vivancos V, Dionne MS, Geissmann F. Macrophage-derived upd3 cytokine causes impaired glucose homeostasis and reduced lifespan in Drosophila fed a lipid-rich diet. Immunity. 2015 Jan 20;42(1):133–44.

177. Yu S, Zhang G, Jin LH. A high-sugar diet affects cellular and humoral immune responses in Drosophila. Exp Cell Res. 2018 Jul;368(2):215–24.

178. Arrese EL, Soulages JL. Insect fat body: energy, metabolism, and regulation. Annu Rev Entomol. 2010;55:207–25.

179. Goyal M, Tomar A, Madhwal S, Mukherjee T. Blood progenitor redox homeostasis through olfaction-derived systemic GABA in hematopoietic growth control in Drosophila. Dev Camb Engl [Internet]. 2022;149(8). Available from: http://www.ncbi.nlm.nih.gov/pubmed/34850846

180. Koranteng F, Cho B, Shim J. Intrinsic and Extrinsic Regulation of Hematopoiesis in Drosophila. Mol Cells. 2022;45(3):101–8.

181. Balaban RS, Nemoto S, Finkel T. Mitochondria, oxidants, and aging. Cell. 2005 Feb 25;120(4):483–95.

182. Boveris A. Mitochondrial production of superoxide radical and hydrogen peroxide. Adv Exp Med Biol. 1977;78:67–82.

183. Chance B, Sies H, Boveris A. Hydroperoxide metabolism in mammalian organs. Physiol Rev. 1979 Jul;59(3):527–605.

184. Finkel T, Holbrook NJ. Oxidants, oxidative stress and the biology of ageing. Nature. 2000 Nov 9;408(6809):239–47.

185. Forman HJ, Kennedy JA. Role of superoxide radical in mitochondrial dehydrogenase reactions. Biochem Biophys Res Commun. 1974 Oct 8;60(3):1044–50.

186. Forman HJ, Kennedy J. Superoxide production and electron transport in mitochondrial oxidation of dihydroorotic acid. J Biol Chem. 1975 Jun 10;250(11):4322–6.

187. Fridovich I. The Biology of Oxygen Radicals: The superoxide radical is an agent of oxygen toxicity; superoxide dismutases provide an important defense. Science. 1978 Sep 8;201(4359):875–80.

188. Lehninger AL. Biochemistry: the molecular basis of cell structure and function. 2d ed. New York: Worth Publishers; 1975. 1104 p.

189. Voet D, Voet JG, Pratt CW. Fundamentals of biochemistry: life at the molecular level. 5th edition. Hoboken, NJ: John Wiley & Sons; 2016. 1098 p.

190. Aykin-Burns N, Slane BG, Liu ATY, Owens KM, O'Malley MS, Smith BJ, et al. Sensitivity to low-dose/low-LET ionizing radiation in mammalian cells harboring mutations in succinate dehydrogenase subunit C is governed by mitochondria-derived reactive oxygen species. Radiat Res. 2011 Feb;175(2):150–8.

191. Ishii N, Fujii M, Hartman PS, Tsuda M, Yasuda K, Senoo-Matsuda N, et al. A mutation in succinate dehydrogenase cytochrome b causes oxidative stress and ageing in nematodes. Nature. 1998 Aug 13;394(6694):694–7.

192. Owens KM, Aykin-Burns N, Dayal D, Coleman MC, Domann FE, Spitz DR. Genomic instability induced by mutant succinate dehydrogenase subunit D (SDHD) is mediated by O2(-•) and H2O2. Free Radic Biol Med. 2012 Jan 1;52(1):160–6.

193. Slane BG, Aykin-Burns N, Smith BJ, Kalen AL, Goswami PC, Domann FE, et al. Mutation of succinate dehydrogenase subunit C results in increased O2.-, oxidative stress, and genomic instability. Cancer Res. 2006 Aug 1;66(15):7615–20.

194. Giorgio M, Migliaccio E, Orsini F, Paolucci D, Moroni M, Contursi C, et al. Electron transfer between cytochrome c and p66Shc generates reactive oxygen species that trigger mitochondrial apoptosis. Cell. 2005 Jul 29;122(2):221–33.

195. Bedard K, Krause KH. The NOX family of ROS-generating NADPH oxidases: physiology and pathophysiology. Physiol Rev. 2007 Jan;87(1):245–313.

196. Lambeth JD. Nox enzymes, ROS, and chronic disease: an example of antagonistic pleiotropy. Free Radic Biol Med. 2007 Aug 1;43(3):332–47.

197. Zhou D, Shao L, Spitz DR. Reactive Oxygen Species in Normal and Tumor Stem Cells. In: Advances in Cancer Research [Internet]. Elsevier; 2014 [cited 2023 Dec 18]. p. 1–67. Available from: https://linkinghub.elsevier.com/retrieve/pii/B9780124201170000013

198. Canton M, Sánchez-Rodríguez R, Spera I, Venegas FC, Favia M, Viola A, et al. Reactive Oxygen Species in Macrophages: Sources and Targets. Front Immunol. 2021 Sep 30;12:734229.

199. De Duve C, Baudhuin P. Peroxisomes (microbodies and related particles). Physiol Rev. 1966 Apr;46(2):323–57.

200. Cheeseman KH, Slater TF. An introduction to free radical biochemistry. Br Med Bull. 1993 Jul;49(3):481–93.

201. Rhee SG, Chae HZ, Kim K. Peroxiredoxins: A historical overview and speculative preview of novel mechanisms and emerging concepts in cell signaling. Free Radic Biol Med. 2005 Jun;38(12):1543–52.

202. Sies H. Oxidative stress: From basic research to clinical application. Am J Med. 1991 Sep;91(3):S31–8.

203. Spitz DR, Azzam EI, Jian Li J, Gius D. Metabolic oxidation/reduction reactions and cellular responses to ionizing radiation: A unifying concept in stress response biology. Cancer Metastasis Rev. 2004 Aug;23(3/4):311–22.

204. Fridovich I. Superoxide anion radical (O2-.), superoxide dismutases, and related matters. J Biol Chem. 1997 Jul 25;272(30):18515–7.

205. Fridovich I. Superoxide dismutases. Annu Rev Biochem. 1975;44:147–59.

206. Iakovleva MN, Sinel'shchikova TA, Perminova IN, Zasukhina GD. [Role of superoxide dismutase in maintaining cellular homeostasis upon exposure to gamma-rays and nickel sulfate]. Radiats Biol Radioecol. 2002;42(3):299–301.

207. Deisseroth A, Dounce AL. Catalase: Physical and chemical properties, mechanism of catalysis, and physiological role. Physiol Rev. 1970 Jul;50(3):319–75.

208. Von Ossowski I, Hausner G, Loewen PC. Molecular evolutionary analysis based on the amino acid sequence of catalase. J Mol Evol. 1993 Jul;37(1):71–6.

209. Lu SC. Glutathione synthesis. Biochim Biophys Acta. 2013 May;1830(5):3143–53.

210. Pompella A, Visvikis A, Paolicchi A, De Tata V, Casini AF. The changing faces of glutathione, a cellular protagonist. Biochem Pharmacol. 2003 Oct 15;66(8):1499–503.

211. Spitz DR, Malcolm RR, Roberts RJ. Cytotoxicity and metabolism of 4-hydroxy-2-nonenal and 2-nonenal in H2O2-resistant cell lines. Do aldehydic by-products of lipid peroxidation contribute to oxidative stress? Biochem J. 1990 Apr 15;267(2):453–9.

212. Spitz DR, Sullivan SJ, Malcolm RR, Roberts RJ. Glutathione dependent metabolism and detoxification of 4-hydroxy-2-nonenal. Free Radic Biol Med. 1991 Jan;11(4):415–23.

213. Marí M, Morales A, Colell A, García-Ruiz C, Fernández-Checa JC. Mitochondrial Glutathione, a Key Survival Antioxidant. Antioxid Redox Signal. 2009 Nov;11(11):2685–700.

214. Valle A, Oliver J, Roca P. Role of Uncoupling Proteins in Cancer. Cancers. 2010 Apr 16;2(2):567–91.

215. Holmström KM, Finkel T. Cellular mechanisms and physiological consequences of redox-dependent signalling. Nat Rev Mol Cell Biol. 2014 Jun;15(6):411–21.

216. Schieber M, Chandel NS. ROS function in redox signaling and oxidative stress. Curr Biol CB. 2014 May 19;24(10):R453-462.

217. Bigarella CL, Liang R, Ghaffari S. Stem cells and the impact of ROS signaling. Development. 2014 Nov 15;141(22):4206–18.

218. Nugud A, Sandeep D, El-Serafi AT. Two faces of the coin: Minireview for dissecting the role of reactive oxygen species in stem cell potency and lineage commitment. J Adv Res. 2018 Nov;14:73–9.

219. Takubo K, Nagamatsu G, Kobayashi CI, Nakamura-Ishizu A, Kobayashi H, Ikeda E, et al. Regulation of Glycolysis by Pdk Functions as a Metabolic Checkpoint for Cell Cycle Quiescence in Hematopoietic Stem Cells. Cell Stem Cell. 2013 Jan;12(1):49–61.

220. Yu WM, Liu X, Shen J, Jovanovic O, Pohl EE, Gerson SL, et al. Metabolic Regulation by the Mitochondrial Phosphatase PTPMT1 Is Required for Hematopoietic Stem Cell Differentiation. Cell Stem Cell. 2013 Jan;12(1):62–74.

221. Zhang J, Khvorostov I, Hong JS, Oktay Y, Vergnes L, Nuebel E, et al. UCP2 regulates energy metabolism and differentiation potential of human pluripotent stem cells: UCP2 regulates hPSC metabolism and differentiation. EMBO J. 2011 Dec 14;30(24):4860–73.

222. Dansen TB, Smits LMM, Van Triest MH, De Keizer PLJ, Van Leenen D, Koerkamp MG, et al. Redox-sensitive cysteines bridge p300/CBP-mediated acetylation and FoxO4 activity. Nat Chem Biol. 2009 Sep;5(9):664–72.

223. Guo Z, Kozlov S, Lavin MF, Person MD, Paull TT. ATM Activation by Oxidative Stress. Science. 2010 Oct 22;330(6003):517–21.

224. Velu CS, Niture SK, Doneanu CE, Pattabiraman N, Srivenugopal KS. Human p53 Is Inhibited by Glutathionylation of Cysteines Present in the Proximal DNA-Binding Domain during Oxidative Stress ·. Biochemistry. 2007 Jul 1;46(26):7765–80.

225. Anastasiou D, Poulogiannis G, Asara JM, Boxer MB, Jiang J kang, Shen M, et al. Inhibition of Pyruvate Kinase M2 by Reactive Oxygen Species Contributes to Cellular Antioxidant Responses. Science. 2011 Dec 2;334(6060):1278–83.

226. Brunelle JK, Bell EL, Quesada NM, Vercauteren K, Tiranti V, Zeviani M, et al. Oxygen sensing requires mitochondrial ROS but not oxidative phosphorylation. Cell Metab. 2005 Jun;1(6):409–14.

227. Sarbassov DD, Sabatini DM. Redox Regulation of the Nutrient-sensitive Raptor-mTOR Pathway and Complex. J Biol Chem. 2005 Nov;280(47):39505–9.

228. Jang YY, Sharkis SJ. A low level of reactive oxygen species selects for primitive hematopoietic stem cells that may reside in the low-oxygenic niche. Blood. 2007 Oct 15;110(8):3056–63.

229. Marty C, Lacout C, Droin N, Le Couédic JP, Ribrag V, Solary E, et al. A role for reactive oxygen species in JAK2V617F myeloproliferative neoplasm progression. Leukemia. 2013 Nov;27(11):2187–95.

230. Yalcin S, Marinkovic D, Mungamuri SK, Zhang X, Tong W, Sellers R, et al. ROS-mediated amplification of AKT/mTOR signalling pathway leads to myeloproliferative syndrome in Foxo3−/− mice. EMBO J. 2010 Dec 15;29(24):4118–31.

231. Ito K, Hirao A, Arai F, Matsuoka S, Takubo K, Hamaguchi I, et al. Regulation of oxidative stress by ATM is required for self-renewal of haematopoietic stem cells. Nature. 2004 Oct;431(7011):997–1002.

232. Miyamoto K, Araki KY, Naka K, Arai F, Takubo K, Yamazaki S, et al. Foxo3a Is Essential for Maintenance of the Hematopoietic Stem Cell Pool. Cell Stem Cell. 2007 Jun;1(1):101–12.

233. Tothova Z, Kollipara R, Huntly BJ, Lee BH, Castrillon DH, Cullen DE, et al. FoxOs Are Critical Mediators of Hematopoietic Stem Cell Resistance to Physiologic Oxidative Stress. Cell. 2007 Jan;128(2):325–39.

234. Yalcin S, Zhang X, Luciano JP, Mungamuri SK, Marinkovic D, Vercherat C, et al. Foxo3 Is Essential for the Regulation of Ataxia Telangiectasia Mutated and Oxidative Stress-mediated Homeostasis of Hematopoietic Stem Cells. J Biol Chem. 2008 Sep;283(37):25692–705.

235. Zhang X, Rielland M, Yalcin S, Ghaffari S. Regulation and Function of FoxO Transcription Factors in Normal and Cancer Stem Cells: What Have We Learned? Curr Drug Targets. 2011 Aug 1;12(9):1267–83.

236. Friedman JS, Lopez MF, Fleming MD, Rivera A, Martin FM, Welsh ML, et al. SOD2-deficiency anemia: protein oxidation and altered protein expression reveal targets of damage, stress response, and antioxidant responsiveness. Blood. 2004 Oct 15;104(8):2565–73.

237. Roberts E, Frankel S. gamma-Aminobutyric acid in brain: its formation from glutamic acid. J Biol Chem. 1950 Nov;187(1):55–63.

238. Basemore AW, Elliot KA, Florey E. Isolation of factor I. J Neurochem. 1957;1(4):334–9.

239. Wang DD, Kriegstein AR. Defining the role of GABA in cortical development. J Physiol. 2009 May 1;587(Pt 9):1873–9.

240. Wu C, Sun D. GABA receptors in brain development, function, and injury. Metab Brain Dis. 2015 Apr;30(2):367–79.

241. Snead OC, Depaulis A, Vergnes M, Marescaux C. Absence epilepsy: advances in experimental animal models. Adv Neurol. 1999;79:253–78.

242. Tiihonen J, Kuikka J, Räsänen P, Lepola U, Koponen H, Liuska A, et al. Cerebral benzodiazepine receptor binding and distribution in generalized anxiety disorder: a fractal analysis. Mol Psychiatry. 1997;2(6):463–71.

243. Stayer C, Meinck HM. Stiff-man syndrome: an overview. Neurol Barc Spain. 1998 Feb;13(2):83–8.

244. Benes F. GABAergic Interneurons Implications for Understanding Schizophrenia and Bipolar Disorder. Neuropsychopharmacology. 2001 Jul;25(1):1–27.

245. Erlander MG, Tillakaratne NJ, Feldblum S, Patel N, Tobin AJ. Two genes encode distinct glutamate decarboxylases. Neuron. 1991 Jul;7(1):91–100.

246. Fon EA, Edwards RH. Molecular mechanisms of neurotransmitter release. Muscle Nerve. 2001 May;24(5):581–601.

247. Macdonald RL, Olsen RW. GABAA receptor channels. Annu Rev Neurosci. 1994;17:569–602.

248. Boue-Grabot E, Roudbaraki M, Bascles L, Tramu G, Bloch B, Garret M. Expression of GABA receptor rho subunits in rat brain. J Neurochem. 1998 Mar;70(3):899–907.

249. Couve A, Moss SJ, Pangalos MN. GABAB Receptors: A New Paradigm in G Protein Signaling. Mol Cell Neurosci. 2000 Oct;16(4):296–312.

250. Luján R, Shigemoto R, López-Bendito G. Glutamate and GABA receptor signalling in the developing brain. Neuroscience. 2005 Jan;130(3):567–80.

251. Misgeld U, Bijak M, Jarolimek W. A physiological role for GABAB receptors and the effects of baclofen in the mammalian central nervous system. Prog Neurobiol. 1995 Jul;46(4):423–62.

252. Owens DF, Kriegstein AR. Is there more to gaba than synaptic inhibition? Nat Rev Neurosci. 2002 Sep;3(9):715–27.

253. Cherubini E, Conti F. Generating diversity at GABAergic synapses. Trends Neurosci. 2001 Mar;24(3):155–62.

254. Squires RF, editor. GABA and benzodiazepine receptors. Boca Raton, Fla: CRC Press; 1988. 2 p.

255. Maitre M. The gamma-hydroxybutyrate signalling system in brain: organization and functional implications. Prog Neurobiol. 1997 Feb;51(3):337–61.

256. Kim K, Yoon H. Gamma-Aminobutyric Acid Signaling in Damage Response, Metabolism, and Disease. Int J Mol Sci. 2023 Feb 26;24(5):4584.

257. Chapman RW, Hey JA, Rizzo CA, Bolser DC. GABAB receptors in the lung. Trends Pharmacol Sci. 1993 Jan;14(1):26–9.

258. Ong J, Kerr DI. GABA-receptors in peripheral tissues. Life Sci. 1990;46(21):1489–501.

259. Steidl U, Bork S, Schaub S, Selbach O, Seres J, Aivado M, et al. Primary human CD34+ hematopoietic stem and progenitor cells express functionally active receptors of neuromediators. Blood. 2004 Jul 1;104(1):81–8.

260. Govindpani K, Calvo-Flores Guzmán B, Vinnakota C, Waldvogel H, Faull R, Kwakowsky A. Towards a Better Understanding of GABAergic Remodeling in Alzheimer's Disease. Int J Mol Sci. 2017 Aug 21;18(8):1813.

261. Zhu F, Feng M, Sinha R, Murphy MP, Luo F, Kao KS, et al. The GABA receptor GABRR1 is expressed on and functional in hematopoietic stem cells and megakaryocyte progenitors. Proc Natl Acad Sci. 2019 Sep 10;116(37):18416–22.

262. Shao L, Elujoba-Bridenstine A, Zink KE, Sanchez LM, Cox BJ, Pollok KE, et al. The neurotransmitter receptor Gabbr1 regulates proliferation and function of hematopoietic stem and progenitor cells. Blood. 2021 Feb 11;137(6):775–87.

263. Zhang B, Vogelzang A, Miyajima M, Sugiura Y, Wu Y, Chamoto K, et al. B cell-derived GABA elicits IL-10+ macrophages to limit anti-tumour immunity. Nature. 2021 Nov;599(7885):471–6.

264. Agarwala S, Tamplin OJ. Neural Crossroads in the Hematopoietic Stem Cell Niche. Trends Cell Biol. 2018 Dec;28(12):987–98.

265. Hanoun M, Maryanovich M, Arnal-Estapé A, Frenette PS. Neural Regulation of Hematopoiesis, Inflammation, and Cancer. Neuron. 2015 Apr;86(2):360–73.

266. Makhijani K, Alexander B, Tanaka T, Rulifson E, Brückner K. The peripheral nervous system supports blood cell homing and survival in the *Drosophila* larva. Development. 2011 Dec 15;138(24):5379–91.

267. Plaitakis A, Kalef-Ezra E, Kotzamani D, Zaganas I, Spanaki C. The Glutamate Dehydrogenase Pathway and Its Roles in Cell and Tissue Biology in Health and Disease. Biology. 2017 Feb 8;6(1):11.

268. Guo Y, Cho SW, Saxena D, Li X. Multifaceted Actions of Succinate as a Signaling Transmitter Vary with Its Cellular Locations. Endocrinol Metab Seoul Korea. 2020 Mar;35(1):36–43.

269. Tretter L, Patocs A, Chinopoulos C. Succinate, an intermediate in metabolism, signal transduction, ROS, hypoxia, and tumorigenesis. Biochim Biophys Acta BBA - Bioenerg. 2016 Aug;1857(8):1086–101.

270. Yuan D, Wu X, Gong B, Huo R, Zhao L, Li J, et al. GABA Metabolism, Transport and Their Roles and Mechanisms in the Regulation of Abiotic Stress (Hypoxia, Salt, Drought) Resistance in Plants. Metabolites. 2023 Feb 26;13(3):347.

271. Kwan W, Cortes M, Frost I, Esain V, Theodore LN, Liu SY, et al. The Central Nervous System Regulates Embryonic HSPC Production via Stress-Responsive Glucocorticoid Receptor Signaling. Cell Stem Cell. 2016 Sep 1;19(3):370–82.

272. Mignini F, Streccioni V, Amenta F. Autonomic innervation of immune organs and neuroimmune modulation. Auton Autacoid Pharmacol. 2003 Feb;23(1):1–25.

273. Calvo W. The innervation of the bone marrow in laboratory animals. Am J Anat. 1968 Sep;123(2):315–28.

274. Katayama Y, Battista M, Kao WM, Hidalgo A, Peired AJ, Thomas SA, et al. Signals from the sympathetic nervous system regulate hematopoietic stem cell egress from bone marrow. Cell. 2006 Jan 27;124(2):407–21.

275. Maestroni GJ, Cosentino M, Marino F, Togni M, Conti A, Lecchini S, et al. Neural and endogenous catecholamines in the bone marrow. Circadian association of norepinephrine with hematopoiesis? Exp Hematol. 1998 Nov;26(12):1172–7.

276. Zangiacomi V, Balon N, Maddens S, Tiberghien P, Versaux-Botteri C, Deschaseaux F. Human cord blood-derived hematopoietic and neural-like stem/progenitor cells are attracted by the neurotransmitter GABA. Stem Cells Dev. 2009 Nov;18(9):1369–78.

277. Chen Y, Lin YC, Kuo TW, Knight ZA. Sensory Detection of Food Rapidly Modulates Arcuate Feeding Circuits. Cell. 2015 Feb;160(5):829–41.

278. Riera CE, Tsaousidou E, Halloran J, Follett P, Hahn O, Pereira MMA, et al. The Sense of Smell Impacts Metabolic Health and Obesity. Cell Metab. 2017 Jul;26(1):198-211.e5.

279. Kreher SA, Kwon JY, Carlson JR. The molecular basis of odor coding in the Drosophila larva. Neuron. 2005 May 5;46(3):445–56.

280. Vosshall LB, Stocker RF. Molecular architecture of smell and taste in Drosophila. Annu Rev Neurosci. 2007;30:505–33.

281. Stocker RF. The organization of the chemosensory system in Drosophila melanogaster: a review. Cell Tissue Res. 1994 Jan;275(1):3–26.

282. Carlson JR. Olfaction in Drosophila: from odor to behavior. Trends Genet TIG. 1996 May;12(5):175–80.

283. de Bruyne M, Foster K, Carlson JR. Odor coding in the Drosophila antenna. Neuron. 2001 May;30(2):537–52.

284. Fishilevich E, Vosshall LB. Genetic and functional subdivision of the Drosophila antennal lobe. Curr Biol CB. 2005 Sep 6;15(17):1548–53.

285. Heimbeck G, Bugnon V, Gendre N, Häberlin C, Stocker RF. Smell and taste perception in Drosophila melanogaster larva: toxin expression studies in chemosensory neurons. J Neurosci Off J Soc Neurosci. 1999 Aug 1;19(15):6599–609.

286. Siddiqi O. Neurogenetics of olfaction in Drosophila melanogaster. Trends Genet. 1987 Jan;3:137–42.

287. Sato K, Pellegrino M, Nakagawa T, Nakagawa T, Vosshall LB, Touhara K. Insect olfactory receptors are heteromeric ligand-gated ion channels. Nature. 2008 Apr 24;452(7190):1002–6.

288. Wicher D, Schäfer R, Bauernfeind R, Stensmyr MC, Heller R, Heinemann SH, et al. Drosophila odorant receptors are both ligand-gated and cyclic-nucleotide-activated cation channels. Nature. 2008 Apr 24;452(7190):1007–11.

289. Masuda-Nakagawa LM, Ito K, Awasaki T, O'Kane CJ. A single GABAergic neuron mediates feedback of odor-evoked signals in the mushroom body of larval Drosophila. Front Neural Circuits. 2014;8:35.

290. Python F, Stocker RF. Adult-like complexity of the larval antennal lobe of D. melanogaster despite markedly low numbers of odorant receptor neurons. J Comp Neurol. 2002 Apr 15;445(4):374–87.

291. Störtkuhl KF, Fiala A. The Smell of Blue Light: A New Approach toward Understanding an Olfactory Neuronal Network. Front Neurosci [Internet]. 2011 [cited 2024 Jan 7];5. Available from: http://journal.frontiersin.org/article/10.3389/fnins.2011.00072/abstract

292. Bigarella CL, Liang R, Ghaffari S. Stem cells and the impact of ROS signaling. Dev Camb. 2014;141(22):4206–18.

293. Harris JM, Esain V, Frechette GM, Harris LJ, Cox AG, Cortes M, et al. Glucose metabolism impacts the spatiotemporal onset and magnitude of HSC induction in vivo. Blood. 2013;121(13):2483–93.

294. Prieto-Bermejo R, Romo-González M, Pérez-Fernández A, Ijurko C, Hernández-Hernández Á. Reactive oxygen species in haematopoiesis: leukaemic cells take a walk on the wild side. J Exp Clin Cancer Res. 2018 Dec;37(1):125.

295. Takubo K, Nagamatsu G, Kobayashi CI, Nakamura-Ishizu A, Kobayashi H, Ikeda E, et al. Regulation of glycolysis by Pdk functions as a metabolic checkpoint for cell cycle quiescence in hematopoietic stem cells. Cell Stem Cell. 2013;12(1):49–61.

296. Tothova Z, Kollipara R, Huntly BJ, Lee BH, Castrillon DH, Cullen DE, et al. FoxOs are critical mediators of hematopoietic stem cell resistance to physiologic oxidative stress. Cell. 2007;128(2):325–39.

297. Vincent A, Crozatier M. Neither too much nor too little: reactive oxygen species levels regulate Drosophila hematopoiesis. J Mol Cell Biol. 2010 Apr;2(2):74–5.

298. Quinlan CL, Orr AL, Perevoshchikova IV, Treberg JR, Ackrell BA, Brand MD. Mitochondrial complex II can generate reactive oxygen species at high rates in both the forward and reverse reactions. J Biol Chem. 2012 Aug 3;287(32):27255–64.

299. Sabharwal SS, Schumacker PT. Mitochondrial ROS in cancer: initiators, amplifiers or an Achilles' heel? Nat Rev Cancer. 2014;14(11):709–21.

300. Kaplon J, Zheng L, Meissl K, Chaneton B, Selivanov VA, Mackay G, et al. A key role for mitochondrial gatekeeper pyruvate dehydrogenase in oncogene-induced senescence. Nature. 2013;498(7452):109–12.

301. Mailloux RJ, Gardiner D, O'Brien M. 2-Oxoglutarate dehydrogenase is a more significant source of O2(.-)/H2O2 than pyruvate dehydrogenase in cardiac and liver tissue. Free Radic Biol Med. 2016;97:501–12.

302. Starkov AA, Fiskum G, Chinopoulos C, Lorenzo BJ, Browne SE, Patel MS, et al. Mitochondrial α-Ketoglutarate Dehydrogenase Complex Generates Reactive Oxygen Species. J Neurosci. 2004 Sep 8;24(36):7779–88.

303. Gray LR, Tompkins SC, Taylor EB. Regulation of pyruvate metabolism and human disease. Cell Mol Life Sci. 2014;71(14):2577–604.

304. Bowker-Kinley MM, Davis WI, Wu P, Harris RA, Popov KM. Evidence for existence of tissue-specific regulation of the mammalian pyruvate dehydrogenase complex. Biochem J. 1998;329 (Pt 1:191–6.

305. Harris RA, Bowker-Kinley MM, Huang B, Wu P. Regulation of the activity of the pyruvate dehydrogenase complex. Adv Enzyme Regul. 2002;42:249–59.

306. Shelp BJ, Bown AW, McLean MD. Metabolism and functions of gamma-aminobutyric acid. Trends Plant Sci. 1999;4(11):446–52.

307. Niraula P, Kim MS. N-Acetylcysteine extends lifespan of Drosophila via modulating ROS scavenger gene expression. Biogerontology. 2019;20(4):533–43.

308. Aldini G, Altomare A, Baron G, Vistoli G, Carini M, Borsani L, et al. N-Acetylcysteine as an antioxidant and disulphide breaking agent: the reasons why. Free Radic Res. 2018;52(7):751–62.

309. Acevedo JM, Centanin L, Dekanty A, Wappner P. Oxygen Sensing in Drosophila: Multiple Isoforms of the Prolyl Hydroxylase Fatiga Have Different Capacity to Regulate HIFα/Sima. Bernhard EJ, editor. PLoS ONE. 2010 Aug 25;5(8):e12390.

310. Thomas D, Surdin-Kerjan Y. Metabolism of sulfur amino acids in Saccharomyces cerevisiae. Microbiol Mol Biol Rev MMBR. 1997 Dec;61(4):503–32.

311. Aitken SM, Kirsch JF. The enzymology of cystathionine biosynthesis: strategies for the control of substrate and reaction specificity. Arch Biochem Biophys. 2005 Jan 1;433(1):166–75.

312. Rodriguez AE, Ducker GS, Billingham LK, Martinez CA, Mainolfi N, Suri V, et al. Serine Metabolism Supports Macrophage IL-1β Production. Cell Metab. 2019;29(4):1003-1011.e4.

313. Geeraerts SL, Heylen E, De Keersmaecker K, Kampen KR. The ins and outs of serine and glycine metabolism in cancer. Nat Metab. 2021 Jan 28;3(2):131–41.

314. Elia I, Rowe JH, Johnson S, Joshi S, Notarangelo G, Kurmi K, et al. Tumor cells dictate anti-tumor immune responses by altering pyruvate utilization and succinate signaling in CD8+ T cells. Cell Metab. 2022 Aug;34(8):1137-1150.e6.

315. Berck ME, Khandelwal A, Claus L, Hernandez-Nunez L, Si G, Tabone CJ, et al. The wiring diagram of a glomerular olfactory system. eLife. 2016 May 13;5:e14859.

316. Ebrahim SAM, Dweck HKM, Stökl J, Hofferberth JE, Trona F, Weniger K, et al. Drosophila Avoids Parasitoids by Sensing Their Semiochemicals via a Dedicated Olfactory Circuit. Benton R, editor. PLOS Biol. 2015 Dec 16;13(12):e1002318.

317. Bailey MS, Puche AC, Shipley MT. Development of the olfactory bulb: evidence for glia-neuron interactions in glomerular formation. J Comp Neurol. 1999 Dec 27;415(4):423–48.

318. Clowney EJ, LeGros MA, Mosley CP, Clowney FG, Markenskoff-Papadimitriou EC, Myllys M, et al. Nuclear aggregation of olfactory receptor genes governs their monogenic expression. Cell. 2012 Nov 9;151(4):724–37.

319. Tsai T, Veitinger S, Peek I, Busse D, Eckardt J, Vladimirova D, et al. Two olfactory receptors— OR 2A4/7 and OR 51B5—differentially affect epidermal proliferation and differentiation. Exp Dermatol. 2017 Jan;26(1):58–65.

320. Tan B, Lu Z, Dong S, Zhao G, Kuo MS. Derivatization of the tricarboxylic acid intermediates with O-benzylhydroxylamine for liquid chromatography-tandem mass spectrometry detection. Anal Biochem. 2014;465:134–47.

321. Walvekar A, Rashida Z, Maddali H, Laxman S. A versatile LC-MS/MS approach for comprehensive, quantitative analysis of central metabolic pathways. Wellcome Open Res. 2018;3:122.

322. Sutton TR, Minnion M, Barbarino F, Koster G, Fernandez BO, Cumpstey AF, et al. A robust and versatile mass spectrometry platform for comprehensive assessment of the thiol redox metabolome. Redox Biol. 2018 Jun;16:359–80.

323. Yuan M, Breitkopf SB, Yang X, Asara JM. A positive/negative ion-switching, targeted mass spectrometry-based metabolomics platform for bodily fluids, cells, and fresh and fixed tissue. Nat Protoc. 2012;7(5):872–81.

324. Shuford CM, Poteat MD, Buchwalter DB, Muddiman DC. Absolute quantification of free glutathione and cysteine in aquatic insects using isotope dilution and selected reaction monitoring. Anal Bioanal Chem. 2012 Jan;402(1):357–66.

325. Owusu-Ansah E, Yavari A, Banerjee U. A protocol for _in vivo_ detection of reactive oxygen species. 2008; Available from: http://dx.doi.org/10.1038/nprot.2008.23

326. Shim J, Mukherjee T, Banerjee U. Direct sensing of systemic and nutritional signals by haematopoietic progenitors in Drosophila. Nat Cell Biol. 2012 Apr;14(4):394–400.

327. Bajgar A, Kucerova K, Jonatova L, Tomcala A, Schneedorferova I, Okrouhlik J, et al. Extracellular Adenosine Mediates a Systemic Metabolic Switch during Immune Response. PLoS Biol. 2015;13(4):1–23.

328. Walvekar A, Rashida Z, Maddali H, Laxman S. A versatile LC-MS/MS approach for comprehensive, quantitative analysis of central metabolic pathways. Wellcome Open Res. 2018 Sep;3(3):122.

329. Tan B, Lu Z, Dong S, Zhao G, Kuo MS. Derivatization of the tricarboxylic acid intermediates with O-benzylhydroxylamine for liquid chromatography-tandem mass spectrometry detection. Anal Biochem. 2014;465:134–47.

330. Florholmen-Kjær Å, Lysså RA ndre, Fuskevåg OM, Goll R, Revhaug A, Mortensen KE rlend. A sensitive method for the analysis of glutathione in porcine hepatocytes. Scand J Gastroenterol. 2014;49(11):1359–66.

331. New LS, Chan ECY. Evaluation of BEH C18, BEH HILIC, and HSS T3 (C18) column chemistries for the UPLC-MS-MS analysis of glutathione, glutathione disulfide, and ophthalmic acid in mouse liver and human plasma. J Chromatogr Sci. 2008;46(3):209–14.

332. Hadjieconomou D, King G, Gaspar P, Mineo A, Blackie L, Ameku T, et al. Enteric neurons increase maternal food intake during reproduction. Nature. 2020 Nov 19;587(7834):455–9.

333. Allen AE, Sun Y, Wei F, Reid MA, Locasale JW. Nucleotide metabolism is linked to cysteine availability. J Biol Chem. 2023 Apr;299(4):103039.

334. Jouandin P, Marelja Z, Shih YH, Parkhitko AA, Dambowsky M, Asara JM, et al. Lysosomal cystine mobilization shapes the response of TORC1 and tissue growth to fasting. Science. 2022 Feb 18;375(6582):eabc4203.

335. Bhat R, Axtell R, Mitra A, Miranda M, Lock C, Tsien RW, et al. Inhibitory role for GABA in autoimmune inflammation. Proc Natl Acad Sci U S A. 2010 Feb 9;107(6):2580–5.

336. Kawashima K, Fujii T. The lymphocytic cholinergic system and its contribution to the regulation of immune activity. Life Sci. 2003 Dec 26;74(6):675–96.

337. Sternberg EM. Neural regulation of innate immunity: a coordinated nonspecific host response to pathogens. Nat Rev Immunol. 2006 Apr;6(4):318–28.

338. Rada B, Leto TL. Oxidative innate immune defenses by Nox/Duox family NADPH oxidases. Contrib Microbiol. 2008;15:164–87.

339. Chouchani ET, Pell VR, Gaude E, Aksentijević D, Sundier SY, Robb EL, et al. Ischaemic accumulation of succinate controls reperfusion injury through mitochondrial ROS. Nature. 2014 Nov 20;515(7527):431–5.

340. Lavoie J. Development of Glutathione Synthesis and γ-Glutamyltranspeptidase Activities in Tissues from Newborn Infants. Free Radic Biol Med. 1998 Apr;24(6):994–1001.

341. Brittain T, Tottle B. Glutathione in the red blood cells of embryonic mice. Comp Biochem Physiol Part B Comp Biochem. 1986 Jan;83(4):843–6.

342. Griffith OW. Biologic and pharmacologic regulation of mammalian glutathione synthesis. Free Radic Biol Med. 1999 Nov;27(9–10):922–35.

343. Lu SC. Regulation of glutathione synthesis. Mol Aspects Med. 2009;30(1–2):42–59.

344. Kim J whan, Tchernyshyov I, Semenza GL, Dang CV. HIF-1-mediated expression of pyruvate dehydrogenase kinase: A metabolic switch required for cellular adaptation to hypoxia. Cell Metab. 2006 Mar;3(3):177–85.

345. Papandreou I, Cairns RA, Fontana L, Lim AL, Denko NC. HIF-1 mediates adaptation to hypoxia by actively downregulating mitochondrial oxygen consumption. Cell Metab. 2006;3(3):187–97.

346. Cummins EP, Berra E, Comerford KM, Ginouves A, Fitzgerald KT, Seeballuck F, et al. Prolyl hydroxylase-1 negatively regulates IkappaB kinase-beta, giving insight into hypoxia-induced NFkappaB activity. Proc Natl Acad Sci U A. 2006;103(48):18154–9.

347. Li X, Jiang O, Wang S. Molecular mechanisms of cellular metabolic homeostasis in stem cells. Int J Oral Sci. 2023 Dec 1;15(1):1–13.

348. Tu WB, Christofk HR, Plath K. Nutrient regulation of development and cell fate decisions. Development. 2023 Oct 15;150(20):dev199961.

349. Baker SA, Rutter J. Metabolites as signalling molecules. Nat Rev Mol Cell Biol. 2023 May;24(5):355–74.

350. Boon R, Silveira GG, Mostoslavsky R. Nuclear metabolism and the regulation of the epigenome. Nat Metab. 2020 Oct 12;2(11):1190–203.

351. Evers TMJ, Holt LJ, Alberti S, Mashaghi A. Reciprocal regulation of cellular mechanics and metabolism. Nat Metab. 2021 Apr 19;3(4):456–68.

352. Miyazawa H, Aulehla A. Revisiting the role of metabolism during development. Development. 2018 Oct 1;145(19):dev131110.

353. DeBerardinis RJ, Lum JJ, Hatzivassiliou G, Thompson CB. The biology of cancer: metabolic reprogramming fuels cell growth and proliferation. Cell Metab. 2008;7(1):11–20.

354. Hasegawa T, Hashimoto KI, Kawasaki H, Nakamatsu T. Changes in enzyme activities at the pyruvate node in glutamate-overproducing Corynebacterium glutamicum. J Biosci Bioeng. 2008 Jan;105(1):12–9.

355. Kinoshita JH, Merola LO. The utilization of pyruvate and its conversion to glutamate in calf lens. Exp Eye Res. 1961 Sep;1(1):53–9.

356. Zangari J, Petrelli F, Maillot B, Martinou JC. The Multifaceted Pyruvate Metabolism: Role of the Mitochondrial Pyruvate Carrier. Biomolecules. 2020 Jul 17;10(7):1068.

357. Schell JC, Wisidagama DR, Bensard C, Zhao H, Wei P, Tanner J, et al. Control of intestinal stem cell function and proliferation by mitochondrial pyruvate metabolism. Nat Cell Biol. 2017 Sep;19(9):1027–36.

358. Petrelli F, Scandella V, Montessuit S, Zamboni N, Martinou JC, Knobloch M. Mitochondrial pyruvate metabolism regulates the activation of quiescent adult neural stem cells. Sci Adv. 2023 Mar 3;9(9):eadd5220.

359. Strous RD, Shoenfeld Y. To smell the immune system: Olfaction, autoimmunity and brain involvement. Autoimmun Rev. 2006 Nov;6(1):54–60.

360. Connor KM, Davidson JR, Churchill LE, Sherwood A, Foa E, Weisler RH. Psychometric properties of the Social Phobia Inventory (SPIN). New self-rating scale. Br J Psychiatry J Ment Sci. 2000 Apr;176:379–86.

361. Hosoi J, Tanida M, Tsuchiya T. Mitigation of stress-induced suppression of contact hypersensitivity by odorant inhalation. Br J Dermatol. 2001 Nov;145(5):716–9.

362. Hosoi J, Tanida M, Tsuchiya T. Regulation of Plasma Substance P and Skin Mast Cells by Odorants. J Cutan Med Surg. 2003 Jul;7(4):287–91.

363. Shibata H, Fujiwara R, Iwamoto M, Matsuoka H, Yokoyama MM. Immunological and Behavioral Effects of Fragrance in Mice. Int J Neurosci. 1991 Jan;57(1–2):151–9.

364. Hsu P, Qu CK. Metabolic Plasticity and Hematopoietic Stem Cell Biology. Curr Opin Hematol. 2013 Jul;20(4):289–94.

365. Morganti C, Cabezas-Wallscheid N, Ito K. Metabolic Regulation of Hematopoietic Stem Cells. HemaSphere. 2022 Jul;6(7):e740.

366. Zuo H, Wan Y. Metabolic Reprogramming in Mitochondria of Myeloid Cells. Cells [Internet]. 2019;9(1). Available from: http://www.ncbi.nlm.nih.gov/pubmed/31861356

Appendix Figure 1

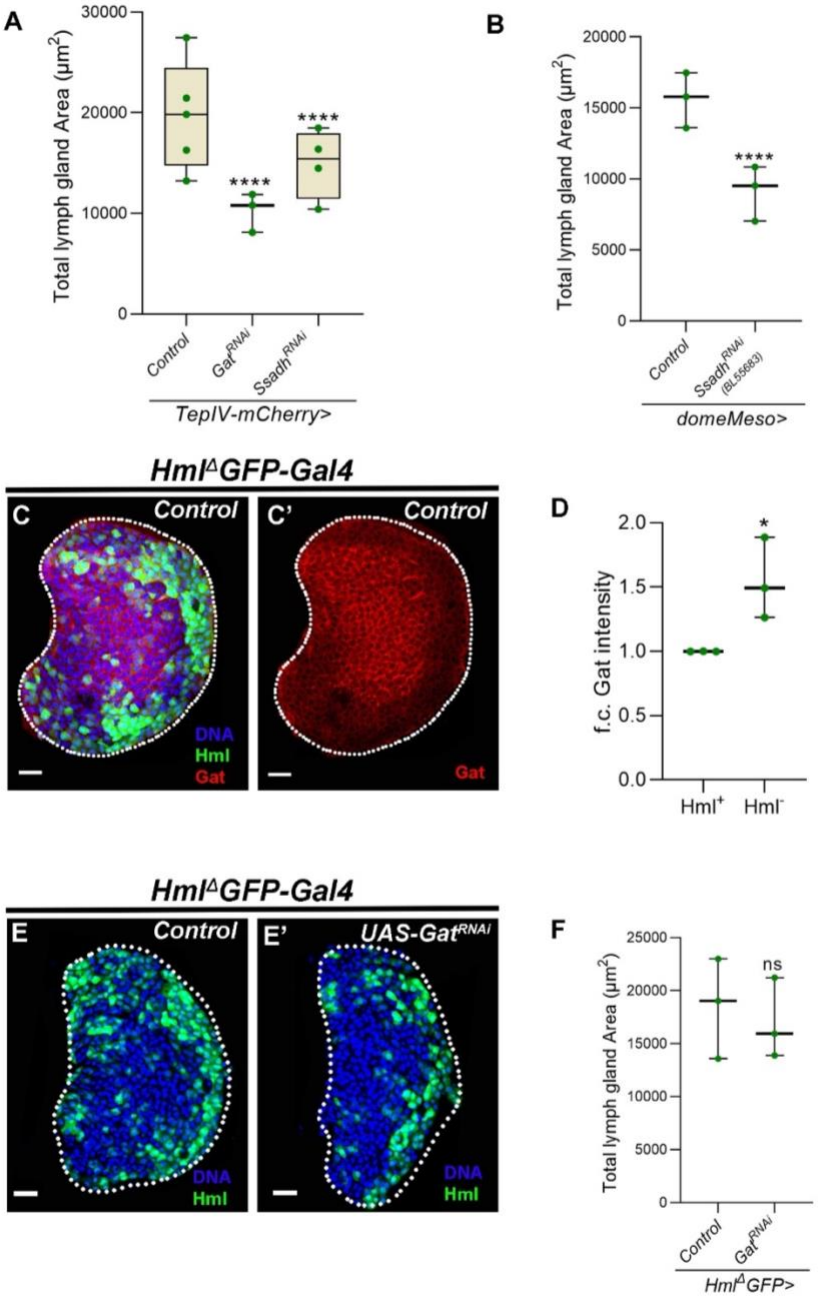

Ap. Fig. 1. GABA catabolism in *Drosophila* blood progenitor cells control lymph gland growth. (A) Quantifications of lymph gland size in *TepIV-Gal4;UAS-mCherry/+* (control, N=5, n=40), *TepIV-Gal4;UAS-mCherry;UAS-Gat^{RNAi}* (N=3, n=32, p<0.0001) and *TepIV-Gal4;UAS-mCherry;UAS-Ssadh^{RNAi}* (N=4, n=30, p<0.0001). **(B)** Quantifications of lymph gland size in *domeMeso>GFP/+* (*control*, N=3, n=30) and *domeMeso>GFP/Ssadh^{RNAi}* (BL55683) (N=3, n=30, p<0.0001). **(C,C')** Representative images showing Gat protein expression in control lymph gland (*Hml^{Δ}-Gal4;UAS-GFP/+*), **(C)** with Hml^{+} overlap (green) and **(C')** without Hml^{+} overlap, Hml^{+} region show lesser Gat levels as compared to Hml^{-}. For quantifications, refer to **D. (D)** Relative fold change in Gat levels in *Hml^{Δ}GFP>/+* in the Hml^{+} (N=3, n=16) and Hml^{-} region (N=3, n=16, p=0.0153) of the lymph gland. **(E-F)** Representative images showing lymph gland size in differentiating cells specific (Hml^{+}) loss of *Gat*, **(F)** expressing *Gat^{RNAi}* (*Hml^{Δ}-Gal4,UAS-GFP;UAS-Gat^{RNAi}*) does not show any reduction in lymph gland

size as compared to (**E)** control (*Hml$^{\Delta}$-Gal4;UAS-GFP/+*). For quantifications, refer to **G**. **(G)** Quantifications of lymph gland size in *Hml$^{\Delta}$GFP>/+* (control, N=3, n=34) and *Hml$^{\Delta}$GFP>/Gat^{RNAi}* (N=3, n=30, p=0.1921). Data is presented as median plots (*p<0.05;**p<0.01;***p<0.001,****p<0.0001,n.s.=non-significant), two-way ANOVA, Tukey's multiple comparisons test. f.c.= fold change. Scale bar: 20µm.'n'=lymph gland lobes. 'N'= number of experimental repeats (green dot). DAPI marks DNA. In this and all the following figures, lymph gland lobes are outlined with a white border and for clarity purpose the accompanying background containing other tissues like ring gland, brain, dorsal vessel etc. have been removed.

Appendix Figure 2

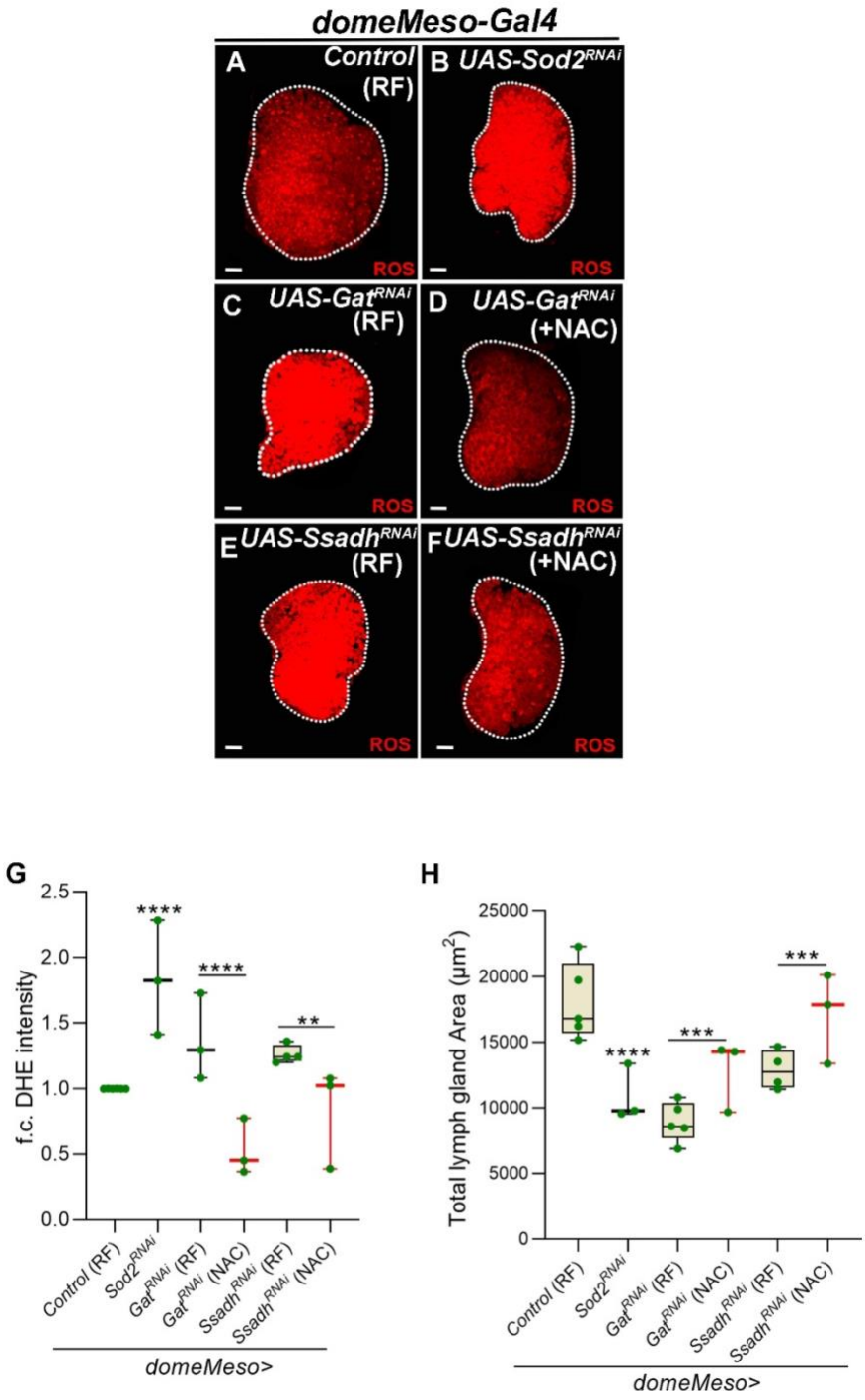

Ap. Fig. 2. ROS regulation by GABA shunt pathway in *Drosophila* blood progenitors is important for lymph gland growth. (A-F) Representative lymph gland images showing ROS levels, **(A)** control (*domeMeso-Gal4,UAS-GFP/+*) lymph gland showing higher ROS levels in the blood progenitor cells,

(B) expressing *Sod2*^{RNAi} (*domeMeso-Gal4,UAS-GFP;UAS-Sod2*^{RNAi}) in blood progenitor cells leads to increase in ROS levels as compared to **(A)** control, **(C-F)** NAC supplementation to (**D)** *domeMeso-Gal4,UAS-GFP;UAS-Gat*^{RNAi} and (**F)** *domeMeso-Gal4,UAS-GFP;UAS-Ssadh*^{RNAi} rescues the increased ROS phenotype as compared to **(C)** *domeMeso-Gal4,UAS-GFP;UAS-Gat*^{RNAi} and **(E)** *domeMeso-Gal4,UAS-GFP;UAS-Ssadh*^{RNAi} on RF respectively. For quantifications, refer to **G**. **(G)** Relative fold change in lymph gland ROS (DHE) levels in *domeMeso>GFP*/+ (control, N=6, n=49), *domeMeso>GFP/Sod2*^{RNAi} (N=3, n=10, p<0.0001), *domeMeso>GFP/Gat*^{RNAi} (RF, N=3, n=24, p=0.0092), *domeMeso>GFP/Gat*^{RNAi} (NAC, N=3, n=28, p<0.0001), *domeMeso>GFP/Ssadh*^{RNAi} (RF, N=4, n=23, p=0.0431) and *domeMeso>GFP/Ssadh*^{RNAi} (NAC, N=3, n=24, p=0.0019). **(H)** Quantifications of lymph gland area in *domeMeso>GFP*/+ (control, N=5, n=37), *domeMeso>GFP/Sod2*^{RNAi} (N=3, n=40, p<0.0001), *domeMeso>GFP/Gat*^{RNAi} (RF, N=5, n=42, p<0.0001), *domeMeso>GFP/Gat*^{RNAi} (NAC, N=3, n=26, p=0.0003), *domeMeso>GFP/Ssadh*^{RNAi} (RF, N=4, n=35, p<0.0001) and *domeMeso>GFP/Ssadh*^{RNAi} (NAC, N=3, n=20, p=0.0001). RF is regular food; SF is succinate food and NAC is N-acetylcysteine supplemented food. Data is presented as median plots (*p<0.05;**p<0.01;***p<0.001,****p<0.0001,n.s.=non-significant), two-way ANOVA, Tukey's multiple comparisons test. f.c.= fold change. Scale bar: 20µm.'n'=lymph gland lobes. 'N'= number of experimental repeats (green dot). DAPI marks DNA. Comparisons for significance are with control values, unless marked by horizontal lines for other respective comparisons and red bars represent rescue combinations.

Appendix Figure 3

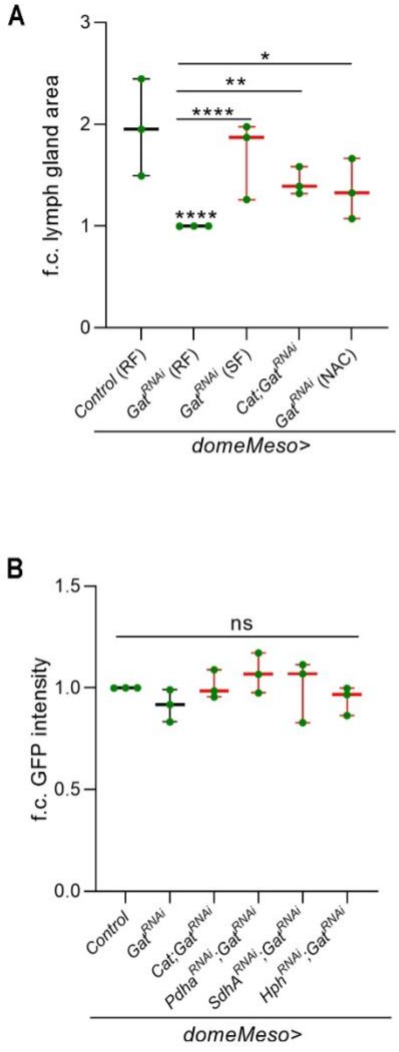

Ap. Fig. 3. GABA catabolism control lymph gland growth by diverse mechanisms.

(A) Relative fold change in lymph gland area in *domeMeso>GFP* /+ (control, N=3, n=26), *domeMeso>GFP/Gat*^{RNAi} (RF, N=3, n=26, p<0.0001 compared to control), *domeMeso>GFP/Gat*^{RNAi} (SF, N=3, n=26, p<0.0001), *domeMeso>GFP/Cat*;*Gat*^{RNAi} (N=3, n=26, p=0.0079) and *domeMeso>GFP/Gat*^{RNAi} (NAC, N=3, n=26, p=0.0162) compared to *domeMeso>GFP/Gat*^{RNAi}. **(B)** Relative fold change in dome^{+} GFP intensity in *domeMeso>GFP* /+(control, N=3, n=23), *domeMeso>GFP/Gat*^{RNAi} (RF, N=3, n=19, n=0.8701), *domeMeso>GFP/Cat*;*Gat*^{RNAi} (N=3, n=19, p>0.9999), *domeMeso>GFP/Pdha*^{RNAi}*;Gat*^{RNAi} (N=3, n=20, p=0.7488), *domeMeso>GFP/SdhA*^{RNAi}*;Gat*^{RNAi} (N=3, n=18, p>0.9999) and *domeMeso>GFP/Hph*^{RNAi};*Gat*^{RNAi} (N=3, n=21, p=0.9565). RF is regular food, SF is succinate food and NAC is N-acetylcysteine supplemented food. Data is presented as median plots (*p<0.05;**p<0.01;***p<0.001,****p<0.0001,n.s.=non-significant), two-way ANOVA, Tukey's multiple comparisons test. f.c.= fold change. 'n'=lymph gland lobes. 'N'= number of experimental repeats (green dot). Comparisons for significance are with control values, unless marked by horizontal lines for other respective comparisons and red bars represent rescue combinations.

Appendix Figure 4

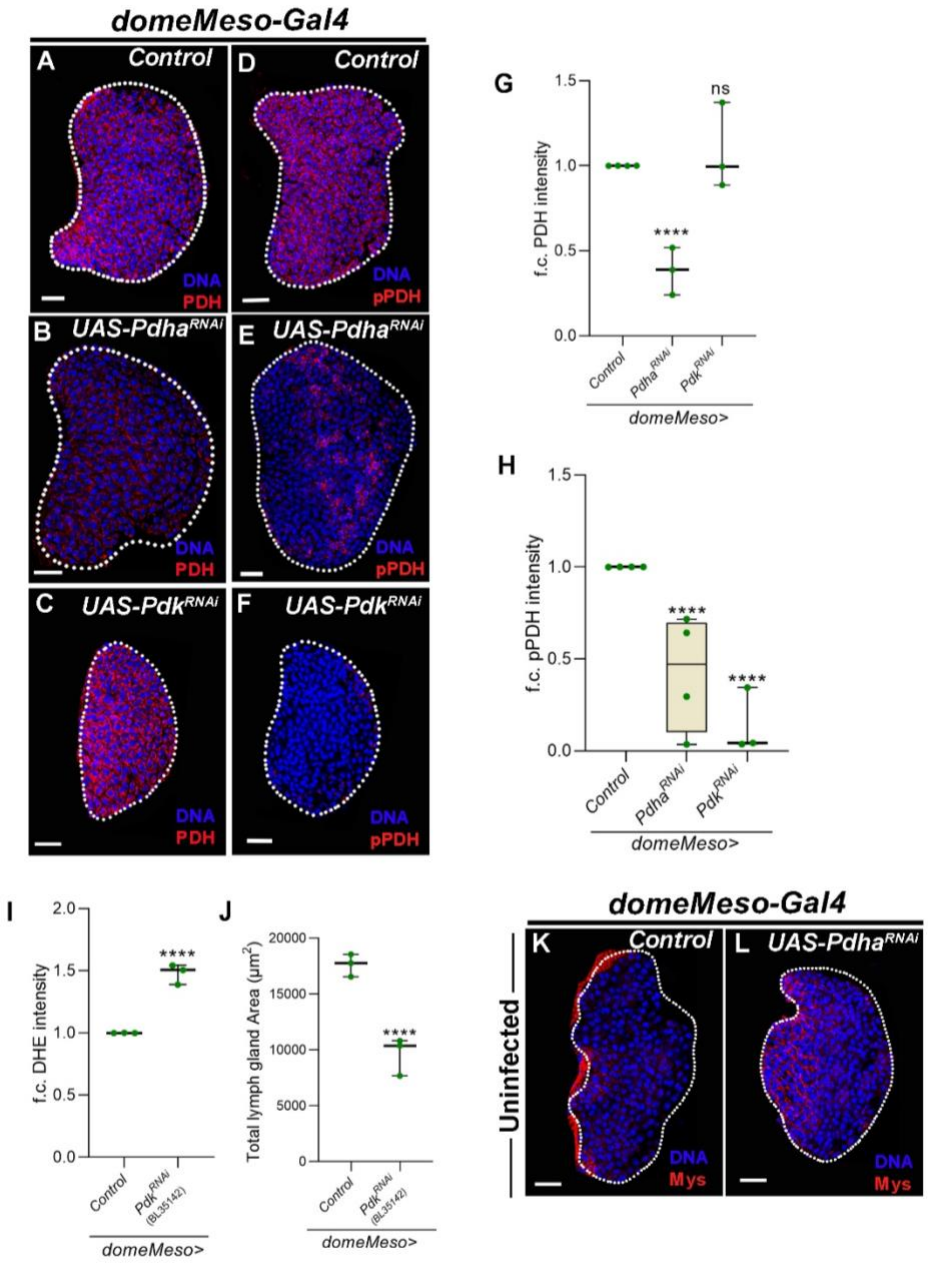

Ap. Fig. 4. TCA activity regulates blood-progenitor ROS levels and lymph gland growth.

(A-C) Representative lymph gland images showing PDH (red), **(A)** control (*domeMeso-Gal4,UAS-GFP/+*)**, (B)** expressing *Pdha*^{RNAi} in progenitor cells (*domeMeso-Gal4,UAS-GFP;UAS-Pdha*^{RNAi}) show reduction in medullary zone PDH levels and **(C)** expressing *Pdk*^{RNAi} in progenitor cells (*domeMeso-Gal4,UAS-GFP;UAS-Pdk*^{RNAi}) does not show reduction in medullary zone PDH levels as compared to **(A)** control**.** For quantifications, refer to **G. (D-F)** Representative lymph gland images showing pPDH (red), **(A)** control (*domeMeso-Gal4,UAS-GFP/+*)**, (B)** expressing *Pdha*^{RNAi} in progenitor cells (*domeMeso-Gal4,UAS-GFP;UAS-Pdha*^{RNAi}) show reduction in medullary zone pPDH levels and **(C)** expressing *Pdk*^{RNAi} in progenitor cells (*domeMeso-Gal4,UAS-GFP;UAS-Pdk*^{RNAi}) also show reduction in medullary zone pPDH levels as compared to **(D)** control**.** For quantifications, refer to **H. (G-H)** Relative fold change in lymph gland MZ **(G)** PDH levels in *domeMeso>GFP/+* (control, N=4, n=41), *domeMeso>GFP/Pdha*^{RNAi} (N=3, n=29, p<0.0001) and *domeMeso>GFP/Pdk*^{RNAi} (N=3, n=33, p=0.9240) and **(H)** pPDH levels in *domeMeso>GFP/+* (control, N=4, n=49), *domeMeso>GFP/Pdha*^{RNAi} (N=4, n=38, p<0.0001), and *domeMeso>GFP/Pdk*^{RNAi} (N=3, n=48, p<0.0001). **(I)** Relative fold change in

lymph gland ROS (DHE) levels in *domeMeso>GFP*/+ (control, N=3, n=37), and *domeMeso>GFP/Pdk*$^{RNAi\ (BL35142)}$ (N=3, n=31, p<0.0001). **(J)** Quantifications of lymph gland area in *domeMeso>GFP*/+ (control, N=3, n=30), and *domeMeso>GFP/Pdk*$^{RNAi\ (BL35142)}$ (N=3, n=30, p<0.0001). **(K-L)** lamellocyte formation in **(K)** control (*domeMeso-Gal4,UAS-GFP*/+) is not seen in uninfected condition, expressing **(L)** *Pdha*^{RNAi} (*domeMeso-Gal4,UAS-GFP;UAS-Pdha*^{RNAi}) does not affect lamellocyte formation in uninfected condition. Data is presented as median plots (*p<0.05;**p<0.01;***p<0.001,****p<0.0001,n.s.=non-significant), two-way ANOVA, Tukey's multiple comparisons test. f.c.= fold change. MZ=Medullary Zone. Scale bar: 20µm.'n'=lymph gland lobes. 'N'= number of experimental repeats (green dot). DAPI marks DNA.

Appendix Figure 5

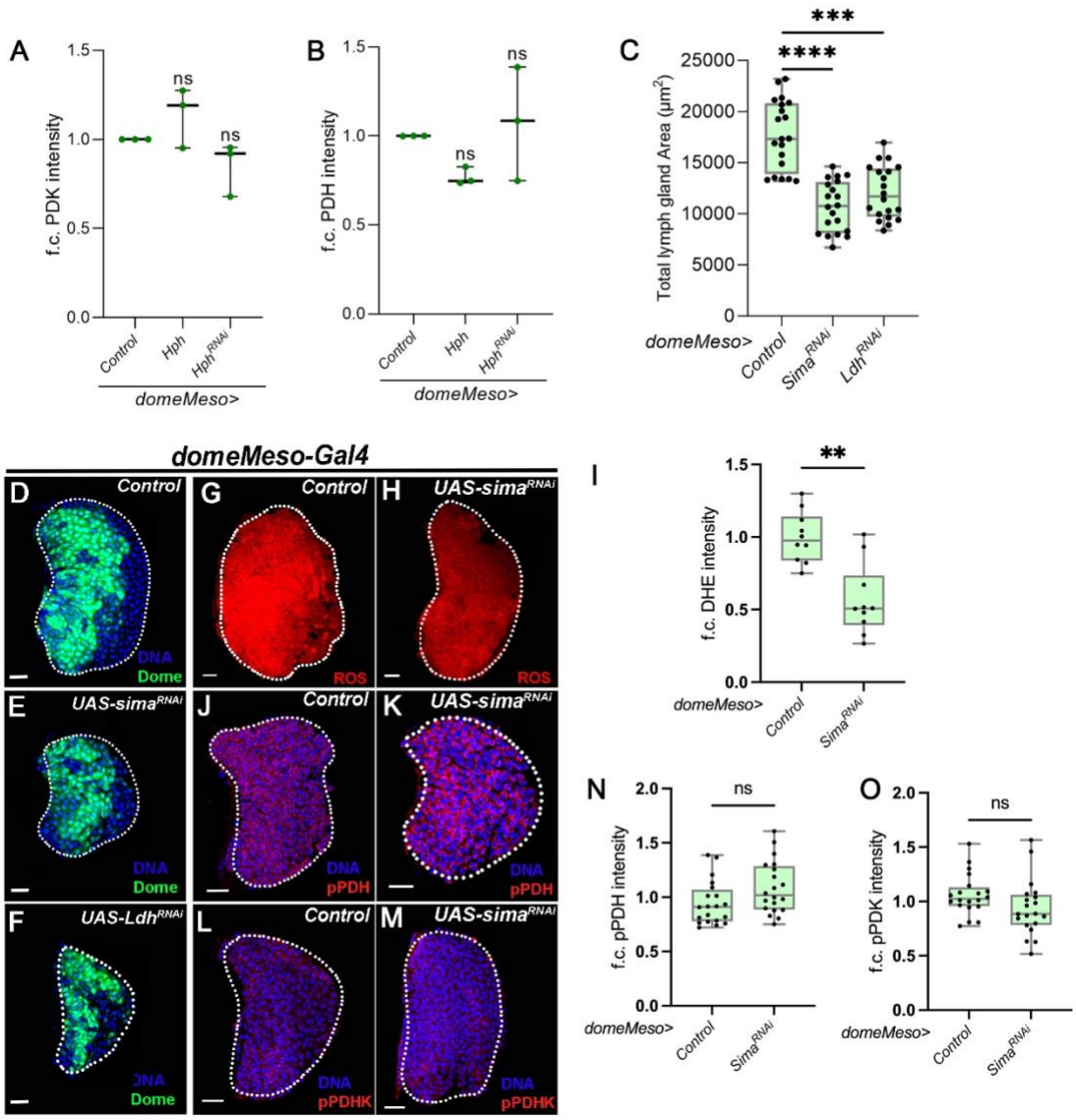

Ap. Fig. 5. Total PDH and Total PDK level in Hph loss and gain of function conditions.

(A-B) Relative fold change in lymph gland MZ **(A)** PDH levels in *domeMeso>GFP*/+ (control, N=3, n=40), *domeMeso>GFP/Hph* (N=3, n=14, p=0.0746), and *domeMeso>GFP/Hph*^{RNAi} (N=3, n=36, p=0.8879) and **(B)** PDK levels in *domeMeso>GFP*/+ (control, N=3, n=35), *domeMeso>GFP/Hph* (N=3, n=24, p=0.1651), and *domeMeso>GFP/Hph*^{RNAi} (N=3, n=28, p=0.0705). Data is presented as median plots (*p<0.05;**p<0.01;***p<0.001,****p<0.0001,n.s.=non-significant), two-way ANOVA, Tukey's

multiple comparisons test. f.c.= fold change. ‘n’=lymph gland lobes. ‘N’= number of experimental repeats (green dot).

Appendix Figure 6

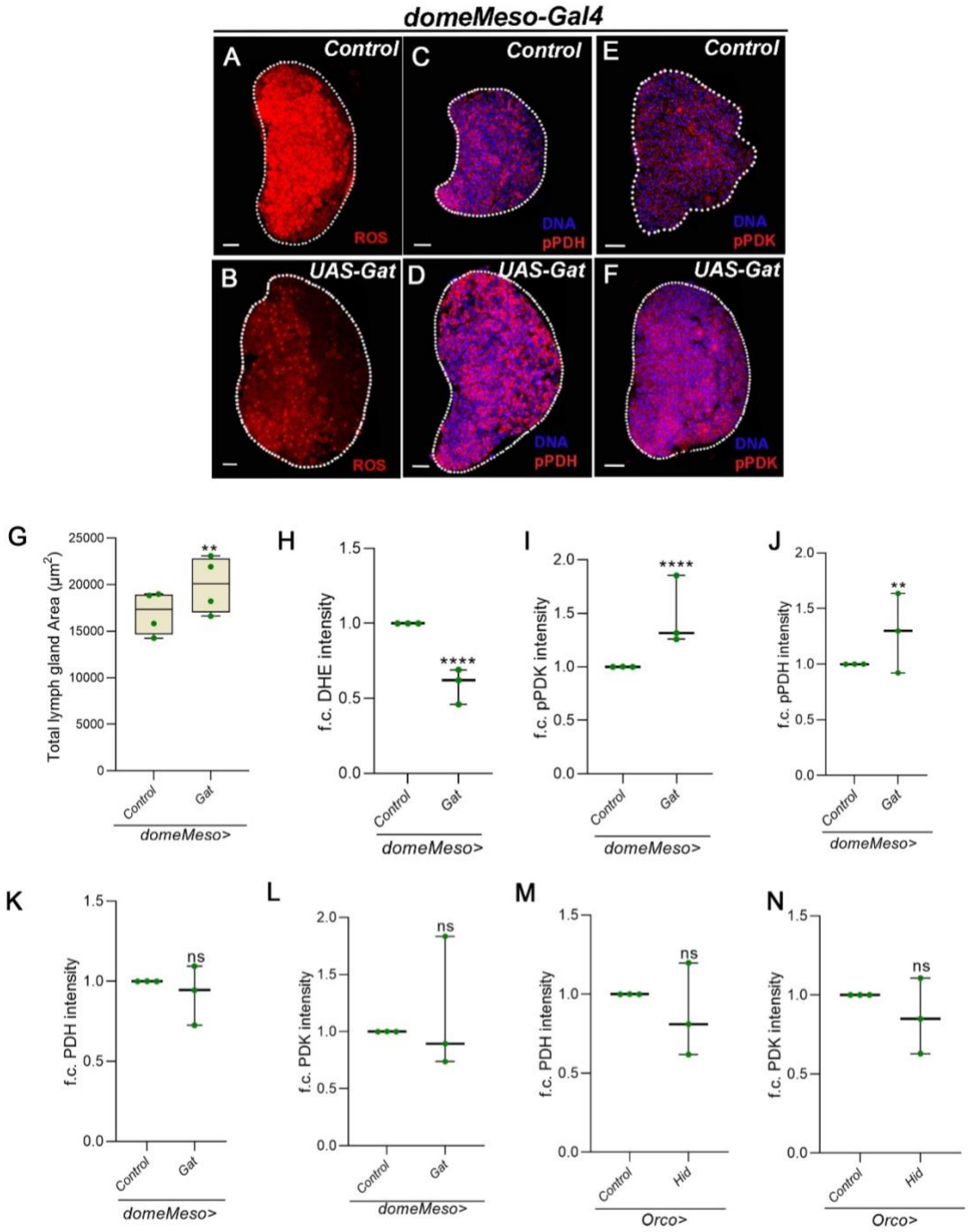

Ap. Fig. 6. Increased GABA uptake increases lymph gland growth and regulates ROS homeostasis. (A-F) Over-expressing **(B, D, F)** *Gat* in progenitor cells (*domeMeso-Gal4,UAS-GFP;UAS-Gat*) leads to significant reduction in **(B)** ROS levels, increase in **(D)** pPDH and **(F)** pPDK levels as compared to **(A, C, E)** control (*domeMeso-Gal4,UAS-GFP/+*). For quantifications, refer to **H, I, J. (G)** Quantification for lymph gland area in *domeMeso>GFP/+* (control, N=4, n=50) and *domeMeso>GFP/Gat* (N=4, n=40, p=0.0023). **(H)** Relative fold change in lymph gland ROS (DHE) levels in *domeMeso>GFP/+* (control, N=3, n=34) and *domeMeso>GFP/Gat* (N=3, n=30, p<0.0001). **(I-L)**, Relative fold change in lymph gland MZ **(I)** pPDH levels in *domeMeso>GFP/+* (control, N=3, n=40) and *domeMeso>GFP/Gat* (N=3, n=31, p=0.0022) **(J)** pPDK levels in *domeMeso>GFP/+* (control, N=3, n=42) and *domeMeso>GFP/Gat* (N=3, n=30, p<0.0001), **(K)** PDH levels in *domeMeso>GFP/+* (control, N=3, n=37) and *domeMeso>GFP/Gat* (N=3, n=17, p=0.4426) and **(L)** PDK levels in *domeMeso>GFP/+* (control, N=3, n=31) and *domeMeso>GFP/Gat* (N=3, n=40, p=0.4377). **(M, N)** Relative fold change in lymph gland

(M) PDH levels in *Orco>/+* (control, N=3, n=24) and *Orco>/Hid* (N=3, n=33, p=0.9983) and **(N)** PDK levels in *Orco>/+* (control, N=3, n=34) and *Orco>/Hid* (N=3, n=32, p=0.1166). Data is presented as median plots (*p<0.05;**p<0.01;***p<0.001,****p<0.0001,n.s.=non-significant), two-way ANOVA, Tukey's multiple comparisons test. f.c.= fold change. MZ=Medullary Zone. Scale bar: 20μm.'n'=lymph gland lobes. 'N'= number of experimental repeats (green dot). DAPI marks DNA.

Appendix Figure 7

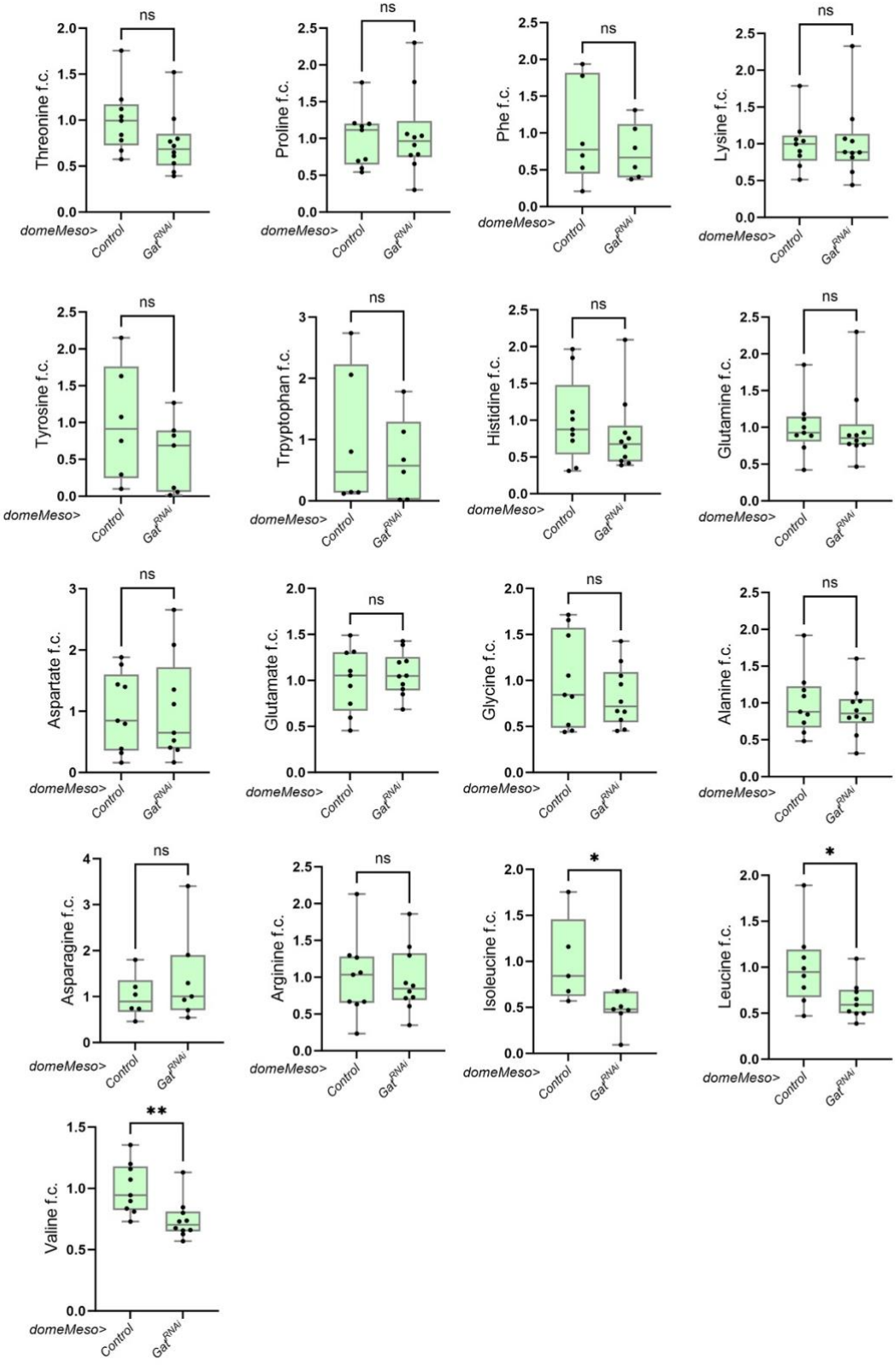

Ap. Fig. 7. GABA catabolic pathway is dispensable for majority of amino acids levels in the lymph glands.

Comparison of various amino acids levels in control (*domeMeso-Gal4,UAS-GFP/+*) and *domeMeso>Gat*^{RNAi} lymph glands. While, majority of the amino acids levels remain comparable between control and *domeMeso>Gat*^{RNAi} conditions, isoleucine, leucine and valine showed a significant reduction

in *domeMeso>Gat*^{RNAi} condition as compared to control lymph glands. For n values and p values, please refer to the appendix table 1.

Appendix Figure 8

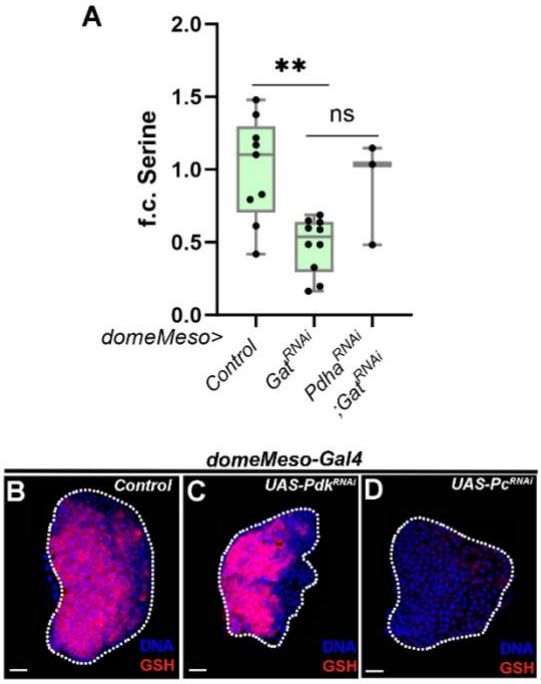

Ap. Fig. 8. GABA catabolism derived PDH regulation is central to control glutathione levels in the lymph gland progenitor cells.

(A) Relative steady state amount (fold change, f.c.) of serine in *domeMeso>GFP/+* (control, RF, n=9), *domeMeso>GFP/Gat*^{RNAi} (RF, n=10, p=0.0081) and *domeMeso>GFP/Pdha*^{RNAi}*;Gat*^{RNAi} (RF, n=3, p=0.3497 in comparison to *Gat*^{RNAi}). **(C)** Expressing *Pdk*^{RNAi} in progenitor cells (*domeMeso-Gal4,UAS-GFP;UAS-Pdk*^{RNAi}) does not reduce blood-progenitor GSH levels and **(D)** expressing *Pc*^{RNAi} in progenitor cells (*domeMeso-Gal4,UAS-GFP;UAS-Pc*^{RNAi}) leads to reduction of blood-progenitor GSH levels in comparison to **(B)** *control* **(***domeMeso>GFP/+*). Kruskal-Wallis test, Dunn's multiple comparisons test.

Appendix Figure 9

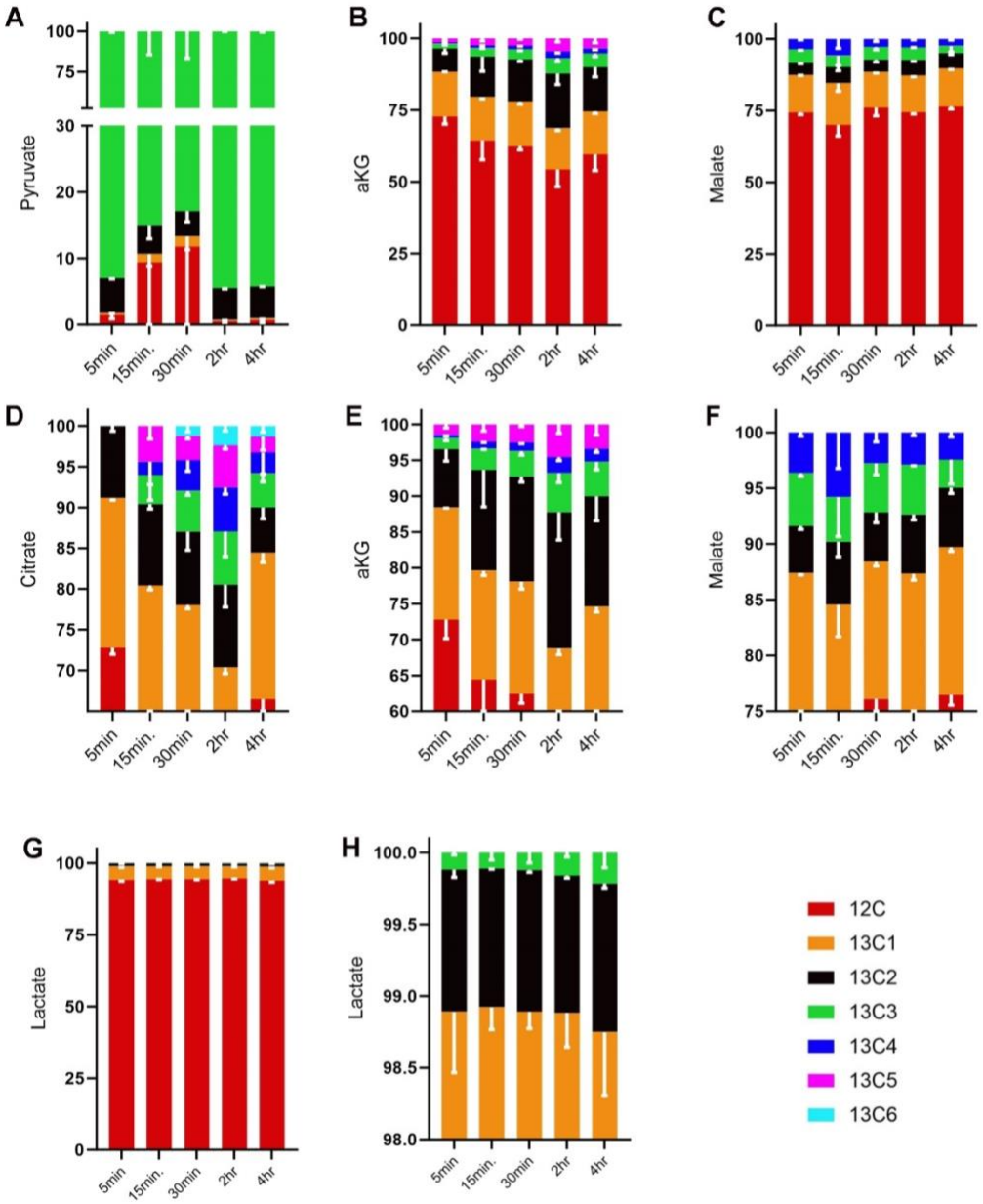

Ap. Fig. 9. Metabolic pathways activity during homeostatic lymph gland development
(A) $U_{13}C$-Pyruvate incubation and labelling analysis in pyruvate metabolite at different time points of 5 min., 15 min., 30 min., 2 hr and 4hr. **(B-C)** $U_{13}C$-pyruvate labelling analysis in wandering 3rd instar control lymph glands showing the label incorporation in **(B, E)** αKG, **(C, F)** Malate, **(D)** citrate and **(G, H)** lactate at different time points of 5 min., 15 min., 30 min., 2 hr and 4hr. 13C label is detected in the TCA metabolites at 5 min. time point and an increase in label incorporation was observed with increase in incubation time and gradually with increase in incubation time a decrease in label incorporation is seen at 4 hr. time point, indicating the flux of pyruvate towards TCA metabolites.

Appendix Figure 10

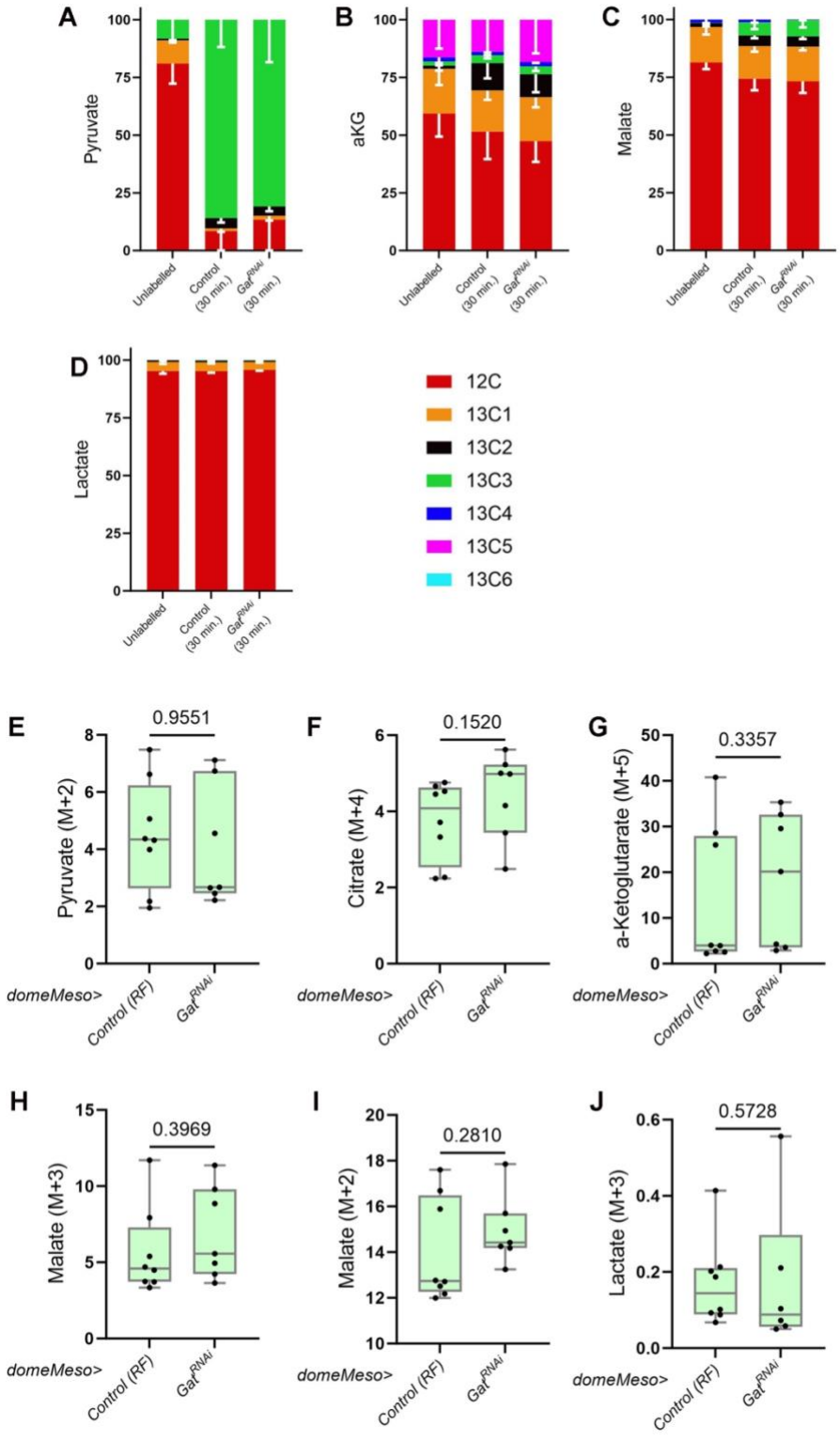

Ap. Fig. 10. GABA catabolic pathway regulates metabolic pathways activity in the lymph gland.

(A-D) Wandering 3rd instar *Control* and *domeMeso>Gat^{RNAi}* lymph glands showing the label incorporation after $U_{13}C$-pyruvate label incubation in **(A)** Pyruvate, **(B)** αKG, **(C)** Malate, and **(D)** lactate, **(E)** $U_{13}C$-pyruvate label incubation in *domeMeso>Gat^{RNAi}* (n=7, p=0.9551) lymph glands show a decrease in relative label incorporation for 13C2 (m+2) in pyruvate as compared to *Control* (n=7). **(F)** $U_{13}C$-pyruvate label incubation in *domeMeso>Gat^{RNAi}* (n=7, p=0.1520) lymph glands show an increase in relative label incorporation for 13C4 (m+4) in citrate as compared to *Control* (n=8). **(G)** $U_{13}C$-pyruvate

label incubation in *domeMeso>Gat*^{RNAi} (n=7, p=0.3357) lymph glands show an in relative label incorporation for 13C5 (m+5) in αKG OAA as compared to *Control* (n=8). **(H)** $U_{13}C$-pyruvate label incubation in *domeMeso>Gat*^{RNAi} (n=6, p=0.3969) lymph glands does not show a change in relative label incorporation for 13C3 (m+3) in malate as compared to *Control* (n=8). **(I)** $U_{13}C$-pyruvate label incubation in *domeMeso>Gat*^{RNAi} (n=6, p=0.2810) lymph glands show an increase in relative label incorporation for 13C2 (m+2) in malate as compared to *Control* (n=8). **(J)** $U_{13}C$-pyruvate label incubation in *domeMeso>Gat*^{RNAi} (n=6, p=0.5728) lymph glands show a decrease in relative label incorporation for 13C3 (m+3) in lactate as compared to *Control* (n=8). Data is presented as median plots (*p<0.05; **p<0.01; ***p<0.001, ****p<0.0001), Mann-Whitney test is applied.

Appendix Figure 11

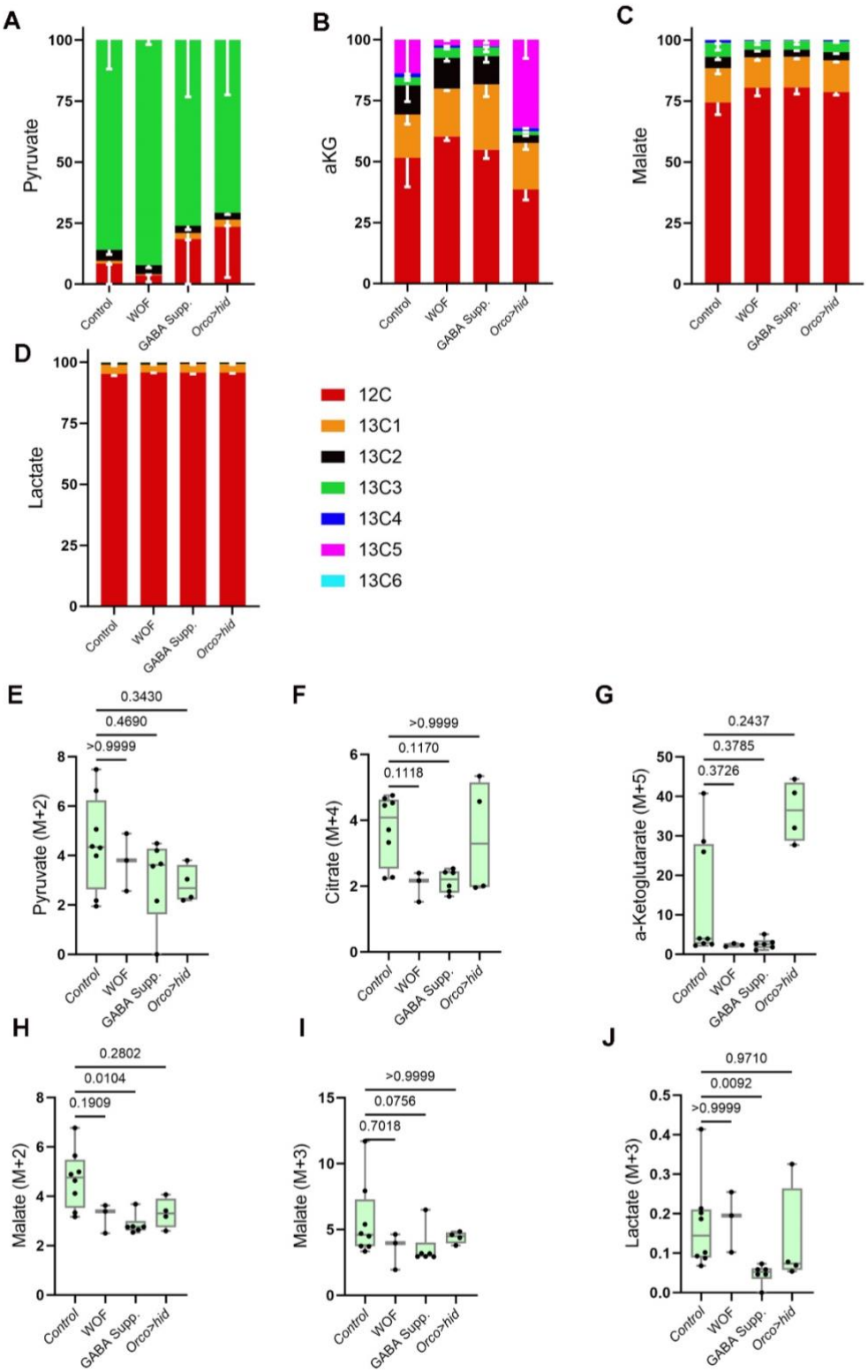

Ap. Fig. 11. Olfactory control of metabolic pathways activity in the lymph gland. (A-D) Wandering 3rd instar *Control*, WOF, GABA feeding (GABA Supp.) and *Orco>hid* lymph glands showing the label incorporation after $U_{13}C$-pyruvate label incubation in **(A)** Pyruvate, **(B)** αKG, **(C)** Malate, and **(D)** lactate, **(E)** $U_{13}C$-pyruvate label incubation in WOF (n=3, p>0.9999) and GABA Supp. (n=6, p=0.4690) lymph glands does not show any change in relative label incorporation and *Orco>hid* (n=4, p=0.3430) lymph glands leads to a decrease in relative label incorporation for 13C2 (m+2) in pyruvate as compared to *Control* (n=8). **(F)** $U_{13}C$-pyruvate label incubation in WOF (n=3, p=0.1118) and GABA Supp. (n=6,

p=0.1170) lymph glands leads to a decrease in relative label incorporation and *Orco>hid* (n=4, p>0.9999) lymph glands does not show any change in relative label incorporation for 13C4 (m+4) in citrate as compared to *Control* (n=8). **(G)** $U_{13}C$-pyruvate label incubation in WOF (n=3, p=0.3726) and GABA Supp. (n=6, p=0.3785) lymph glands leads to a decrease in relative label incorporation and *Orco>hid* (n=4, p=0.2437) lymph glands show an increase in relative label incorporation for 13C5 (m+5) in α-ketoglutarate (αKG) as compared to *Control* (n=8). **(H)** $U_{13}C$-pyruvate label incubation in WOF (n=3, p=0.1909), GABA Supp. (n=6, p=0.0104) and *Orco>hid* (n=4, p=0.2802) lymph glands leads to a decrease in relative label incorporation for 13C2 (m+2) in malate as compared to *Control* (n=8). **(I)** $U_{13}C$-pyruvate label incubation in WOF (n=3, p=0.7018) and GABA Supp. (n=6, p=0.0756) lymph glands leads to a decrease in relative label incorporation and *Orco>hid* (n=4, p>0.9999) lymph glands does not show any change in relative label incorporation for 13C3 (m+3) in malate as compared to *Control* (n=8). **(J)** $U_{13}C$-pyruvate label incubation in WOF (n=3, p>0.9999), lymph glands show a mild increase in relative label incorporation, GABA Supp. and (n=6, p=0.3092) *Orco>hid* (n=4, p=0.9710) lymph glands leads to a decrease in relative label incorporation for 13C3 (m+3) in lactate as compared to *Control* (n=8).

Appendix Table 1

Amino acid level in *Control* and *domeMeso>Gat^{RNAi}* lymph glands

Amino acids	**n value**	**p-value**
Threonine	Control= 9 *Gat^{RNAi}*= 10	0.0653
Proline	Control= 9 *Gat^{RNAi}*= 10	0.9682
Phenylalanine	Control= 6 *Gat^{RNAi}*= 6	0.6991
Lysine	Control= 9 *Gat^{RNAi}*= 10	0.7802
Tyrosine	Control= 6 *Gat^{RNAi}*= 7	0.2949
Tryptophan	Control= 6 *Gat^{RNAi}*= 6	0.5887
Histidine	Control= 9 *Gat^{RNAi}*= 10	0.4470
Glutamine	Control= 9 *Gat^{RNAi}*= 10	0.6038
Aspartate	Control= 9 *Gat^{RNAi}*= 9	>0.9999
Glutamate	Control= 9 *Gat^{RNAi}*= 10	0.8421
Glycine	Control= 9 *Gat^{RNAi}*= 10	0.5490
Alanine	Control= 9 *Gat^{RNAi}*= 10	0.6607
Asparagine	Control= 6 *Gat^{RNAi}*= 7	0.6282
Arginine	Control= 9 *Gat^{RNAi}*= 10	>0.9999
Isoleucine	Control= 6 *Gat^{RNAi}*= 7	0.0177
Leucine	Control= 8 *Gat^{RNAi}*=9	0.0464
Valine	Control= 9 *Gat^{RNAi}*=10	0.0057

Appendix Table 2

Peak areas and R_T for metabolite isotopes for flux analysis (QQQ3) with OBHA derivatization method

Analyte	Q1/Q3	Retention Time (R_T)
a-ketoglutaric acid [M+0]	462.1 -> 91.1	6.224
a-ketoglutaric acid [M+1]	463.1 -> 91.1	6.224
a-ketoglutaric acid [M+2]	464.1 -> 91.1	6.224
a-ketoglutaric acid [M+3]	465.1 -> 91.1	6.224
a-ketoglutaric acid [M+4]	466.1 -> 91.1	6.224
a-ketoglutaric acid [M+5]	467.1 -> 91.1	6.224
citric acid [M+0]	508.1 -> 91.1	5.329
citric acid [M+1]	509.1 -> 91.1	5.329
citric acid [M+2]	510.1 -> 91.1	5.329
citric acid [M+3]	511.1 -> 91.1	5.329
citric acid [M+4]	512.1 -> 91.1	5.329
citric acid [M+5]	513.1 -> 91.1	5.329
citric acid [M+6]	514.1 -> 91.1	5.329
fumaric acid [M+0]	327.1 -> 91.1	5.877
fumaric acid [M+1]	328.1 -> 91.1	5.877
fumaric acid [M+2]	329.1 -> 91.1	5.877
fumaric acid [M+3]	330.1 -> 91.1	5.877
fumaric acid [M+4]	331.1 -> 91.1	5.877
Glutamate [M+0]	253.1 -> 91.1	3.651
Glutamate [M+1]	254.1 -> 91.1	3.651
Glutamate [M+2]	255.1 -> 91.1	3.651
Glutamate [M+3]	256.1 -> 91.1	3.651
Glutamate [M+4]	257.1 -> 91.1	3.651
Glutamate [M+5]	258.1 -> 91.1	3.651
Glycine [M+0]	181.1 -> 91.1	3.628
Glycine [M+1]	182.1 -> 91.1	3.628

Glycine [M+2]	183.1 -> 91.1	3.628
lactic acid [M+0]	196.1 -> 91.1	3.032
lactic acid [M+1]	197.1 -> 91.1	3.032
lactic acid [M+2]	198.1 -> 91.1	3.032
lactic acid [M+3]	199.1 -> 91.1	3.032
malic acid [M+0]	345.1 -> 91.1	4.207
malic acid [M+1]	346.1 -> 91.1	4.207
malic acid [M+2]	347.1 -> 91.1	4.207
malic acid [M+3]	348.1 -> 91.1	4.207
malic acid [M+4]	349.1 -> 91.1	4.207
oxaloacetic acid [M+0]	448.1 -> 91.1	7.357
oxaloacetic acid [M+1]	449.1 -> 91.1	7.357
oxaloacetic acid [M+2]	450.1 -> 91.1	7.357
oxaloacetic acid [M+3]	451.1 -> 91.1	7.357
oxaloacetic acid [M+4]	452.1 -> 91.1	7.357
pyruvate [M+0]	299.1 -> 91.1	6.354
pyruvate [M+1]	300.1 -> 91.1	6.354
pyruvate [M+2]	301.1 -> 91.1	6.354
pyruvate [M+3]	302.1 -> 91.1	6.354
Serine [M+0]	211.1 -> 91.1	4.396
Serine [M+1]	212.1 -> 91.1	4.396
Serine [M+2]	213.1 -> 91.1	4.396
Serine [M+3]	214.1 -> 91.1	4.396
succinic acid [M+0]	329.1 -> 91.1	4.477
succinic acid [M+1]	330.1 -> 91.1	4.477
succinic acid [M+2]	331.1 -> 91.1	4.477
succinic acid [M+3]	332.1 -> 91.1	4.477
succinic acid [M+4]	333.1 -> 91.1	4.477

Appendix Table 3

Peak areas and R_T for amino acid (HILIC method) extracted from TCA precipitation

Amino acids	**R_T**	**Q1/Q3**
Alanine	10.067	90.1/44.1
Arginine	22.13	175.2/116.2
Asparagine	5.688	133.2/87.1
Aspartate	11.406	134.2/88.1
Cysteine	8.402	122.2/76.1
Glutamine	15.053	147.2/84.1
Glutamate	20.557	148.2/130.2
Glycine	10.598	76.1/30.1
Histidine	11.057	156.2/110.2
Isoleucine	5.689	132.2/86.1
Leucine	5.689	132.2/86.1
Lysine	20.557	147.2/84.1
Methionine	6.419	150.2/104.2
Phenylalanine	4.988	166.2/120.2
Proline	7.292	116.2/70.1
Serine	11.581	106.2/60.1
Threonine	10.309	120.2/74.1
Tryptophan	5.243	205.2/146.2
Tyrosine	6.661	182.2/165.2
Valine	7.462	118.2/72.1

Appendix Table 4

Peak areas and R_T for analytes

Analyte	**Retention Time (R_T)**	**Q1/Q3**
Glutathione (GSH, reduced) [M+0]	5.517	433.5/201.1 304.5
Glutathione (GSSG, oxidized)	4.308	613.7/231.4 355.4 484.2
N-Acetyl Cysteine	6.805	289.5/201.5
Cysteine	4.309	247.1/158.1 201.1 230.1
Homocysteine	3.654	261.1/56.1
NAD+	8.184	664.5/136.1
NADH	8.710	666.5/514.3
Acetyl CoA	9.835	810.2/303.1
Malonyl CoA	10.264	855.5/347.1
GSH [M+2] (from cysteine)	5.517	435/203 306
GSH [M+2] (from glutamate/glycine)	5.517	435/201 304

Appendix Table 5

Reagents utilized for LC/MS

Sr. No.	Reagent name	Supplier	Catalog Number
1	OBHA	Sigma	B22984
2	EDC	Sigma	03450
3	SODIUM PYRUVATE (13C3, 99%)	Cambridge Isotope Lab.	CLM-2440-0.5
4	D-GLUCOSE (U-13C6, 99%)	Cambridge Isotope Lab.	CLM-1396-PK
5	Hamilton® syringe, 1000 series GASTIGHT®, removable needle	Hamilton	22192-U
6	Pyridine	Sigma	270407-100ML
7	Lactate	Sigma	L1750
8	Pyruvate	Sigma	P2256
9	Citrate	Sigma	C3674
10	a-Ketoglutarate	Sigma	K3752
11	Succinate	Sigma	S2378
12	Malate	Sigma	112577
13	Fumarate	Sigma	F1506
14	OAA	Sigma	O4126
15	Glutamate	Sigma	G1251
16	Glycine	Sigma	G7126
17	Serine	Sigma	S4500
18	GABA	Sigma	A5835
19	Ethyl Acetate	Sigma	270989
20	Waters, XBridge BEH C18 Column, 130Å, 3.5 µm, 2.1 mm X 100 mm	Waters	SKU: 186003022

21	Waters, Atlantis Silica T3 Column, 100Å, 3 µm, 2.1 mm X 75 mm	Waters	SKU: 186005652
22	Pierce™ Formic Acid, LC-MS Grade	Thermo Scientific	28905
23	Acetonitrile, LC-MS Grade, 99.8%	Thermo Scientific	047138
24	Pierce™ Water, LC-MS Grade	Thermo Scientific	85189
25	Gibco™ PBS (10X), pH 7.4,	Thermo Scientific	70011044
26	Eppendorf: Protein LoBind Tubes, Protein LoBind®, 1.5 mL, PCR clean, colourless, 1 bag × 500 tubes Catalog	Eppendorf	0030108442
27	N-Ethylmaleimide	Sigma	04260
28	Dichloromethane	Thermo Scientific	610050040
29	Glutathione Disulfide-13C4,15N2 Ammonium Salt (ISTD: https://www.trc-canada.com/product-detail/?G597972)	Toronto Research Chemicals (TRC)	G597972
30	Glutathione (glycine-13C2,15N) Sodium Salt (ISTD: https://www.trc-canada.com/product-detail/?G597952)	Toronto Research Chemicals (TRC)	G597952